

POLITECNICO DI TORINO

Scuola di Dottorato (SCUDO)

Dottorato di Ricerca in Ingegneria Aerospaziale - XXIV ciclo
Ecole Doctorale "Connaissance, Langage, Modélisation" (ED139)
Doctorat en mécanique de l'Université Paris Ouest - Nanterre La
Défense

Ph.D. Dissertation

Refined and advanced shell models for the analysis of advanced structures



MARIA CINEFRA

Tutors

prof. Erasmo Carrera
prof. Olivier Polit

January 2012

ai miei migliori amici

Acknowledgements

First of all, I am grateful to Prof. Erasmo Carrera, my supervisor at Politecnico di Torino, for the suggestions and the opportunities he offered me in these years.

I would like to express my gratitude also to Prof. Olivier Polit, my supervisor at Université Paris Ouest - Nanterre La Défense, for his support in the development of the shell finite element presented in this thesis.

Finally, I acknowledge Professors Claudia Chinosi and Lucia Della Croce, from the University of Pavia, for their help in the formulation of the shell finite element presented in this thesis; and the Professor Ferreira, for our fruitful collaboration about meshless computational methods.

Torino, January 2012

Maria Cinefra

UNIVERSITÉ
FRANCO
ITALIENNE

UNIVERSITÀ
ITALO
FRANCESE

Summary

Structures technology for aerospace systems includes a wide range of component technologies from materials development to analysis, design and testing of the structures. The main improvements in future aircraft and spacecraft could depend on an increasing use of conventional and unconventional multilayered structures. New unconventional materials could be used in the near future: e.g. piezoelectric ones, which are commonly used in the so-called smart structures and functionally graded materials, which have a continuous variation of physical properties in a particular direction. The most of multilayered structures are subjected to different loadings: mechanical, thermal and/or electric loads. This fact leads to the definition of multifield problems.

In particular applications, the aforementioned structures appear as two-dimensional and they are known as shells. The advent of new materials in aerospace structures and the use of multilayered configurations has led to a significant increase in the development of refined theories for the modelling of shells. Classical two-dimensional models, which were frequently used in the past, are inappropriate for the analysis of these new structures: their modelling involves complicated effects that are not considered in the hypotheses used in classical models. To overcome these limitations, a new set of two-dimensional models, which employ Carrera's Unified Formulation (CUF), are presented.

The dissertation is organized in three main parts: - the refined and advanced shell models contained in the CUF; - the computational methods used to calculate the solution of differential equations; - the results obtained from the analysis of several problems.

In the first part, the different refined and advanced shell models contained in the CUF are presented. The CUF permits to obtain, in a general and unified manner, several models that can differ by the chosen order of expansion in the thickness direction, by the equivalent single layer or layer wise approach and by the variational statement used. These models are here defined directly for the shells, according to different geometrical assumptions. Both the cylindrical and the double-curvature geometries are considered. The constitutive equations of the advanced materials are provided. The constitutive equations for multi-field problems are obtained in a generalized way by employing thermodynamic considerations and they are opportunely rewritten for the case of mixed models. Depending on the variational statement used, one can define the refined theories, that are based on the principle of virtual displacements, and the advanced theories, based upon the Reissner's mixed variational theorem, in which secondary variables are "a priori" modelled. A complete system of acronyms is introduced to characterize these two-dimensional models.

The second part is devoted to the derivation of the governing equations by means of different methods: an analytical method, that is the Navier method, and two approximated numerical methods, that are the Finite Element Method (FEM) and the Radial Basis Functions (RBF)

method. The RBF method is based on a meshless approach and it can be considered a good alternative to the FEM. It is demonstrated that the Unified Formulation permits to derive the governing equations in terms of some few basic elements called fundamental nuclei. Expanding them by means of opportune indexes and loops, it is possible to obtain the stiffness matrix of the global structure. The use of such nuclei permits to obtain in a unified manner the different refined and advanced models contained in the CUF. The governing equations can be obtained in weak form for the Finite Element Method or strong form for the Navier method and the Radial Basis Functions method. A review of these solution methods is also provided, with particular attention to the finite element method that is the most common method in literature and it is the main topic of this thesis.

In the last part, different problems are analyzed. The thermo-mechanical analysis of FGM shells, the electromechanical analysis of piezoelectric shells and the dynamic analysis of carbon nanotubes are performed by means of the Navier method. The aim of this study is to demonstrate the efficiency of the models contained in the CUF in the analysis of multifield problems in advanced structures. Then, the CUF shell finite element, presented in this thesis, is tested and used for the analysis of composite and FGM shells. The superiority of this element in respect to finite elements based on classical theories is shown. Finally, the RBF method is combined with the CUF for the analysis of composite and FGM shells in order to overcome the numerical problems relative to the mesh that usually affect the finite elements.

Sommario

La tecnologia delle strutture per i sistemi aerospaziali include un'ampia gamma di tecnologie dei componenti, dallo sviluppo dei materiali all'analisi, al progetto e alla sperimentazione delle strutture. I principali miglioramenti nei futuri velivoli aeronautici e spaziali possono dipendere dall'uso crescente di strutture multistrato convenzionali e non convenzionali. Nuovi materiali non convenzionali possono essere usati in un prossimo futuro, quali i materiali piezoelettrici, che sono comunemente usati nelle cosiddette 'strutture intelligenti', e i materiali funzionalmente graduati (FGM), che sono caratterizzati da una variazione continua delle proprietà fisiche in una particolare direzione spaziale. La maggior parte delle strutture multistrato sono soggette a diversi tipi di carico: meccanico, termico e/o elettrico. Questo porta alla definizione dei problemi multi-campo.

In particolari applicazioni, le strutture sopra menzionate appaiono come bi-dimensionali e sono conosciute come 'gusci'. L'avvento di nuovi materiali nelle strutture aerospaziali e l'uso di configurazioni multistrato ha portato a una crescita significativa nello sviluppo di teorie raffinate per la modellazione dei gusci. I modelli bidimensionali classici, che sono stati spesso usati nel passato, non sono adatti per l'analisi di queste nuove strutture: la loro modellazione implica effetti complicati che non sono considerati nelle ipotesi usate per i modelli classici. Per superare questi limiti, un nuovo gruppo di modelli bidimensionali raggruppati nella Carrera's Unified Formulation (CUF) viene qui presentato.

La tesi è organizzata in tre parti principali: - i modelli guscio raffinati e avanzati che sono contenuti nella CUF; - i metodi computazionali utilizzati per calcolare la soluzione delle equazioni differenziali; - i risultati ottenuti dall'analisi di diversi problemi.

Nella prima parte, i modelli guscio raffinati e avanzati contenuti nella CUF vengono presentati. La CUF permette di ottenere, in maniera generale e unificata, molti modelli che differiscono per l'ordine di espansione scelto per le variabili primarie in direzione dello spessore, per il tipo di approccio, equivalent-single-layer o layer-wise, e per il principio variazionale usato. Questi modelli sono qui definiti direttamente per i gusci, in base a differenti assunzioni geometriche. Sia la geometria cilindrica che quella a doppia curvatura sono considerate. Inoltre, vengono fornite le equazioni costitutive per i materiali avanzati considerati. Le equazioni costitutive per i problemi multi-campo sono ottenute in modo generalizzato impiegando i principi della termodinamica ed esse vengono opportunamente riscritte nel caso di modelli misti. A seconda del principio variazionale utilizzato, si possono definire le teorie 'raffinate', che si basano sul Principle of Virtual Displacements (PVD), e le teorie 'avanzate', che si basano sul Reissner's Mixed Variational Theorem (RMVT), in cui anche le variabili secondarie sono modellate a priori. Un sistema completo di acronimi è stato introdotto per distinguere i diversi modelli bi-dimensionali.

La seconda parte della tesi è dedicata alla derivazione delle equazioni di governo per mezzo

di diversi metodi: il metodo analitico di Navier e due metodi numerici approssimati, quali il Finite Element Method (FEM) e il metodo delle collocazione tramite Radial Basis Functions (RBF). Il metodo RBF si basa su un approccio 'meshless' e può essere considerato una valida alternativa al FEM. Viene qui dimostrato che la Unified Formulation permette di derivare le equazioni di governo in termini di alcuni elementi base, detti 'nuclei fondamentali', che sono delle matrici di dimensioni 3×3 . Espandendo questi nuclei per mezzo di alcuni indici e cicli, è possibile ottenere la matrice di rigidezza della struttura globale. L'uso di tali nuclei permette di ottenere, in maniera unificata, i diversi modelli raffinati e avanzati contenuti nella CUF. Le equazioni di governo possono essere ottenute in forma debole per l'applicazione del metodo degli elementi finiti o in forma forte per l'applicazione del metodo di Navier o del metodo RBF. Viene data anche una visione d'insieme di questi metodi di risoluzione, con particolare attenzione al metodo degli elementi finiti che è il metodo più utilizzato in letteratura ed è l'argomento principale di questa tesi.

Nell'ultima parte, diversi problemi vengono studiati tramite il metodo di Navier: l'analisi termo-meccanica di gusci in FGM, l'analisi elettromeccanica di gusci in materiale piezoelettrico e l'analisi dinamica di nanotubi di carbonio (CNT). Lo scopo di questo studio è dimostrare l'efficienza dei modelli contenuti nella CUF nell'analisi di problemi multi campo. Successivamente, l'elemento finito guscio basato sulla CUF, presentato in questa tesi, viene testato e utilizzato per l'analisi di gusci compositi e FGM. I risultati ottenuti dimostrano la superiorità di questo elemento rispetto agli elementi finiti basati su teorie classiche nell'analisi dei materiali avanzati. Infine, il metodo RBF viene combinato con la CUF per l'analisi di gusci compositi e FGM in modo da superare i problemi numerici legati alla mesh che spesso si hanno negli elementi finiti.

Résumé

La technologie des structures pour les systèmes aérospatiaux doit tenir compte d'une vaste gamme de facteurs: le développement des matériels, la conception, le dimensionnement et l'expérimentation des structures. Les principales améliorations pour les futurs véhicules aéronautiques et spatiaux peuvent dépendre de l'utilisation croissante de structures multicouches conventionnelles et non conventionnelles. De nouveaux matériaux non conventionnels pourront être utilisés: les matériaux piézo-électriques, utilisés dans les "smart structures", et les matériaux à gradient de propriétés FGM qui sont caractérisés par une variation continue des propriétés physiques dans une direction spatiale déterminée. La plupart des structures multicouches sont sujettes à différents types de chargement: mécanique, thermique et/ou électrique. Cela nous amène donc à situer ce travail dans le cadre des problèmes multi-physiques.

Sous certaines conditions, ces structures sont dites bidimensionnelles et sont appelées "coques". L'avènement de nouveaux matériels dans les structures aérospatiales et l'utilisation de matériaux hétérogènes ont conduit au développement de théories raffinées pour modéliser les coques. Les modèles de coques classiques, développés par le passé, ne sont pas appropriés pour l'analyse de ces nouvelles structures: les phénomènes complexes induits dans ces nouvelles structures ne sont pas pris en compte dans ces modèles classiques. Ainsi, une nouvelle famille de modèles bi-dimensionnels, regroupés au sein de la "Carrera's Unified Formulation" (CUF), est présentée dans ce travail.

La thèse est décomposée en trois parties: - les modèles raffinées et avancées de coque de la CUF; - les méthodes numériques utilisées afin de résoudre le problème; - les résultats obtenus pour différents problèmes.

Dans la première partie, les modèles raffinée et avancée de coque de la CUF sont présentés. En effet, la CUF permet d'obtenir, dans un formalisme générale, de nombreux modèles qui diffèrent 1) selon l'ordre d'expansion dans l'épaisseur choisie pour les variables primaires; 2) selon le type de modèle: modèles couche équivalente (ESL) ou couche discrète (LW); 3) selon le principe variationnel. Ces modèles sont directement définis pour les coques, en explicitant les différentes hypothèses géométriques qui peuvent être introduits. Des géométries cylindrique et à double courbure sont traités. Dans un cadre multi-physique, les équations constitutives associées aux matériaux avancés abordés dans cette étude, sont obtenues de façon générale à partir des principes de la thermodynamique. Elles sont par ailleurs définies pour les approches variationnelles mixtes. On peut définir les théories raffinées, basées sur le "Principe of Virtual Displacements" (PVD) et les théories avancées, qui utilisent le "Reissner's Mixed Variational Theorem" (RMVT) où les variables secondaires sont approximées a priori. Des acronymes sont introduits pour classer et organiser les différents modèles obtenus.

La deuxième partie de la thèse est consacrée à l'obtention des équations fondamentales en

utilisant différentes méthodes: la méthode analytique de Navier (NAVIER) et deux méthodes numériques approchées; la "Finite Element Method" (FEM) et la "Radial Basis Functions" (RBF). La méthode RBF est une méthode sans maillage "meshless" et peut être considérée comme une méthode alternative à la FEM. On démontre ici que la CUF permet d'obtenir les équations fondamentales à l'aide d'éléments de base, appelés "fundamental nuclei" (FU), qui sont des matrices élémentaires de dimensions 3×3 . En assemblant ces FU par des boucles sur les indices caractéristiques, il est possible d'obtenir la matrice de rigidité de la structure globale. L'utilisation de ces FU permet donc d'obtenir de manière automatique et compacte les différents modèles raffinés et avancés de la CUF. Les équations fondamentales peuvent ainsi être obtenues sous une forme faible pour la FEM, ou sous une forme forte pour Navier et RBF. Ainsi, une vue d'ensemble est proposée pour ces différentes méthodes de résolution, en insistant plus particulièrement sur la FEM, qui est la plus utilisée dans la littérature et le sujet principal de cette thèse.

Dans la dernière partie, différents problèmes sont proposés et résolus afin d'illustrer les développements introduits dans les deux premières parties. Navier est utilisé pour l'analyse thermomécanique de coques FGM, l'analyse de coques piézo-électrique et l'analyse dynamique de nanotubes de carbone (CNT). Afin de démontrer l'efficacité des différents modèles CUF pour l'analyse de problèmes multi-physiques, un élément fini coque présenté dans cette thèse, est utilisé pour l'analyse de coques composites et FGM. Les résultats obtenus démontrent la supériorité de cet élément par rapport aux éléments finis basés sur les théories classiques pour l'analyse des matériaux avancés. Enfin, la méthode RBF est utilisée pour l'analyse de coques composites, permettant d'illustrer l'avantage des méthodes sans maillage.

Contents

1	Introduction	15
1.1	Advanced composite structures	15
1.1.1	Composite materials	16
1.1.2	Piezoelectric materials	17
1.1.3	Functionally graded materials	18
1.1.4	Carbon nanotubes	20
1.2	Theoretical models for thin-walled composites structures	20
1.2.1	Modelling of piezoelectric structures	23
1.2.2	Modelling of FGM structures	24
1.2.3	Modelling of CNTs	25
2	Refined and advanced shell models	27
2.1	Unified Formulation	27
2.2	Geometrical relations	28
2.2.1	Strain-displacement relations	29
2.2.2	Multifield geometrical relations	35
2.3	Constitutive equations	35
2.3.1	Composite materials	36
2.3.2	Multifield problems	39
2.3.3	Functionally graded materials	40
2.4	Variational statements	41
2.4.1	Principle of Virtual Displacements	41
2.4.2	Reissner's Mixed Variational Theorem	42
2.5	Acronyms of CUF models	44
3	Differential equations and solution methods	47
3.1	Governing equations	47
3.2	Navier method	50
3.2.1	Free vibration analysis	52
3.3	Finite element method	53
3.3.1	CUF MITC9 shell element	54
3.4	RBF collocation method	59
3.4.1	The static problem	60
3.4.2	The eigenproblem	62

4	Analytical solutions	65
4.1	Thermo-mechanical analysis of FGM shells	65
4.1.1	Governing equations	66
4.1.2	Results and discussion	68
4.2	Electromechanical analysis of piezoelectric shells	74
4.2.1	Governing equations	74
4.2.2	Results and discussion	77
4.3	Dynamic analysis of Double Walled Carbon Nanotubes (DWNT)	78
4.3.1	Results and discussion	90
5	FEM solutions	95
5.1	Governing equations	95
5.2	Assessment	100
5.3	Analysis of composite shells	104
5.3.1	Analysis of thick shells	118
5.4	Analysis of FGM shells	119
6	RBF solutions	123
6.1	Governing equations	123
6.2	Analysis of laminated shells	126
6.2.1	Results and discussion	127
6.3	Free vibration analysis of FGM shells	130
6.3.1	Results and discussion	133
7	Conclusions	143
7.1	Outlooks	146
	Bibliography	152

Chapter 1

Introduction

Structures technology for aerospace systems includes a wide range of component technologies from materials development to analysis, design and testing of the structures. Materials and structures are largely responsible for major performance improvements in many aerospace systems. The maturation of computational structures technology and the development of advanced composite materials obtained in the last 30 years have improved the structural performance, reduced the operational risk and shortened the development time. The design of future aerospace systems must meet additional demanding challenges. For aircraft, these includes cheapness, safety and environmental compatibility. For military aircraft, there will be a change in emphasis from best performance to low cost at acceptable performance. For space systems, new challenges are a result of a shift in strategy from long term, complex and expensive missions to those that are simple, inexpensive and fast.

Materials and structures, in addition to enabling technologies for future aeronautical and space systems, continue to be the key elements in determining the reliability, performance, testability and cost effectiveness of these systems. For some of the future air vehicles, the development and deployment of new structures technologies can have more impact on reducing the operating cost and the gross weight than any other technology area. An overview of advanced composite materials studied in the recent years and structural models used to analyze them is given in this chapter.

1.1 Advanced composite structures

Advanced structures considered in this work are multilayered two-dimensional structures embedding several layers with different properties: mechanical, thermal or electrical. As two-dimensional structures we consider those with a dimension, usually the thickness, negligible with respect to the other two in the in-plane directions. Typical two-dimensional structures are plates and shells. Plates do not have any curvature along the two in-plane directions, they are flat panels. Shells are two-dimensional structures with curvature along the two in-plane directions. In the case of plates, a rectilinear Cartesian reference system is employed. In the case of shells, the introduction of a curvilinear reference system is necessary (see Fig. 1.1). In both plate and shell cases, the third axis in the thickness direction is always rectilinear.

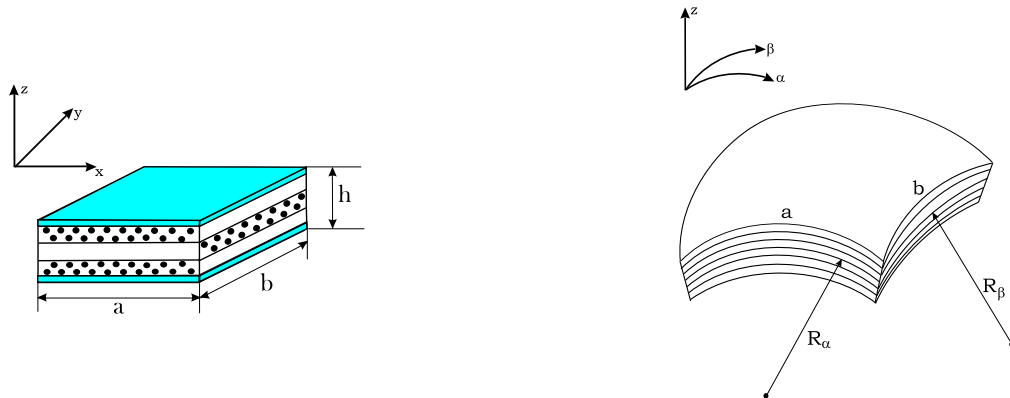


Figure 1.1: Examples of multilayered plate and shell.

Several materials are considered for layers embedded in multilayered structures. A first possibility are the homogeneous materials. Typical homogeneous materials used in aeronautics and space field are the aluminium and titanium alloys [1]. They present high strength-to-weight ratio and excellent mechanical properties. A natural development are *composite materials*, where two or more materials are combined on a macroscopic scale in order to obtain better engineering properties than the conventional materials (for example metals). Other typical aeronautics multilayered structures are the so-called sandwich structures. They are used to provide a stronger and stiffer structure for the same weight, or conversely a lighter structure to carry the same load as a homogeneous or compact-laminate flexural member. These structures are constituted by two stiff skins (faces) and a soft core, and they are widely used to build large parts of aircraft, spacecraft, ship and automotive vehicle structures. Most of the recent applications have used skins constituted by layered structures made of anisotropic composite materials. In the case of *smart structures*, some layers are in piezoelectric materials, they use the so-called *piezoelectric effect* which connects the electrical and mechanical fields. Also the so-called *Functionally Graded Materials (FGMs)* can be embedded in multilayered structures. They are used to provide the desired thermo-mechanical and piezoelectric properties, via the spatial variation in their composition. FGMs vary the elastic, electric and thermal properties in the thickness direction via a gradually changing of the volume fraction of the constituents. Finally, the *Carbon Nanotubes (CNTs)* are considered in these work. CNTs exhibit superior mechanical properties and are extremely promising due to their strong, light, and high toughness characteristics. In particular, they can be used as superfibers for nanocomposites materials.

The above proposed materials are discussed in depth in next sections.

1.1.1 Composite materials

Composite materials consist of two or more combined materials which have desirable properties that cannot be obtained with any of the constituents alone [2],[3]. Typical examples are fiber-reinforced composite materials which have high strength and high modulus *fibers* in a *matrix* material. In such composites, fibers are the main load-

carrying members and the matrix material keeps the fibers together, acts as a load-transfer medium between fibers, and protects them from being exposed to the environment. Fibers have a very high length-to-diameter ratio and their properties are maximized in a given direction. Paradoxically, short fibers (whiskers) exhibit better structural properties than long fibers. The fibers and matrix materials usually employed in composites can be metallic or non-metallic. The fiber materials can be common metals like aluminum, copper, iron, nickel, steel, titanium, or organic material like glass, boron and graphite [2].

In the case of structural applications, for example in aeronautics field, fiber-reinforced composite materials are often a thin layer called *lamina*. Typical structural elements, such as bars, beams, plates or shells are formed by stacking the layers to obtain desired strength and stiffness. Fiber orientation in each lamina and stacking sequence of the layers can be chosen to achieve desired strength and stiffness for a specific application.

The main disadvantages of laminates made of fiber-reinforced composite materials are the delamination and the fiber debonding. Delamination is caused by the mismatch of material properties between layers, which produces shear stresses between the layers, especially at the edges of a laminate. Fiber debonding is caused by the mismatch of material properties between matrix and fiber. Also, during manufacturing of laminates, material defects such as interlaminar voids, delamination, incorrect orientation, damaged fibers and variation in thickness may be introduced [4].

In formulating the constitutive equations of a lamina we assume that: (a) a lamina is a continuum: no gaps or empty spaces exist; (b) a lamina behaves as a linear elastic material. The assumption (a) permits to consider the macromechanical behavior of a lamina. The assumption (b) implies that the generalized Hooke's law is valid.

Sandwich structures are a kind of composite structures that are widely used in the aerospace, aircraft, marine, and automotive industries because they are lightweight with high bending stiffness. In general, the face sheets of sandwich panels consist of metals or laminated composites while the core is made of corrugated sheet, foam, or honeycomb. The commonly used core materials include aluminum, alloys, titanium, stainless steel, and polymer composites. The core supports the skin, increases bending and torsional stiffness, and carries most of the shear load [5],[6]. Structural sandwiches most often have two faces, identical in material and thickness, which primarily resist the in-plane and lateral (bending) loads. However, in special cases the faces may differ in either thickness or material or both, because one face is the primary load-carrying and low-temperature portion, while the other face must withstand an elevated temperature, corrosive environment, etc.

1.1.2 Piezoelectric materials

The phenomena of piezoelectricity is a peculiarity of certain class of crystalline materials. The piezoelectric effect is a linear energy conversion between mechanical and electrical fields. The linear conversion between the two fields is in both directions, defining a direct or converse piezoelectric effect. The *direct piezoelectric effect* generates

an electric polarization by applying mechanical stresses. On the contrary, the *converse piezoelectric effect* induces mechanical stresses or strains by applying an electric field. These two effects represent the coupling between the mechanical and electrical field, that is mathematically expressed by means of piezoelectric coefficients. First applications for piezoelectric materials were sound, ultrasound sensors and sources. These are still actual, but, in recent years, piezoelectricity has found renewed interest, as active intelligent structures with self-monitoring and self-adaptive capabilities [7]-[9]. Typical applications of piezoelectric materials in aerospace field are listed below.

Vibration damping. Nearly every structure in aerospace engineering is subjected to vibrations. In some cases such dynamic loads can be more dangerous than the applied static loads. By implementing sensors and actuators in such structures, the dynamic vibrations can be measured and then actively damped. Typical examples are vibration problems for the rotor wings in helicopters, sound damping in the cockpit or cabin of civil planes.

Shape adaption of aerodynamics surfaces. In modern airplane the aerodynamic surfaces can be optimized only for a certain airspeed and flight altitude. Wings that are able to change their geometry according to the actual demands could lead to an increase in efficiency.

Active aeroelastic control. Typical problems of aeroelasticity like flutter or buffeting can be reduced by the use of adaptive materials.

Shape control of optical and electromagnetic devices. Structures in aerospace field are subjected to rapid and high temperature variations due to changing exposure to the sunlight. Optical surfaces like mirrors and lenses, electromagnetic antennas and reflectors are highly sensitive to thermal deformations. A remedy to these problems could be the use of adaptive materials.

Health monitoring. In aerospace structures microscopic cracks are tolerable up to a certain limit. Smart structures could monitor these stresses and then apply an additional control mechanism to maintain the safety.

1.1.3 Functionally graded materials

The severe temperature loads involved in many engineering applications, such as thermal barrier coatings, engine components or rocket nozzles, require high temperature resistant materials. In Japan in the late 1980s the concept of Functionally Graded Materials (FGMs) has been proposed as a thermal barrier material. FGMs are advanced composite materials wherein the composition of each material constituent varies gradually with respect to spatial coordinates [10]. Therefore, in FGMs the macroscopic material properties vary continuously, distinguishing them from laminated composite materials in which the abrupt change of material properties across layer interfaces leads to large interlaminar stresses allowing for damage development [11].

Functionally Graded Materials (FGMs) have a large variety of applications, due to their properties, not only to provide the desired thermomechanical properties, but also to obtain appropriate piezoelectric, and magnetic properties, via the spatial variation in their composition. An alternative application of FGMs could be the use of piezoelectric materials, functionally graded in the thickness direction (FGPM), in order to build smart structures which are extensively used as sensors and actuators. A typical example of a material functionally graded in the thickness direction and employed as thermal barrier coating is given in Figure 1.2. The special feature of graded spatial compositions associated to FGMs provides freedom in the design and manufacturing of novel structures; on the other hand, it also poses great challenges in numerical modeling and simulation of the FGM structures [12].

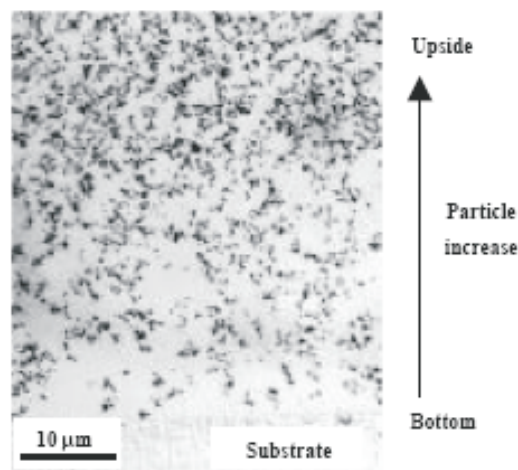


Figure 1.2: Typical microstructure of a thermal barrier coating functionally graded in a desired direction.

It is well known that the response of macroscopically homogeneous systems can be described in terms of certain thermoelastic moduli that are evaluated for a selected representative volume element, subjected to uniform overall thermomechanical fields. However, such representative volumes are not easily defined for systems with variable phase volume fractions, subjected to nonuniform overall fields. The characterization of an FGM is not easy and it changes depending the considered material. The most common methods based on micromechanical models are the rule of mixtures [13], the 3-D phases distribution micromechanical models [14], the Voronoi Cell Finite Element Method (VCFEM) [15], the stress waves methods [16], and the stochastic micromechanical models [17][18]. Among the various topics related to FGM, reference can be made to the review articles by Birman and Bird (2007) (Da articolo vibration FGM shells).

1.1.4 Carbon nanotubes

Carbon nanotubes (CNT) have exceptional mechanical properties (Young's modulus, tensile strength, toughness, etc), which are due to their molecular structure consisting of single or multiple sheets of graphite wrapped into seamless hollow cylinders [19]. Due to the large stiffness, strength and high aspect ratio of CNTs, it is expected that by evenly dispersing them throughout a polymer matrix one can produce composites with considerably improved overall effective mechanical properties. Furthermore, CNTs have a relatively low density of about 1.75 g/cm^{-3} and, therefore, nanotube reinforced polymers (NRPs) excel due to their extremely high specific stiffness, strength and toughness. This has already been demonstrated in experiments, both for thermoplastic [20] and thermosetting [21] polymer matrices.

The study of the vibration and frequency analysis of embedded CNTs is a major topic of current interest. Since controlled experiments to measure the properties of individual CNT at the nanoscale are extremely difficult, computational simulations have been regarded as a powerful tool. However, computational simulations for predicting properties of CNTs fall into two major categories: molecular dynamics (MD) and continuum mechanics. Although MD simulation has been successfully used for simulating the properties of the material with microstructures, this method is time consuming and formidable especially for large-scale complex systems. Recently, solid mechanics with continuum elastic models, such as beam and shell models, have been widely and successfully used to study mechanical behavior of CNTs [22],[23]. Moreover, interest in double-walled nanotubes (DWNTs) is rising due to the progress in large-scale synthesis of DWNTs. In these cases, it is anticipated that intertube radial displacements of Multiwalled carbon nanotubes (MWNTs), defined by substantially non-coincident axes of the nested nanotubes, would come to play a significant role and it must be accounted in the considered continuum model [24].

1.2 Theoretical models for thin-walled composites structures

In recent years, considerable attention has been paid to the development of appropriate two-dimensional shell theories that can accurately describe the response of multilayered anisotropic thick shells. In fact, thick shell component analysis and fatigue design require an accurate description of local stress fields to include highly accurate assessment of localized regions where damage is likely to take place. As mentioned in the previous section, examples of multilayered shell structures used in modern aerospace vehicles are laminated constructions made of anisotropic composite materials, sandwich panels, layered structures used as thermal protection, or intelligent structural system embedding piezolayers.

It was pointed out by Koiter [25] that, for traditional isotropic one-layer shells, refinements of Love's first approximation theory are meaningless unless the effects of transverse shear and normal stress are both taken into account in a refined theory.

Layered shells deserve special attention. These are characterized by a noncontinuous material properties distribution in the thickness direction and further requisites become essential for a reliable modelling of such structures. Among these, the fulfillment of both continuity of displacement and transverse shear and normal stresses at the interface between two adjacent layers is such a necessary desideratum. In Ref. [26] these requisites are referred to as C_z^0 requirements that state that both displacements and transverse stress components are C^0 -continuous functions in the thickness shell coordinate z . An increasing role is played by the C_z^0 requirements and by Koiter's recommendation in the case of laminated shells made of composite materials presently used in aerospace structures. These materials exhibit higher values of Young's moduli orthotropic ratio ($E_L/E_T = E_L/E_z = 5 \div 40$; L denotes the fiber directions, whereas T and z are two-direction orthogonal to L) and the lower transverse shear moduli ratio ($G_{LT}/E_L \approx G_{TT}/E_L = \frac{1}{10} \div \frac{1}{200}$) leading to higher transverse shear and normal stress deformability in comparison to isotropic cases. Approximated three-dimensional solutions by Noor and Rarig [27] and Noor and Peters [28],[29] and more recent exact three-dimensional solutions by Ren [30] and Varadan and Bhaskar [31] have numerically confirmed the need of the previously mentioned refinements for static and dynamic cylindrical shell problems. In particular, the fundamental role played by transverse normal stress σ_{zz} was underlined. Nevertheless, three-dimensional elasticity solutions are only available in a very few cases and these are mainly related to simple geometries, a specific stacking sequence of the lamina, and linear problems. In the most general cases and to minimize the computational effort, two-dimensional models are preferred in practice.

Starting from the early work by Shtayerman [32] many two-dimensional models have been proposed for anisotropic layered shells. The so-called axiomatic approach [33] (where a certain displacement or stress field is postulated in the shell thickness direction) and asymptotic methods [34]-[40] (where the three-dimensional equations are expanded in terms of an introduced shell parameter) have both been applied to derive simplified analysis. Exhaustive overviews on these topics can be found in many published review papers. Classical theories were reviewed by Bert [41]. An interesting overview, including works that appeared in Russian literature, can be found in the book by Librescu [42]. Recent developments in the Russian school concerning the fulfillment of the C_z^0 requirements were overviewed by Grigolyuk and Kulikov [43]. Reviews on finite element shell formulations can be found in the work by Dennis and Palazotto [44], Merk [45], and Di and Ramm [46]. Recent articles on the application of asymptotic methods to anisotropic shells can be found in Fettahlioglu and Steele [47], Widera and Logan [48], Widera and Fan [49] and Spencer et al. [50]. Two exhaustive and more recent surveys have been provided by Kapania [51] and Noor and Burton [183] that address a complete overview of different aspects of multilayered shells modelings. Herein, attention is focused on the axiomatic approach. A short review of this approach follows.

Classical displacement formulations start by assuming a linear or higher-order expansion for the displacement fields in the thickness direction. In-plane and transverse stresses are then computed by means of Hooke's law. According to this procedure, it is

found that transverse stresses (both shear and normal components) are discontinuous at the interfaces. To overcome these difficulties, these stresses are evaluated a posteriori in most applications by implementing a post-processing procedure, e.g., through the thickness integration of the three-dimensional indefinite equation of equilibrium. A few examples in which a layer-wise model (LWM) description is used (the number of the unknowns depends on the number of layers) are works by Hsu and Wang [53], Cheung and Wu [54], and Barbero et al. [55]. Others, in which an equivalent single-layer model (ESLM) description was preferred, are the works by Hildebrand et al. [56], Whitney and Sun [57], Reddy and Liu [234], Librescu et al. [59], and Dennis and Palazotto [44],[60]. The interesting theory by Rath and Das [61] should be mentioned from the ESLM analysis, where interlaminar transverse shear continuity was a priori fulfilled in both the symmetrical and unsymmetrical case through the thickness response of layered shells. A particular example of the theory in Ref. [61] was analyzed in Ref. [62] for symmetrically laminated cylinders. The numerical analysis reported in the cited works conclude the following:

1. An a priori description of transverse stress cannot account for LWMs based on the displacement formulation.
2. Layer-wise (LW) analysis usually lead to a better description than ESLM ones; such a superiority is more evident for arbitrarily laminated shells with increasing layers.
3. The ESLM analysis experienced difficulties in accurately describing a σ_{zz} and the related consequences.
4. The mentioned post-processing procedure for the calculation of transverse stresses cannot be implemented for most of the available models in the general case of asymmetric in-plane displacement fields (i.e., two different results could be obtained for the stress distributions by starting from the top or from the bottom shell surface).

Reissner [63],[64] proposed a mixed variational equation for the purpose of overcoming the impossibility of fulfilling a priori the interlaminar continuity for both transverse shear and normal stresses, which furnishes equilibrium and constitutive equations that are consistent with an assumed displacement and transverse stress field. Similar discussion and conclusions can be read in the overview paper by Grigolyuk and Kulikov [43]. This tool was applied to shells by Bhaskar and Varadan [65] and Jing and Tzeng [66] for the case of ESLM analysis. Both works neglected the transverse normal stress. Related results confirmed that the use of Reissner's mixed variational equations associated to an ESLM description is not sufficient to describe accurately the σ_{zz} effects. Therefore, the use of Reissner equation requires a layer-wise description. The convenience of referring to a Reissner mixed variational equation was shown in [26],[67]-[73]. In particular, it was shown that the proposed layer-mixed description gives an excellent a priori description of the transverse shear and normal stress fields.

It is a well-established result obtained from traditional isotropic shell structures analysis [74]-[77] that accurate two-dimensional shell modelling cannot come without an equivalently accurate description of the curvature terms. The neglectfulness of terms of type $h = R$ (thickness to radii shell ratio) or the use of Donnell's shallow-shell type approximations could be very restrictive in thick-shell analysis. In fact, as shown by Soldatos [78], Carrera [79], and Jing and Tzeng [66] any refinement related to the fulfillment of C_z^0 requirements would be meaningless unless curvature terms are well described. For this reason, no assumption will be introduced in this work concerning curvature terms.

1.2.1 Modelling of piezoelectric structures

In most applications, the piezoelectric layers are embedded in multilayer structures made of anisotropic composite materials. The efficient use of piezoelectric materials in multilayer structures requires accurate evaluation of mechanical and electric variables in each layer. Classical shell models such as classical lamination theory (CLT) and first-order shear deformation theory (FSDT) can lead to large discrepancies with respect to the exact solution. Improvements can be introduced by using equivalent single-layer models with higher-order kinematics. However, much better results can be obtained through the use of layerwise models. For recent indications of the superiority of LWMs over ESLMs, see [80].

The advantages of the Reissner Mixed Variational Theorem (RMVT) with respect to other approaches that mostly make use of the Principle of Virtual Displacement (PVD) were shown in [81],[82]. The Unified Formulation (UF) was used there to create an hierarchical shell formulation with variable kinematics (relative to displacements and transverse stresses) in each layer. Attention was restricted to pure mechanical problems. UF has been extended to closed-form and finite-element solutions of a piezoelectric plate in [83] and [84], respectively; PVD was used and only the displacements and the electrical potential were considered as unknown variables. The main advantage of RMVT is the possibility of fulfilling a priori the continuity conditions for the transverse electromechanical variables (electric displacement and stresses). Indeed, the discontinuity of electromechanical properties at the layer interface requires a discontinuous first derivative of the same variables.

Attempts to introduce the C_z^0 -requirements in piezoelectric continua have been made in [85],[86]. Closed form and FEs solutions were considered in these last papers, respectively. Attention was restricted to the fulfillment of C_z^0 -requirements for transverse shear and normal stress components. Such an extension is herein stated as a "partial" RMVT application. The complete fulfillment of the C_z^0 -requirements to both electrical and mechanical variables has been provided in the companion paper [87], devoted to FE analysis and plate geometries. Such a contribution has been called a "full" extension of RMVT to piezoelectric continua.

A few papers on piezoelectric shells exist in the literature, in particular for the FE method. Layerwise methods were considered in [220]. FE piezoelectric shells have been considered in [89]. Cho and Roh [90] proposed geometrically exact shell elements,

while Kögl and Bucalem [91] gave the extension of MITC4 type element to piezoelectric shell structures. Review and assessment have been given in [92]. Three dimensional piezoelectricity solutions have been addressed in [93]-[96]. Wang et al. [93] and Shakeri et al. [94] dealt with vibration problems. Chen et al. [95] addressed cylindrical shell with very thin piezoelectric layers. Only a piezoelectric layer was instead considered in [96]. No results are available in which both mechanical and piezoelectric layers (with thickness comparable to the mechanical layers) are analyzed.

The full version of RMVT has been extended to piezoelectric shells in [97] and [98]. These are the natural extension of the previous works [72],[73],[219],[100] that deal with the plates.

1.2.2 Modelling of FGM structures

The concept of Functionally Graded Material was first proposed as thermal barrier material. Therefore, the thermo-mechanical problem in FGMs is a major topic of current interest.

Over the last decade, extensive research has been carried out on the modeling of shells comprising FGM layers. Pelletier and Vel, in [101], have provided an exact solution for the steady-state thermoelastic response of functionally graded orthotropic cylindrical shells. The equilibrium equations are solved by the power series method and the temperature field are obtained by solving the heat conduction equations. The cylindrical shells are analyzed using the Flugge and the Donnell theories. In [102] Shao has derived a series solution for a functionally graded circular hollow cylinder, using a multi-layered approach based on the laminated composite theory. The material properties are assumed to be temperature-independent and radial dependent, but are assumed to be homogenous in each layer. The temperature profile along the thickness is calculated by means of the heat conduction equations. A functionally graded circular hollow cylinder has also been analyzed by Liew et al. in [103]. In this case, the solutions are obtained through a novel limiting process that employs the solutions of homogeneous hollow circular cylinders. The temperature distribution is assumed in the radial direction. Vel and Baskiyar [104] have presented an analytical solution for a functionally graded tube with arbitrary variation of the material properties in the radial direction and subjected to steady thermomechanical loads. The heat conduction and thermoelasticity equations are solved using the power series method. In [105] Abrinia et al. have proposed an analytical method to compute the radial and circumferential stresses in a thick FGM cylindrical vessel under the influence of internal pressure and temperature. In this paper it is assumed that the modulus of elasticity and thermal coefficient of expansion vary through the thickness of the FGM material, according to a power law relationship. Shao and Wang [106] have performed a three-dimensional thermo-elastic analysis of a functionally graded cylindrical panel with finite length and subjected to non uniform mechanical and steady-state thermal loads. The thermal and mechanical properties are assumed to be temperature independent and continuously vary in the radial direction of the panel.

1.2.3 Modelling of CNTs

Two basic methods are used to simulate the mechanical behavior of nanostructures: atomistic-based modelling approaches and continuum approaches. In the former, the vibrational behavior of CNTs is investigated using an atomistic finite element model with beam elements and concentrated masses [107],[108]. But, the computational effort necessary for these methods does not permit simulations of real size multi-walled CNTs. For these reasons, continuum approaches are preferred to atomistic-based ones.

In literature, many researchers have used beam models to analyze the mechanical behavior of carbon nanotubes. Among these, Wang [109] and Aydogdu [110],[221] have studied the vibration problem in multi-walled carbon nanotubes (MWCNTs) via the Timoshenko beam model and the generalized shear deformation theory, respectively. In [112], Amin et al. have presented a double elastic beam model for frequency analysis in a double-walled carbon nanotube (DWNT) embedded in an elastic matrix. The analysis has been based on both Euler-Bernoulli and Timoshenko beam theories, considering intertube radial displacements. Chang and Lee have also employed the Timoshenko beam model, in [113], to study the vibration frequency of a fluid-conveying SWCNT. An assessment of the Timoshenko beam models has been accomplished by Zhang et al. in [114] in determining the vibration frequencies of SWCNTs.

However, it is also possible to analyze carbon nanotubes using shell models. In [115], Dong et al. have presented an analytical method to investigate wave propagation in MWNTs, using a laminated cylindrical shell model. Each of the concentric tubes of the MWNT was an individual elastic shell and is coupled to adjacent tubes through the van der Waals interaction. Foo has adopted the Donnell thin shell theory for the vibration analysis of SWCNTs [116]. Wang and Zhang [117] have also proposed a two-dimensional elastic shell model to characterize the deformation of single-walled carbon nanotubes and they have concluded that this model can be established with well-defined effective thickness. He et al. have developed an elastic multiple shell model for the vibration and buckling analysis of MWCNTs [118],[119], which accounts for the dependence of vdW interaction coefficients on the change of interlayer spacing and the radii of the tubes. Finally, in [120] a continuum elastic double-shell model, based on von Kàrmàn-Donnell-type non-linear differential equations, has been employed to study the buckling and post-buckling behavior of DWNTs subjected to torsional load. Each DWNT tube has been described as an individual elastic shell, which is subject to the van der Waals interaction between the inner and outer nanotubes.

Chapter 2

Refined and advanced shell models

Different refined and advanced shell/plate models are contained in the Carrera's Unified Formulation (CUF). The CUF permits to obtain, in a general and unified manner, several models that can differ by the chosen order of expansion in the thickness direction, by the equivalent single layer or layer wise approach and by the variational statement used. These models are here defined directly for the shells, according to different geometrical assumptions: plates are particular cases when the shell has infinite curvature radius. By considering the appropriate constitutive equations, the CUF can be applied to the analysis of the advanced materials described in the previous section. The refined theories are higher order theories based on the principle of virtual displacements and they can be extended to multifield problems by considering the modelling of temperature and electric potential. Advanced theories are theories based upon the Reissner's mixed variational theorem in which secondary variables, such as the transverse shear/normal stresses and the transverse normal electric displacement, are "a priori" modelled. A complete system of acronyms is introduced to characterize these two-dimensional theories.

2.1 Unified Formulation

The main feature of the Unified Formulation by Carrera [26] (CUF) is the unified manner in which the field variables are handled. If one considers a displacements formulation, the displacement field is written by means of approximating functions in the thickness direction as follows:

$$\delta \mathbf{u}^k(\xi^1, \xi^2, \xi^3) = F_\tau(\xi^3) \delta \mathbf{u}_\tau^k(\xi^1, \xi^2), \quad \mathbf{u}^k(\xi^1, \xi^2, \xi^3) = F_s(\xi^3) \mathbf{u}_s^k(\xi^1, \xi^2), \quad \tau, s = 0, 1, \dots, N, \quad (2.1)$$

where (ξ^1, ξ^2, ξ^3) is a curvilinear reference system, defined in the next section, and the displacement $\mathbf{u} = \{u, v, w\}$ is referred to such system. δ indicates the virtual variation and k identifies the layer. F_τ and F_s are the so-called thickness functions depending only on ξ^3 . \mathbf{u}_s are the unknown variables depending on the coordinates ξ^1 and ξ^2 . τ and s are sum indexes and N is the order of expansion in the thickness direction assumed for the displacements.

In the case of Equivalent Single Layer (ESL) models, a Taylor expansion is em-

ployed as thickness functions:

$$\mathbf{u} = F_0 \mathbf{u}_0 + F_1 \mathbf{u}_1 + \dots + F_N \mathbf{u}_N = F_s \mathbf{u}_s, \quad s = 0, 1, \dots, N, \quad (2.2)$$

$$F_0 = (\xi^3)^0 = 1, \quad F_1 = (\xi^3)^1 = \xi^3, \quad \dots, \quad F_N = (\xi^3)^N. \quad (2.3)$$

Classical theories, such as the First-order Shear Deformation Theory (FSDT), can be obtained from an ESL model with $N = 1$, by imposing a constant transverse displacement through the thickness via penalty techniques. The Classical Lamination Theory (CLT) can be also obtained from FSDT via an opportune penalty technique which imposes an infinite shear correction factor. It is important to remember that the ESL theories which have transverse displacement constant and transverse normal strain ε_{zz} equal to zero and the first order ESL theory, show Poisson's locking phenomena; this can be overcome via plane stress conditions in constitutive equations [121],[122].

In the case of Layer-Wise (LW) models, the displacement is defined at k -layer level:

$$\mathbf{u}^k = F_t \mathbf{u}_t^k + F_b \mathbf{u}_b^k + F_r \mathbf{u}_r^k = F_s \mathbf{u}_s^k, \quad s = t, b, r, \quad r = 2, \dots, N, \quad (2.4)$$

$$F_t = \frac{P_0 + P_1}{2}, \quad F_b = \frac{P_0 - P_1}{2}, \quad F_r = P_r - P_{r-2}. \quad (2.5)$$

in which $P_j = P_j(\zeta_k)$ is the Legendre polynomial of j -order defined in the ζ_k -domain: $-1 < \zeta_k < 1$. The top (t) and bottom (b) values of the displacements are used as unknown variables and one can impose the following compatibility conditions:

$$u_t^k = u_b^{k+1}, \quad k = 1, N_l - 1. \quad (2.6)$$

The LW models, in respect to the ESLs, allow the zig-zag form of the displacement distribution in layered structures to be modelled. It is possible to reproduce the zig-zag effects also in the framework of the ESL description by employing the Murakami theory. According to reference [123], a zig-zag term can be introduced into equation (2.7) as follows:

$$\mathbf{u}^k = F_0 \mathbf{u}_0^k + \dots + F_N \mathbf{u}_N^k + (-1)^k \zeta_k \mathbf{u}_Z^k. \quad (2.7)$$

Subscript Z refers to the introduced term. Such theories are called zig-zag (ZZ) theories.

2.2 Geometrical relations

We define a thin shell as a three-dimensional body bounded by two closely spaced curved surfaces, the distance between the two surfaces must be small in comparison with the other dimensions. The middle surface of the shell is the locus of points which lie midway between these surfaces. The distance between the surfaces measured along the normal to the middle surface is the thickness of the shell at that point [124]. Shells may be seen as generalizations of a flat plate [125]; conversely, a flat plate is a special

case of a shell having no curvature. In this section the fundamental equations of thin shell theory are presented in order to obtain the geometrical relations also for multifield problems. Geometrical relations for plates are seen as particular case of those for shells. The material is assumed to be linearly elastic and homogeneous, displacements are assumed to be small, thereby yielding linear equations; shear deformation and rotary inertia effects are neglected, and the thickness is taken to be small.

2.2.1 Strain-displacement relations

The shell can be considered as a solid medium geometrically defined by a midsurface, given by the coordinates ξ^1, ξ^2 , immersed in the physical space and a parameter representing the thickness ξ^3 of the medium around this surface. The geometrical relations for shells are derived by considering the linear part of the 3D Green-Lagrange strain tensor [126], that is expressed in the following formula:

$$\varepsilon'_{ij} = (\mathbf{g}_i \mathbf{u}_{,j} + \mathbf{g}_j \mathbf{u}_{,i}), \quad i, j = 1, 2, 3, \quad (2.8)$$

where comma indicates the partial derivative of the displacements in respect to the curvilinear coordinates (ξ^1, ξ^2, ξ^3) and \mathbf{g}_i are the 3D base vectors of the curvilinear reference system.

In order to calculate the derivatives of the displacements and the 3D base vectors, one needs to define the 3D chart Φ , that allows to express the cartesian coordinates (x, y, z) in function of the curvilinear coordinates:

$$\Phi(\xi^1, \xi^2, \xi^3) = \phi(\xi^1, \xi^2) + \xi^3 \mathbf{a}_3(\xi^1, \xi^2). \quad (2.9)$$

It is defined by means of the 2D chart ϕ and the unit vector \mathbf{a}_3 , that will be introduced below (see Fig.2.1). Starting from Φ , one can calculate the 3D *covariant basis* $(\mathbf{g}_1, \mathbf{g}_2, \mathbf{g}_3)$ as follows:

$$\mathbf{g}_m = \frac{\partial \Phi(\xi^1, \xi^2, \xi^3)}{\partial \xi^m} \quad m = 1, 2, 3, \quad (2.10)$$

that is a local basis and it is defined in each point of the shell volume. The 3D *contravariant basis* $(\mathbf{g}^1, \mathbf{g}^2, \mathbf{g}^3)$ can be inferred from the 3D covariant basis by the relations:

$$\mathbf{g}_m \cdot \mathbf{g}^n = \delta_m^n \quad m, n = 1, 2, 3, \quad (2.11)$$

where δ denotes the Kronecker symbol ($\delta_m^n = 1$ if $m = n$ and 0 otherwise).

The vectors \mathbf{a}_α and \mathbf{a}_3 , that form the covariant basis of the plane tangent to the midsurface at each point, are calculated from the 2D chart as follows:

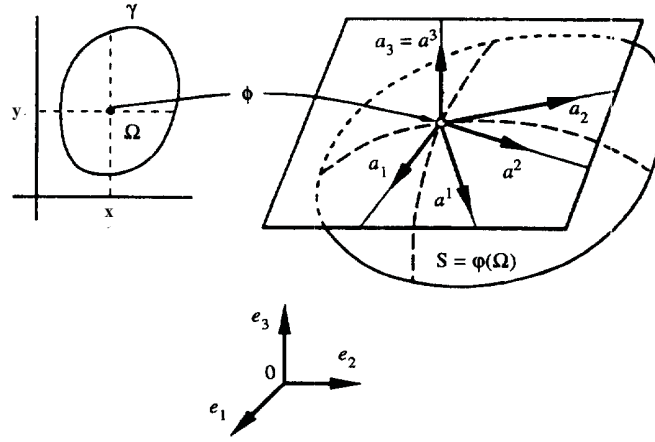


Figure 2.1: 2D chart.

$$\mathbf{a}_\alpha = \frac{\partial \phi(\xi^1, \xi^2)}{\partial \xi^\alpha} \quad \alpha, \beta = 1, 2, \quad \mathbf{a}_3 = \frac{\mathbf{a}_1 \wedge \mathbf{a}_2}{\|\mathbf{a}_1 \wedge \mathbf{a}_2\|}. \quad (2.12)$$

In a manner very similar to the 3D case, a contravariant basis of the tangent plane ($\mathbf{a}^1, \mathbf{a}^2$) can be defined by the relations:

$$\mathbf{a}_\alpha \cdot \mathbf{a}^\beta = \delta_\alpha^\beta \quad \alpha, \beta = 1, 2. \quad (2.13)$$

The 3D base vectors can be defined by means of the basis of the tangent plane, using the following relations:

$$\begin{aligned} \mathbf{g}_\alpha &= (\delta_\alpha^\lambda - \xi^3 b_\alpha^\lambda) \mathbf{a}_\lambda = \mu_\alpha^\lambda \mathbf{a}_\lambda \quad \alpha, \lambda = 1, 2, \\ \mathbf{g}_3 &= \mathbf{a}_3, \end{aligned} \quad (2.14)$$

where the tensor b_α^λ takes into account the curvature of the shell and it is:

$$b_\alpha^\lambda = \mathbf{a}_{,\alpha}^\lambda \cdot \mathbf{a}_3.$$

In the case of the contravariant basis, one has:

$$\mathbf{g}^\alpha = m_\lambda^\alpha \mathbf{a}^\lambda \quad \alpha, \lambda = 1, 2, \quad (2.15)$$

where m_λ^α is the inverse of the tensor μ_α^λ introduced in the previous relations (2.14):

$$m_\lambda^\alpha = (\mu^{-1})_\lambda^\alpha .$$

The derivatives of the displacements are calculated in the following way:

$$\frac{\partial \mathbf{u}}{\partial \xi^\alpha} = F_\tau \frac{\partial \mathbf{u}_\tau}{\partial \xi^\alpha} , \quad \alpha = 1, 2, 3 , \quad (2.16)$$

where:

$$\frac{\partial \mathbf{u}_\tau}{\partial \xi^\alpha} = \frac{\partial}{\partial \xi^\alpha} (u_{\tau\lambda} \mathbf{a}^\lambda + u_{\tau 3} \mathbf{a}^3) , \quad \lambda = 1, 2 , \quad (2.17)$$

and, for convenience reasons, it is here assumed that $(u, v, w) = (u_1, u_2, u_3)$. Then, one has:

$$\frac{\partial}{\partial \xi^\alpha} (u_{\tau\lambda} \mathbf{a}^\lambda) = u_{\tau\lambda|\alpha} \mathbf{a}^\lambda + b_\alpha^\lambda u_{\tau\lambda} \mathbf{a}_3 , \quad \alpha, \lambda = 1, 2 , \quad (2.18)$$

where $|$ indicates the covariant derivative, that is defined as follows:

$$u_{\tau\lambda|\alpha} = u_{\tau\lambda,\alpha} - \Gamma_{\lambda\alpha}^\gamma u_{\tau\gamma} , \quad \gamma = 1, 2 . \quad (2.19)$$

The $\Gamma_{\lambda\alpha}^\gamma$ is the surface *Christoffel symbol* and it reads:

$$\Gamma_{\lambda\alpha}^\gamma = \mathbf{a}_{\lambda,\alpha} \cdot \mathbf{a}^\gamma .$$

For more details about the mathematical definitions, one can refer to the book of Chapelle and Bathe [126].

Cylindrical geometry

If one considers the cylindrical geometry (see Fig.2.2), the 2D-chart is the following:

$$\{x, y, z\}^T = \phi(\xi^1, \xi^2) = \begin{bmatrix} \xi^1 \\ R \sin(\xi^2/R) \\ R \cos(\xi^2/R) \end{bmatrix} , \quad (2.20)$$

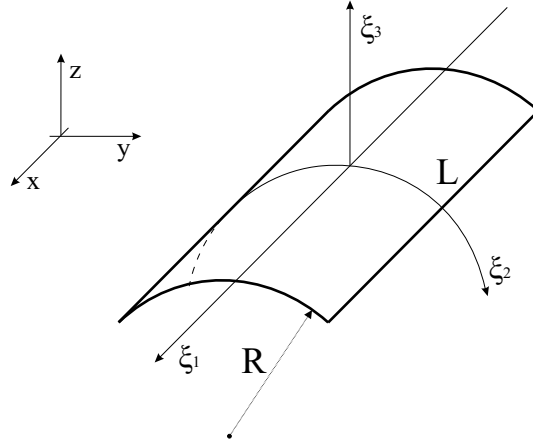


Figure 2.2: Cylindrical geometry.

where R is the curvature radius of the cylinder, as indicated in the Figure 1.1. Using the 2D chart, one can calculate the 3D base vectors (2.14) and the derivatives of the displacements (2.16), following the procedure explained in the previous section. Substituting in the 3D Green-Lagrange strain tensor (2.8), one obtains the following strain-displacement relations, valid for the cylinder:

$$\begin{aligned}
 \varepsilon'_{11} &= F_\tau u_{\tau,1}, \\
 \varepsilon'_{22} &= F_\tau \left[\left(1 + \frac{\xi^3}{R}\right) \frac{w_\tau}{R} + \left(1 + \frac{\xi^3}{R}\right) v_{\tau,2} \right], \\
 \varepsilon'_{12} &= F_\tau \left[u_{\tau,2} + \left(1 + \frac{\xi^3}{R}\right) v_{\tau,1} \right] = \varepsilon_{21}, \\
 \varepsilon'_{13} &= w_{\tau,1} F_\tau + u_\tau F_{\tau,3}, \\
 \varepsilon'_{23} &= F_\tau \left[w_{\tau,2} - \frac{v_\tau}{R} \right] + F_{\tau,3} \left[\left(1 + \frac{\xi^3}{R}\right) v_\tau \right], \\
 \varepsilon'_{33} &= w_\tau F_{\tau,3}.
 \end{aligned} \tag{2.21}$$

The geometrical relations in matrix form are:

$$\begin{aligned}
 \boldsymbol{\varepsilon}_p &= (\mathbf{D}_p + \mathbf{A}_p) \mathbf{u}, \\
 \boldsymbol{\varepsilon}_n &= (\mathbf{D}_{np} + \mathbf{D}_{nz} - \mathbf{A}_n) \mathbf{u},
 \end{aligned} \tag{2.22}$$

where (p) indicates the in-plane strain components $(\varepsilon'_{11}, \varepsilon'_{22}, \varepsilon'_{12})$ and (n) the transverse components $(\varepsilon'_{13}, \varepsilon'_{23}, \varepsilon'_{33})$. The differential operators used above are defined as follows:

$$\mathbf{D}_p = \begin{bmatrix} \partial_1 & 0 & 0 \\ 0 & H \partial_2 & 0 \\ \partial_2 & H \partial_1 & 0 \end{bmatrix}, \quad \mathbf{D}_{np} = \begin{bmatrix} 0 & 0 & \partial_1 \\ 0 & 0 & \partial_2 \\ 0 & 0 & 0 \end{bmatrix}, \quad \mathbf{D}_{nz} = \partial_3 \cdot \mathbf{A}_{nz} = \partial_3 \cdot \begin{bmatrix} 1 & 0 & 0 \\ 0 & H & 0 \\ 0 & 0 & 1 \end{bmatrix}, \tag{2.23}$$

$$\mathbf{A}_p = \begin{bmatrix} 0 & 0 & 0 \\ 0 & 0 & \frac{1}{R}H \\ 0 & 0 & 0 \end{bmatrix}, \quad \mathbf{A}_n = \begin{bmatrix} 0 & 0 & 0 \\ 0 & \frac{1}{R} & 0 \\ 0 & 0 & 0 \end{bmatrix}, \quad (2.24)$$

and $H = (1 + \frac{\xi^3}{R})$.

The strain components ε'_{ij} are expressed in the 3D contravariant basis $(\mathbf{g}^1, \mathbf{g}^2, \mathbf{g}^3)$. In order to derive the governing equations, it is necessary to refer all the quantities (displacements, strains and stresses) to the basis $(\mathbf{a}^1, \mathbf{a}^2, \mathbf{a}^3)$. Therefore, the strains ε'_{ij} must be transformed in ε_{ij} according to the following relations:

$$\begin{aligned} \varepsilon_{ij} &= m_i^\alpha m_j^\beta \varepsilon'_{\alpha\beta}, \\ \varepsilon_{\alpha 3} &= m_\alpha^\beta \varepsilon'_{\beta 3}, \quad i, j, \alpha, \beta = 1, 2, \\ \varepsilon_{33} &= \varepsilon'_{33}, \end{aligned} \quad (2.25)$$

where \mathbf{m} is the tensor introduced in Eq.(2.15) and, in the case of cylindrical geometry, its components are:

$$m_1^1 = 1, \quad m_2^1 = m_1^2 = 0, \quad m_2^2 = (1 + \frac{\xi^3}{R})^{-1} = H^{-1} \quad (2.26)$$

In this case, the matrixes of differential operators in Eqs.(2.22) are:

$$\mathbf{D}_p = \begin{bmatrix} \partial_1 & 0 & 0 \\ 0 & \frac{\partial_2}{H} & 0 \\ \frac{\partial_2}{H} & \partial_1 & 0 \end{bmatrix}, \quad \mathbf{D}_{np} = \begin{bmatrix} 0 & 0 & \partial_1 \\ 0 & 0 & \frac{\partial_2}{H} \\ 0 & 0 & 0 \end{bmatrix}, \quad \mathbf{D}_{nz} = \partial_3 \cdot \mathbf{A}_{nz} = \partial_3 \cdot \begin{bmatrix} 1 & 0 & 0 \\ 0 & 1 & 0 \\ 0 & 0 & 1 \end{bmatrix}, \quad (2.27)$$

$$\mathbf{A}_p = \begin{bmatrix} 0 & 0 & 0 \\ 0 & 0 & \frac{1}{HR} \\ 0 & 0 & 0 \end{bmatrix}, \quad \mathbf{A}_n = \begin{bmatrix} 0 & 0 & 0 \\ 0 & \frac{1}{HR} & 0 \\ 0 & 0 & 0 \end{bmatrix}, \quad (2.28)$$

If the shell is very thin, the basis $(\mathbf{g}^1, \mathbf{g}^2, \mathbf{g}^3)$ can be considered coincident with $(\mathbf{a}^1, \mathbf{a}^2, \mathbf{a}^3)$ and this transformation can be neglected $\varepsilon'_{ij} = \varepsilon_{ij}$. From this point on, $\varepsilon_p/\varepsilon_n$ can be contain ε'_{ij} or ε_{ij} . When it is necessary, it will be specified which strain components are considered.

The geometrical relations (2.22) are valid for the plate when the radius of curvature R is infinite.

In the study of multilayered structures, these relations are referred to the midsurface of each layer if the model used is layer-wise, while they are referred to the midsurface of the global laminate if the model is equivalent single layer. For more details about the geometrical relations for the cylindrical geometry, written according to the CUF, one can refer to [127].

Double-curvature geometry

According to [124], the geometrical relations for a shell with double curvature are derived in this paragraph. The passages are similar to those in the previous section but they are here omitted for the sake of brevity. By considering a shell with constant radii of curvature (Fig.2.3) and renaming the curvilinear reference system as (α, β, z) , the geometrical relations can be written in matrix form as in Eq.(2.22):

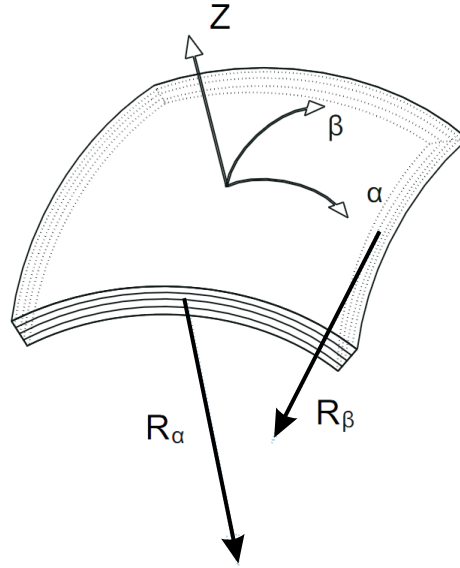


Figure 2.3: Double-curvature geometry.

$$\begin{aligned}\boldsymbol{\varepsilon}_p &= [\varepsilon_{\alpha\alpha}, \varepsilon_{\beta\beta}, \varepsilon_{\alpha\beta}] = (\mathbf{D}_p + \mathbf{A}_p)\mathbf{u}, \\ \boldsymbol{\varepsilon}_n &= [\varepsilon_{\alpha z}, \varepsilon_{\beta z}, \varepsilon_{zz}] = (\mathbf{D}_{np} + \mathbf{D}_{nz} - \mathbf{A}_n)\mathbf{u},\end{aligned}\tag{2.29}$$

where the differential operators are:

$$\mathbf{D}_p = \begin{bmatrix} \frac{\partial_\alpha}{H_\alpha} & 0 & 0 \\ 0 & \frac{\partial_\beta}{H_\beta} & 0 \\ \frac{\partial_\beta}{H_\beta} & \frac{\partial_\alpha}{H_\alpha} & 0 \end{bmatrix}, \quad \mathbf{D}_{np} = \begin{bmatrix} 0 & 0 & \frac{\partial_\alpha}{H_\alpha} \\ 0 & 0 & \frac{\partial_\beta}{H_\beta} \\ 0 & 0 & 0 \end{bmatrix}, \quad \mathbf{D}_{nz} = \begin{bmatrix} \partial_z & 0 & 0 \\ 0 & \partial_z & 0 \\ 0 & 0 & \partial_z \end{bmatrix},\tag{2.30}$$

$$\mathbf{A}_p = \begin{bmatrix} 0 & 0 & \frac{1}{H_\alpha R_\alpha} \\ 0 & 0 & \frac{1}{H_\beta R_\beta} \\ 0 & 0 & 0 \end{bmatrix}, \quad \mathbf{A}_n = \begin{bmatrix} \frac{1}{H_\alpha R_\alpha} & 0 & 0 \\ 0 & \frac{1}{H_\beta R_\beta} & 0 \\ 0 & 0 & 0 \end{bmatrix}.\tag{2.31}$$

In these arrays, the metric coefficients are:

$$H_\alpha = (1 + z/R_\alpha), \quad H_\beta = (1 + z/R_\beta), \quad H_z = 1.\tag{2.32}$$

where R_α and R_β are the principal radii of curvature along the coordinates α and β , respectively. The square of an infinitesimal linear segment in the layer, the associated infinitesimal area and the volume are given by:

$$\begin{aligned} ds^2 &= H_\alpha^2 d\alpha^2 + H_\beta^2 d\beta^2 + H_z^2 dz^2, \\ d\Omega &= H_\alpha H_\beta d\alpha d\beta, \\ dV &= H_\alpha H_\beta H_z d\alpha d\beta dz. \end{aligned} \quad (2.33)$$

The geometrical relations (2.29) are valid for the cylinder when one radius of curvature is infinite (one can check by assuming $R_\alpha \rightarrow \infty$ and comparing with ε_{ij} in the previous paragraph).

In the study of multilayered structures, these relations are referred to the midsurface of each layer if the model used is layer-wise, while they are referred to the midsurface of the global laminate if the model is equivalent single layer. For more details about the geometrical relations for double-curvature geometry, written according to the CUF, one can refer to [128].

2.2.2 Multifield geometrical relations

In [97], the geometrical relations that link the electrical field \mathcal{E} with the electric potential Φ , are also given:

$$\begin{aligned} \mathcal{E}_p &= [\mathcal{E}_\alpha, \mathcal{E}_\beta]^T = -\mathbf{D}_{ep} \Phi, \\ \mathcal{E}_n &= [\mathcal{E}_z]^T = -\mathbf{D}_{en} \Phi, \end{aligned} \quad (2.34)$$

where the meaning of arrays is:

$$\mathbf{D}_{ep} = \begin{bmatrix} \frac{\partial_\alpha}{H_\alpha} \\ \frac{\partial_\beta}{H_\beta} \end{bmatrix}, \quad \mathbf{D}_{en} = [\partial_z].$$

In analogy with equations 2.35, it is possible to define geometrical relations between the temperature θ and its spatial gradient ϑ :

$$\begin{aligned} \vartheta_p &= [\vartheta_\alpha, \vartheta_\beta]^T = -\mathbf{D}_{ep} \theta, \\ \vartheta_n &= [\vartheta_z]^T = -\mathbf{D}_{en} \theta. \end{aligned} \quad (2.35)$$

2.3 Constitutive equations

Constitutive equations characterize the individual material and its reaction to applied loads. According to Reddy [2], generalized Hooke's law is considered for mechanical case by employing a linear constitutive model for infinitesimal deformations. These equations are obtained in material coordinates and then modified in a general reference

system depending by the problem. In the case of shell geometry, such equations are referred to the basis (a^1, a^2, a^3) . The plane stress conditions are shortly discussed in order to avoid the Poisson's locking phenomena. The constitutive equations for the thermo-mechanical and electro-mechanical case are obtained by using the Gibbs free energy. The constitutive equations are also extended to functionally graded materials by considering the coefficients involved depending on the thickness coordinate.

2.3.1 Composite materials

When the elastic coefficients at a point have the same value for every pair of coordinate systems which are the mirror images of each other with respect to a plane, the material is called *monoclinic*. In this general case, the constitutive equations that link the stresses to the strains are written as follows:

$$\begin{aligned}\sigma_p &= C_{pp}\epsilon_p + C_{pn}\epsilon_n, \\ \sigma_n &= C_{np}\epsilon_p + C_{nn}\epsilon_n,\end{aligned}\tag{2.36}$$

with:

$$\begin{aligned}C_{pp} &= \begin{bmatrix} C_{11} & C_{12} & C_{16} \\ C_{12} & C_{22} & C_{26} \\ C_{16} & C_{26} & C_{66} \end{bmatrix}, & C_{pn} &= \begin{bmatrix} 0 & 0 & C_{13} \\ 0 & 0 & C_{23} \\ 0 & 0 & C_{36} \end{bmatrix}, \\ C_{np} &= \begin{bmatrix} 0 & 0 & 0 \\ 0 & 0 & 0 \\ C_{13} & C_{23} & C_{36} \end{bmatrix}, & C_{nn} &= \begin{bmatrix} C_{55} & C_{45} & 0 \\ C_{45} & C_{44} & 0 \\ 0 & 0 & C_{33} \end{bmatrix},\end{aligned}\tag{2.37}$$

where the independent material parameters C_{ij} are 13.

If one considers an *orthotropic* material, there are three mutually orthogonal planes of symmetry, so the number of independent elastic coefficients is reduced from 13 to 9:

$$C_{16} = C_{26} = C_{36} = C_{45} = 0.$$

Most often, the material properties are determined in a laboratory in terms of the engineering constants such as Young's modulus, shear modulus and Poisson's ratios. The 9 independent material coefficients in Eq.(2.37) can be expressed by 9 independent material engineering constants:

$$E_1, E_2, E_3, G_{23}, G_{13}, G_{12}, \nu_{12}, \nu_{13}, \nu_{23},$$

the relations between material coefficients and engineering constants are:

$$\begin{aligned}
 C_{11} &= \frac{1 - \nu_{23}\nu_{23}}{E_2 E_3 \Delta}, \quad C_{12} = \frac{\nu_{21} + \nu_{31}\nu_{23}}{E_2 E_3 \Delta} = \frac{\nu_{12} + \nu_{32}\nu_{13}}{E_1 E_3 \Delta}, \\
 C_{13} &= \frac{\nu_{31} + \nu_{21}\nu_{32}}{E_2 E_3 \Delta} = \frac{\nu_{13} + \nu_{12}\nu_{23}}{E_1 E_2 \Delta}, \\
 C_{22} &= \frac{1 - \nu_{13}\nu_{31}}{E_1 E_3 \Delta}, \quad C_{23} = \frac{\nu_{32} + \nu_{12}\nu_{31}}{E_1 E_3 \Delta} = \frac{\nu_{23} + \nu_{21}\nu_{13}}{E_1 E_3 \Delta}, \\
 C_{33} &= \frac{1 - \nu_{13}\nu_{31}}{E_1 E_3 \Delta}, \quad C_{44} = G_{23}, \quad C_{55} = G_{31}, \quad C_{66} = G_{12}, \\
 \Delta &= \frac{1 - \nu_{12}\nu_{21} - \nu_{23}\nu_{32} - \nu_{31}\nu_{13} - 2\nu_{21}\nu_{32}\nu_{13}}{E_1 E_2 E_3}.
 \end{aligned} \tag{2.38}$$

For the Poisson's ratio is valid the following relation:

$$\frac{\nu_{ij}}{E_i} = \frac{\nu_{ji}}{E_j} \quad (\text{no sum on } i, j). \tag{2.39}$$

When there exist no preferred directions in the material, infinite number of planes of material symmetry are considered. Such materials are called *isotropic* and the number of independent elastic coefficients are reduced from 9 to 2:

$$E_1 = E_2 = E_3 = E, \quad G_{23} = G_{13} = G_{12} = G, \quad \nu_{12} = \nu_{13} = \nu_{23} = \nu.$$

The constitutive relations for an orthotropic material are written in terms of stress and strain components referred to the principal material coordinate system (x_1, x_2, x_3) . In composite laminates each orthotropic layer has a different orientation with respect to the global laminate system, called problem coordinate system (x, y, z) . In Figure 2.4 the material coordinate system and the problem coordinate system are clearly indicated for a layer embedded in a laminate. The angle ϕ between the in-plane material coordinates x_1, x_2 and the problem coordinates x, y is considered counterclockwise. The third coordinates coincide ($x_3 = z$). The relations between the two reference systems are:

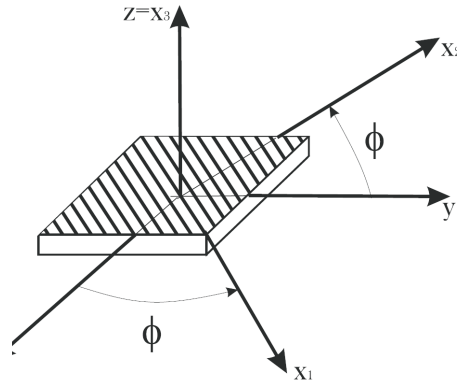


Figure 2.4: Material coordinate system and problem coordinate system.

$$\begin{Bmatrix} x_1 \\ x_2 \\ x_3 \end{Bmatrix} = \begin{bmatrix} \cos \phi & \sin \phi & 0 \\ -\sin \phi & \cos \phi & 0 \\ 0 & 0 & 1 \end{bmatrix} \begin{Bmatrix} x \\ y \\ z \end{Bmatrix}. \quad (2.40)$$

Applying this rotation to the stress tensor σ_{ij} and rearranging in terms of a single-column stress array, one obtains:

$$\begin{Bmatrix} \sigma_{xx} \\ \sigma_{yy} \\ \sigma_{zz} \\ \sigma_{yz} \\ \sigma_{xz} \\ \sigma_{xy} \end{Bmatrix} = \begin{bmatrix} \cos^2 \phi & \sin^2 \phi & 0 & 0 & 0 & -\sin 2\phi \\ \sin^2 \phi & \cos^2 \phi & 0 & 0 & 0 & \sin 2\phi \\ 0 & 0 & 1 & 0 & 0 & 0 \\ 0 & 0 & 0 & \cos \phi & \sin \phi & 0 \\ 0 & 0 & 0 & -\sin \phi & \cos \phi & 0 \\ \sin \phi \cos \phi & \sin \phi \cos \phi & 0 & 0 & 0 & \cos^2 \phi - \sin^2 \phi \end{bmatrix} \begin{Bmatrix} \sigma_{11} \\ \sigma_{22} \\ \sigma_{33} \\ \sigma_{23} \\ \sigma_{13} \\ \sigma_{12} \end{Bmatrix}. \quad (2.41)$$

The equations (2.41) can be expressed in compact form as:

$$\{\sigma\}_p = [T]\{\sigma\}_m, \quad (2.42)$$

where p indicates quantities related to the problem reference system and m to the material reference system.

The same procedure can be applied for the transformation of strain components, therefore one has:

$$\{\varepsilon\}_m = [T]^T \{\varepsilon\}_p. \quad (2.43)$$

The only remaining quantities that need to be transformed from material coordinate system to the problem coordinates are the material parameters C_{ij} . These can be easily obtained considering the Eqs.(2.42) and (2.43):

$$\{\sigma\}_p = [T]\{\sigma\}_m = \{\sigma\}_p = [T][C]_m\{\varepsilon\}_m = [T][C]_m[T]^T\{\varepsilon\}_p = [C]_p\{\varepsilon\}_p. \quad (2.44)$$

$[C]_p$ is the material stiffness matrix in the problem coordinates and it can be rearranged as in Eqs. (2.37).

The *thickness locking* (TL) mechanism, also known as Poisson's locking phenomena, affects the plate/shell analysis [121],[122]. The TL doesn't permit to an equivalent single layer theory with transverse displacement w constant or linear through the thickness (that means transverse strain ε_{zz} zero or constant) to lead to the 3D solution in thin plate/shell problems. A known technique to contrast TL consists in modifying the elastic stiffness coefficients by forcing the 'contradictory' condition of transverse normal stress equal to zero:

$$\sigma_{zz} = 0.$$

By imposing this condition in the constitutive equations (2.36), the modified stiffness coefficients in material reference system (reduced stiffness coefficients) can be obtained:

$$\tilde{C}_{11} = \frac{E_1}{1 - \nu_{12}\nu_{21}}, \quad \tilde{C}_{22} = \frac{E_2}{1 - \nu_{12}\nu_{21}}, \quad \tilde{C}_{12} = \frac{\nu_{12}E_2}{1 - \nu_{12}\nu_{21}}. \quad (2.45)$$

In order to avoid the TL, these coefficients must be used in $[C]_m$ in the place of C_{11}, C_{22}, C_{12} and then rotated according to Eq.(2.44).

2.3.2 Multifield problems

Constitutive equations for the electro-thermo-mechanical problem can be obtained according to [129] and [130]. The coupling between the mechanical, thermal and electrical fields can be determined by using the thermodynamical principles and Maxwell's relations [131]. For this aim, it is necessary to define a Gibbs free energy [132]. For more details about the mathematical passages, one can refer to [129] and [130]. In this work, three particular cases are discussed: pure mechanical problem (seen in the previous section); thermo-mechanical problem; electro-mechanical problem.

In the case of *thermo-mechanical* problems, electrical loads are not applied on the structure. The coupling between the mechanical and electrical fields, and between the thermal and electrical fields are not considered. The constitutive equations are:

$$\begin{aligned}\sigma_p &= C_{pp}\varepsilon_p + C_{pn}\varepsilon_n - \lambda_p\theta, \\ \sigma_n &= C_{np}\varepsilon_p + C_{nn}\varepsilon_n - \lambda_n\theta, \\ h_p &= \kappa_{pp}\vartheta_p + \kappa_{pn}\vartheta_n, \\ h_n &= \kappa_{np}\vartheta_p + \kappa_{nn}\vartheta_n,\end{aligned}\tag{2.46}$$

where the variation of entropy is not considered because, in this work, the temperature is imposed on the structure surfaces. While, the information about the heat flux h are fundamental to understand how the temperature profile evolves along the thickness of the structure.

The matrixes introduced are:

- Heat flux:

$$h_p = \begin{Bmatrix} h_\alpha \\ h_\beta \end{Bmatrix}, \quad h_n = \{h_z\} .\tag{2.47}$$

- Thermo-mechanical coupling coefficients:

$$\lambda_p = \begin{bmatrix} \lambda_1 \\ \lambda_2 \\ \lambda_6 \end{bmatrix}, \quad \lambda_n = \begin{bmatrix} 0 \\ 0 \\ \lambda_3 \end{bmatrix} .\tag{2.48}$$

- Conductivity coefficients:

$$\begin{aligned}\kappa_{pp} &= \begin{bmatrix} \kappa_{11} & \kappa_{12} \\ \kappa_{12} & \kappa_{22} \end{bmatrix}, \quad \kappa_{pn} = \begin{bmatrix} 0 \\ 0 \end{bmatrix}, \\ \kappa_{np} &= \begin{bmatrix} 0 & 0 \end{bmatrix}, \quad \kappa_{nn} = [\kappa_{33}] .\end{aligned}\tag{2.49}$$

In the case of *electro-mechanical* problem, two physical fields interact, no thermal loads and spatial temperature gradients are applied on the structure. The couplings between

mechanical and thermal fields, and between electrical and thermal fields are not considered. In this case, the constitutive equations are:

$$\begin{aligned}\sigma_p &= C_{pp}\epsilon_p + C_{pn}\epsilon_n - e_{pp}^T \mathcal{E}_p - e_{pn}^T \mathcal{E}_n, \\ \sigma_n &= C_{np}\epsilon_p + C_{nn}\epsilon_n - e_{np}^T \mathcal{E}_p - e_{nn}^T \mathcal{E}_n, \\ \mathcal{D}_p &= e_{pp}\epsilon_p + e_{pn}\epsilon_n + \epsilon_{pp}\mathcal{E}_p + \epsilon_{pn}\mathcal{E}_n, \\ \mathcal{D}_n &= e_{np}\epsilon_p + e_{nn}\epsilon_n + \epsilon_{np}\mathcal{E}_p + \epsilon_{nn}\mathcal{E}_n.\end{aligned}\tag{2.50}$$

The matrixes introduced are:

- Electrical displacement:

$$\mathcal{D}_p = \left\{ \begin{matrix} \mathcal{D}_\alpha \\ \mathcal{D}_\beta \end{matrix} \right\}, \quad \mathcal{D}_n = \{ \mathcal{D}_z \} .\tag{2.51}$$

- Piezoelectric coefficients:

$$\begin{aligned}e_{pp} &= \begin{bmatrix} 0 & 0 & 0 \\ 0 & 0 & 0 \end{bmatrix}, \quad e_{pn} = \begin{bmatrix} e_{15} & e_{14} & 0 \\ e_{25} & e_{24} & 0 \end{bmatrix}, \\ e_{np} &= [e_{31} \quad e_{32} \quad e_{36}], \quad e_{nn} = [0 \quad 0 \quad e_{33}].\end{aligned}\tag{2.52}$$

- Permittivity coefficients:

$$\begin{aligned}\epsilon_{pp} &= \begin{bmatrix} \epsilon_{11} & \epsilon_{12} \\ \epsilon_{12} & \epsilon_{22} \end{bmatrix}, \quad \epsilon_{pn} = \begin{bmatrix} 0 \\ 0 \end{bmatrix}, \\ \epsilon_{np} &= [0 \quad 0], \quad \epsilon_{nn} = [\epsilon_{33}].\end{aligned}\tag{2.53}$$

The meaning of these constitutive equations are clarified in next sections, where the opportune variational statements and governing equations are discussed.

2.3.3 Functionally graded materials

In the case of Functionally Graded Materials (FGMs), the properties change with continuity along a particular direction of plate/shell, usually along the thickness. The matrices of elastic coefficients, piezoelectric coefficients, thermo-mechanical coupling coefficients and conductivity coefficients are general continuous functions of the thickness coordinate z (or ξ^3).

It is possible to describe the variation in z of the material properties via particular thickness functions that are a combination of Legendre polynomials (Eqs.(2.5)), that is:

$$\begin{aligned}C(z) &= F_b(z)C_b + F_\gamma(z)C_\gamma + F_t(z)C_t, \\ \lambda(z) &= F_b(z)\lambda_b + F_\gamma(z)\lambda_\gamma + F_t(z)\lambda_t, \\ \kappa(z) &= F_b(z)\kappa_b + F_\gamma(z)\kappa_\gamma + F_t(z)\kappa_t, \\ e(z) &= F_b(z)e_b + F_\gamma(z)e_\gamma + F_t(z)e_t, \\ \epsilon(z) &= F_b(z)\epsilon_b + F_\gamma(z)\epsilon_\gamma + F_t(z)\epsilon_t.\end{aligned}\tag{2.54}$$

t and b are the top and bottom values. γ denotes the higher order terms of the expansion and it goes from 2 to 10, that is enough to guarantee a good approximation of the FGMs properties. The constants $C_b, C_\gamma, C_t, \lambda_b, \dots$ and so on, can be calculated knowing the value of the related property in 10 different locations along the thickness. For more details, one can refer to [133] and [134].

Alternatively, one can directly integrate the material properties as general function of z . Since the thickness functions F_τ, F_s are arbitrary, the integrals in the thickness direction are numerically calculated in this work. For this reason, any function of the material properties can be integrated.

2.4 Variational statements

The variational statements considered in this work are the Principle of Virtual Displacements (PVD) and the Reissner's Mixed Variational Theorem (RMVT). The PVD extended to thermo-electro-mechanical problems is easily obtained by considering the thermal, electrical and mechanical internal works and the opportune constitutive equations. In this way, the use of Carrera's Unified Formulation (CUF) permits to obtain several refined two-dimensional models. Particular cases of the PVD are simply obtained by discarding thermal, electrical or mechanical internal works. The extension of the RMVT to multifield problems is obtained by rearranging the constitutive equations seen in the previous section and using opportune Lagrange multipliers in the variational statement. Such two-dimensional models, obtained via the RMVT, are called advanced models.

2.4.1 Principle of Virtual Displacements

The Principle of Virtual Displacements in the general case of a thermo-electro-elastic problem can be derived from the Hamilton's principle as indicated in [129] and [130]. Omitting the mathematical passages and neglecting the terms that are not involved in our problems, the final form of the PVD is the following:

$$\int_V (\delta \epsilon_{pG}^T \sigma_{pC} + \delta \epsilon_{nG}^T \sigma_{nC} - \delta \mathcal{E}_{pG}^T \mathcal{D}_{pC} - \delta \mathcal{E}_{nG}^T \mathcal{D}_{nC} - \delta \vartheta_{pG}^T \mathbf{h}_{pC} - \delta \vartheta_{nG}^T \mathbf{h}_{nC}) dV = \delta L_e - \delta L_{in} . \quad (2.55)$$

V is the volume of the structure. Subscripts C and G suggest the substitution of constitutive and geometrical relations, respectively. T means the transpose of a vector and δ the virtual variation.

δL_e is the virtual variation of the work done by the external loads, that are mechanical \mathbf{p}_u , thermal \mathbf{p}_θ and electrical \mathbf{p}_Φ . The explicit expression of the external work is:

$$\delta L_e = \int_V (\delta \mathbf{u} \mathbf{p}_u + \delta \theta \mathbf{p}_\theta + \delta \Phi \mathbf{p}_\Phi) dV , \quad (2.56)$$

while the expression of the inertial work δL_{in} is:

$$\delta L_{in} = \int_V \delta \mathbf{u} \rho \ddot{\mathbf{u}} dV , \quad (2.57)$$

where ρ is the density of the material and double dots indicate the second temporal derivative.

In the case of pure mechanical problems, the PVD has only the displacement u as primary variable and is simplified by discarding the internal thermal and electrical works:

$$\int_V (\delta \boldsymbol{\varepsilon}_{pG}^T \boldsymbol{\sigma}_{pC} + \delta \boldsymbol{\varepsilon}_{nG}^T \boldsymbol{\sigma}_{nC}) dV = \delta L_e - \delta L_{in} . \quad (2.58)$$

In the case of thermo-mechanical problems, two approaches can be considered. If the temperature is seen as an external load, it produces thermal stresses according to the constitutive equations (2.46), but there is no heat flux produced by the mechanical strains. In this case, the PVD used is in the form of Eq.(2.58). If the coupling between the thermal and mechanical fields is accounted, the PVD becomes the following:

$$\int_V (\delta \boldsymbol{\varepsilon}_{pG}^T \boldsymbol{\sigma}_{pC} + \delta \boldsymbol{\varepsilon}_{nG}^T \boldsymbol{\sigma}_{nC} - \delta \boldsymbol{\vartheta}_{pG}^T \mathbf{h}_{pC} - \delta \boldsymbol{\vartheta}_{nG}^T \mathbf{h}_{nC}) dV = \delta L_e - \delta L_{in} . \quad (2.59)$$

In this work, only the first approach is considered.

In the case of electro-mechanical coupling, for example the use of piezoelectric materials and/or the application of an electrical load, the relative PVD can be simply obtained by discarding the internal thermal work:

$$\int_V (\delta \boldsymbol{\varepsilon}_{pG}^T \boldsymbol{\sigma}_{pC} + \delta \boldsymbol{\varepsilon}_{nG}^T \boldsymbol{\sigma}_{nC} - \delta \boldsymbol{\varepsilon}_{pG}^T \mathbf{D}_{pC} - \delta \boldsymbol{\varepsilon}_{nG}^T \mathbf{D}_{nC}) dV = \delta L_e - \delta L_{in} . \quad (2.60)$$

For more details about this topic, one can refer to [128] and [129].

2.4.2 Reissner's Mixed Variational Theorem

The Reissner's Mixed Variational Theorem (RMVT) [63] permits to assume two independent sets of variables: a set of primary unknowns as the PVD case, and a set of extensive variables which are modelled a priori in the thickness direction. The main advantage of using the RMVT is a priori and complete fulfillment of the C_z^0 -requirements for the modelled extensive variables [81]. In this work, the RMVT is used only for the analysis of pure-mechanical and electromechanical problems. Therefore, the thermal terms seen in the PVD will be discarded in the following equations.

It is possible to obtain different extensions of RMVT by adding a Lagrange's multiplier in the PVD for each extensive variable considered (transverse stresses, normal electric displacement and so on). When a new Lagrange's multiplier is added [63], the constitutive equations must be rearranged in order to explicit the modelled variables. For this reason, each proposed extension of RMVT cannot be seen as a particular case of the other two. The extensive variables are modelled by means of the Unified Formulation (2.1). The approach in this case is always layer wise, independently on the modelling of the displacements (ESL or LW), because it permits to directly satisfy the interlaminar continuity conditions.

The first extension of RMVT, that can be considered, is the a-priori modelling of the transverse stresses $\boldsymbol{\sigma}_{nM}$ (the new subscript M is introduced to remark that the

transverse stresses are now modelled and not obtained via constitutive equations). The added Lagrange's multiplier is $\delta\sigma_{nM}^T(\epsilon_{nG} - \epsilon_{nC})$. The condition to add this multiplier is that the transverse strains ϵ_n calculated by means of geometrical relations (G) and by using the constitutive equations (C) must be the same or almost the same. In this way the balance of the internal work does not change or remains almost the same. In the case of pure mechanical problems, the RMVT reads:

$$\int_V (\delta\epsilon_{pG}^T \sigma_{pC} + \delta\epsilon_{nG}^T \sigma_{nM} + \delta\sigma_{nM}^T (\epsilon_{nG} - \epsilon_{nC})) dV = \delta L_e - \delta L_{in} . \quad (2.61)$$

The relative constitutive equations are obtained from Eqs.(2.36) considering the transverse stresses σ_{nM} as modelled and the transverse strains ϵ_{nC} as obtained from constitutive equations:

$$\begin{aligned} \sigma_p &= \hat{C}_{pp} \epsilon_p + \hat{C}_{pn} \sigma_n , \\ \epsilon_n &= \hat{C}_{np} \epsilon_p + \hat{C}_{nn} \sigma_n . \end{aligned} \quad (2.62)$$

The material coefficients are rearranged in the matrixes \hat{C}_{pp} , \hat{C}_{pn} , \hat{C}_{np} , \hat{C}_{nn} in order to express ϵ_n in function of σ_n . If one considers also the contribution of the electrical field, the RMVT becomes:

$$\int_V (\delta\epsilon_{pG}^T \sigma_{pC} + \delta\epsilon_{nG}^T \sigma_{nM} + \delta\sigma_{nM}^T (\epsilon_{nG} - \epsilon_{nC}) - \delta\mathcal{E}_{pG}^T \mathcal{D}_{pC} - \delta\mathcal{E}_{nG}^T \mathcal{D}_{nC}) dV = \delta L_e - \delta L_{in} , \quad (2.63)$$

and the constitutive equations (2.50) are modified as follows:

$$\begin{aligned} \sigma_p &= \hat{C}_{pp} \epsilon_p + \hat{C}_{pn} \sigma_n + \hat{e}_{pp}^T \mathcal{E}_p + \hat{e}_{pn}^T \mathcal{E}_n , \\ \epsilon_n &= \hat{C}_{np} \epsilon_p + \hat{C}_{nn} \sigma_n + \hat{e}_{np}^T \mathcal{E}_p + \hat{e}_{nn}^T \mathcal{E}_n , \\ \mathcal{D}_p &= \hat{e}_{pp} \epsilon_p + \hat{e}_{pn} \sigma_n + \hat{\epsilon}_{pp} \mathcal{E}_p + \hat{\epsilon}_{pn} \mathcal{E}_n , \\ \mathcal{D}_n &= \hat{e}_{np} \epsilon_p + \hat{e}_{nn} \sigma_n + \hat{\epsilon}_{np} \mathcal{E}_p + \hat{\epsilon}_{nn} \mathcal{E}_n . \end{aligned} \quad (2.64)$$

All the material coefficients, also the electrical ones, are recalculated.

In the analysis of electro-mechanical problems, other transverse variables can be modelled a priori, such as the transverse normal electric displacement \mathcal{D}_z . So other two extensions of the RMVT are possible: - introduction of a new Lagrange's multiplier for the modelling of the transverse normal electric displacement; - introduction of two Lagrange's multipliers for both transverse stresses and transverse normal electric displacement. The first one cannot be considered a particular case of the second one because the constitutive equations change.

In the first case, the variational statement is:

$$\int_V (\delta\epsilon_{pG}^T \sigma_{pC} + \delta\epsilon_{nG}^T \sigma_{nC} - \delta\mathcal{E}_{pG}^T \mathcal{D}_{pC} - \delta\mathcal{E}_{nG}^T \mathcal{D}_{nM} - \delta\mathcal{D}_{nM}^T (\mathcal{E}_{nG} - \mathcal{E}_{nC})) dV = \delta L_e - \delta L_{in} , \quad (2.65)$$

the Lagrange's multiplier $\delta \mathcal{D}_{nM}^T(\boldsymbol{\varepsilon}_{nG} - \boldsymbol{\varepsilon}_{nC})$ has been added. The constitutive equations are re-written in function of \mathcal{D}_n :

$$\begin{aligned}\sigma_p &= \hat{C}_{pp}\varepsilon_p + \hat{C}_{pn}\varepsilon_n + \hat{e}_{pp}^T \mathcal{E}_p + \hat{e}_{pn}^T \mathcal{D}_n, \\ \sigma_n &= \hat{C}_{np}\varepsilon_p + \hat{C}_{nn}\varepsilon_n + \hat{e}_{np}^T \mathcal{E}_p + \hat{e}_{nn}^T \mathcal{D}_n, \\ \mathcal{D}_p &= \hat{e}_{pp}\varepsilon_p + \hat{e}_{pn}\varepsilon_n + \hat{\epsilon}_{pp}\mathcal{E}_p + \hat{\epsilon}_{pn}\mathcal{D}_n, \\ \mathcal{E}_n &= \hat{e}_{np}\varepsilon_p + \hat{e}_{nn}\varepsilon_n + \hat{\epsilon}_{np}\mathcal{E}_p + \hat{\epsilon}_{nn}\mathcal{D}_n.\end{aligned}\tag{2.66}$$

In the second case, both the Lagrange's multipliers seen above are added:

$$\begin{aligned}\int_V (\delta \varepsilon_{pG}^T \sigma_{pC} + \delta \varepsilon_{nG}^T \sigma_{nM} + \delta \sigma_{nM}^T (\varepsilon_{nG} - \varepsilon_{nC}) - \delta \mathcal{E}_{pG}^T \mathcal{D}_{pC} - \delta \mathcal{E}_{nG}^T \mathcal{D}_{nM} - \delta \mathcal{D}_{nM}^T (\varepsilon_{nG} - \varepsilon_{nC})) dV \\ = \delta L_e - \delta L_{in},\end{aligned}\tag{2.67}$$

and the constitutive equations are:

$$\begin{aligned}\sigma_p &= \hat{C}_{pp}\varepsilon_p + \hat{C}_{pn}\sigma_n + \hat{e}_{pp}^T \mathcal{E}_p + \hat{e}_{pn}^T \mathcal{D}_n, \\ \varepsilon_n &= \hat{C}_{np}\varepsilon_p + \hat{C}_{nn}\sigma_n + \hat{e}_{np}^T \mathcal{E}_p + \hat{e}_{nn}^T \mathcal{D}_n, \\ \mathcal{D}_p &= \hat{e}_{pp}\varepsilon_p + \hat{e}_{pn}\sigma_n + \hat{\epsilon}_{pp}\mathcal{E}_p + \hat{\epsilon}_{pn}\mathcal{D}_n, \\ \mathcal{E}_n &= \hat{e}_{np}\varepsilon_p + \hat{e}_{nn}\sigma_n + \hat{\epsilon}_{np}\mathcal{E}_p + \hat{\epsilon}_{nn}\mathcal{D}_n.\end{aligned}\tag{2.68}$$

One has to pay attention that the coefficients with the hat are not always the same, but they must be derived for each variational statement. For more details about this topic, one can refer to [128] and [129].

2.5 Acronyms of CUF models

Several refined and advanced two-dimensional models are contained in the Unified Formulation. Depending on the variables description (LW, ESL or ZZ), the order of expansion in the thickness direction and the variational statement used, a large variety of kinematics shell theories can be obtained. A system of acronyms is given in order to denote these models. The first letter indicates the multi-layer approach which can be Equivalent Single Layer (E) or Layer Wise (L). The second letter refers to the employed variational statement: (D) for the Principle of Virtual Displacements and (M) for the Reissner's Mixed Variational Theorem. A number in the third position indicates the order of expansion (N) (from 1 to 4). In the case of ESL approach, a letter (Z) can be added if the zig-zag effects of displacements are considered by means of Murakami's zig-zag function. Summarizing, ED1-ED4 are ESL models based on PVD. If Murakami's zigzag function is used, these models are indicated as EDZ1-EDZ3. Classical theories such as Classical Lamination Theory (CLT) and First order Shear Deformation Theory (FSDT), can be obtained as particular cases of ED1 theory simply imposing constant value of the transversal displacement through the thickness direction. An appropriate application of penalty technique to shear moduli of the material leads to CLT. In the case of

layer wise approaches, the letter L is considered in place of E, so the acronyms are LD1-LD4. Finally, if the RMVT is used, the acronyms become: EM1-EM4 and LM1-LM4. In this case, the Murakami's function is not applied. When the structure is made of one single layer, the ESL and LW approaches provide the same results, thus just the order of expansion N will be indicated in the tables to distinguish the theories.

Chapter 3

Differential equations and solution methods

Anisotropy, nonlinear analysis as well as complicating effects, such as the C_z^0 - Requirements (zig-zag effects in the displacements and interlaminar continuity for the stresses), the couplings between in-plane and out-of-plane strains, make the analysis of layered composite structures complicated in practice. Analytical, closed form solutions are available in very few cases. In most of the practical problems, the solution demand applications of approximated computational methods.

In this work, an analytical method, that is the Navier method, and two approximated numerical methods, that are the Finite Element Method and the Radial Basis Functions method, are employed to solve the governing equations of the problems considered. The Unified Formulation permits to derive the governing equations in terms of some few basic elements called fundamental nuclei. Expanding them by means of opportune indexes and loops, it is possible to obtain the stiffness matrix of the global structure. The use of such nuclei permits to obtain in a unified manner several refined and advanced models which differ for the order of expansion in the thickness direction, for the choice of the modelled multifield variables, and for the multi-layer description, ESL or LW. As an example, the PVD variational statement is here developed to obtain the differential equations for the analysis of multilayered structures. The governing equations can be obtained in weak form for the Finite Element Method or strong form for the Navier method or the Radial Basis Functions method. A review of these solution methods is also provided, with particular attention to the finite element method that is the most common method in literature and it is the main topic of this thesis.

3.1 Governing equations

In the case of pure mechanical problems, the Principle of Virtual Displacements (PVD) states as indicated in Eq.(2.58):

$$\int_V (\delta \epsilon_p^T \sigma_p + \delta \epsilon_n^T \sigma_n) dV = \delta L_e - \delta L_{in} . \quad (3.1)$$

If the structure analyzed is a laminate of N_l layers, the integral on the volume V_k of a generic layer k is split into an integral on the in-plane domain Ω_k plus an integral in the thickness domain A_k :

$$\int_{\Omega_k} \int_{A_k} (\delta \boldsymbol{\varepsilon}_p^{kT} \boldsymbol{\sigma}_p^k + \delta \boldsymbol{\varepsilon}_n^{kT} \boldsymbol{\sigma}_n^k) H d\Omega_k dA_k = \delta L_e^k - \delta L_{in}^k . \quad (3.2)$$

where δL_e^k and δL_{in}^k are the external and the inertial virtual works at the k -layer level, respectively. The factor H has been introduced according to the Eqs.(2.33) (here cylindrical geometry is considered). The relative constitutive equations are those obtained in Eq.(2.36), but written for each layer k :

$$\begin{aligned} \boldsymbol{\sigma}_p^k &= \mathbf{C}_{pp}^k \boldsymbol{\varepsilon}_p^k + \mathbf{C}_{pn}^k \boldsymbol{\varepsilon}_n^k , \\ \boldsymbol{\sigma}_n^k &= \mathbf{C}_{np}^k \boldsymbol{\varepsilon}_p^k + \mathbf{C}_{nn}^k \boldsymbol{\varepsilon}_n^k , \end{aligned} \quad (3.3)$$

By substituting the constitutive equations (3.3) in the variational statement (3.2), one obtains:

$$\int_{\Omega_k} \int_{A_k} (\delta \boldsymbol{\varepsilon}_p^{kT} (\mathbf{C}_{pp}^k \boldsymbol{\varepsilon}_p^k + \mathbf{C}_{pn}^k \boldsymbol{\varepsilon}_n^k) + \delta \boldsymbol{\varepsilon}_n^{kT} (\mathbf{C}_{np}^k \boldsymbol{\varepsilon}_p^k + \mathbf{C}_{nn}^k \boldsymbol{\varepsilon}_n^k)) H d\Omega_k d\xi_k^3 = \delta L_e^k - \delta L_{in}^k . \quad (3.4)$$

The following step is the substitution of the geometrical relations of Eq.(2.22), written for a generic layer k :

$$\begin{aligned} \boldsymbol{\varepsilon}_p^k &= (\mathbf{D}_p^k + \mathbf{A}_p^k) \mathbf{u}^k , \\ \boldsymbol{\varepsilon}_n^k &= (\mathbf{D}_{np}^k + \mathbf{D}_{nz}^k - \mathbf{A}_n^k) \mathbf{u}^k , \end{aligned} \quad (3.5)$$

in which the factor H^k (see Eqs.(2.23) and (2.24)) is calculated in two different ways:

- $H = (1 + \frac{\xi^3}{R})$ if the variable description is equivalent single layer and it doesn't depend on the layer k ;
- $H^k = (1 + \frac{\xi_k}{R^k})$, where R^k is the curvature radius of the midsurface of the layer k , if the variable description is layer wise.

The same for the factors H_α and H_β (see Eqs.(2.30) and (2.31)) in the case of double-curvature geometry. After the substitution of geometrical relations, one has:

$$\begin{aligned} \int_{\Omega_k} \int_{A_k} &(((\mathbf{D}_p^k + \mathbf{A}_p^k) \delta \mathbf{u}^k)^T (\mathbf{C}_{pp}^k (\mathbf{D}_p^k + \mathbf{A}_p^k) + \mathbf{C}_{pn}^k (\mathbf{D}_{np}^k + \mathbf{D}_{nz}^k - \mathbf{A}_n^k)) \mathbf{u}^k + \\ &((\mathbf{D}_{np}^k + \mathbf{D}_{nz}^k - \mathbf{A}_n^k) \delta \mathbf{u}^k)^T (\mathbf{C}_{np}^k (\mathbf{D}_p^k + \mathbf{A}_p^k) + \mathbf{C}_{nn}^k (\mathbf{D}_{np}^k + \mathbf{D}_{nz}^k - \mathbf{A}_n^k)) \mathbf{u}^k) H d\Omega_k d\xi_k^3 = \\ &\delta L_e^k - \delta L_{in}^k . \end{aligned} \quad (3.6)$$

Finally, the Unified Formulation is introduced, as in Eq.(2.1):

$$\delta \mathbf{u}^k = F_\tau \delta \mathbf{u}_\tau^k , \quad \mathbf{u}^k = F_s \mathbf{u}_s^k , \quad \tau, s = 0, 1, \dots, N , \quad (3.7)$$

where, in practice, the displacement \mathbf{u} depends on k only if the approach is LW. Substituting in the previous equation (3.6), one obtains the governing equations in weak form that are:

$$\begin{aligned} \int_{\Omega_k} \int_{A_k} & (((\mathbf{D}_p^k + \mathbf{A}_p^k) F_\tau \delta \mathbf{u}_\tau^k)^T (C_{pp}^k (\mathbf{D}_p^k + \mathbf{A}_p^k) + C_{pn}^k (\mathbf{D}_{np}^k + \mathbf{D}_{nz}^k - \mathbf{A}_n^k)) F_s \mathbf{u}_s^k + \\ & ((\mathbf{D}_{np}^k + \mathbf{D}_{nz}^k - \mathbf{A}_n^k) F_\tau \delta \mathbf{u}_\tau^k)^T (C_{np}^k (\mathbf{D}_p^k + \mathbf{A}_p^k) + C_{nn}^k (\mathbf{D}_{np}^k + \mathbf{D}_{nz}^k - \mathbf{A}_n^k)) F_s \mathbf{u}_s^k) H d\Omega_k d\xi_k^3 = \\ & \delta L_e^k - \delta L_{in}^k. \end{aligned} \quad (3.8)$$

At this step, it is possible to apply the Finite Element Method because the boundary conditions are applied in weak form (more details will be provided below). While, if the Navier method or meshless methods, such as the Radial Basis Functions, are employed to solve the governing equations, one needs to derive the equations in strong form. In this way, one has a set of differential equations on the domain Ω_k , that are the governing equations, and a set of equations on the edge Γ_k , that are the relative boundary conditions.

For this aim, the integration by part is used, that permits to move the differential operators from the infinitesimal variation of the displacement $\delta \mathbf{u}^k$ to the finite quantity \mathbf{u}^k . For a generic variable \mathbf{a} , the integration by parts states:

$$\int_{\Omega_k} ((\mathbf{D}_\Omega^k) \delta \mathbf{a}^k)^T \mathbf{a}^k d\Omega_k = - \int_{\Omega_k} \delta \mathbf{a}^{kT} ((\mathbf{D}_\Omega^{kT}) \mathbf{a}^k) d\Omega_k + \int_{\Gamma_k} \delta \mathbf{a}^{kT} ((\mathbf{I}_\Omega^k) \mathbf{a}^k) d\Gamma_k \quad (3.9)$$

where $\Omega = p, np$. The matrix \mathbf{I}_Ω is obtained applying the *Gradient theorem*:

$$\int_{\Omega_k} \frac{\partial \mathbf{a}^k}{\partial \xi^i} d\Omega_k = \oint_{\Gamma_k} n_i \mathbf{a}^k d\Gamma_k \quad (3.10)$$

in which n_i are the components of the vector $\hat{\mathbf{n}}$, that is the normal to the boundary Γ_k , along the direction ξ^i .

After integration by parts, the governing equations and the relative boundary conditions are obtained from Eq.(3.8):

$$\begin{aligned} \int_{\Omega_k} \int_{A_k} & \delta \mathbf{u}_\tau^{kT} ((-\mathbf{D}_p^k + \mathbf{A}_p^k)^T (C_{pp}^k (\mathbf{D}_p^k + \mathbf{A}_p^k) + C_{pn}^k (\mathbf{D}_{np}^k + \mathbf{D}_{nz}^k - \mathbf{A}_n^k)) + \\ & (-\mathbf{D}_{np}^k + \mathbf{D}_{nz}^k - \mathbf{A}_n^k)^T (C_{np}^k (\mathbf{D}_p^k + \mathbf{A}_p^k) + C_{nn}^k (\mathbf{D}_{np}^k + \mathbf{D}_{nz}^k - \mathbf{A}_n^k))) \mathbf{u}_s^k F_\tau F_s H d\Omega_k d\xi_k^3 + \\ \int_{\Gamma_k} \int_{A_k} & \delta \mathbf{u}_\tau^{kT} (\mathbf{I}_p^{kT} (C_{pp}^k (\mathbf{D}_p^k + \mathbf{A}_p^k) + C_{pn}^k (\mathbf{D}_{np}^k + \mathbf{D}_{nz}^k - \mathbf{A}_n^k)) + \\ & \mathbf{I}_{np}^{kT} (C_{np}^k (\mathbf{D}_p^k + \mathbf{A}_p^k) + C_{nn}^k (\mathbf{D}_{np}^k + \mathbf{D}_{nz}^k - \mathbf{A}_n^k))) \mathbf{u}_s^k F_\tau F_s H d\Gamma_k d\xi_k^3 = \\ \int_{\Omega_k} \int_{A_k} & (\delta \mathbf{u}_\tau^{kT} \mathbf{p}_u) F_\tau H d\Omega_k d\xi_k^3 - \int_{\Omega_k} \int_{A_k} (\delta \mathbf{u}_\tau^{kT} \rho^k \ddot{\mathbf{u}}_s^k) F_\tau F_s H d\Omega_k d\xi_k^3. \end{aligned} \quad (3.11)$$

The matrices to perform the integration by parts \mathbf{I}_p^k and \mathbf{I}_{np}^k have the following form, in analogy with the matrices for the geometrical relations:

$$\mathbf{I}_p^k = \begin{bmatrix} n_1 & 0 & 0 \\ 0 & n_1 & 0 \\ n_2 & n_1 & 0 \end{bmatrix}, \quad \mathbf{I}_{np}^k = \begin{bmatrix} 0 & 0 & n_1 \\ 0 & 0 & n_2 \\ 0 & 0 & 0 \end{bmatrix}. \quad (3.12)$$

n_1 and n_2 are the components of the normal to the boundary of domain Ω that is:

$$\hat{\mathbf{n}} = \begin{bmatrix} n_1 \\ n_2 \end{bmatrix} = \begin{bmatrix} \cos(\varphi_1) \\ \cos(\varphi_2) \end{bmatrix} \quad (3.13)$$

φ_1 and φ_2 are the angles between the normal $\hat{\mathbf{n}}$ and the direction ξ^1 and ξ^2 , respectively. Whether the Finite Element Method or the Navier and Radial Basis Functions methods are applied, the final form of the governing equations is:

$$\delta \mathbf{u}_\tau^{kT} : \quad \mathbf{K}_{uu}^{k\tau s} \mathbf{u}_s^k = \mathbf{P}_{u\tau}^k - \mathbf{M}_{uu}^{k\tau s} \ddot{\mathbf{u}}_s^k \quad (3.14)$$

In the case of strong form solution, one has also the related Neumann-type boundary conditions on the edge Γ_k :

$$\mathbf{\Pi}_{uu}^{k\tau s} \mathbf{u}_s^k = \mathbf{\Pi}_{uu}^{k\tau s} \bar{\mathbf{u}}_s^k, \quad (3.15)$$

In these equations, $\mathbf{K}_{uu}^{k\tau s}$ is the so-called fundamental nucleus for the stiffness matrix, $\mathbf{P}_{u\tau}^k$ is the vector of the external mechanical loads, $\mathbf{M}_{uu}^{k\tau s}$ is the matrix of the inertial contribution, written in form of fundamental nucleus, and $\mathbf{\Pi}_{uu}^{k\tau s}$ is the fundamental nucleus for the boundary conditions. \mathbf{u}_s^k is the vector of degrees of freedom, $\ddot{\mathbf{u}}_s^k$ is the second temporal derivative of \mathbf{u}_s^k and $\bar{\mathbf{u}}_s^k$ is the vector of the displacements assigned on the boundary.

The stiffness matrix of each layer k is calculated by expanding the fundamental nucleus $\mathbf{K}_{uu}^{k\tau s}$ on the indexes τ and s . Then, the stiffness matrix of the global structure is obtained by assembling these matrices at multilayer level. Two different assembling procedures are used, depending on the variable description: if the approach is equivalent single layer, the assembling procedure is shown in Fig.3.1; if the approach is layer wise, the procedure is that of Fig.3.2.

3.2 Navier method

The Navier method permits to calculate the closed form solution of the governing equations under particular conditions of geometry, boundary and material. These conditions are:

- the geometry in the plane of the plate or shell must be rectangular;
- the structure must be simply supported on the boundary;

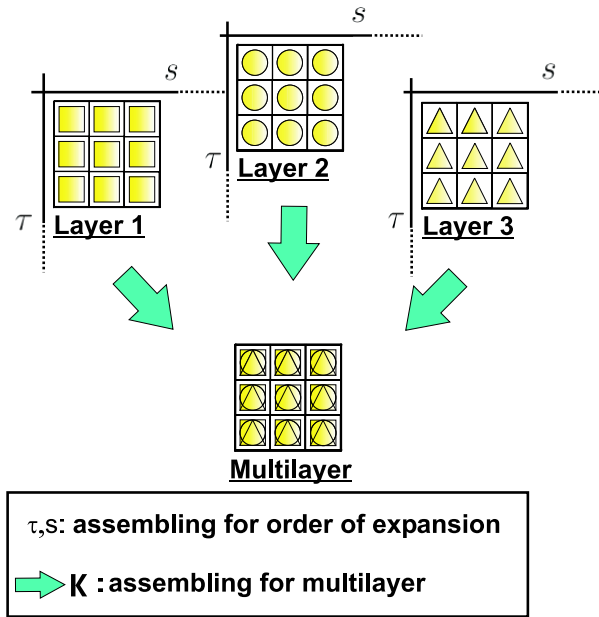


Figure 3.1: Assembling procedure for ESL approach.

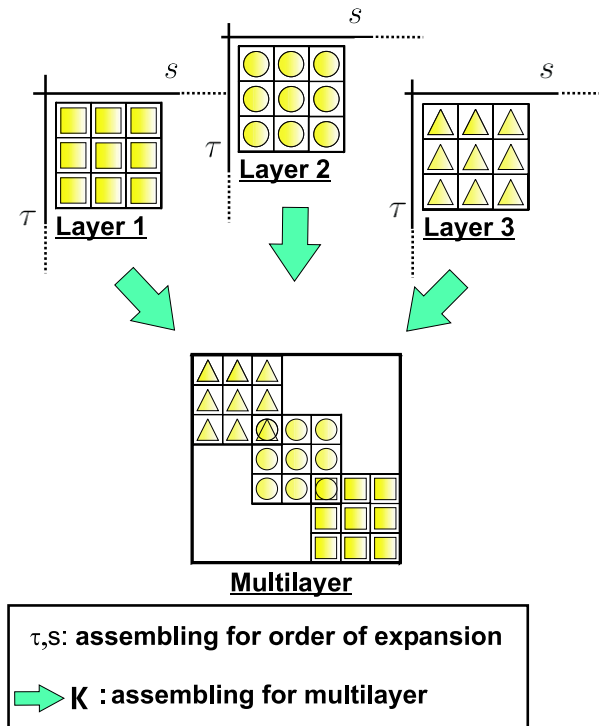


Figure 3.2: Assembling procedure for LW approach.

- some material constants must be zero, that are:

$$C_{16} = C_{26} = C_{63} = C_{36} = C_{45} = 0. \quad (3.16)$$

In the case of thermal or electrical problems, also the following constants must be considered:

$$\lambda_6 = 0, \quad e_{25} = e_{14} = e_{36} = \epsilon_{12} = \epsilon_{21} = 0. \quad (3.17)$$

Thanks to the first and the second conditions, the Eq.s(3.15) are directly satisfied. The last condition is always verified in the case of isotropic and orthotropic materials and it permits to eliminate some terms in the governing equations in order to find the strong solution.

According to the Navier method, the following harmonic assumptions are made for the field variables (displacements in this case, but they can be made also for stresses, temperature, electric potential and electric displacement):

$$\begin{aligned} u_s^k &= \sum_{m,n} (\hat{U}_s^k) \cos\left(\frac{m\pi\xi^1}{a}\right) \sin\left(\frac{n\pi\xi^2}{b}\right) e^{i\omega_{mn}t} & k = 1, N_l \\ v_s^k &= \sum_{m,n} (\hat{V}_s^k) \sin\left(\frac{m\pi\xi^1}{a}\right) \cos\left(\frac{n\pi\xi^2}{b}\right) e^{i\omega_{mn}t} & \tau = t, b, r \quad \text{or} \quad \tau = 0, 1, r \\ w_s^k &= \sum_{m,n} (\hat{W}_s^k) \sin\left(\frac{m\pi\xi^1}{a}\right) \sin\left(\frac{n\pi\xi^2}{b}\right) e^{i\omega_{mn}t} & r = 2, N \end{aligned} \quad (3.18)$$

The same assumptions are made for the virtual displacements $\delta \mathbf{u}_\tau^k$. In these equations, $\hat{U}_s^k, \hat{V}_s^k, \hat{W}_s^k$ are the amplitudes of sinusoidal displacements, m, n are the wave numbers and a, b are the dimensions of the shell/plate in the ξ^1 and ξ^2 direction, respectively. $i = \sqrt{-1}$, t is the time and ω_{mn} is the circular frequency depending on m and n .

Substituting the expressions (3.18) in the governing equations (3.11), one obtains the explicit form of the fundamental nuclei $\mathbf{K}_{uu}^{k\tau s}, \mathbf{M}_{uu}^{k\tau s}$ and $\mathbf{\Pi}_{uu}^{k\tau s}$ in the equations (5.3) and (3.15). The vector of the unknowns \mathbf{u}_s^k contains the amplitudes $\hat{U}_s^k, \hat{V}_s^k, \hat{W}_s^k$.

3.2.1 Free vibration analysis

The free vibration analysis leads to an eigenvalue problem. Upon substitution of Eqs.(3.18), the governing equations assume the form of a linear system of algebraic equations in the Ω_k domain:

$$\mathbf{K}\hat{\mathbf{U}} = \omega_{mn}^2 \mathbf{M}\hat{\mathbf{U}}, \quad (3.19)$$

By defining $\lambda_{mn} = \omega_{mn}^2$, the solution of the associated eigenvalue problem becomes:

$$||\mathbf{K} - \lambda_{mn}\mathbf{M}|| = 0. \quad (3.20)$$

The eigenvectors $\hat{\mathbf{U}}$ associated to the eigenvalues λ_{mn} (or to circular frequencies ω_{mn}) define the vibration modes of the structure in terms of primary variables. Once the

waves number (m,n) has been defined in the in-plane directions, the number of obtained frequencies becomes equal to the degrees of freedom of the employed two-dimensional model. It is possible to obtain the relative eigenvector, in terms of primary variables, for each value of frequency, in order to obtain the modes plotted in the thickness direction.

3.3 Finite element method

Among the computational techniques implemented for the analysis of layered structures, a predominant role has been played by Finite Element Method (FEM). The most of the finite elements, available in literature, are formulated on the bases of axiomatic-type theories. According to MacNeal [135] the first FEM analysis was published in 1961. The majority of early FEM calculations were performed with the classical Kirchhoff-Love theory and some examples are given in [136]-[140]. But, it was difficult to satisfy the requirements of compatibility in thin shell analysis because the rotations were derived from the transversal displacement. For this reason, plate/shell elements including classical transverse shear effects (FSDT) were developed by Pryor and Barker [141], Noor [142], Hughes [143], Panda and Natarayan [144], Parisch [145], Ferreira [146] and many others. However, early FSDT type elements showed severe stiffening in thin plate/shell limits. Such a numerical mechanism, known as shear or membrane locking, was first contrasted by implementation of numerical tricks, such as reduced/selective integration schemes [147]-[151]. But, spurious zero energy modes are introduced by these sub-integration techniques. In [152] and [153], Chinosi et al. developed a hierarchic finite element for thin Naghdi shell model [154] that was able to contrast locking for the shell problem in its displacement formulation. However, in the case of very small thickness and when the element is not of degree as high as needed, the numerical solution exhibits a loss in the rate of convergence. The so-called Mixed Interpolation of Tensorial Components (MITC) was implemented to overcome both these problems. Many articles by Bathe and others are available on that topic: examples are the papers [155]-[160]. Arnold and Brezzi [161] dealt with a mixed formulation of the Naghdi model, giving a family of locking free elements and proving the convergence of their numerical approach. Similarly, Ramm and Bischoff [162]-[166] developed a shell finite element based on a 7-parameter theory, in which the extra strain term is incorporated via the enhanced assumed strain concept proposed by Simo and Rafai [167].

Also a large variety of plate/shell finite element implementations of higher-order theories (HOT) have been proposed in the last twenty years literature. HOT-based C^0 finite elements (C^0 means that the continuity is required only for the unknown variables and not for their derivatives) were discussed by Kant and co-authors [168],[169]. In [170]-[174], Polit et al. proposed a C^1 six-nodes triangular finite element in which the transverse shear strains are represented by cosine functions. This element is able to ensure both the continuity conditions for displacements and transverse shear stresses at the interfaces between layers of laminated structures. A comprehensive discussion of HOT-type theories and related finite element suitability has been provided by Tessler

[175]. Many other papers are available in which HOTs have been implemented for plates and shells, details can be found in the books by Reddy [176] and Palazotto and Dennis [177].

Dozens of finite elements have been proposed based on zig-zag theories [178],[179]. An application of Reissner Mixed Variational Theorem (RMVT) [180] to develop standard finite elements was proposed by Rao and Meyer-Piening [181]. A generalization of RMVT as a tool to develop approximate solutions was given by Carrera [26]. The obtained finite elements represent the FE implementation of the Murakami theory [123] and were denoted by the acronym RMZC, (Reissner Mindlin Zigzag interlaminar Continuity). Full extensions of RMZC to shell geometries have been done by Brank and Carrera [182].

Finite element implementations of layer-wise theories in the framework of axiomatic-type theories have been proposed by many authors, among which Noor and Burton [183], Reddy [184], Mawenya and Davies [185], Pinsky and Kim [186], Chaudhuri and Seide [189], Rammerstorfer et al. [188]. Finally, the finite element presented in this work is based on both equivalent-single-layer, zig-zag and layer-wise models contained in the CUF [81],[82],[127] and it employs the MITC method to contrast the membrane and shear locking.

3.3.1 CUF MITC9 shell element

According to the Finite Element Method (FEM), the displacement field (see Eqs.(2.1)) is interpolated by means of the shape functions N_i, N_j :

$$\delta \mathbf{u}^k = F_\tau N_i \delta \mathbf{q}_{\tau_i}^k, \quad \mathbf{u}^k = F_s N_j \mathbf{q}_{s_j}^k, \quad (3.21)$$

where $\tau, s = 0, 1, \dots, N$, $i, j = 1, \dots, N_n$ and N_n is the number of nodes of the element. $\mathbf{q}_{s_j}^k$ and $\delta \mathbf{q}_{\tau_i}^k$ are the nodal displacements and their virtual variations. The element considered in this work has 9 nodes and the Lagrangian shape functions are used to interpolate the displacements. These functions are obtained by imposing that N_i assumes the value 1 in the node i and 0 in the others, and they are expressed in the local reference system of the element (ξ, η) (see Figure 3.3), as follows:

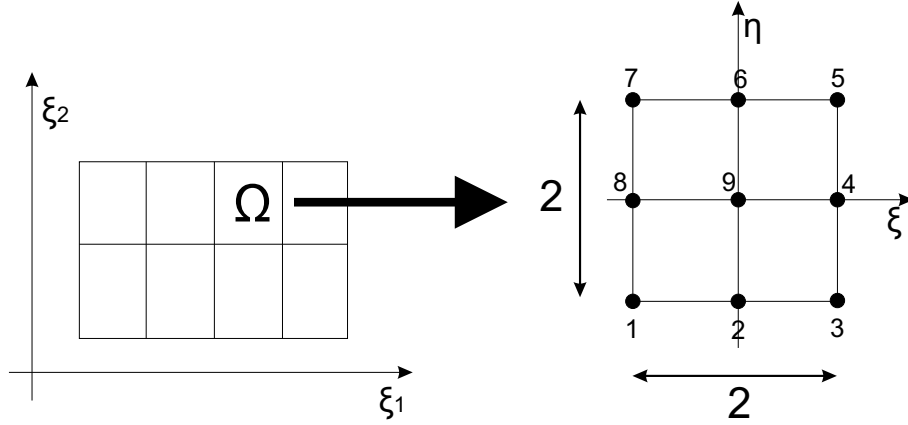


Figure 3.3: Local reference system of the element.

$$\begin{aligned}
 N_1 &= \frac{1}{4}(\xi^2 - \xi)(\eta^2 - \eta), \\
 N_2 &= \frac{1}{2}(1 - \xi^2)(\eta^2 - \eta), \\
 N_3 &= \frac{1}{4}(\xi^2 + \xi)(\eta^2 - \eta), \\
 N_4 &= \frac{1}{2}(\xi^2 + \xi)(1 - \eta^2), \\
 N_5 &= \frac{1}{4}(\xi^2 + \xi)(\eta^2 + \eta), \\
 N_6 &= \frac{1}{2}(1 - \xi^2)(\eta^2 + \eta), \\
 N_7 &= \frac{1}{4}(\xi^2 - \xi)(\eta^2 + \eta), \\
 N_8 &= \frac{1}{2}(\xi^2 - \xi)(1 - \eta^2), \\
 N_9 &= (1 - \xi^2)(1 - \eta^2).
 \end{aligned} \tag{3.22}$$

Substituting the displacements (7.2) in the geometrical relations (2.22), one has:

$$\begin{aligned}
 \epsilon_p^k &= F_\tau(\mathbf{D}_p^k + \mathbf{A}_p^k)(N_i \mathbf{I}) \mathbf{q}_{\tau_i}^k, \\
 \epsilon_n^k &= F_\tau(\mathbf{D}_{n\Omega}^k - \mathbf{A}_n^k)(N_i \mathbf{I}) \mathbf{q}_{\tau_i}^k + F_{\tau,z} \mathbf{A}_{nz}^k (N_i \mathbf{I}) \mathbf{q}_{\tau_i}^k,
 \end{aligned} \tag{3.23}$$

where \mathbf{I} is 3×3 identity matrix.

Considering the components of the strain tensor in the local coordinate system (ξ, η) , the MITC shell elements are formulated by using - instead of the strain components directly computed from the displacements - an interpolation of these strain components within each element using a specific interpolation strategy for each component. The corresponding interpolation points, called the *tying points*, are shown in the Figure 3.4 for nine-nodes shell elements.

The strain components ϵ_{11} and ϵ_{13} are interpolated on the points $(A1, B1, C1, D1, E1, F1)$ by means of the following functions (that are obtained as the shape functions):

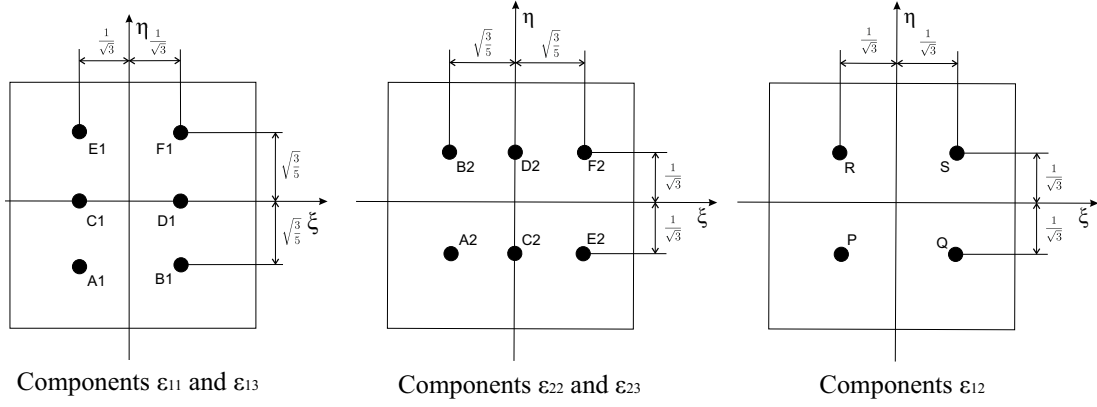


Figure 3.4: Tying points for MITC9 shell finite elements.

$$\begin{aligned}
 N_{A1} &= \frac{5\sqrt{3}}{12} \eta \left(\eta - \sqrt{\frac{3}{5}} \right) \left(\frac{1}{\sqrt{3}} - \xi \right), \\
 N_{B1} &= \frac{5\sqrt{3}}{12} \eta \left(\eta - \sqrt{\frac{3}{5}} \right) \left(\frac{1}{\sqrt{3}} + \xi \right), \\
 N_{C1} &= -\frac{5\sqrt{3}}{6} \left(\eta + \sqrt{\frac{3}{5}} \right) \left(\eta - \sqrt{\frac{3}{5}} \right) \left(\frac{1}{\sqrt{3}} - \xi \right), \\
 N_{D1} &= -\frac{5\sqrt{3}}{6} \left(\eta + \sqrt{\frac{3}{5}} \right) \left(\eta - \sqrt{\frac{3}{5}} \right) \left(\frac{1}{\sqrt{3}} + \xi \right), \\
 N_{E1} &= \frac{5\sqrt{3}}{12} \left(\eta + \sqrt{\frac{3}{5}} \right) \eta \left(\frac{1}{\sqrt{3}} - \xi \right), \\
 N_{F1} &= \frac{5\sqrt{3}}{12} \left(\eta + \sqrt{\frac{3}{5}} \right) \eta \left(\frac{1}{\sqrt{3}} + \xi \right).
 \end{aligned} \tag{3.24}$$

For the components ε_{22} and ε_{23} , the interpolating functions on the points $(A2, B2, C2, D2, E2, F2)$ are:

$$\begin{aligned}
 N_{A2} &= \frac{5\sqrt{3}}{12} \xi \left(\xi - \sqrt{\frac{3}{5}} \right) \left(\frac{1}{\sqrt{3}} - \eta \right), \\
 N_{B2} &= \frac{5\sqrt{3}}{12} \xi \left(\xi - \sqrt{\frac{3}{5}} \right) \left(\frac{1}{\sqrt{3}} + \eta \right), \\
 N_{C2} &= -\frac{5\sqrt{3}}{6} \left(\xi + \sqrt{\frac{3}{5}} \right) \left(\xi - \sqrt{\frac{3}{5}} \right) \left(\frac{1}{\sqrt{3}} - \eta \right), \\
 N_{D2} &= -\frac{5\sqrt{3}}{6} \left(\xi + \sqrt{\frac{3}{5}} \right) \left(\xi - \sqrt{\frac{3}{5}} \right) \left(\frac{1}{\sqrt{3}} + \eta \right), \\
 N_{E2} &= \frac{5\sqrt{3}}{12} \left(\xi + \sqrt{\frac{3}{5}} \right) \xi \left(\frac{1}{\sqrt{3}} - \eta \right), \\
 N_{F2} &= \frac{5\sqrt{3}}{12} \left(\xi + \sqrt{\frac{3}{5}} \right) \xi \left(\frac{1}{\sqrt{3}} + \eta \right).
 \end{aligned} \tag{3.25}$$

Finally, the interpolating functions on the points (P, Q, R, S) for the strain ε_{12} are:

$$\begin{aligned}
 N_P &= \frac{3}{4} \left(\frac{1}{\sqrt{3}} - \xi \right) \left(\frac{1}{\sqrt{3}} - \eta \right), \\
 N_Q &= \frac{3}{4} \left(\frac{1}{\sqrt{3}} + \xi \right) \left(\frac{1}{\sqrt{3}} - \eta \right), \\
 N_R &= \frac{3}{4} \left(\frac{1}{\sqrt{3}} - \xi \right) \left(\frac{1}{\sqrt{3}} + \eta \right), \\
 N_S &= \frac{3}{4} \left(\frac{1}{\sqrt{3}} + \xi \right) \left(\frac{1}{\sqrt{3}} + \eta \right).
 \end{aligned} \tag{3.26}$$

The strain component ε_{33} is directly calculated from the displacements.

For convenience reasons, the interpolating functions can be arranged in the following vectors:

$$\begin{aligned}
 \mathbf{N}_{m1} &= [N_{A1}, N_{B1}, N_{C1}, N_{D1}, N_{E1}, N_{F1}], \\
 \mathbf{N}_{m2} &= [N_{A2}, N_{B2}, N_{C2}, N_{D2}, N_{E2}, N_{F2}], \\
 \mathbf{N}_{m3} &= [N_P, N_Q, N_R, N_S].
 \end{aligned} \tag{3.27}$$

According to the MITC method, the strain components are written as follows:

$$\boldsymbol{\varepsilon}_p = \begin{Bmatrix} \varepsilon_{11} \\ \varepsilon_{22} \\ \varepsilon_{12} \end{Bmatrix} = \begin{bmatrix} \mathbf{N}_{m1} & 0 & 0 \\ 0 & \mathbf{N}_{m2} & 0 \\ 0 & 0 & \mathbf{N}_{m3} \end{bmatrix} \begin{Bmatrix} \boldsymbol{\varepsilon}_{11_{m1}} \\ \boldsymbol{\varepsilon}_{22_{m2}} \\ \boldsymbol{\varepsilon}_{12_{m3}} \end{Bmatrix} = \mathbf{N}_1 \begin{Bmatrix} \boldsymbol{\varepsilon}_{11_{m1}} \\ \boldsymbol{\varepsilon}_{22_{m2}} \\ \boldsymbol{\varepsilon}_{12_{m3}} \end{Bmatrix}, \tag{3.28}$$

$$\boldsymbol{\varepsilon}_n = \begin{Bmatrix} \varepsilon_{13} \\ \varepsilon_{23} \\ \varepsilon_{33} \end{Bmatrix} = \begin{bmatrix} \mathbf{N}_{m1} & 0 & 0 \\ 0 & \mathbf{N}_{m2} & 0 \\ 0 & 0 & 1 \end{bmatrix} \begin{Bmatrix} \boldsymbol{\varepsilon}_{13_{m1}} \\ \boldsymbol{\varepsilon}_{23_{m2}} \\ \varepsilon_{33} \end{Bmatrix} = \mathbf{N}_2 \begin{Bmatrix} \boldsymbol{\varepsilon}_{13_{m1}} \\ \boldsymbol{\varepsilon}_{23_{m2}} \\ \varepsilon_{33} \end{Bmatrix},$$

where the matrixes N_1 and N_2 have been introduced and the vectors of the strains are:

$$\epsilon_{11_{m1}} = \begin{Bmatrix} \epsilon_{11}(A1) \\ \epsilon_{11}(B1) \\ \epsilon_{11}(C1) \\ \epsilon_{11}(D1) \\ \epsilon_{11}(E1) \\ \epsilon_{11}(F1) \end{Bmatrix}, \quad \epsilon_{22_{m2}} = \begin{Bmatrix} \epsilon_{22}(A2) \\ \epsilon_{22}(B2) \\ \epsilon_{22}(C2) \\ \epsilon_{22}(D2) \\ \epsilon_{22}(E2) \\ \epsilon_{22}(F2) \end{Bmatrix}, \quad \epsilon_{12_{m3}} = \begin{Bmatrix} \epsilon_{12}(P) \\ \epsilon_{12}(Q) \\ \epsilon_{12}(R) \\ \epsilon_{12}(S) \end{Bmatrix}, \quad (3.29)$$

$$\epsilon_{13_{m1}} = \begin{Bmatrix} \epsilon_{13}(A1) \\ \epsilon_{13}(B1) \\ \epsilon_{13}(C1) \\ \epsilon_{13}(D1) \\ \epsilon_{13}(E1) \\ \epsilon_{13}(F1) \end{Bmatrix}, \quad \epsilon_{23_{m2}} = \begin{Bmatrix} \epsilon_{23}(A2) \\ \epsilon_{23}(B2) \\ \epsilon_{23}(C2) \\ \epsilon_{23}(D2) \\ \epsilon_{23}(E2) \\ \epsilon_{23}(F2) \end{Bmatrix}.$$

The notation (m) indicates that the strain is calculated in the tying point m using the geometrical relations (3.23). For example, if one considers the strain ϵ_{11} calculated in the point $A1$, one has:

$$\epsilon_{11}(A1) = F_\tau (\mathbf{D}_p + \mathbf{A}_p)_{(1,:)} N_i(\xi_{A1}, \eta_{A1}) \mathbf{q}_{\tau_i}, \quad (3.30)$$

where $(1, :)$ means that the first row of the matrix $(\mathbf{D}_p + \mathbf{A}_p)$ is considered and ξ_{A1}, η_{A1} are the coordinates of the point $A1$.

According to this interpolation, the geometrical relations can be rewritten as follows:

$$\begin{aligned} \epsilon_{p_{im}}^{k\tau} &= F_\tau \mathbf{C}_{3_{im}}^k \mathbf{q}_{\tau_i}^k, \\ \epsilon_{n_{im}}^{k\tau} &= F_\tau \mathbf{C}_{1_{im}}^k \mathbf{q}_{\tau_i}^k + F_{\tau,z} \mathbf{C}_{2_{im}}^k \mathbf{q}_{\tau_i}^k, \end{aligned} \quad (3.31)$$

where m indicates a loop on the tying points and the matrixes introduced are:

$$\begin{aligned} \mathbf{C}_{1_{im}}^k &= \mathbf{N}_2 \begin{bmatrix} (\mathbf{D}_{n\Omega}^k - \mathbf{A}_n^k)_{(1,:)} (N_i \mathbf{I})_{m1} \\ (\mathbf{D}_{n\Omega}^k - \mathbf{A}_n^k)_{(2,:)} (N_i \mathbf{I})_{m2} \\ (\mathbf{D}_{n\Omega}^k - \mathbf{A}_n^k)_{(3,:)} (N_i \mathbf{I})_{m3} \end{bmatrix}, \\ \mathbf{C}_{2_{im}}^k &= \mathbf{N}_2 \begin{bmatrix} \mathbf{A}_{nz(1,:)}^k (N_i \mathbf{I})_{m1} \\ \mathbf{A}_{nz(2,:)}^k (N_i \mathbf{I})_{m2} \\ \mathbf{A}_{nz(3,:)}^k (N_i \mathbf{I})_{m3} \end{bmatrix}, \\ \mathbf{C}_{3_{im}}^k &= \mathbf{N}_1 \begin{bmatrix} (\mathbf{D}_p^k + \mathbf{A}_p^k)_{(1,:)} (N_i \mathbf{I})_{m1} \\ (\mathbf{D}_p^k + \mathbf{A}_p^k)_{(2,:)} (N_i \mathbf{I})_{m2} \\ (\mathbf{D}_p^k + \mathbf{A}_p^k)_{(3,:)} (N_i \mathbf{I})_{m3} \end{bmatrix}. \end{aligned} \quad (3.32)$$

Also the constitutive equations are rewritten considering the loop on the tying points by means of the index n :

$$\begin{aligned}\sigma_{p_{jn}}^{ks} &= C_{pp}^k \epsilon_{p_{jn}}^{ks} + C_{pn}^k \epsilon_{n_{jn}}^{ks}, \\ \sigma_{n_{jn}}^{ks} &= C_{np}^k \epsilon_{p_{jn}}^{ks} + C_{nn}^k \epsilon_{n_{jn}}^{ks}.\end{aligned}\quad (3.33)$$

By exploiting the constitutive equations (3.33), the geometrical relations (3.31) and the displacement field (7.2) in the PVD (3.2), one obtains:

$$\begin{aligned}& \delta \mathbf{q}_{\tau_i}^{kT} \left\{ \int_{A_k} F_{\tau} \left(\int_{\Omega_k} [C_{3im}^{kT} (C_{pp}^k C_{3jn}^k + C_{pn}^k C_{1jn}^k) + C_{1im}^{kT} (C_{np}^k C_{3jn}^k + C_{nn}^k C_{1jn}^k)] d\Omega_k \right) F_s H_k d\xi_k^3 \right\} \mathbf{q}_{s_j}^k + \\& \delta \mathbf{q}_{\tau_i}^{kT} \left\{ \int_{A_k} F_{\tau} \left(\int_{\Omega_k} [(C_{3im}^{kT} C_{pn}^k + C_{1im}^{kT} C_{nn}^k) C_{2jn}^k] d\Omega_k \right) F_{s,3} H_k d\xi_k^3 \right\} \mathbf{q}_{s_j}^k + \\& \delta \mathbf{q}_{\tau_i}^{kT} \left\{ \int_{A_k} F_{\tau,3} \left(\int_{\Omega_k} [C_{2im}^{kT} (C_{np}^k C_{3jn}^k + C_{nn}^k C_{1jn}^k)] d\Omega_k \right) F_s H_k d\xi_k^3 \right\} \mathbf{q}_{s_j}^k + \\& \delta \mathbf{q}_{\tau_i}^{kT} \left\{ \int_{A_k} F_{\tau,3} \left(\int_{\Omega_k} [C_{2im}^{kT} C_{nn}^k C_{2jn}^k] d\Omega_k \right) F_{s,3} H_k d\xi_k^3 \right\} \mathbf{q}_{s_j}^k = \\& \delta \mathbf{q}_{\tau_i}^{kT} \left\{ \int_{A_k} F_{\tau} \left(\int_{\Omega_k} N_i \mathbf{p} d\Omega_k \right) H_k d\xi_k^3 \right\},\end{aligned}\quad (3.34)$$

Therefore, the following governing equation system is written:

$$\delta \mathbf{q}_{\tau_i}^k : \mathbf{K}^{k\tau s i j} \mathbf{q}_{s_j}^k = \mathbf{P}_{\tau_i}^k \quad (3.35)$$

where the vector of unknowns is given by the nodal displacements $\mathbf{q}_{s_j}^k$ and the fundamental nucleus is dependent on the indexes i, j .

3.4 RBF collocation method

Recently, radial basis functions (RBFs) have enjoyed considerable success and research as a technique for interpolating data and functions. A radial basis function, $\phi(\|x - x_j\|)$ is a spline that depends on the Euclidian distance between distinct data centers $x_j, j = 1, 2, \dots, N \in \mathbb{R}^n$, also called nodal or collocation points. Although most work to date on RBFs relates to scattered data approximation and in general to interpolation theory, there has recently been an increased interest in their use for solving partial differential equations (PDEs). This approach, which approximates the whole solution of the PDE directly using RBFs, is truly a mesh-free technique. Kansa [190] introduced the concept of solving PDEs by an unsymmetric RBF collocation method based upon the Multi Quadratic (MQ) interpolation functions, in which the shape parameter may vary across the problem domain. The use of alternative methods to the Finite Element Methods for the analysis of plates and shells, such as the meshless methods based on radial

basis functions is attractive due to the absence of a mesh and the ease of collocation methods. The use of radial basis function for the analysis of structures and materials has been previously studied by numerous authors [191]-[204].

Radial basis functions (RBF) approximations are mesh-free numerical schemes that can exploit accurate representations of the boundary, are easy to implement and can be spectrally accurate. In this section, the formulation of a global unsymmetrical collocation RBF-based method to compute elliptic operators is presented.

The radial basis function (ϕ) approximation of a function (\mathbf{u}) is given by:

$$\tilde{\mathbf{u}}(\mathbf{x}) = \sum_{i=1}^N \alpha_i \phi(\|x - y_i\|_2), \mathbf{x} \in \mathbb{R}^n, \quad (3.36)$$

where $y_i, i = 1, \dots, N$ is a finite set of distinct points (centers) in \mathbb{R}^n . The most common RBFs are:

$$\begin{aligned} \text{Cubic:} \quad & \phi(r) = r^3, \\ \text{Thin plate splines:} \quad & \phi(r) = r^2 \log(r), \\ \text{Wendland functions:} \quad & \phi(r) = (1 - r)_+^m p(r), \\ \text{Gaussian:} \quad & \phi(r) = e^{-(cr)^2}, \\ \text{Multiquadrics:} \quad & \phi(r) = \sqrt{c^2 + r^2}, \\ \text{Inverse Multiquadrics:} \quad & \phi(r) = (c^2 + r^2)^{-1/2}, \end{aligned}$$

where the Euclidian distance r is real and non-negative and c is a positive shape parameter. Hardy [205] introduced multiquadrics in the analysis of scattered geographical data. In the 1990's Kansa [190] used multiquadrics for the solution of partial differential equations. Considering N distinct interpolations, and knowing $u(x_j), j = 1, 2, \dots, N, \alpha_i$ are found by the solution of a $N \times N$ linear system:

$$\mathbf{A}\boldsymbol{\alpha} = \mathbf{u}, \quad (3.37)$$

where $\mathbf{A} = [\phi(\|x - y_i\|_2)]_{N \times N}$, $\boldsymbol{\alpha} = [\alpha_1, \alpha_2, \dots, \alpha_N]^T$ and $\mathbf{u} = [u(x_1), u(x_2), \dots, u(x_N)]^T$.

3.4.1 The static problem

Consider a linear elliptic partial differential operator L and a bounded region Ω in \mathbb{R}^n with some boundary $\partial\Omega$. In the static problems, one seeks the computation of displacements (\mathbf{u}) from the global system of equations:

$$\mathcal{L}\mathbf{u} = \mathbf{f} \text{ in } \Omega, \quad (3.38)$$

$$\mathcal{L}_B\mathbf{u} = \mathbf{g} \text{ on } \partial\Omega, \quad (3.39)$$

where \mathcal{L} , \mathcal{L}_B are linear operators in the domain and on the boundary, respectively. The right-hand side of (3.38) and (3.39) represent the external forces applied on the shell and the boundary conditions applied along the perimeter of the shell, respectively. The PDE problem defined in (3.38) and (3.39) will be replaced by a finite problem, defined by an algebraic system of equations, after the radial basis expansions.

The solution of a static problem by radial basis functions considers N_I nodes in the domain and N_B nodes on the boundary, with a total number of nodes $N = N_I + N_B$. The sampling points are denoted by $x_i \in \Omega, i = 1, \dots, N_I$ and $x_i \in \partial\Omega, i = N_I + 1, \dots, N$. At the points in the domain, the following system of equations is solved:

$$\sum_{i=1}^N \alpha_i \mathcal{L}\phi(\|x - y_i\|_2) = \mathbf{f}(x_j), j = 1, 2, \dots, N_I, \quad (3.40)$$

or:

$$\mathcal{L}^I \boldsymbol{\alpha} = \mathbf{F}, \quad (3.41)$$

where:

$$\mathcal{L}^I = [\mathcal{L}\phi(\|x - y_i\|_2)]_{N_I \times N}. \quad (3.42)$$

At the points on the boundary, one can impose the boundary conditions as:

$$\sum_{i=1}^N \alpha_i \mathcal{L}_B\phi(\|x - y_i\|_2) = \mathbf{g}(x_j), j = N_I + 1, \dots, N, \quad (3.43)$$

or:

$$\mathbf{B}\boldsymbol{\alpha} = \mathbf{G}, \quad (3.44)$$

where:

$$\mathbf{B} = [\mathcal{L}_B\phi(\|x_{N_I+1} - y_j\|_2)]_{N_B \times N}.$$

Therefore, one can write a finite-dimensional static problem as:

$$\begin{bmatrix} \mathcal{L}^I \\ \mathbf{B} \end{bmatrix} \boldsymbol{\alpha} = \begin{bmatrix} \mathbf{F} \\ \mathbf{G} \end{bmatrix}. \quad (3.45)$$

By inverting the system (3.45), one obtains the vector $\boldsymbol{\alpha}$. Then, the solution \mathbf{u} is obtained using the interpolation equation (3.36).

The radial basis collocation method follows a simple implementation procedure. Taking equation (3.11), one computes:

$$\boldsymbol{\alpha} = \begin{bmatrix} \mathcal{L}^I \\ \mathbf{B} \end{bmatrix}^{-1} \begin{bmatrix} \mathbf{F} \\ \mathbf{G} \end{bmatrix}. \quad (3.46)$$

This $\boldsymbol{\alpha}$ vector is then used to obtain solution $\tilde{\mathbf{u}}$, by using (2.1). If derivatives of $\tilde{\mathbf{u}}$ are needed, such derivatives are computed as:

$$\frac{\partial \tilde{\mathbf{u}}}{\partial x} = \sum_{j=1}^N \alpha_j \frac{\partial \phi_j}{\partial x}, \quad (3.47)$$

$$\frac{\partial^2 \tilde{\mathbf{u}}}{\partial x^2} = \sum_{j=1}^N \alpha_j \frac{\partial^2 \phi_j}{\partial x^2}, \text{etc.} \quad (3.48)$$

In the present collocation approach, one needs to impose essential and natural boundary conditions. Consider, for example, the condition $w = 0$, on a simply supported or clamped edge. The conditions are enforced by interpolating as:

$$w = 0 \rightarrow \sum_{j=1}^N \alpha_j^W \phi_j = 0. \quad (3.49)$$

Other boundary conditions are interpolated in a similar way.

3.4.2 The eigenproblem

The eigenproblem looks for eigenvalues (λ) and eigenvectors (\mathbf{u}) that satisfy:

$$\mathcal{L}\mathbf{u} + \lambda\mathbf{u} = 0 \text{ in } \Omega, \quad (3.50)$$

$$\mathcal{L}_B\mathbf{u} = 0 \text{ on } \partial\Omega. \quad (3.51)$$

As in the static problem, the eigenproblem defined in (3.50) and (3.51) is replaced by a finite-dimensional eigenvalue problem, based on RBF approximations. N_I nodes in the interior of the domain and N_B nodes on the boundary are considered, with $N = N_I + N_B$. The interpolation points are denoted by $x_i \in \Omega, i = 1, \dots, N_I$ and $x_i \in \partial\Omega, i = N_I + 1, \dots, N$. At the points in the domain, one can define the eigenproblem as:

$$\sum_{i=1}^N \alpha_i \mathcal{L}\phi(\|x - y_i\|_2) = \lambda \tilde{\mathbf{u}}(x_j), j = 1, 2, \dots, N_I, \quad (3.52)$$

or:

$$\mathcal{L}^I \boldsymbol{\alpha} = \lambda \tilde{\mathbf{u}}^I, \quad (3.53)$$

where:

$$\mathcal{L}^I = [\mathcal{L}\phi(\|x - y_i\|_2)]_{N_I \times N}. \quad (3.54)$$

At the points on the boundary, the boundary conditions are enforced as:

$$\sum_{i=1}^N \alpha_i \mathcal{L}_B\phi(\|x - y_i\|_2) = 0, j = N_I + 1, \dots, N, \quad (3.55)$$

or:

$$\mathbf{B}\boldsymbol{\alpha} = 0. \quad (3.56)$$

Equations (3.53) and (3.56) can now be solved as a generalized eigenvalue problem:

$$\begin{bmatrix} \mathcal{L}^I \\ \mathbf{B} \end{bmatrix} \boldsymbol{\alpha} = \lambda \begin{bmatrix} \mathbf{A}^I \\ \mathbf{0} \end{bmatrix} \boldsymbol{\alpha}, \quad (3.57)$$

where:

$$\mathbf{A}^I = \phi [(\|x_{N_I} - y_j\|_2)]_{N_I \times N} .$$

For free vibration problems, the external force is set to zero, and the solution is assumed harmonic in terms of displacements u_τ, v_τ, w_τ , as:

$$u_\tau = U_\tau(w, y)e^{i\omega t}, \quad v_\tau = V_\tau(w, y)e^{i\omega t}, \quad w_\tau = W_\tau(w, y)e^{i\omega t}, \quad (3.58)$$

where ω is the frequency of natural vibration. Substituting the harmonic expansion into equations (3.57) in terms of the amplitudes U_τ, V_τ, W_τ , one can obtain the natural frequencies and vibration modes for the shell problem, by solving the eigenproblem:

$$[\mathcal{L} - \omega^2 \mathcal{G}] \mathbf{X} = \mathbf{0}, \quad (3.59)$$

where \mathcal{L} collects all stiffness terms and \mathcal{G} collects all terms related to the inertial terms. In (3.59) \mathbf{X} are the modes of vibration associated with the natural frequencies defined as ω .

Chapter 4

Analytical solutions

This chapter discusses the analysis of some shell structures performed by means of the Navier method. First, the thermo-mechanical static analysis of functionally graded shells is considered. Here, the temperature profile along the thickness is not assumed but it is calculated by solving the Fourier's heat conduction equation. Then, shell structures that include piezoelectric layers are analyzed. Only the free vibration analysis is performed and particular attention is given to the effect of the electro-mechanical coupling on the solution. Finally, the dynamic analysis of a double-walled carbon nanotube is presented. In this case, an equivalent continuum shell model is formulated in the framework of the CUF, that permits to take into account the van der Waals interaction between the tubes. Different models contained in the CUF, refined and advanced, are used for these analyses and the capability of each model to reproduce the quasi-3D results is evaluated. Note that, in this chapter, every calculation is made referring to the double-curvature geometry and relative notation (see Section 2.2.1), even when the shell is cylindrical.

4.1 Thermo-mechanical analysis of FGM shells

In the present analysis, the temperature is seen as an external load. If the values of the temperature are known at the top and bottom surface of the plate, the thermal load can be considered in two different ways. The first method introduces an assumed profile $T(z)$ that varies linearly from the top to the bottom; the second one computes $T(z)$ by solving Fourier's heat conduction equation [210]. In this paper only the second way is considered because even for a very thin FGM layer the temperature profile is nonlinear. Therefore, the assumption of a linear $T(z)$ would cause very large errors. The temperature profile is described in the same way as the displacements in case of the Layer Wise approach:

$$T^k(\alpha, \beta, z) = F_\tau \theta_\tau^k \quad \text{with} \quad \tau = t, b, l \quad \text{and} \quad l = 2, \dots, 14, \quad (4.1)$$

The thickness functions F_τ are a combination of Legendre polynomials.

In general, for the k^{th} homogeneous orthotropic layer, the differential Fourier's equation of heat conduction reads:

$$\left(\frac{K_1^k}{H_\alpha^2} \right) \frac{\partial^2 T}{\partial \alpha^2} + \left(\frac{K_2^k}{H_\beta^2} \right) \frac{\partial^2 T}{\partial \beta^2} + K_3^k \frac{\partial^2 T}{\partial z^2} = 0. \quad (4.2)$$

The coefficients K_1^k , K_2^k and K_3^k depend on z because some layers k can be in FGM. In case of shell we can define three new coefficients $K_1^{*k} = \frac{K_1^k(z)}{H_\alpha^2}$, $K_2^{*k} = \frac{K_2^k(z)}{H_\beta^2}$ and $K_3^{*k} = K_3^k(z)$, which in a generic layer k depend on the thickness coordinate of the shell. K_1^{*k} and K_2^{*k} can depend by the thickness coordinate z for two reasons: possible use of FGM layers and/or presence of curvature in case of shells; K_3^{*k} can depend by z coordinate only in case of FGM layers. So Fourier's equation becomes:

$$K_1^{*k} \frac{\partial^2 T}{\partial \alpha^2} + K_2^{*k} \frac{\partial^2 T}{\partial \beta^2} + K_3^{*k} \frac{\partial^2 T}{\partial z^2} = 0. \quad (4.3)$$

The Eq.(4.3) has not constant coefficients in the layer k . It can be solved by introducing, for each layer k , a given number of mathematical layers (N_{ml}) in which K_1^{*k} , K_2^{*k} and K_3^{*k} can be supposed constant. In each mathematical layer, the values of H_α and H_β and the material properties of the FGM layer can be calculated at a given value of the coordinate z , so the mean value between the values at the top and bottom of mathematical layer is taken for K_1^j , K_2^j and K_3^j , while the value at the midsurface is taken for H_α and H_β . The complete procedure to calculate the temperature profile $T(z)$ and to obtain the values of θ_τ^k for the Eq.(4.1) is reported in [211], where the plate case is considered, but the Fourier's equation is formally the same ($K_1^{*k} = K_1^k$, $K_2^{*k} = K_2^k$ and $K_3^{*k} = K_3^k$ for the plate).

4.1.1 Governing equations

The procedure to obtain the governing equations is that exposed in the previous chapter (Section 3.1) for the closed form solution. Substituting the geometrical relations (Eqs.(2.29)) and the constitutive equations (Eqs.(2.46 without considering the heat flux h)) in the variational statement (Eq.2.58), one obtains the following differential equilibrium equations, for a FGM multi-layered shell subjected to thermal and mechanical loadings:

$$\delta \mathbf{u}_s^{kT} : \quad \mathbf{K}_{uu}^{k\tau sr} \mathbf{u}_\tau^k = \mathbf{K}_{u\theta}^{k\tau sr} \boldsymbol{\theta}_\tau^k + \mathbf{P}_{u\tau}^k, \quad (4.4)$$

where $(\mathbf{K}_{u\theta}^{k\tau sr} \boldsymbol{\theta}_\tau^k)$ is the thermal load. In this analysis, the material properties of FGM layers are written using the Legendre polynomials (see Eqs.(2.54)).

In order to apply the Navier method, the harmonic assumptions of Eqs.3.18 are made for the displacements and for the temperature one has:

$$\theta_s^k = \sum_{m,n} (\hat{\theta}_s^k) \sin\left(\frac{m\pi\alpha_k}{a_k}\right) \sin\left(\frac{n\pi\beta_k}{b_k}\right). \quad (4.5)$$

Therefore, the explicit expressions of fundamental nuclei $\mathbf{K}_{uu}^{k\tau sr}$ and $\mathbf{K}_{u\theta}^{k\tau sr}$ are:

- K_{uu}

$$K_{uu_{11}} = C_{55}^k J_{\alpha\beta}^{k\tau_z s_z r} + \frac{1}{R_\alpha^k} C_{55}^k (-J_\beta^{k\tau_z sr} - J_\beta^{k\tau s_z r} + \frac{1}{R_\alpha^k} J_{\beta/\alpha}^{k\tau sr}) + C_{11}^k J_{\beta/\alpha}^{k\tau sr} \alpha^2 + C_{66}^k J_{\alpha/\beta}^{k\tau sr} \beta^2,$$

$$K_{uu_{12}} = J^{k\tau sr} \alpha \beta (C_{12}^k + C_{66}^k) = K_{uu_{21}},$$

$$K_{uu_{13}} = C_{55}^k (J_\beta^{k\tau_z sr} \alpha - \frac{1}{R_\alpha^k} J_{\beta/\alpha}^{k\tau sr} \alpha) - C_{13}^k J_\beta^{k\tau s_z r} \alpha - \frac{1}{R_\alpha^k} C_{11}^k J_{\beta/\alpha}^{k\tau sr} \alpha - C_{12}^k J^{k\tau sr} \alpha \frac{1}{R_\beta^k},$$

$$K_{uu_{22}} = C_{44}^k J_{\alpha\beta}^{k\tau_z s_z r} + \frac{1}{R_\beta^k} C_{44}^k (-J_\alpha^{k\tau_z sr} - J_\alpha^{k\tau s_z r} + \frac{1}{R_\beta^k} J_{\alpha/\beta}^{k\tau sr}) + C_{22}^k J_{\alpha/\beta}^{k\tau sr} \beta^2 + C_{66}^k J_{\beta/\alpha}^{k\tau sr} \alpha^2,$$

$$K_{uu_{23}} = C_{44}^k (J_\alpha^{k\tau_z sr} \beta - \frac{1}{R_\beta^k} J_{\alpha/\beta}^{k\tau sr} \beta) - C_{23}^k J_\alpha^{k\tau s_z r} \beta - \frac{1}{R_\beta^k} C_{22}^k J_{\alpha/\beta}^{k\tau sr} \beta - \frac{1}{R_\alpha^k} C_{12}^k J^{k\tau sr} \beta,$$

$$K_{uu_{31}} = C_{55}^k J_\beta^{k\tau s_z r} \alpha - C_{55}^k \frac{1}{R_\alpha^k} J_{\beta/\alpha}^{k\tau sr} \alpha - C_{13}^k J_\beta^{k\tau_z sr} \alpha - \frac{1}{R_\alpha^k} C_{11}^k J_{\beta/\alpha}^{k\tau sr} \alpha - \frac{1}{R_\beta^k} C_{12}^k J^{k\tau sr} \alpha,$$

$$K_{uu_{32}} = C_{44}^k (J_\alpha^{k\tau s_z r} \beta - \frac{1}{R_\beta^k} J_{\alpha/\beta}^{k\tau sr} \beta) - C_{23}^k J_\alpha^{k\tau_z sr} \beta - \frac{1}{R_\beta^k} C_{22}^k J_{\alpha/\beta}^{k\tau sr} \beta - \frac{1}{R_\alpha^k} C_{12}^k J^{k\tau sr} \beta,$$

$$\begin{aligned} K_{uu_{33}} &= C_{55}^k J_{\beta/\alpha}^{k\tau sr} \alpha^2 + C_{44}^k J_{\alpha/\beta}^{k\tau sr} \beta^2 + C_{33}^k J_{\alpha\beta}^{k\tau_z s_z r} + \frac{1}{R_\alpha^k} (\frac{1}{R_\alpha^k} C_{11}^k J_{\beta/\alpha}^{k\tau sr} + C_{13}^k J_\beta^{k\tau s_z r} + C_{13}^k J_\beta^{k\tau_z sr}), \\ &+ \frac{2}{R_\alpha^k R_\beta^k} J^{k\tau sr} C_{12}^k + \frac{1}{R_\beta^k} (\frac{1}{R_\beta^k} C_{22}^k J_{\alpha/\beta}^{k\tau sr} + C_{23}^k J_\alpha^{k\tau_z sr} + C_{23}^k J_\alpha^{k\tau s_z r}), \end{aligned}$$

- $K_{u\theta}$

$$K_{u\theta_1} = \alpha J_\beta^{k\tau sr} \lambda_{p1}^k,$$

$$K_{u\theta_2} = \beta J_\alpha^{k\tau sr} \lambda_{p2}^k,$$

$$K_{u\theta_3} = -J_\beta^{k\tau sr} \frac{1}{R_\alpha^k} \lambda_{p1}^k - J_\alpha^{k\tau sr} \frac{1}{R_\beta^k} \lambda_{p2}^k - J_{\alpha\beta}^{k\tau_z sr} \lambda_{n3}^k,$$

where the following notation is introduced:

$$\begin{aligned}
(J^{k\tau sr}, J_{\alpha}^{k\tau sr}, J_{\beta}^{k\tau sr}, J_{\frac{\alpha}{\beta}}^{k\tau sr}, J_{\frac{\beta}{\alpha}}^{k\tau sr}, J_{\alpha\beta}^{k\tau sr}) &= \int_{A_k} F_r F_{\tau} F_s \left(1, H_{\alpha}^k, H_{\beta}^k, \frac{H_{\alpha}^k}{H_{\beta}^k}, \frac{H_{\beta}^k}{H_{\alpha}^k}, H_{\alpha}^k H_{\beta}^k \right) dz, \\
(J^{k\tau_z sr}, J_{\alpha}^{k\tau_z sr}, J_{\beta}^{k\tau_z sr}, J_{\frac{\alpha}{\beta}}^{k\tau_z sr}, J_{\frac{\beta}{\alpha}}^{k\tau_z sr}, J_{\alpha\beta}^{k\tau_z sr}) &= \int_{A_k} F_r \frac{\partial F_{\tau}}{\partial z} F_s \left(1, H_{\alpha}^k, H_{\beta}^k, \frac{H_{\alpha}^k}{H_{\beta}^k}, \frac{H_{\beta}^k}{H_{\alpha}^k}, H_{\alpha}^k H_{\beta}^k \right) dz, \\
(J^{k\tau s_z r}, J_{\alpha}^{k\tau s_z r}, J_{\beta}^{k\tau s_z r}, J_{\frac{\alpha}{\beta}}^{k\tau s_z r}, J_{\frac{\beta}{\alpha}}^{k\tau s_z r}, J_{\alpha\beta}^{k\tau s_z r}) &= \int_{A_k} F_r F_{\tau} \frac{\partial F_s}{\partial z} \left(1, H_{\alpha}^k, H_{\beta}^k, \frac{H_{\alpha}^k}{H_{\beta}^k}, \frac{H_{\beta}^k}{H_{\alpha}^k}, H_{\alpha}^k H_{\beta}^k \right) dz, \\
(J^{k\tau_z s_z r}, J_{\alpha}^{k\tau_z s_z r}, J_{\beta}^{k\tau_z s_z r}, J_{\frac{\alpha}{\beta}}^{k\tau_z s_z r}, J_{\frac{\beta}{\alpha}}^{k\tau_z s_z r}, J_{\alpha\beta}^{k\tau_z s_z r}) &= \int_{A_k} F_r \frac{\partial F_{\tau}}{\partial z} \frac{\partial F_s}{\partial z} \left(1, H_{\alpha}^k, H_{\beta}^k, \frac{H_{\alpha}^k}{H_{\beta}^k}, \frac{H_{\beta}^k}{H_{\alpha}^k}, H_{\alpha}^k H_{\beta}^k \right) dz,
\end{aligned}$$

and $\alpha = m\pi/a$, $\beta = n\pi/b$.

If $\theta_{\tau}^k = 0$ in Eq.(5.3), only a mechanical load is considered. Vice versa, if $\mathbf{P}_{u\tau}^k = 0$, only a thermal load is applied. The fundamental nuclei are formally the same in case of "classical" or FGM layers, the only difference is the assembling loop on index r which accounts for the variation of the material properties through the thickness.

4.1.2 Results and discussion

In this section a shell comprising a single functionally graded layer, is analyzed. The geometry is given by Ren: $R_{\alpha} \rightarrow \infty$, $R_{\beta} = 10\text{m}$, span angle in β -direction $\phi = \pi/3$, $a = 1\text{m}$. As a typical example for high-temperature applications, the constituent materials of the functionally graded shell are taken to be Monel (70Ni-30Cu), a nickel-based alloy, and the ceramic zirconia (ZrO_2). The required material properties are those reported in [212]:

$$\begin{aligned}
B_m &= 227.24 \text{ GPa}, \quad \mu_m = 65.55 \text{ GPa}, \quad \alpha_m = 15 \times 10^{-6} / \text{K}, \quad K_m = 25 \text{ W/mK}, \quad \text{for Monel}, \\
B_c &= 125.83 \text{ GPa}, \quad \mu_c = 58.08 \text{ GPa}, \quad \alpha_c = 10 \times 10^{-6} / \text{K}, \quad K_c = 2.09 \text{ W/mK}, \quad \text{for zirconia}.
\end{aligned}$$

For this two-phase composite material different micromechanical models can be applied for the computation of the effective local material properties. According to [212], the following formulas are chosen:

- The effective bulk modulus B and shear modulus μ are given by the mean field estimate of Mori and Tanaka [213],[214]:

$$\frac{B - B_m}{B_c - B_m} = \frac{V_2}{1 + (1 - V_2) \frac{B_c - B_m}{B_m + \frac{4}{3}\mu_m}}, \quad (4.6)$$

$$\frac{\mu - \mu_m}{\mu_c - \mu_m} = \frac{V_2}{1 + (1 - V_2) \frac{\mu_c - \mu_m}{\mu_m + f_1}}, \quad \text{with} \quad f_1 = \frac{\mu_m(9B_m + 8\mu_m)}{6(B_m + 2\mu_m)}. \quad (4.7)$$

- The effective heat conduction coefficient K is given by the model of Hatta and Taya [215]:

$$\frac{K - K_m}{K_c - K_m} = \frac{V_2}{1 + (1 - V_2) \frac{K_c - K_m}{3K_m}}. \quad (4.8)$$

- For the coefficient of thermal expansion α a correspondence relation holds [216],[217], reading:

$$\frac{\alpha - \alpha_m}{\alpha_c - \alpha_m} = \frac{\frac{1}{B} - \frac{1}{B_m}}{\frac{1}{B_c} - \frac{1}{B_m}}. \quad (4.9)$$

In Eqs.(4.6) to (4.9), the indices m and c refer to the metallic and ceramic phase, respectively. V_2 is the volume fraction of the ceramic phase that is assumed for the computations as:

$$V_2 = V_c = (z/h)^{n_g}, \quad (4.10)$$

where by changing the exponent n_g different material gradients can be accomplished. Figure 4.1 shows the through-thickness distribution of the volume fraction V_c of the ceramic phase and the resulting evolution of the bulk modulus. The Young's modulus and the Poisson's ratio can be calculated directly from the bulk modulus and the shear modulus.

At the top surface, the shell is subjected to pure mechanical or pure thermal, transverse

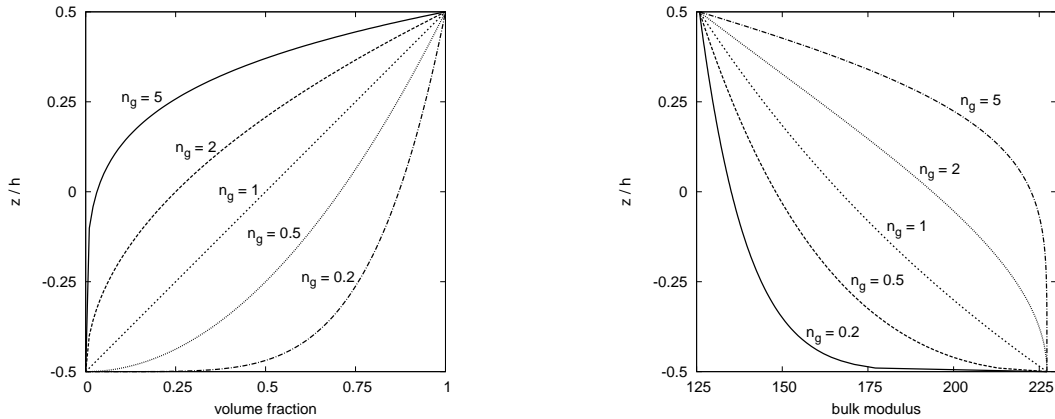


Figure 4.1: Through-thickness distribution of the volume fraction V_c of the ceramic phase (left) and of the bulk modulus (right).

bi-sinusoidal loads, reading:

$$p_z^+ = \hat{p}_z^+ \sin\left(\frac{m\pi\alpha}{a}\right) \sin\left(\frac{n\pi\beta}{b}\right), \quad T^+ = \hat{T}^+ \sin\left(\frac{m\pi\alpha}{a}\right) \sin\left(\frac{n\pi\beta}{b}\right). \quad (4.11)$$

Here m, n are the wave numbers and a, b the shell dimensions, respectively. A quantity with a superimposed hat denotes the amplitude of the respective load. Since a linear theory is considered, more complicated load cases can be accomplished by superimposing the pure thermal and mechanical contributions.

As an analytical Navier-type solution is employed, the shell is assumed to be simply supported, i.e. the boundary conditions read:

$$\begin{aligned} u_\beta = u_z = 0 \quad \text{at} \quad \alpha = 0, a, \\ u_\alpha = u_z = 0 \quad \text{at} \quad \beta = 0, b, \\ T = 0 \quad \text{at} \quad \alpha = 0, a \quad \text{and} \quad \beta = 0, b, \end{aligned} \quad (4.12)$$

which is fulfilled by the assumed harmonic in-plane displacement and temperature fields, compare Eqs.(3.18). In addition, $m = n = 1$ is assumed for the wave numbers. As done in [212], non-dimensionalized quantities are introduced:

$$\bar{u}_i = \frac{\hat{u}_i(z)}{P a}, \quad \bar{\sigma}_{ij} = \frac{\hat{\sigma}_{ij}(z)}{P B^*}, \quad \bar{T} = \frac{\alpha^* \hat{T}(z)}{P}, \quad (4.13)$$

where either $P = \hat{p}_z^+ / B^*$ or $P = \alpha^* \hat{T}^+$ is taken for the applied load p_z^+ or for the applied temperature T^+ at the top, respectively. The scale factors are $B^* = 1$ GPa and $\alpha^* = 1 \times 10^6$. The indices i and j can be α, β and z .

Exact solutions about thermo-mechanical analysis of FGM shells have not been found in literature. To validate the considered shell theories, a quasi-3D solution is considered. This solution is obtained by introducing a number of fictitious mathematical layers in the FGM layer, in which the material properties are taken constant in the thickness direction. The number of mathematical layers is chosen to coincide with the one leading to convergent solutions, that is 100. A layer-wise theory with an order of expansion equal to 4 is used to calculate the solution.

Considering that the values of the temperature at the top and bottom surface of the shell are, respectively:

$$\bar{T}^+ = 1 \quad \text{at} \quad z = +\frac{h}{2}, \quad \bar{T}^- = 0 \quad \text{at} \quad z = -\frac{h}{2}, \quad (4.14)$$

where h is the thickness of the shell, the Figure 4.2 depicts the through-thickness distribution of the non-dimensionalized temperature \bar{T} for a shell thickness ratio of $R_\beta / h = 10$, $n_g = 2$ and different orders of expansion N . It can be seen that it is necessary an order of expansion equal to 14 to reach the convergence for temperature. For implementation reasons, the same order of expansion is used to approximate the displacement components, but it will be shown that in pure-mechanical case a lower value of N is sufficient to obtain the required accuracy. Furthermore, one can note that the temperature distribution is strongly nonlinear which contradicts the assumption of a linear temperature variation often found in the literature. In [211] it is demonstrated that a linear profile can be assumed only for very thin "classical" layers; as far as the alteration of the temperature distribution due to different material gradients n_g , the influence of the material composition is shown to be considerable.

The results obtained by CUF extended to FGM shells under pure thermal or pure mechanical loading are compared with quasi-3D solution. Tables 4.1 and 4.2 provide results for the displacement components in non-dimensionalized form for different

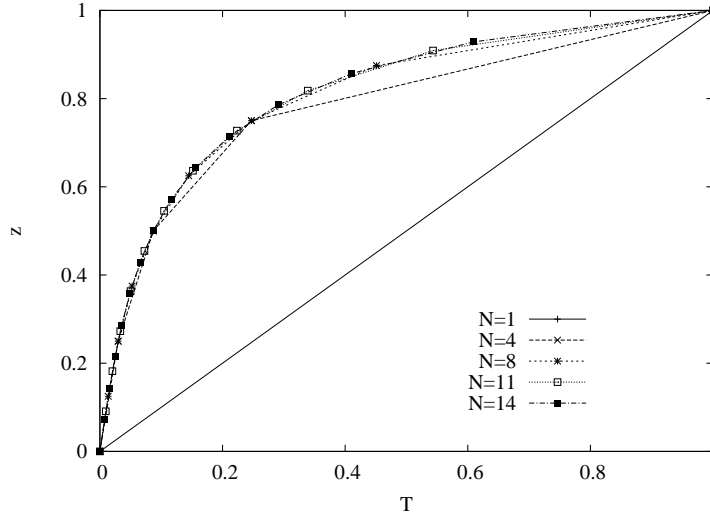


Figure 4.2: Ren shell ($n_g = 2$, $R_\beta/h = 10$). Calculated temperature profile T .

shell thickness ratios and exponential index $n_g = 2$. It can be concluded that Unified Formulation yields very accurate results compared to quasi-3D solution for both mechanical and thermal case and even for very thick shells.

In Figure 4.3 the through-thickness distribution of the transverse deflection u_z is

	<i>Ref</i>	$R_\beta/h = 10$			<i>Ref</i>	$R_\beta/h = 500$		
		$N = 1$	$N = 3$	$N = 6$		$N = 1$	$N = 3$	$N = 6$
$\bar{w}(t)$	0.0039	0.0032	0.0040	0.0039	2.2199	2.0431	2.2199	2.2199
$\bar{w}(m)$	0.0021	0.0021	0.0022	0.0021	2.2212	2.0437	2.2211	2.2212
$\bar{w}(b)$	0.0013	0.0011	0.0013	0.0013	2.2214	2.0443	2.2214	2.2214
$\bar{u}(t)$	-0.0012	-0.0004	-0.0011	-0.0012	-0.4870	-0.4580	-0.4870	-0.4870
$\bar{u}(m)$	0.0006	0.0003	0.0006	0.0006	0.2099	0.1832	0.2100	0.2100
$\bar{u}(b)$	0.0010	0.0011	0.0010	0.0010	0.9072	0.8244	0.9071	0.9072

Table 4.1: Mechanical load. Non-dimensional transverse displacement \bar{w} and in-plane displacement \bar{u} at top (t), middle (m) and bottom (b) of the considered shell ($n_g = 2$). *Ref* is the solution obtained with $N_{ml} = 100$ mathematical layers.

shown for different material gradients n_g . It can be clearly seen that in the case of thermal loading the transverse deflection varies considerably through the thickness, in respect to the pure-mechanical case, even if the shell is very thin ($R_\beta/h = 100$). This is due to the combined effects of the varying thermal field (see Fig.4.2) as well as the altering mechanical properties. Therefore, the usual assumption of a constant through-thickness distribution of u_z made by most lower order shell theories is not justified in the thermal case. However, in the case of a pure mechanical loading, the influence of different material gradients n_g is less pronounced. Furthermore, the variation of the

	<i>Ref</i>	$R_\beta/h = 50$			<i>Ref</i>	$R_\beta/h = 1000$		
		$N = 2$	$N = 8$	$N = 14$		$N = 2$	$N = 8$	$N = 14$
$\bar{w}(t)$	7.1337	8.8684	7.1548	7.1361	43.590	48.034	43.653	43.600
$\bar{w}(m)$	6.4131	8.0312	6.4331	6.4153	43.553	47.990	43.617	43.563
$\bar{w}(b)$	6.1942	7.8766	6.2143	6.1964	43.554	47.997	43.618	43.564
$\bar{u}(t)$	-3.5466	-4.1620	-3.5545	-3.5477	-1.7868	-1.8872	-1.7886	-1.7871
$\bar{u}(m)$	-1.4532	-1.5217	-1.4547	-1.4535	-1.1021	-1.1326	-1.1029	-1.1023
$\bar{u}(b)$	0.4833	0.9074	0.4880	0.4837	-0.4178	-0.3785	-0.4176	-0.4178

Table 4.2: Thermal load. Non-dimensional transverse displacement \bar{w} and in-plane displacement \bar{u} at top (t), middle (m) and bottom (b) of the considered shell ($n_g = 2$). *Ref* is the solution obtained with $N_{ml} = 100$ mathematical layers.

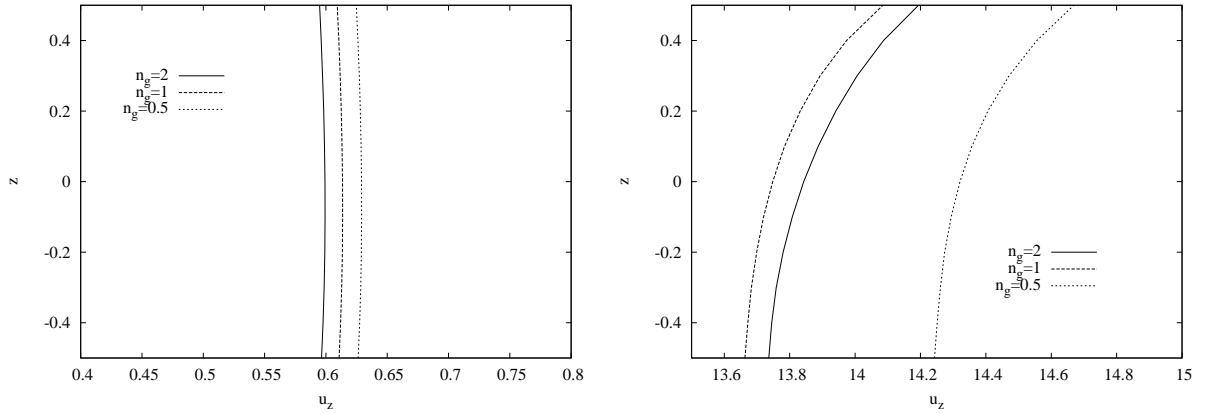


Figure 4.3: Ren shell ($R_\beta/h = 100$). Transverse displacement u_z : mechanical load [N=6](left); thermal load [N=14] (right).

transverse deflection u_z through the thickness is small so in the mechanical case the assumption of a constant through-thickness distribution is valid.

Figures 4.4 and 4.5 show the through-thickness distribution of the transverse shear and normal stresses, respectively. It can be seen that load boundary conditions are verified for $N = 6$ in the mechanical case and for $N = 14$ in the thermal case.

One can conclude that the use of higher order shell theories is mandatory in order

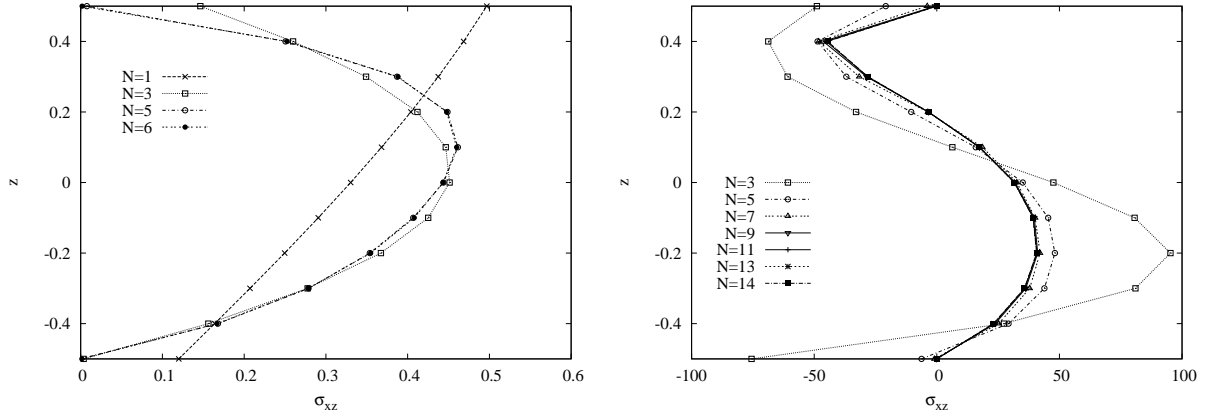


Figure 4.4: Ren shell ($n_g = 2$, $R_\beta/h = 10$). Transverse shear stress $\sigma_{\alpha z}$: mechanical load (left); thermal load (right).

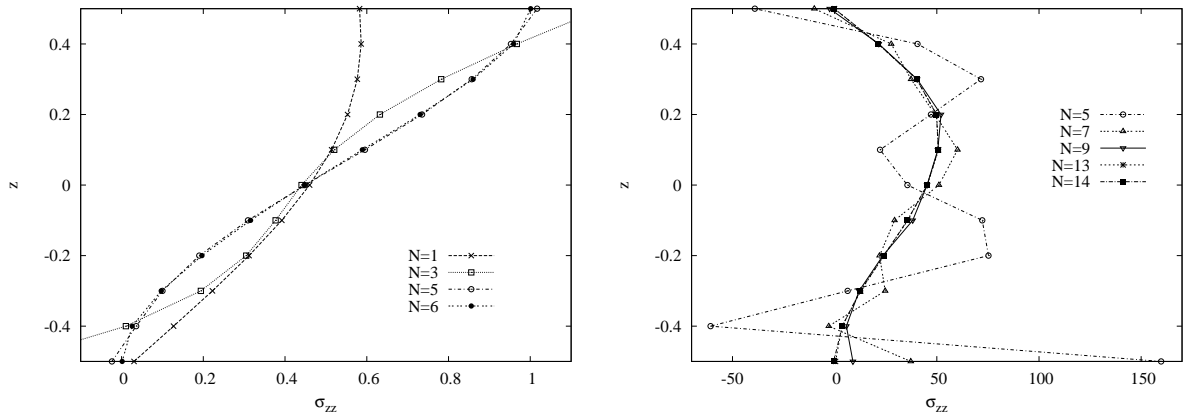


Figure 4.5: Ren shell ($n_g = 2$, $R_\beta/h = 10$). Transverse normal stress σ_{zz} : mechanical load (left); thermal load (right).

to capture all the effects of the displacement and stress distributions. By comparing the cases of thermal and mechanical loading, it is shown that a thermal load requires higher order thickness assumptions. As stated in the previous section, this is due to the coupling between the thermal and the mechanical field which claims higher order thickness assumptions to obtain the same accuracy.

For more details about the thermo-mechanical analysis of FGM shells, one can refer to [133].

4.2 Electromechanical analysis of piezoelectric shells

In case of electro-mechanical problem the assumed variables are the displacements \mathbf{u} and the electric potential Φ . If Reissner's Mixed Variational Theorem (RMVT) is used, other variables such as transverse shear/normal stresses σ_n and/or transverse normal electric displacement \mathcal{D}_n can be also assumed. In this work only the displacement \mathbf{u} can be modelled as ESL or LW, the other variables are always assumed in LW form. So a model is said ESL or LW depending on the choice made for the displacement variables.

Therefore, the expansions of variables in z direction are:

$$(\mathbf{u}^k, \sigma_{nM}^k, \Phi^k, \mathcal{D}_{nM}^k) = F_\tau (\mathbf{u}^k, \sigma_{nM}^k, \Phi^k, \mathcal{D}_{nM}^k)_\tau, \quad (4.15)$$

where $\tau = t, b, r$, with $r = 2, \dots, N$ or $\tau = 0, 1, \dots, N$ only for the displacements, if the description is ESL.

4.2.1 Governing equations

In the electro-mechanical case, there are four different ways to derive the differential equilibrium equations, depending on the variational statement used.

The first is the simple derivation from the PVD (Eq.(2.60)), in which the displacements \mathbf{u} and the electric potential Φ are modelled. Substituting the geometrical relations that link the strains to the displacements (Eqs.(2.29)) and the electrical field to the electric potential (Eqs.(2.35)), the constitutive equations (Eqs.(2.50)) and the variable assumptions (Eqs.(4.15)) in the PVD, the following governing equations are obtained:

$$\begin{aligned} \delta \mathbf{u}_s^k : \mathbf{K}_{uu}^{k\tau s} \mathbf{u}_\tau^k + \mathbf{K}_{u\Phi}^{k\tau s} \Phi_\tau^k &= \mathbf{P}_{us}^k - \mathbf{M}^{k\tau s} \ddot{\mathbf{u}}_\tau^k, \\ \delta \Phi_s^k : \mathbf{K}_{\Phi u}^{k\tau s} \mathbf{u}_\tau^k + \mathbf{K}_{\Phi\Phi}^{k\tau s} \Phi_\tau^k &= \mathbf{P}_{\Phi s}^k, \end{aligned} \quad (4.16)$$

where $\ddot{\mathbf{u}}_\tau^k$ denotes the second derivative with respect to the time of the displacement components. $\mathbf{M}^{k\tau s}$ is the fundamental nucleus for the inertial array. $\mathbf{K}_{uu}^{k\tau s}$, $\mathbf{K}_{u\Phi}^{k\tau s}$, $\mathbf{K}_{\Phi u}^{k\tau s}$ and $\mathbf{K}_{\Phi\Phi}^{k\tau s}$ are the so-called fundamental nuclei of electro-mechanical stiffness array. \mathbf{P}_{us}^k and $\mathbf{P}_{\Phi s}^k$ are the consistent variationally mechanical and electric loads, respectively. Boundary conditions of Dirichlet type are:

$$\begin{aligned} \mathbf{u}_\tau^k &= \bar{\mathbf{u}}_\tau^k, \\ \Phi_\tau^k &= \bar{\Phi}_\tau^k, \end{aligned} \quad (4.17)$$

Boundary conditions of Neumann type are:

$$\begin{aligned} \Pi_{uu}^{k\tau s} \mathbf{u}_\tau^k + \Pi_{u\Phi}^{k\tau s} \Phi_\tau^k &= \Pi_{uu}^{k\tau s} \bar{\mathbf{u}}_\tau^k + \Pi_{u\Phi}^{k\tau s} \bar{\Phi}_\tau^k, \\ \Pi_{\Phi u}^{k\tau s} \mathbf{u}_\tau^k + \Pi_{\Phi\Phi}^{k\tau s} \Phi_\tau^k &= \Pi_{\Phi u}^{k\tau s} \bar{\mathbf{u}}_\tau^k + \Pi_{\Phi\Phi}^{k\tau s} \bar{\Phi}_\tau^k, \end{aligned} \quad (4.18)$$

where $\Pi_{uu}^{k\tau s}$, $\Pi_{u\Phi}^{k\tau s}$, $\Pi_{\Phi u}^{k\tau s}$ and $\Pi_{\Phi\Phi}^{k\tau s}$ are the fundamental nuclei of electro-mechanical boundary conditions.

Another way to derive the governing equations is the use of the RMVT (Eq.(2.63)) in which the stresses σ_n are modelled with the displacements and the electric potential. Substituting the geometrical relations (Eqs.(2.29) and (2.35)) and the modified constitutive equations (Eqs.(2.64)) in the Eq.(2.63), one has:

$$\begin{aligned}\delta \mathbf{u}_s^k : \mathbf{K}_{uu}^{k\tau s} \mathbf{u}_\tau^k + \mathbf{K}_{u\sigma}^{k\tau s} \sigma_{n\tau}^k + \mathbf{K}_{u\Phi}^{k\tau s} \Phi_\tau^k &= \mathbf{P}_{us}^k - \mathbf{M}^{k\tau s} \ddot{\mathbf{u}}_\tau^k, \\ \delta \sigma_{ns}^k : \mathbf{K}_{\sigma u}^{k\tau s} \mathbf{u}_\tau^k + \mathbf{K}_{\sigma\sigma}^{k\tau s} \sigma_{n\tau}^k + \mathbf{K}_{\sigma\Phi}^{k\tau s} \Phi_\tau^k &= 0, \\ \delta \Phi_s^k : \mathbf{K}_{\Phi u}^{k\tau s} \mathbf{u}_\tau^k + \mathbf{K}_{\Phi\sigma}^{k\tau s} \sigma_{n\tau}^k + \mathbf{K}_{\Phi\Phi}^{k\tau s} \Phi_\tau^k &= \mathbf{P}_{\Phi s}^k.\end{aligned}\quad (4.19)$$

Nine fundamental nuclei are obtained which are completely different from those obtained from the PVD.

Corresponding boundary conditions of Dirichlet type are:

$$\begin{aligned}\mathbf{u}_\tau^k &= \bar{\mathbf{u}}_\tau^k, \\ \Phi_\tau^k &= \bar{\Phi}_\tau^k,\end{aligned}\quad (4.20)$$

while the Neumann ones are:

$$\begin{aligned}\Pi_{uu}^{k\tau s} \mathbf{u}_\tau^k + \Pi_{u\sigma}^{k\tau s} \sigma_{n\tau}^k + \Pi_{u\Phi}^{k\tau s} \Phi_\tau^k &= \Pi_{uu}^{k\tau s} \bar{\mathbf{u}}_\tau^k + \Pi_{u\sigma}^{k\tau s} \bar{\sigma}_{n\tau}^k + \Pi_{u\Phi}^{k\tau s} \bar{\Phi}_\tau^k, \\ \Pi_{\Phi u}^{k\tau s} \mathbf{u}_\tau^k + \Pi_{\Phi\sigma}^{k\tau s} \sigma_{n\tau}^k + \Pi_{\Phi\Phi}^{k\tau s} \Phi_\tau^k &= \Pi_{\Phi u}^{k\tau s} \bar{\mathbf{u}}_\tau^k + \Pi_{\Phi\sigma}^{k\tau s} \bar{\sigma}_{n\tau}^k + \Pi_{\Phi\Phi}^{k\tau s} \bar{\Phi}_\tau^k.\end{aligned}\quad (4.21)$$

It is possible to conveniently model a priori the transverse normal electric displacement \mathcal{D}_z in the place of transverse stresses by using the RMVT in the form of Eq.(2.65). In this case, the governing equations, obtained by substituting in Eq.(2.65) the geometrical relations (Eqs.(2.29) and (2.35)) and the modified constitutive equations (Eqs.(2.66)), read:

$$\begin{aligned}\delta \mathbf{u}_s^k : \mathbf{K}_{uu}^{k\tau s} \mathbf{u}_\tau^k + \mathbf{K}_{uD}^{k\tau s} \mathcal{D}_{n\tau}^k + \mathbf{K}_{u\Phi}^{k\tau s} \Phi_\tau^k &= \mathbf{P}_{us}^k - \mathbf{M}^{k\tau s} \ddot{\mathbf{u}}_\tau^k, \\ \delta \mathcal{D}_{ns}^k : \mathbf{K}_{Du}^{k\tau s} \mathbf{u}_\tau^k + \mathbf{K}_{DD}^{k\tau s} \mathcal{D}_{n\tau}^k + \mathbf{K}_{D\Phi}^{k\tau s} \Phi_\tau^k &= 0, \\ \delta \Phi_s^k : \mathbf{K}_{\Phi u}^{k\tau s} \mathbf{u}_\tau^k + \mathbf{K}_{\Phi D}^{k\tau s} \mathcal{D}_{n\tau}^k + \mathbf{K}_{\Phi\Phi}^{k\tau s} \Phi_\tau^k &= \mathbf{P}_{\Phi s}^k.\end{aligned}\quad (4.22)$$

Corresponding boundary conditions of Dirichlet type are:

$$\begin{aligned}\mathbf{u}_s^k &= \bar{\mathbf{u}}_s^k, \\ \Phi_s^k &= \bar{\Phi}_s^k,\end{aligned}\quad (4.23)$$

the corresponding Neumann ones are:

$$\begin{aligned}\Pi_{uu}^{k\tau s} \mathbf{u}_\tau^k + \Pi_{uD}^{k\tau s} \mathcal{D}_{n\tau}^k + \Pi_{u\Phi}^{k\tau s} \Phi_\tau^k &= \Pi_{uu}^{k\tau s} \bar{\mathbf{u}}_\tau^k + \Pi_{uD}^{k\tau s} \bar{\mathcal{D}}_{n\tau}^k + \Pi_{u\Phi}^{k\tau s} \bar{\Phi}_\tau^k, \\ \Pi_{\Phi u}^{k\tau s} \mathbf{u}_\tau^k + \Pi_{\Phi D}^{k\tau s} \mathcal{D}_{n\tau}^k + \Pi_{\Phi\Phi}^{k\tau s} \Phi_\tau^k &= \Pi_{\Phi u}^{k\tau s} \bar{\mathbf{u}}_\tau^k + \Pi_{\Phi D}^{k\tau s} \bar{\mathcal{D}}_{n\tau}^k + \Pi_{\Phi\Phi}^{k\tau s} \bar{\Phi}_\tau^k.\end{aligned}\quad (4.24)$$

Finally, one can decide to model a priori both the transverse stresses and the transverse normal electric displacement and the governing equations can be derived from the RMVT in the form of Eqs.(2.67), substituting the geometrical relations (Eqs.(2.29) and

(2.35)) and the modified constitutive equations (Eqs.(2.68)). In this case, the equations are:

$$\begin{aligned}
\delta \mathbf{u}_s^k : \mathbf{K}_{uu}^{k\tau s} \mathbf{u}_\tau^k + \mathbf{K}_{u\sigma}^{k\tau s} \boldsymbol{\sigma}_{n\tau}^k + \mathbf{K}_{u\Phi}^{k\tau s} \Phi_\tau^k + \mathbf{K}_{uD}^{k\tau s} \mathcal{D}_{n\tau}^k &= \mathbf{P}_{us}^k - \mathbf{M}^{k\tau s} \ddot{\mathbf{u}}_\tau^k , \\
\delta \boldsymbol{\sigma}_{ns}^k : \mathbf{K}_{\sigma u}^{k\tau s} \mathbf{u}_\tau^k + \mathbf{K}_{\sigma\sigma}^{k\tau s} \boldsymbol{\sigma}_{n\tau}^k + \mathbf{K}_{\sigma\Phi}^{k\tau s} \Phi_\tau^k + \mathbf{K}_{\sigma\mathcal{D}}^{k\tau s} \mathcal{D}_{n\tau}^k &= 0 , \\
\delta \Phi_s^k : \mathbf{K}_{\Phi u}^{k\tau s} \mathbf{u}_\tau^k + \mathbf{K}_{\Phi\sigma}^{k\tau s} \boldsymbol{\sigma}_{n\tau}^k + \mathbf{K}_{\Phi\Phi}^{k\tau s} \Phi_\tau^k + \mathbf{K}_{\Phi\mathcal{D}}^{k\tau s} \mathcal{D}_{n\tau}^k &= \mathbf{P}_{\Phi s}^k , \\
\delta \mathcal{D}_{ns}^k : \mathbf{K}_{\mathcal{D}u}^{k\tau s} \mathbf{u}_\tau^k + \mathbf{K}_{\mathcal{D}\sigma}^{k\tau s} \boldsymbol{\sigma}_{n\tau}^k + \mathbf{K}_{\mathcal{D}\Phi}^{k\tau s} \Phi_\tau^k + \mathbf{K}_{\mathcal{D}\mathcal{D}}^{k\tau s} \mathcal{D}_{n\tau}^k &= 0 .
\end{aligned} \tag{4.25}$$

Dirichlet type boundary conditions are:

$$\begin{aligned}
\mathbf{u}_\tau^k &= \bar{\mathbf{u}}_\tau^k , \\
\Phi_\tau^k &= \bar{\Phi}_\tau^k ,
\end{aligned} \tag{4.26}$$

the Neumann ones are:

$$\begin{aligned}
\Pi_{uu}^{k\tau s} \mathbf{u}_\tau^k + \Pi_{u\sigma}^{k\tau s} \boldsymbol{\sigma}_{nM\tau}^k + \Pi_{u\Phi}^{k\tau s} \Phi_\tau^k + \Pi_{uD}^{k\tau s} \mathcal{D}_{nM\tau}^k &= \Pi_{uu}^{k\tau s} \bar{\mathbf{u}}_\tau^k + \Pi_{u\sigma}^{k\tau s} \bar{\boldsymbol{\sigma}}_{nM\tau}^k \\
+ \Pi_{u\Phi}^{k\tau s} \bar{\Phi}_\tau^k + \Pi_{uD}^{k\tau s} \bar{\mathcal{D}}_{nM\tau}^k , \\
\Pi_{\Phi u}^{k\tau s} \mathbf{u}_\tau^k + \Pi_{\Phi\sigma}^{k\tau s} \boldsymbol{\sigma}_{nM\tau}^k + \Pi_{\Phi\Phi}^{k\tau s} \Phi_\tau^k + \Pi_{\Phi\mathcal{D}}^{k\tau s} \mathcal{D}_{nM\tau}^k &= \Pi_{\Phi u}^{k\tau s} \bar{\mathbf{u}}_\tau^k + \Pi_{\Phi\sigma}^{k\tau s} \bar{\boldsymbol{\sigma}}_{nM\tau}^k \\
+ \Pi_{\Phi\Phi}^{k\tau s} \bar{\Phi}_\tau^k + \Pi_{\Phi\mathcal{D}}^{k\tau s} \bar{\mathcal{D}}_{nM\tau}^k .
\end{aligned} \tag{4.27}$$

In all the cases, the inertial array has the following expression:

$$\mathbf{M}^{k\tau s} = \int_{A_k} \mathbf{I} \rho^k F_\tau F_s H_\alpha^k H_\beta^k dz , \tag{4.28}$$

where ρ^k is the mass density for each layer k , and \mathbf{I} is the identity matrix of dimension $[3 \times 3]$.

Navier-type closed form solutions are applied to the proposed governing equations and the following harmonic assumptions can be made for the field variables:

$$\begin{aligned}
(u_{\alpha\tau}^k, \sigma_{\alpha z\tau}^k) &= \sum_{m,n} (\hat{U}_{\alpha\tau}^k, \hat{S}_{\alpha z\tau}^k) \cos \frac{m\pi\alpha_k}{a_k} \sin \frac{n\pi\beta_k}{b_k} e^{i\omega_{mn}\hat{t}} , & k = 1, N_l \\
(u_{\beta\tau}^k, \sigma_{\beta z\tau}^k) &= \sum_{m,n} (\hat{U}_{\beta\tau}^k, \hat{S}_{\beta z\tau}^k) \sin \frac{m\pi\alpha_k}{a_k} \cos \frac{n\pi\beta_k}{b_k} e^{i\omega_{mn}\hat{t}} , & \tau = t, b, r \\
(u_{z\tau}^k, \sigma_{zz\tau}^k, \Phi_\tau^k, \mathcal{D}_{n\tau}^k) &= \sum_{m,n} (\hat{U}_{z\tau}^k, \hat{S}_{zz\tau}^k, \hat{\Phi}_\tau^k, \hat{\mathcal{D}}_{n\tau}^k) \sin \frac{m\pi\alpha_k}{a_k} \sin \frac{n\pi\beta_k}{b_k} e^{i\omega_{mn}\hat{t}} , & r = 2, N
\end{aligned} \tag{4.29}$$

in which the quantities with $\hat{}$ indicate the amplitudes. These assumptions correspond to the simply-supported boundary conditions. Upon substitution of Eq.(4.29), the governing equations on Ω^k assume the form of a linear system of algebraic equations in the domain while the boundary conditions are exactly fulfilled. For the sake of brevity, the explicit expression of all the fundamental nuclei in closed-algebraic form is here omitted but it can be found in [98].

In the electromechanical case, the free vibration analysis leads to the following eigenvalue problem:

$$\mathbf{K}^* \hat{\mathbf{U}} = \omega_{mn}^2 \mathbf{M} \hat{\mathbf{U}} , \tag{4.30}$$

where \mathbf{K}^* is the equivalent stiffness matrix obtained by means of static condensation (for further details see [218], [219]). Only the free vibration analysis is investigated in this work and the external loadings (mechanical and electrical) are therefore set to zero and the relative boundary conditions are exactly fulfilled.

4.2.2 Results and discussion

The free vibrations problem for multilayered shells including piezoelectric layers has been investigated. By imposing the waves number in the in-plane directions, the corresponding vibration modes are obtained. The number of frequencies is equal to the number of degrees of freedom through the thickness according to the considered kinematics.

For the analysis, a multilayered ring shell is investigated. The geometry of the ring is given in Figure 4.6. The free vibrations problem is investigated by considering the closed circuit configuration ($\Phi_t = \Phi_b = 0$). The elastic and piezoelectric properties of the employed materials and the geometrical parameters are given in Table 4.3.

The cylindrical ring shell is made of two layers, an internal layer in Titanium and an external one in piezoelectric PZT-4 with a thickness that is 1/4 of the total thickness. The free dimensional solution for this case is given by Heyliger et alii [220]: the first fundamental frequency in Hz ($f = \frac{\omega}{2\pi}$) is given by imposing $m = 0$ and $n = 4, 8, 12, 16, 20$. The thickness ratio is a constant and it is around 70.

Table 4.4 gives the first fundamental frequencies in the case of CLT and FSDT. Tables 4.5 and 4.6 consider the ESL models and the ESL models with the Murakami zigzag function in the case of PVD extended to an electro-mechanical problem (PVD(\mathbf{u}, Φ)). LW theories are investigated in Table 4.7 using the same variational statement (PVD(\mathbf{u}, Φ)). Tables 4.8-4.13 give the results of the first fundamental frequencies in the case of the three possible extensions of RMVT to the electro-mechanical case; the same kinematics models introduced for the PVD case are considered.

The results obtained in all cases (ESL or LW and PVD or RMVT model) are very close to the 3D solution if higher orders of expansion are used, the maximum error is 2.68%. When lower orders of expansion are employed, if the variational statement is PVD, ESL models gives smaller errors than LW ones; if the variational statement is RMVT one has the opposite situation. In general, the error doesn't depend on the wave number because by varying n one obtain completely different modes of vibration. Table 4.4 shows that classical theories, such as CLT and FSDT, don't give very large errors but the results are not so near to the 3D solution as in the other cases. The use of mixed models does not appear mandatory to obtain the frequencies: the kinematic based PVD leads to a quasi-3D evaluation of the first fundamental frequencies for every wave number n . The use of mixed models instead appears mandatory to obtain the correct evaluation of modes through the thickness in terms of displacements, stresses, electric potential and electric displacement. This fact is illustrated in the following analysis.

The mode through the thickness for the fundamental frequency is given in Figs.(4.7)-(4.10) in terms of displacements, stresses, electric potential and electric displacement.

The distribution of the transverse displacement u_z through the thickness is given in Fig.(4.7); in this case, there are no differences for the considered variational statements because the displacement is a primary variable in all them. The mode is given in Fig.(4.8) in terms of electric potential. The potential Φ consists of a primary variable in each considered model; as a consequence, the same considerations made for the displacements are confirmed: the electric potential is continuous and satisfies the closed-circuit boundary conditions. In order to give the mode through the thickness in terms of stress σ_{zz} , the use of mixed models in which σ_{zz} is a primary variable is mandatory: these models permit the interlaminar continuity and the correct boundary homogeneous conditions to be obtained (see Fig.(4.9)). Finally, Fig.(4.10) gives the modes in terms of transverse normal electric displacement \mathcal{D}_z . As in the case of stress σ_{zz} , mixed models, where normal electric displacement is a primary variable, are necessary in order to achieve the interlaminar continuity of \mathcal{D}_z at the interfaces.

The frequencies calculated using a pure mechanical model are quoted in Table 4.14. In order to estimate the piezoelectric effect, the following parameter is evaluated:

$$\Delta^p[\%] = \sqrt{\frac{\omega^2 - \omega_{el}^2}{\omega^2}} \cdot 100, \quad (4.31)$$

where the eigenfrequency ω is obtained by considering the electric effect, whereas ω_{el} is computed neglecting the electric part (only the elastic properties of the piezoelectric layers are considered). Due to the employed high orders of expansion, each model gives the same value of the parameter Δ^p , this is quite large so we can conclude that in this particular case the electrical effect can't be neglected. In addition to what demonstrated in [98] (the effect produced by the electromechanical interaction is not predictable and does not depend on the thickness ratio and the order of the considered mode), one can note that the parameter Δ^p doesn't depend on the wave number n . For more details about the electromechanical analysis of piezoelectric shells, one can refer to [98].

4.3 Dynamic analysis of Double Walled Carbon Nanotubes (DWNT)

It has been demonstrated by Aydogdu [221] that single-beam continuum models, which are often used in literature to study CNTs, can not represent the behavior of individual tubes in a MWNT and relative deformation between adjacent tubes, because they assume that all the originally concentric tubes of a MWNT remain coaxial during vibration. Therefore, refined MWNTs models are needed, in which also van der Waals (vdW) forces must be taken into consideration and which consider interlayer radial displacements and individual deflection curves of nested tubes within the MWNT.

In this work, the discrete DWNT is considered as an equivalent continuum cylindrical shell composed of two adjacent layers (see Fig.4.11). As multi-beam models, CUF

permits to consider each tube of the DWNT as independent by simply modifying the assembling procedure of the stiffness matrix on the layer k , as shown in Figure 4.12. In this way, the condition of continuity for the displacements at the layer interface is not fulfilled and the inner and outer tubes can vibrate separately.

In order to apply a continuum model for the free vibration analysis of the DWNT is necessary to determine its equivalent mechanical properties. In literature, there are many dissenting opinions about the mechanical characterization of carbon nanotubes. This work is directed to validate the refined shell theories contained in CUF for the analysis of DWNTs. According to [221] the effective wall thickness of the single carbon nanotube t is assumed to be equal to the interplanar spacing of graphite layers (0.35 nm) and the mechanical properties are consequently calculated. The diameters of the inner and the outer walls of the double-walled nanotube are taken as $d_1 = 0.7$ nm and $d_2 = 1.4$ nm, respectively (see Fig.4.11). Young's modulus and the shear modulus of double-walled carbon nano tubes are assumed to be approximately insensitive to tube chirality. For the present DWNT and tube geometry, each tube is assumed to have the same Young's modulus of 1 TPa, shear modulus of 0.4 TPa, Poisson ratio of 0.25, and mass density of 2.3 g/cm^3 with the effective thickness of 0.35 nm.

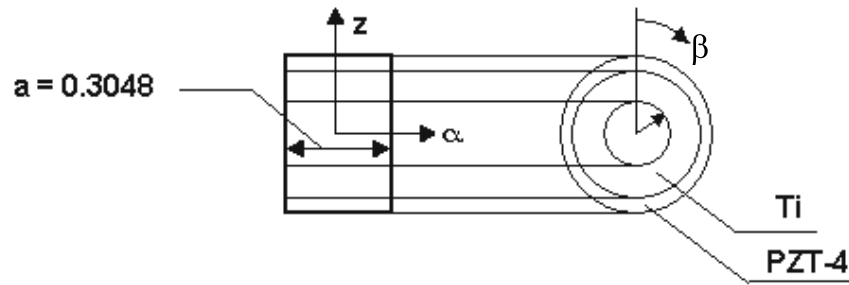


Figure 4.6: Geometry of multilayered piezoelectric ring for closed circuit vibration problem.

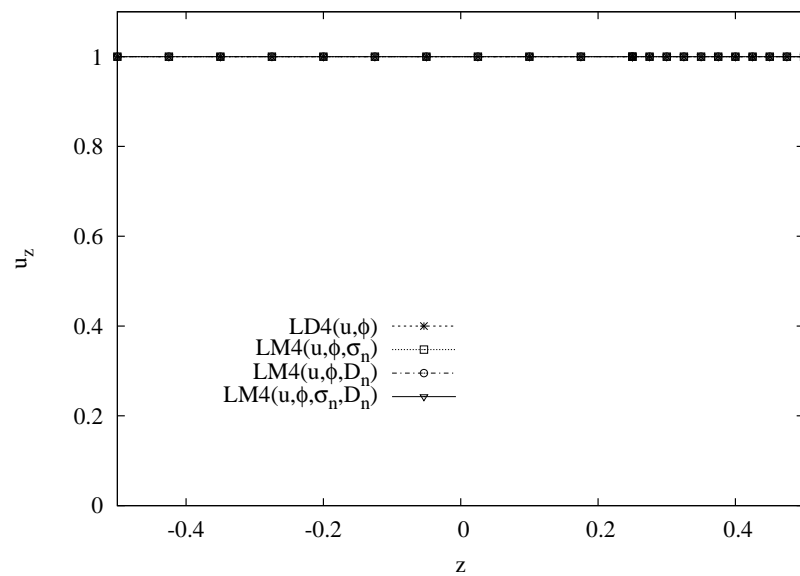


Figure 4.7: Mechanical transverse displacement u_z vs z . First mode for $m = 0$ and $n = 4$.

Properties	$PZT - 4$		<i>Titanium</i>
$E_1[GP a]$	81.3		114
$E_2[GP a]$	81.3		114
$E_3[GP a]$	64.5		114
$\nu_{12}[-]$	0.329		0.3
$\nu_{13}[-]$	0.432		0.3
$\nu_{23}[-]$	0.432		0.3
$G_{23}[GP a]$	25.6		43.85
$G_{13}[GP a]$	25.6		43.85
$G_{12}[GP a]$	30.6		43.85
$e_{15}[C/m^2]$	12.72		0
$e_{24}[C/m^2]$	12.72		0
$e_{31}[C/m^2]$	-5.20		0
$e_{32}[C/m^2]$	-5.20		0
$e_{33}[C/m^2]$	15.08		0
$\varepsilon_{11}[pC/Vm]$	1.306E4		8.850
$\varepsilon_{22}[pC/Vm]$	1.306E4		8.850
$\varepsilon_{33}[pC/Vm]$	1.151E4		8.850
$\rho[Kg/m^3]$	7600		2768
$h_{PZT4}[m]$	0.001	—	—
$h_T[m]$	—	—	0.003
$h_{TOT}[m]$	—	0.004	—
$a[m]$	—	0.3048	—
$b = 2\pi R_\beta[m]$	—	1.82841	—
$R_\alpha[m](at\ midsurface)$	—	∞	—
$R_\beta[m](at\ midsurface)$	—	$0.289 + 0.002$	—

Table 4.3: Geometrical, elastic and piezoelectric properties of ring in PZT4 and titanium for closed circuit vibration problem.

	$n = 4$	$n = 8$	$n = 12$	$n = 16$	$n = 20$
$3D$	31.27	170.42	407.29	745.21	1190.48
$PVD(\mathbf{u}, \Phi)$					
CLT	30.71	166.63	395.29	715.59	1127.24
$Err(\%)$	(1.79)	(2.22)	(2.95)	(3.97)	(5.31)
$FSDT$	30.71	166.57	394.98	714.60	1124.79
$Err(\%)$	(1.79)	(2.26)	(3.02)	(4.11)	(5.52)

Table 4.4: Ring in PTZ4 and Titanium, closed circuit configuration. 3D results vs CLT and FSDT analysis.

	$n = 4$	$n = 8$	$n = 12$	$n = 16$	$n = 20$
$3D$	31.27	170.42	407.29	745.21	1190.48
$PVD(\mathbf{u}, \Phi)$					
$ED1$	30.65	166.28	394.29	713.35	1122.85
$Err(\%)$	(1.98)	(2.43)	(3.19)	(4.27)	(5.68)
$ED2$	31.65	171.67	407.05	736.45	1159.21
$Err(\%)$	(-1.21)	(-0.73)	(0.06)	(1.17)	(2.63)
$ED3$	31.64	171.62	406.93	736.18	1158.70
$Err(\%)$	(-1.18)	(-0.70)	(0.09)	(1.21)	(2.67)
$ED4$	31.64	171.61	406.91	736.14	1158.64
$Err(\%)$	(-1.18)	(-0.70)	(0.09)	(1.22)	(2.67)

Table 4.5: Ring in PTZ4 and Titanium, closed circuit configuration. 3D results vs Equivalent Single Layer (ESL) theories.

	$n = 4$	$n = 8$	$n = 12$	$n = 16$	$n = 20$
$3D$	31.27	170.42	407.29	745.21	1190.48
$PVD(\mathbf{u}, \Phi)$					
$EDZ1$	33.28	180.53	428.05	774.35	1218.71
$Err(\%)$	(-6.43)	(-5.93)	(-5.10)	(-3.91)	(-2.37)
$EDZ2$	31.64	171.60	406.90	736.16	1158.73
$Err(\%)$	(-1.18)	(-0.69)	(0.10)	(1.21)	(2.67)
$EDZ3$	31.64	171.60	406.88	736.08	1158.55
$Err(\%)$	(-1.18)	(-0.69)	(0.10)	(1.22)	(2.68)

Table 4.6: Ring in PTZ4 and Titanium, closed circuit configuration. 3D results vs ESL zig-zag theories.

	$n = 4$	$n = 8$	$n = 12$	$n = 16$	$n = 20$
$3D$	31.27	170.42	407.29	745.21	1190.48
$PVD(\mathbf{u}, \Phi)$					
$LD1$	33.28	180.51	427.99	774.24	1218.54
$Err(\%)$	(-6.43)	(-5.92)	(-5.08)	(-3.89)	(-2.36)
$LD2$	31.64	171.60	406.88	736.11	1158.61
$Err(\%)$	(-1.18)	(-0.69)	(0.10)	(1.22)	(2.68)
$LD3$	31.64	171.59	406.87	736.07	1158.51
$Err(\%)$	(-1.18)	(-0.69)	(0.10)	(1.23)	(2.68)
$LD4$	31.64	171.59	406.87	736.07	1158.51
$Err(\%)$	(-1.18)	(-0.69)	(0.10)	(1.23)	(2.68)

Table 4.7: Ring in PTZ4 and Titanium, closed circuit configuration. 3D results vs Layer Wise (LW) theories.

	$n = 4$	$n = 8$	$n = 12$	$n = 16$	$n = 20$
$3D$	31.27	170.42	407.29	745.21	1190.48
$RMVT(\mathbf{u}, \Phi, \boldsymbol{\sigma}_n)$					
$EM1$	35.53	192.70	456.86	826.39	1300.41
$Err(\%)$	(-13.62)	(-13.07)	(-12.17)	(-10.89)	(-9.23)
$EM2$	31.65	171.65	407.03	736.40	1159.13
$Err(\%)$	(-1.21)	(-0.72)	(0.06)	(1.18)	(2.63)
$EM3$	31.64	171.61	406.91	736.15	1158.65
$Err(\%)$	(-1.18)	(-0.70)	(0.10)	(1.22)	(2.67)
$EM4$	31.64	171.61	406.90	736.13	1158.62
$Err(\%)$	(-1.18)	(-0.70)	(0.10)	(1.22)	(2.68)

Table 4.8: Ring in PTZ4 and Titanium, closed circuit configuration. 3D results vs mixed ESL theories with Interlaminar Continuous transverse stress components.

	$n = 4$	$n = 8$	$n = 12$	$n = 16$	$n = 20$
$3D$	31.27	170.42	407.29	745.21	1190.48
$RMVT(\mathbf{u}, \Phi, \mathcal{D}_n)$					
$EM1$	35.54	192.73	456.93	826.51	1300.61
$Err(\%)$	(-13.65)	(-13.09)	(-12.19)	(-10.91)	(-9.25)
$EM2$	31.65	171.67	407.05	736.45	1159.21
$Err(\%)$	(-1.21)	(-0.73)	(0.06)	(1.17)	(2.63)
$EM3$	31.64	171.62	406.93	736.18	1158.70
$Err(\%)$	(-1.18)	(-0.70)	(0.09)	(1.21)	(2.67)
$EM4$	31.64	171.62	406.91	736.14	1158.64
$Err(\%)$	(-1.18)	(-0.70)	(0.09)	(1.22)	(2.67)

Table 4.9: Ring in PTZ4 and Titanium, closed circuit configuration. 3D results vs mixed ESL theories with Interlaminar Continuous transverse normal electrical displacement.

	$n = 4$	$n = 8$	$n = 12$	$n = 16$	$n = 20$
$3D$	31.27	170.42	407.29	745.21	1190.48
$RMVT(\mathbf{u}, \Phi, \sigma_n, \mathcal{D}_n)$					
$EM1$	35.54	192.73	456.92	826.49	1300.57
$Err(\%)$	(-13.65)	(-13.09)	(-12.18)	(-10.91)	(-9.25)
$EM2$	31.65	171.66	407.03	736.40	1159.13
$Err(\%)$	(-1.21)	(-0.73)	(0.06)	(1.18)	(2.63)
$EM3$	31.64	171.61	406.91	736.15	1158.65
$Err(\%)$	(-1.18)	(-0.70)	(0.09)	(1.22)	(2.67)
$EM4$	31.64	171.61	406.90	736.13	1158.62
$Err(\%)$	(-1.18)	(-0.70)	(0.10)	(1.22)	(2.68)

Table 4.10: Ring in PTZ4 and Titanium, closed circuit configuration. 3D results vs mixed ESL theories with Interlaminar Continuous transverse stresses and transverse normal electrical displacement.

	$n = 4$	$n = 8$	$n = 12$	$n = 16$	$n = 20$
$3D$	31.27	170.42	407.29	745.21	1190.48
$RMVT(\mathbf{u}, \Phi, \boldsymbol{\sigma}_n)$					
$LM1$	32.39	175.66	416.50	753.47	1185.87
$Err(\%)$	(-3.58)	(-3.07)	(-2.26)	(-1.11)	(0.39)
$LM2$	31.64	171.60	406.88	736.10	1158.58
$Err(\%)$	(-1.18)	(-0.69)	(0.10)	(1.22)	(2.68)
$LM3$	31.64	171.59	406.87	736.07	1158.51
$Err(\%)$	(-1.18)	(-0.69)	(0.10)	(1.23)	(2.68)
$LM4$	31.64	171.59	406.87	736.07	1158.51
$Err(\%)$	(-1.18)	(-0.69)	(0.10)	(1.23)	(2.68)

Table 4.11: Ring in PTZ4 and Titanium, closed circuit configuration. 3D results vs mixed LW theories with Interlaminar Continuous transverse stress components.

	$n = 4$	$n = 8$	$n = 12$	$n = 16$	$n = 20$
$3D$	31.27	170.42	407.29	745.21	1190.48
$RMVT(\mathbf{u}, \Phi, \boldsymbol{\mathcal{D}}_n)$					
$LM1$	33.28	180.53	428.05	774.35	1218.71
$Err(\%)$	(-6.43)	(-5.93)	(-5.10)	(-3.91)	(-2.37)
$LM2$	31.64	171.60	406.88	736.11	1158.61
$Err(\%)$	(-1.18)	(-0.69)	(0.10)	(1.22)	(2.68)
$LM3$	31.64	171.59	406.87	736.07	1158.51
$Err(\%)$	(-1.18)	(-0.69)	(0.10)	(1.23)	(2.68)
$LM4$	31.64	171.59	406.87	736.07	1158.51
$Err(\%)$	(-1.18)	(-0.69)	(0.10)	(1.23)	(2.68)

Table 4.12: Ring in PTZ4 and Titanium, closed circuit configuration. 3D results vs mixed LW theories with Interlaminar Continuous transverse normal electrical displacement.

	$n = 4$	$n = 8$	$n = 12$	$n = 16$	$n = 20$
$3D$	31.27	170.42	407.29	745.21	1190.48
$RMVT(\mathbf{u}, \Phi, \boldsymbol{\sigma}_n, \mathcal{D}_n)$					
$LM1$	32.53	176.42	418.30	756.73	1191.00
$Err(\%)$	(-4.03)	(-3.52)	(-2.70)	(-1.55)	(-0.04)
$LM2$	31.64	171.60	406.88	736.09	1158.58
$Err(\%)$	(-1.18)	(-0.69)	(0.10)	(1.22)	(2.68)
$LM3$	31.64	171.59	406.87	736.07	1158.51
$Err(\%)$	(-1.18)	(-0.69)	(0.10)	(1.23)	(2.68)
$LM4$	31.64	171.59	406.87	736.07	1158.51
$Err(\%)$	(-1.18)	(-0.69)	(0.10)	(1.23)	(2.68)

Table 4.13: Ring in PTZ4 and Titanium, closed circuit configuration. 3D results vs mixed LW theories with Interlaminar Continuous transverse stresses and transverse normal electrical displacement.

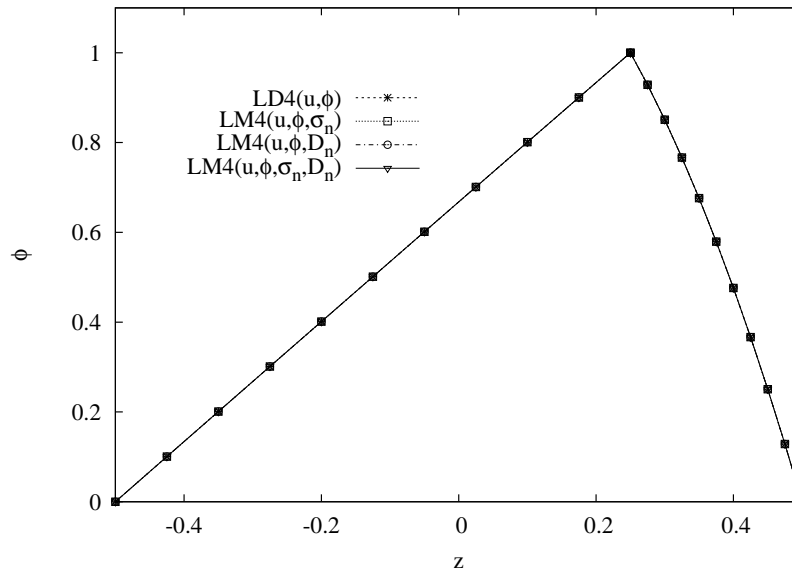


Figure 4.8: Electric potential Φ vs z . First mode for $m = 0$ and $n = 4$.

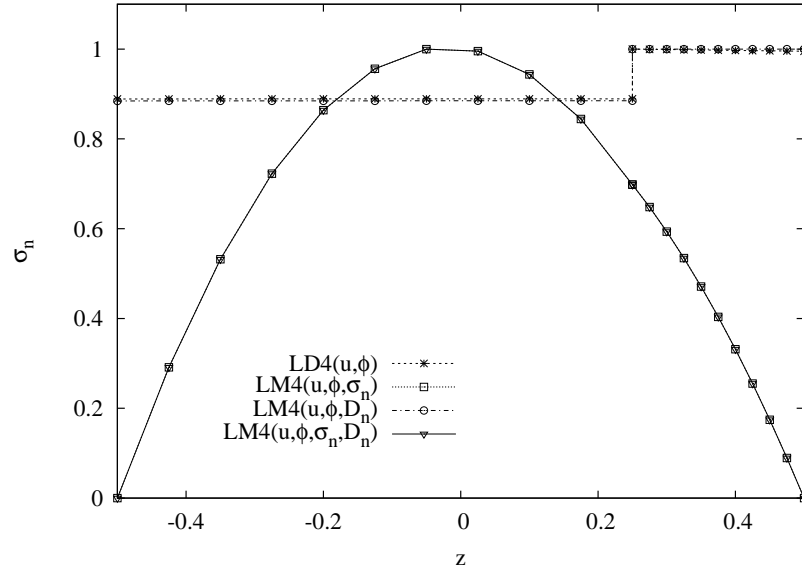


Figure 4.9: Transverse normal stress σ_{zz} vs z . First mode for $m = 0$ and $n = 4$.

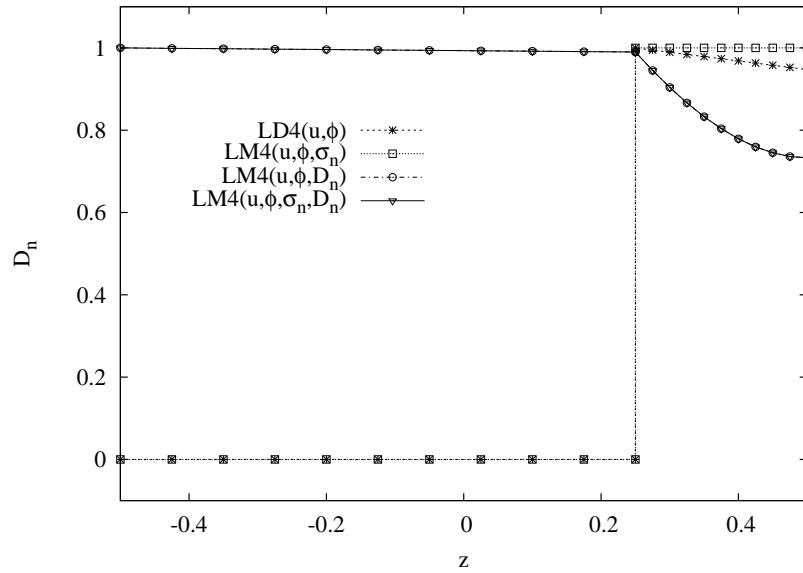


Figure 4.10: Transverse normal electric displacement D_z vs z . First mode for $m = 0$ and $n = 4$.

	$n = 4$	$n = 8$	$n = 12$	$n = 16$	$n = 20$
$LD4(u)$	30.55	165.69	392.87	710.78	1118.77
$LD4(u, \Phi)$	31.64	171.59	406.87	736.07	1158.51
$LM4(u, \Phi, \mathcal{D}_n)$	31.64	171.59	406.87	736.07	1158.51
$\Delta^p[\%]$	(26.02)	(26.00)	(26.00)	(26.00)	(26.00)
$LM4(u, \sigma_n)$	30.55	165.69	392.87	710.78	1118.77
$LM4(u, \Phi, \sigma_n)$	31.64	171.59	406.87	736.07	1158.51
$LM4(u, \Phi, \sigma_n, \mathcal{D}_n)$	31.64	171.59	406.87	736.07	1158.51
$\Delta^p[\%]$	(26.02)	(26.00)	(26.00)	(26.00)	(26.00)

Table 4.14: Ring in PTZ4 and Titanium, closed circuit configuration. Comparison between frequency response of pure mechanical problem and electro-mechanical problem.

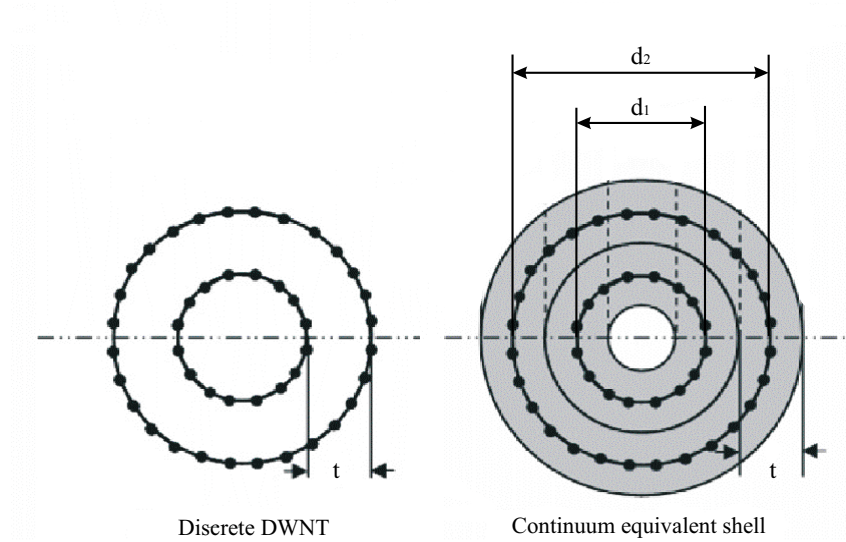


Figure 4.11: DWNT: continuum equivalent shell.

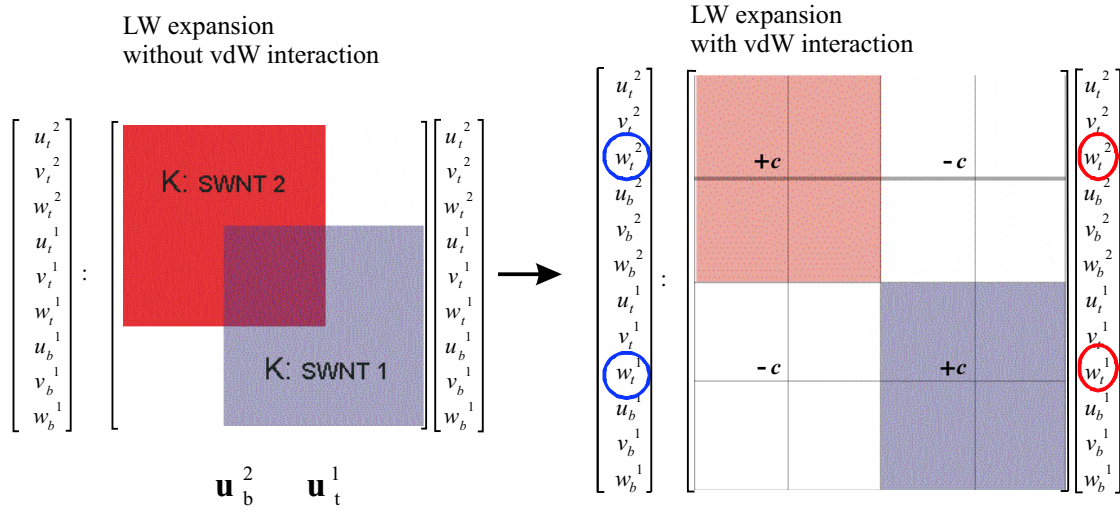


Figure 4.12: Assembling procedure of the global stiffness matrix of a DWNT, taking account for van der Waals interaction.

The deflections of two tubes are coupled through the van der Waals intertube interaction pressure. Since the inner and outer tubes of a DWNT are originally concentric and the van der Waals interaction is determined by the interlayer spacing, the net van der Waals interaction pressure remains zero for each tube, provided they deform coaxially. For small-amplitude linear transverse vibrations, interaction pressure at any point between the tubes depends linearly on the difference between their deflection curves at that point. The van der Waals pressure on tube 1 due to tube 2 (see Fig.4.13), which is positive inward, is given in [221]:

$$P_{1,2} = c(w_2 - w_1), \quad (4.32)$$

and, for the equilibrium, $P_{2,1} = -P_{1,2}$. w_1 and w_2 are the displacements of the tubes in the radial direction and c is the van der Waals interaction coefficient, estimated at the initial interlayer spacing (~ 0.34 nm):

$$c = \frac{320 \text{ erg/cm}^2}{0.16d^2}, \quad (4.33)$$

where $d = 0.142$ nm is the length of C-C bond and $1 \text{ erg} = 10^{-7} \text{ J}$.

Since the coefficient c has the physical dimensions of a stiffness, it is possible to account for vdW interaction in the CUF by opportunely introducing c in the stiffness matrix, as shown in Figure 4.12. This is equivalent to consider the van der Waals forces $P_{2,1}$ and $P_{1,2}$ as external loads applied at the top of the layers 1 and 2, respectively. The free vibration analysis of DWNTs is performed solving the eigenvalue problem in Section 3.2.1, formulated on the basis of Navier method, and the stiffness matrix is obtained following the procedure exposed in Section 3.1.

4.3.1 Results and discussion

In this section, the results obtained using the CUF extended to free vibrations analysis of a double-walled carbon nanotube are proposed. The global thickness of DWNT is $h = 1.75$ and the thickness ratio L/h , where L is the axial length of the nanotube, assumes the values 10 and 50.

In the Tables 4.15 and 4.16, the tubes of DWNT are supposed to remain coaxial during vibration, while in Table 4.17 and 4.18, each tube of DWNT is considered as independent and the vdW interaction is accounted for. These results are compared with the beam solutions provided in [221], by Aydogdu: Tables 4.15, 4.16 refer to the single third-order beam (STOB) theory and Tables 4.17, 4.18 to the double third-order beam (DTOB) theory. The proposed values are calculated employing different two-dimensional shell models contained in the CUF: Classical Lamination Theory (CLT), First order Shear Deformation Theory (FSDT), Equivalent Single Layer and Layer Wise models with order of expansion for the displacements in the thickness direction from 1 to 4.

In the tables, the wave numbers of the vibration modal shapes of DWNT in terms

n	<i>STOB</i>	<i>CLT</i>	<i>FSDT</i>	<i>ED1</i>	<i>ED2</i>	<i>ED3</i>	<i>ED4</i>
1	3.1278	3.1278	3.1254	3.1310	3.1220	3.1219	3.1219
2	6.1735	6.1604	6.1422	6.1538	6.1356	6.1345	6.1344
3	9.0418	9.0283	8.9772	8.9955	8.9675	8.9644	8.9641
4	11.612	11.704	11.601	11.627	11.589	11.582	11.582
5	13.757	14.190	14.016	14.050	14.001	13.991	13.989

Table 4.15: Natural frequencies parameter Ω of DWNT. STOB results are provided in [221]. $L/h = 10$ and $m = 2$.

n	<i>STOB</i>	<i>CLT</i>	<i>FSDT</i>	<i>ED1</i>	<i>ED2</i>	<i>ED3</i>	<i>ED4</i>
1	3.1410	3.1455	3.1442	3.1497	3.1408	3.1408	3.1408
2	6.2787	6.2867	6.2835	6.2947	6.2768	6.2768	6.2768
3	9.4102	9.4194	9.4135	9.4302	9.4034	9.4032	9.4032
4	12.531	12.540	12.529	12.552	12.516	12.516	12.515
5	15.640	15.644	15.627	15.655	15.610	15.609	15.609

Table 4.16: Natural frequencies parameter Ω of DWNT. STOB results are provided in [221]. $L/h = 50$ and $m = 2$.

of displacements, in the axial and circumferential directions, are taken as $n = 1, \dots, 5$ and $m = 2$, respectively. Only first-order frequencies are considered and these are

n	$DTOB$	$LD1$	$LD2$	$LD3$	$LD4$
1	3.1199	3.1155	3.1135	3.1135	3.1135
2	6.1275	6.0776	6.0733	6.0732	6.0732
3	8.9633	8.7914	8.7866	8.7841	8.7841
4	11.547	11.230	11.220	11.219	11.219
5	13.761	13.410	13.386	13.395	13.395

Table 4.17: Natural frequencies parameter Ω of DWNT. DTOB results are provided in [221]. vdW forces are taken into consideration. $L/h = 10$ and $m = 2$.

n	$DTOB$	$LD1$	$LD2$	$LD3$	$LD4$
1	3.1406	3.1425	3.1404	3.1404	3.1404
2	6.2760	6.2781	6.2740	6.2740	6.2740
3	9.4008	9.4000	9.3939	9.3939	9.3939
4	12.510	12.502	12.494	12.494	12.494
5	15.599	15.578	15.567	15.567	15.567

Table 4.18: Natural frequencies parameter Ω of DWNT. DTOB results are provided in [221]. vdW forces are taken into consideration. $L/h = 50$ and $m = 2$.

n	$L/h = 10$			$L/h = 50$		
	$ED4$	$LD4$ (vdW)	$\Delta(\%)$	$ED4$	$LD4$ (vdW)	$\Delta(\%)$
1	3.1219	3.1135	0.27	3.1408	3.1404	0.01
2	6.1344	6.0732	1.00	6.2768	6.2740	0.04
3	8.9641	8.7841	2.00	9.4032	9.3939	0.10
4	11.582	11.219	3.13	12.515	12.494	0.17
5	13.989	13.395	4.25	15.609	15.567	0.27

Table 4.19: Natural frequencies parameter Ω of DWNT. Comparison between ESL models and LW models which account for vdW forces: $\Delta(\%) = \frac{ED4-LD4}{ED4} \times 100$

normalized according to the formula:

$$\Omega = \sqrt[4]{\frac{\rho A \omega^2 L^4}{EI}}, \quad (4.34)$$

where A and I are the area and moment of inertia of the DWNT cross section.

Tables 4.15-4.18 show that the CUF results are in good agreement with the reference solution by increasing the order of expansion of the theory. It should be considered that shell models are compared with beam models, therefore some differences between them remain even though high orders of expansion ($N = 4$) are used. However, these differences become smaller when the nanotube is longer ($L/h = 50$), because the beam hypotheses are fulfilled, and lower frequencies are considered (low n). In particular, looking at the Tables 4.15 and 4.16 it is possible to note that in general CLT and FSDT theories give results that are further from the reference solution, compared with the ESL models. In some cases, such as in Table 4.16 for $n = 4$ and $n = 5$, CLT and FSDT theories give a smaller error in respect to high-order equivalent single layer theories, but this inconsistency is due to the error that a beam model, as is the STOB, produces on high frequencies. ED4 and LD4 models are compared in Table 4.19. The percentage difference $\Delta(\%) = \frac{ED4-LD4}{ED4} \times 100$ between them increases for short DWNTs and higher frequencies, therefore it is possible to conclude that in these cases it is necessary to consider the vdW interaction between the DWNT tubes in order to avoid overestimated results.

For more details about the free vibration analysis of DWNTs, one can refer to [222].

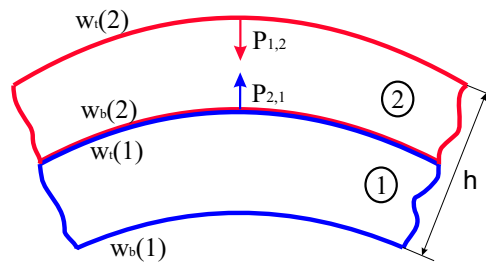


Figure 4.13: Van der Waals interaction in a DWNT.

Chapter 5

FEM solutions

The FEM model here presented for the analysis of shells does not involve any approximation of the geometry and it is able to accurately describe the curvature of cylindrical shells. Note that, in this chapter, the notation presented in Section 2.2.1 for cylindrical geometry is used. Such a model is combined with a simple displacement formulation and the MITC method is employed to overcome the membrane and shear locking phenomenon.

Firstly, the derivation of the governing equations in the framework of FEM is presented. Then, an assessment of the CUF MITC9 shell element is performed. Some discriminating problems from the literature are considered and the efficiency and the robustness of the shell element are tested. Finally, the results obtained from the analysis of composite and FGM shells are provided. In this case, the superiority of the models contained in the CUF in respect to the classical finite elements based on the FSDT is demonstrated. For these reasons, it seems reasonable to extend in future the CUF shell element to the analysis of multi-field problems, as made in Chapter 4.

5.1 Governing equations

The governing equations for the static analysis of cylindrical shells subjected to pure mechanical loads are derived from the PVD, written in the following form:

$$\int_{\Omega} \int_A \{ \delta \epsilon_p^T \sigma_p + \delta \epsilon_n^T \sigma_n \} H d\Omega d\xi^3 = \int_{\Omega} \int_A \{ \delta \mathbf{u} p \} H d\Omega d\xi^3 \quad (5.1)$$

where $p = p(\xi_1, \xi_2, \xi_3)$ is the load applied to the structure.

Exploiting the geometrical relations (Eqs.(3.31)) and the constitutive equations (Eqs.(3.33)), in which the FEM approximation and the MITC method have been applied, the PVD

becomes:

$$\begin{aligned}
& \delta \mathbf{q}_{\tau_i}^T \left\{ \int_A F_\tau \left(\int_\Omega [C_{3im}^T (C_{pp} C_{3jn} + C_{pn} C_{1jn}) + C_{1im}^T (C_{np} C_{3jn} + C_{nn} C_{1jn})] d\Omega \right) F_s H d\xi^3 \right\} \mathbf{q}_{s_j} + \\
& \delta \mathbf{q}_{\tau_i}^T \left\{ \int_A F_\tau \left(\int_\Omega [(C_{3im}^T C_{pn} + C_{1im}^T C_{nn}) C_{2jn}] d\Omega \right) F_{s,3} H d\xi^3 \right\} \mathbf{q}_{s_j} + \\
& \delta \mathbf{q}_{\tau_i}^T \left\{ \int_A F_{\tau,3} \left(\int_\Omega [C_{2im}^T (C_{np} C_{3jn} + C_{nn} C_{1jn})] d\Omega \right) F_s H d\xi^3 \right\} \mathbf{q}_{s_j} + \\
& \delta \mathbf{q}_{\tau_i}^T \left\{ \int_A F_{\tau,3} \left(\int_\Omega [C_{2im}^T C_{nn} C_{2jn}] d\Omega \right) F_{s,3} H d\xi^3 \right\} \mathbf{q}_{s_j} = \\
& \delta \mathbf{q}_{\tau_i}^T \left\{ \int_A F_\tau \left(\int_\Omega N_i \mathbf{p} d\Omega \right) H d\xi^3 \right\},
\end{aligned} \tag{5.2}$$

Therefore, the following governing equation system can be obtained:

$$\delta \mathbf{q}_{\tau_i}^T : \quad \mathbf{K}_{uu}^{\tau sij} \mathbf{q}_{s_j} = \mathbf{P}_{s_j} \tag{5.3}$$

In the case of FEM analysis, the boundary conditions are imposed in weak form by applying penalty techniques to the stiffness matrix.

In order to write the explicit expression of the fundamental nucleus of the stiffness matrix, the following matrixes are introduced:

$$N_m = \begin{bmatrix} N_{A1} & N_{A2} & N_P \\ N_{B1} & N_{B2} & N_Q \\ N_{C1} & N_{C2} & N_R \\ N_{D1} & N_{D2} & N_S \\ N_{E1} & N_{E2} & 0 \\ N_{F1} & N_{F2} & 0 \end{bmatrix}, \tag{5.4}$$

where it is assumed that $N_m(:, 1) = N_{m1}$, $N_m(:, 2) = N_{m2}$ e $N_m(:, 3) = N_{m3}$. Similarly, the shape functions and the respective derivatives in respect to ξ_1 and ξ_2 are calculated in the tying points and arranged in the following matrixes:

$$N_{im} = \begin{bmatrix} N_{iA1} & N_{iA2} & N_{iP} \\ N_{iB1} & N_{iB2} & N_{iQ} \\ N_{iC1} & N_{iC2} & N_{iR} \\ N_{iD1} & N_{iD2} & N_{iS} \\ N_{iE1} & N_{iE2} & 0 \\ N_{iF1} & N_{iF2} & 0 \end{bmatrix}, \quad N_{i,1m} = \begin{bmatrix} N_{i,1A1} & N_{i,1A2} & N_{i,1P} \\ N_{i,1B1} & N_{i,1B2} & N_{i,1Q} \\ N_{i,1C1} & N_{i,1C2} & N_{i,1R} \\ N_{i,1D1} & N_{i,1D2} & N_{i,1S} \\ N_{i,1E1} & N_{i,1E2} & 0 \\ N_{i,1F1} & N_{i,1F2} & 0 \end{bmatrix}, \quad N_{i,2m} = \begin{bmatrix} N_{i,2A1} & N_{i,2A2} & N_{i,2P} \\ N_{i,2B1} & N_{i,2B2} & N_{i,2Q} \\ N_{i,2C1} & N_{i,2C2} & N_{i,2R} \\ N_{i,2D1} & N_{i,2D2} & N_{i,2S} \\ N_{i,2E1} & N_{i,2E2} & 0 \\ N_{i,2F1} & N_{i,2F2} & 0 \end{bmatrix}, \tag{5.5}$$

and it is assumed that:

$$\begin{aligned}
 N_{i_m}(:, 1) &= N_{i_{m1}}, & N_{i_m}(:, 2) &= N_{i_{m2}}, & N_{i_m}(:, 3) &= N_{i_{m3}} \\
 N_{i,1_m}(:, 1) &= N_{i,1_{m1}}, & N_{i,1_m}(:, 2) &= N_{i,1_{m2}}, & N_{i,1_m}(:, 3) &= N_{i,1_{m3}} \\
 N_{i,2_m}(:, 1) &= N_{i,2_{m1}}, & N_{i,2_m}(:, 2) &= N_{i,2_{m2}}, & N_{i,2_m}(:, 3) &= N_{i,2_{m3}}
 \end{aligned} \tag{5.6}$$

Therefore the components of the fundamental nucleus $\mathbf{K}_{uu}^{\tau sij}$ are:

$$\begin{aligned}
 K_{11}^{\tau sijmn} &= C_{55}^k N_{i_{m1}} \triangleleft N_{m1} N_{n1} \triangleright_{\Omega} N_{j_{n1}} \triangleleft H F_{\tau,3} F_{s,3} \triangleright_A + \\
 &\quad C_{11} N_{i,1_{m1}} \triangleleft N_{m1} N_{n1} \triangleright_{\Omega} N_{j,1_{n1}} \triangleleft H F_{\tau} F_s \triangleright_A + \\
 &\quad C_{16} N_{i,2_{m3}} \triangleleft N_{m3} N_{n1} \triangleright_{\Omega} N_{j,1_{n1}} \triangleleft H F_{\tau} F_s \triangleright_A + \\
 &\quad C_{16} N_{i,1_{m1}} \triangleleft N_{m1} N_{n3} \triangleright_{\Omega} N_{j,2_{n3}} \triangleleft H F_{\tau} F_s \triangleright_A + \\
 &\quad C_{66} N_{i,2_{m3}} \triangleleft N_{m3} N_{n3} \triangleright_{\Omega} N_{j,2_{n3}} \triangleleft H F_{\tau} F_s \triangleright_A \\
 \\
 K_{12}^{\tau sijmn} &= -C_{45}^k \frac{1}{R} N_{i_{m1}} \triangleleft N_{m1} N_{n2} \triangleright_{\Omega} N_{j_{n2}} \triangleleft H F_{\tau,3} F_s \triangleright_A + \\
 &\quad C_{45} N_{i_{m1}} \triangleleft N_{m1} N_{n2} \triangleright_{\Omega} N_{j_{n2}} \triangleleft H^2 F_{\tau,3} F_{s,3} \triangleright_A + \\
 &\quad C_{12} N_{i,1_{m1}} \triangleleft N_{m1} N_{n2} \triangleright_{\Omega} N_{j,2_{n2}} \triangleleft H^2 F_{\tau} F_s \triangleright_A + \\
 &\quad C_{16} N_{i,1_{m1}} \triangleleft N_{m1} N_{n3} \triangleright_{\Omega} N_{j,1_{n3}} \triangleleft H^2 F_{\tau} F_s \triangleright_A + \\
 &\quad C_{26} N_{i,2_{m3}} \triangleleft N_{m3} N_{n2} \triangleright_{\Omega} N_{j,2_{n2}} \triangleleft H^2 F_{\tau} F_s \triangleright_A + \\
 &\quad C_{66} N_{i,2_{m3}} \triangleleft N_{m3} N_{n3} \triangleright_{\Omega} N_{j,1_{n3}} \triangleleft H^2 F_{\tau} F_s \triangleright_A \\
 \\
 K_{13}^{\tau sijmn} &= C_{13}^k N_{i,1_{m1}} \triangleleft N_{m1} N_j \triangleright_{\Omega} \triangleleft H F_{\tau} F_{s,3} \triangleright_A + \\
 &\quad C_{36} N_{i,2_{m3}} \triangleleft N_{m3} N_j \triangleright_{\Omega} \triangleleft H F_{\tau} F_{s,3} \triangleright_A + \\
 &\quad C_{12} \frac{1}{R} N_{i,1_{m1}} \triangleleft N_{m1} N_{n2} \triangleright_{\Omega} N_{j_{n2}} \triangleleft H^2 F_{\tau} F_s \triangleright_A + \\
 &\quad C_{26} \frac{1}{R} N_{i,2_{m3}} \triangleleft N_{m3} N_{n2} \triangleright_{\Omega} N_{j_{n2}} \triangleleft H^2 F_{\tau} F_s \triangleright_A + \\
 &\quad C_{55} N_{i_{m1}} \triangleleft N_{m1} N_{n1} \triangleright_{\Omega} N_{j,1_{n1}} \triangleleft H F_{\tau,3} F_s \triangleright_A + \\
 &\quad C_{45} N_{i_{m1}} \triangleleft N_{m1} N_{n2} \triangleright_{\Omega} N_{j,2_{n2}} \triangleleft H F_{\tau,3} F_s \triangleright_A
 \end{aligned} \tag{5.7}$$

$$\begin{aligned}
K_{21}^{\tau sijmn} = & -C_{45}^k \frac{1}{R} N_{i_{m2}} \triangleleft N_{m2} N_{n1} \triangleright_{\Omega} N_{j_{n1}} \triangleleft H F_{\tau} F_{s,3} \triangleright_A + \\
& C_{45} N_{i_{m2}} \triangleleft N_{m2} N_{n1} \triangleright_{\Omega} N_{j_{n1}} \triangleleft H^2 F_{\tau,3} F_{s,3} \triangleright_A + \\
& C_{12} N_{i,2_{m2}} \triangleleft N_{m2} N_{n1} \triangleright_{\Omega} N_{j,1_{n1}} \triangleleft H^2 F_{\tau} F_s \triangleright_A + \\
& C_{16} N_{i,1_{m3}} \triangleleft N_{m3} N_{n1} \triangleright_{\Omega} N_{j,1_{n1}} \triangleleft H^2 F_{\tau} F_s \triangleright_A + \\
& C_{26} N_{i,2_{m2}} \triangleleft N_{m2} N_{n3} \triangleright_{\Omega} N_{j,2_{n3}} \triangleleft H^2 F_{\tau} F_s \triangleright_A + \\
& C_{66} N_{i,1_{m3}} \triangleleft N_{m3} N_{n3} \triangleright_{\Omega} N_{j,2_{n3}} \triangleleft H^2 F_{\tau} F_s \triangleright_A \\
\\
K_{22}^{\tau sijmn} = & C_{22}^k N_{i,2_{m2}} \triangleleft N_{m2} N_{n2} \triangleright_{\Omega} N_{j,2_{n2}} \triangleleft H^3 F_{\tau} F_s \triangleright_A + \\
& C_{26} N_{i,2_{m2}} \triangleleft N_{m2} N_{n3} \triangleright_{\Omega} N_{j,1_{n3}} \triangleleft H^3 F_{\tau} F_s \triangleright_A \\
& C_{26} N_{i,1_{m3}} \triangleleft N_{m3} N_{n2} \triangleright_{\Omega} N_{j,2_{n2}} \triangleleft H^3 F_{\tau} F_s \triangleright_A + \\
& C_{66} N_{i,1_{m3}} \triangleleft N_{m3} N_{n3} \triangleright_{\Omega} N_{j,1_{n3}} \triangleleft H^3 F_{\tau} F_s \triangleright_A + \\
& C_{44} \frac{1}{R^2} N_{i_{m2}} \triangleleft N_{m2} N_{n2} \triangleright_{\Omega} N_{j_{n2}} \triangleleft H F_{\tau} F_s \triangleright_A - \\
& C_{44} \frac{1}{R} N_{i_{m2}} \triangleleft N_{m2} N_{n2} \triangleright_{\Omega} N_{j_{n2}} \triangleleft H^2 F_{\tau} F_{s,3} \triangleright_A - \\
& C_{44} \frac{1}{R} N_{i_{m2}} \triangleleft N_{m2} N_{n2} \triangleright_{\Omega} N_{j_{n2}} \triangleleft H^2 F_{\tau,3} F_s \triangleright_A + \\
& C_{44} N_{i_{m2}} \triangleleft N_{m2} N_{n2} \triangleright_{\Omega} N_{j_{n2}} \triangleleft H^3 F_{\tau,3} F_{s,3} \triangleright_A \\
\\
K_{23}^{\tau sijmn} = & C_{22}^k \frac{1}{R} N_{i,2_{m2}} \triangleleft N_{m2} N_{n2} \triangleright_{\Omega} N_{j_{n2}} \triangleleft H^3 F_{\tau} F_s \triangleright_A + \\
& C_{23} N_{i,2_{m2}} \triangleleft N_{m2} N_j \triangleright_{\Omega} \triangleleft H^2 F_{\tau} F_{s,3} \triangleright_A + \\
& C_{26} \frac{1}{R} N_{i,1_{m3}} \triangleleft N_{m3} N_{n2} \triangleright_{\Omega} N_{j_{n2}} \triangleleft H^3 F_{\tau} F_s \triangleright_A + \\
& C_{36} N_{i,1_{m3}} \triangleleft N_{m3} N_j \triangleright_{\Omega} \triangleleft H^2 F_{\tau} F_{s,3} \triangleright_A - \\
& C_{45} \frac{1}{R} N_{i_{m2}} \triangleleft N_{m2} N_{n1} \triangleright_{\Omega} N_{j,1_{n1}} \triangleleft H F_{\tau} F_s \triangleright_A - \\
& C_{44} \frac{1}{R} N_{i_{m2}} \triangleleft N_{m2} N_{n2} \triangleright_{\Omega} N_{j,2_{n2}} \triangleleft H F_{\tau} F_s \triangleright_A + \\
& C_{45} N_{i_{m2}} \triangleleft N_{m2} N_{n1} \triangleright_{\Omega} N_{j,1_{n1}} \triangleleft H^2 F_{\tau,3} F_s \triangleright_A + \\
& C_{44} N_{i_{m2}} \triangleleft N_{m2} N_{n2} \triangleright_{\Omega} N_{j,2_{n2}} \triangleleft H^2 F_{\tau,3} F_s \triangleright_A
\end{aligned} \tag{5.8}$$

$$\begin{aligned}
K_{31}^{\tau s i j m n} = & C_{55}^k N_{i,1_{m1}} \triangleleft N_{m1} N_{n1} \triangleright_{\Omega} N_{j_{n1}} \triangleleft H F_{\tau} F_{s,3} \triangleright_A + \\
& C_{45} N_{i,2_{m2}} \triangleleft N_{m2} N_{n1} \triangleright_{\Omega} N_{j_{n1}} \triangleleft H F_{\tau} F_{s,3} \triangleright_A + \\
& C_{12} \frac{1}{R} N_{i_{m2}} \triangleleft N_{m2} N_{n1} \triangleright_{\Omega} N_{j,1_{n1}} \triangleleft H^2 F_{\tau} F_s \triangleright_A + \\
& C_{13} \triangleleft N_i N_{n1} \triangleright_{\Omega} N_{j,1_{n1}} \triangleleft H F_{\tau,3} F_s \triangleright_A + \\
& C_{26} \frac{1}{R} N_{i_{m2}} \triangleleft N_{m2} N_{n3} \triangleright_{\Omega} N_{j,2_{n3}} \triangleleft H^2 F_{\tau} F_s \triangleright_A + \\
& C_{36} \triangleleft N_i N_{n3} \triangleright_{\Omega} N_{j,2_{n3}} \triangleleft H F_{\tau,3} F_s \triangleright_A \\
\\
K_{32}^{\tau s i j m n} = & C_{22}^k \frac{1}{R} N_{i_{m2}} \triangleleft N_{m2} N_{n2} \triangleright_{\Omega} N_{j,2_{n2}} \triangleleft H^3 F_{\tau} F_s \triangleright_A + \\
& C_{23} \triangleleft N_i N_{n2} \triangleright_{\Omega} N_{j,2_{n2}} \triangleleft H^2 F_{\tau,3} F_s \triangleright_A + \\
& C_{26} \frac{1}{R} N_{i_{m2}} \triangleleft N_{m2} N_{n3} \triangleright_{\Omega} N_{j,1_{n3}} \triangleleft H^3 F_{\tau} F_s \triangleright_A + \\
& C_{36} \triangleleft N_i N_{n3} \triangleright_{\Omega} N_{j,1_{n3}} \triangleleft H^2 F_{\tau,3} F_s \triangleright_A - \\
& C_{45} \frac{1}{R} N_{i,1_{m1}} \triangleleft N_{m1} N_{n2} \triangleright_{\Omega} N_{j_{n2}} \triangleleft H F_{\tau} F_s \triangleright_A - \\
& C_{44} \frac{1}{R} N_{i,2_{m2}} \triangleleft N_{m2} N_{n2} \triangleright_{\Omega} N_{j_{n2}} \triangleleft H F_{\tau} F_s \triangleright_A + \\
& C_{45} N_{i,1_{m1}} \triangleleft N_{m1} N_{n2} \triangleright_{\Omega} N_{j_{n2}} \triangleleft H^2 F_{\tau} F_{s,3} \triangleright_A + \\
& C_{44} N_{i,2_{m2}} \triangleleft N_{m2} N_{n2} \triangleright_{\Omega} N_{j_{n2}} \triangleleft H^2 F_{\tau} F_s \triangleright_A \\
\\
K_{33}^{\tau s i j m n} = & C_{22}^k \frac{1}{R^2} N_{i_{m2}} \triangleleft N_{m2} N_{n2} \triangleright_{\Omega} N_{j_{n2}} \triangleleft H^3 F_{\tau} F_s \triangleright_A + \\
& C_{23} \frac{1}{R} N_{i_{m2}} \triangleleft N_{m2} N_j \triangleright_{\Omega} \triangleleft H^2 F_{\tau} F_{s,3} \triangleright_A + \\
& C_{23} \frac{1}{R} \triangleleft N_i N_{n2} \triangleright_{\Omega} N_{j_{n2}} \triangleleft H^2 F_{\tau,3} F_s \triangleright_A + \\
& C_{33} \triangleleft N_i N_j \triangleright_{\Omega} \triangleleft H F_{\tau,3} F_{s,3} \triangleright_A + \\
& C_{55} N_{i,1_{m1}} \triangleleft N_{m1} N_{n1} \triangleright_{\Omega} N_{j,1_{n1}} \triangleleft H F_{\tau} F_s \triangleright_A + \\
& C_{45} N_{i,2_{m2}} \triangleleft N_{m2} N_{n1} \triangleright_{\Omega} N_{j,1_{n1}} \triangleleft H F_{\tau} F_s \triangleright_A + \\
& C_{45} N_{i,1_{m1}} \triangleleft N_{m1} N_{n2} \triangleright_{\Omega} N_{j,2_{n2}} \triangleleft H F_{\tau} F_s \triangleright_A + \\
& C_{44} N_{i,2_{m2}} \triangleleft N_{m2} N_{n2} \triangleright_{\Omega} N_{j,2_{n2}} \triangleleft H F_{\tau} F_s \triangleright_A
\end{aligned} \tag{5.9}$$

where:

$$\triangleleft(\dots)\triangleright_{\Omega} = \int_{\Omega} (\dots) d\Omega, \quad \triangleleft(\dots)\triangleright_A = \int_A (\dots) d\xi_3 \tag{5.10}$$

The fundamental nucleus is expanded on the sum indexes $m, n = 1, \dots, 6$ (that is a loop on the tying points), $i, j = 1, \dots, 9$ and $\tau, s = 0, \dots, N$ in order to build the stiffness matrix of each element. Then, the stiffness matrixes are assembled at element level

by imposing the compatibility conditions. Moreover, if the shell is multilayered, the stiffness matrix is calculated for each layer k , by following two approach: if the variable description is ESL, the geometrical parameters, such as R and H , are referred to the global midsurface of the structure, but the different material constants of each layer are used; if the variable description is LW, the parameters R and H are referred to the midsurface of the layer k . Finally, the stiffness matrixes are assembled at multilayer level following the procedure explained in Section 3.1. For more details about the derivation of the governing equations, one can refer to [223].

5.2 Assessment

Some discriminating problems from the literature are considered in order to test the efficiency and the robustness of the shell element. The first test is the one called *pinched shell*. The essential shape of this structure is shown in Fig. 5.1. The pinched shell is simply supported at each end by rigid diaphragm and singularly loaded by two opposed forces acting at midpoint of the shell. Due to the symmetry of the structure the computations have been performed, using a uniform decomposition, on a octave of the shell (\overline{ABCD}). The physical data given in Table 5.1 have been assumed.

The following symmetry conditions are applied:

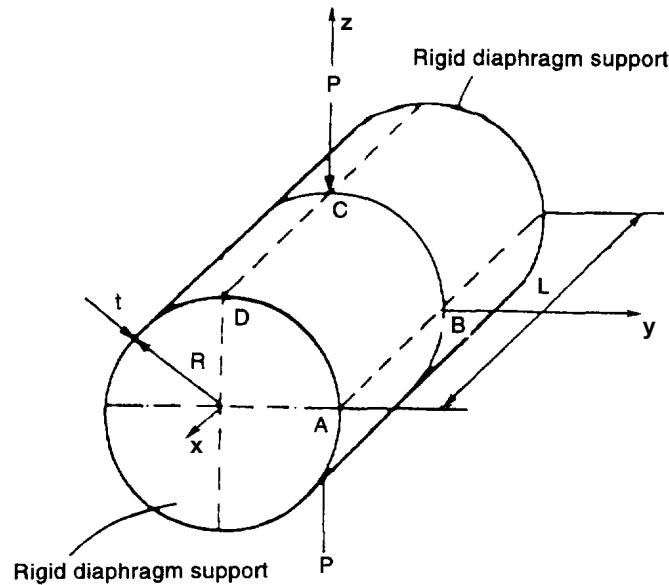


Figure 5.1: Pinched shell.

$$\begin{aligned} v_s(\xi_1, 0) &= 0, \\ u_s(0, \xi_2) &= 0, \\ v_s(\xi_1, R\pi/2) &= 0, \end{aligned} \tag{5.11}$$

Pinched shell		
Young's modulus	E	3×10^6 psi
Poisson's ratio	ν	0.3
load	P	1 lb
length	L	600 in
radius	R	300 in
thickness	t	3 in

Table 5.1: Physical data for pinched shell.

and the following simply-supported conditions are prescribed on the boundary:

$$v_s(L/2, \xi_2) = w_s(L/2, \xi_2) = 0, \quad (5.12)$$

with $s = 0, 1, \dots, N$.

In Table 5.2 the transversal displacement at the loaded point C is presented for several decompositions $n \times n$ and different theories. The exact solution is given by Flügge [224] and it is 1.8248×10^{-5} [in]. The results show that the element has good properties of convergence and robustness by increasing the mesh. The results obtained with high-order theories are grater than the reference value because Flügge refers to a classical shell theory. Indeed, the solution calculated with the CLT model is very close to the exact solution for mesh 13×13 , while the FSDT model that takes into account the shear energy gives a higher value, as one can expect. The ESL theory with linear expansion (ESL1) produces such a high value because the correction of Poisson locking it has been applied, but in the case of cylindrical shell structures this correction gives some problems. The remaining theories provide almost the same results and they converge to the same value (1.842×10^{-5} [in]) by increasing the order of expansion and the number of used elements.

Mesh	4×4	10×10	13×13
CLT	1.7891	1.8230	1.8251
FSDT	1.7984	1.8363	1.8396
ED1	1.9212	1.9582	1.9615
ED2	1.7805	1.8359	1.8406
ED3	1.7818	1.8379	1.8427
ED4	1.7818	1.8379	1.8427

Table 5.2: Pinched shell. Transversal displacement $w[\text{in}] \times 10^5$ at the loaded point C of the midsurface.(exact solution: 1.8248×10^{-5} [in])

The second test deals with a cylindrical shell known in the literature as *barrel vault*. The shell is described in Fig.5.2. This typical shell is used in civil engineering using

conventional processes by Scordelis and Lo [225]. The shell is simply-supported on diaphragms and is free on the other sides. The shell is loaded by its own weight P . The physical data given in Table 5.3 have been assumed.

The covariant components of the vertical load are: $p_1 = 0$, $p_2 = -P \sin(\xi_2/R)$, $p_3 =$

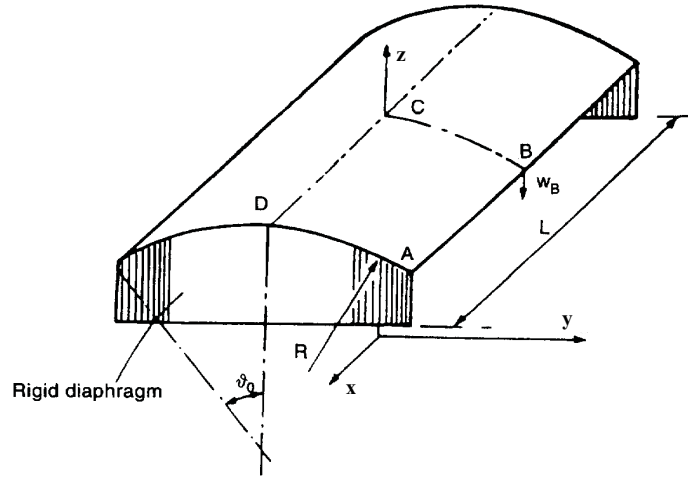


Figure 5.2: Scordelis-Lo roof.

Barrel vault		
Young's modulus	E	4.32×10^8 lb/ft ²
Poisson's ratio	ν	0.0
load	P	90 lb/ft ²
length	L	50 ft
radius	R	25 ft
thickness	t	0.25 ft
angle	θ_0	$2\pi/9$ rad

Table 5.3: Physical data for barrel vault.

$P \cos(\xi_2/R)$. The barrel vault has a symmetric structure. Thus, the computations have been performed only on a quarter of the shell, using a uniform decomposition. The following symmetry conditions have been assumed:

$$\begin{aligned} v_s(\xi_1, 0) &= 0, \\ u_s(0, \xi_2) &= 0, \end{aligned} \tag{5.13}$$

and the following boundary conditions are prescribed:

$$v_s(L/2, \xi_2) = w_s(L/2, \xi_2) = 0, \tag{5.14}$$

with $s = 0, 1, \dots, N$.

The exact solution for the present problem is given by McNeal and Harder [226] in terms of transversal displacement at the point B and it is 0.3024[ft]. In Table 5.4 this quantity is calculated for several decompositions $n \times n$ and different theories. The Table confirms the considerations done for the pinched shell: the results converge to the exact solution by increasing the order of expansion and the number of elements. Another difference regarding to the pinched shell is that the high-order theories and the classical theories provide almost the same results, because in this case we don't have local stretching effects in the thickness direction due to the concentrated load. In Figure 5.3, the ED4 solution in which the correction of both shear and membrane locking has been applied ($m+$) is compared with the solution in which only the shear locking has been corrected (s). One can note that the membrane locking phenomenon is remarkable in the barrel vault and the shell element shows high performances in terms of convergence, by increasing the number of elements. One can conclude that the shell element based on the CUF is completely locking free. For more details about

Mesh	13×13	16×16	20×20
FSDT	0.30091	0.30097	0.30104
ED1	0.30091	0.30097	0.30104
ED2	0.30091	0.30097	0.30104
ED3	0.30091	0.30097	0.30104
ED4	0.30091	0.30097	0.30104

Table 5.4: Barrel vault. Transversal displacement w [ft] at the point B of the midsurface S .(exact solution: 0.3024[ft]).

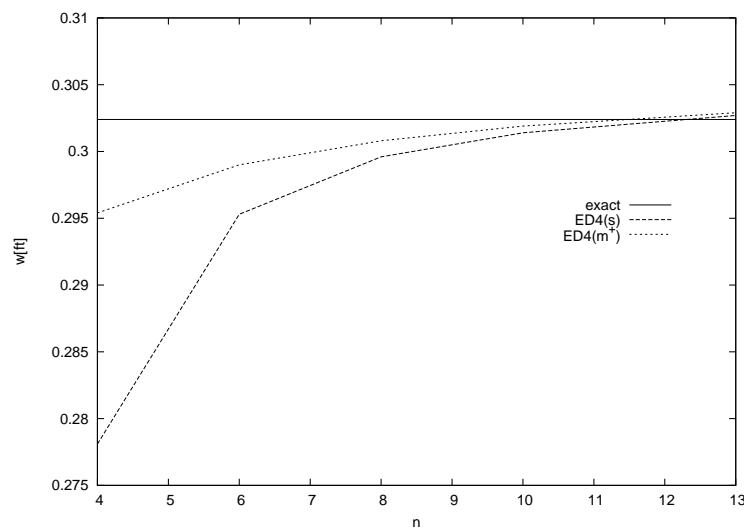


Figure 5.3: Barrel vault. Transversal displacement w [ft] at the point B of the midsurface S by varying the mesh $n \times n$.

the assessment of the CUF MITC9 shell element, one can refer to [223].

5.3 Analysis of composite shells

In order to test the efficiency of the different models contained in the CUF (classical, ESL, ZZ and LW) combined with the finite element scheme two classical reference problems are analyzed and the numerical results are compared with the ones obtained by the 3D elasticity approach.

The first problem is the structure analyzed by Ren [30] (see Fig.5.4). It is a composite cylindrical panel made of three orthotropic layers with lamination $(90^\circ/0^\circ/90^\circ)$, where the lamination angle is measured with respect to the ξ_1 axis. The layers have equal thickness and the physical properties of the shell are given in Table 5.5 (L is the direction parallel to the fibres and T is the transverse direction).

A sinusoidal distribution of transverse pressure applied at the top shell surface is

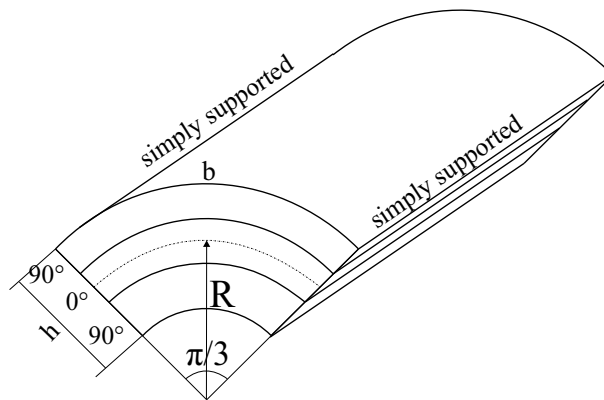


Figure 5.4: Ren cylindrical shell.

Ren cylindrical shell		
Young's modulus	E_L/E_T	25
Shear modulus	G_{LT}/E_T	0.5
Shear modulus	G_{TT}/E_T	0.2
Poisson's ratio	$\nu_{LT} = \nu_{TT}$	0.25
radius	R	10
angle span	φ	$\pi/3$

Table 5.5: Physical data for Ren cylindrical shell.

considered (cylindrical bending problem):

$$p_3^+ = \hat{p}_3^+ \sin \left(\frac{n \pi \xi_2}{b} \right), \quad (5.15)$$

with amplitude $\hat{p}_3^+ = 1$ and wave number $n = 1$.

In order to reproduce the property of infinite length in the finite element scheme, the following plane-strain conditions (respect to the plane ξ_2, ξ_3) are imposed in each point of the cylinder:

$$\begin{aligned} u_s(\xi_1, \xi_2) &= 0, \\ (u_s, v_s, w_s)_{,1}(\xi_1, \xi_2) &= 0, \end{aligned} \quad (5.16)$$

that is any variation along the axis of the cylinder is equal to zero.

Due to the symmetry of both the geometry and the load, half cylinder is analyzed in the circumferential direction and the following symmetry and boundary conditions (simply-supported) are applied:

$$\begin{aligned} v_s(\xi_1, 0) &= 0, \\ w_s(L/2, \xi_2) &= 0, \end{aligned} \quad (5.17)$$

with $s = 0, 1, \dots, N$.

The results are presented for different thickness ratios R/h in terms of non-dimensional transversal displacement:

$$\bar{w} = \frac{w 10 E_L h^3}{\hat{p}_3^+ R^4}, \quad (5.18)$$

measured in the middle of the shell surface, where the load has its maximum amplitude.

The Figure 5.5 shows the convergence of the parameter \bar{w} by varying the number of the elements n in the circumferential direction (only one element is taken in the axial direction) for the theory LD4 and the thickness ratio $R/h = 100$: (MITC) is the FEM solution obtained by applying the MITC method; (FEM_s) is the FEM solution with the correction of the shear locking only; and (FEM) is the FEM solution without any correction. One can see that the first curve converge very fast to the 3D solution, as confirmed in Table 5.6 where the percentage error ($\text{err} = \frac{|3\text{D} - \text{MITC}|}{3\text{D}} \times 100$) is calculated. One can see that the error becomes steady for $n = 6$. The other curves are more slow, even when the shear locking is corrected. This demonstrates that the membrane locking is a very important phenomenon in the shell elements and the MITC technique is very efficient in contrasting both the membrane and shear locking. After this analysis, 6 elements are taken to perform the following analysis.

Finally, the Figure 5.6 shows the convergence of the parameter \bar{w} by varying the thickness ratio R/h for the theory LD4. In this Figure, also the analytical solution (anal), obtained by solving the governing equations with the Navier method, is presented for comparison reasons. One can note that the MITC solution coincides with the analytical one for the different thickness ratios. Therefore, the error of the MITC solution in

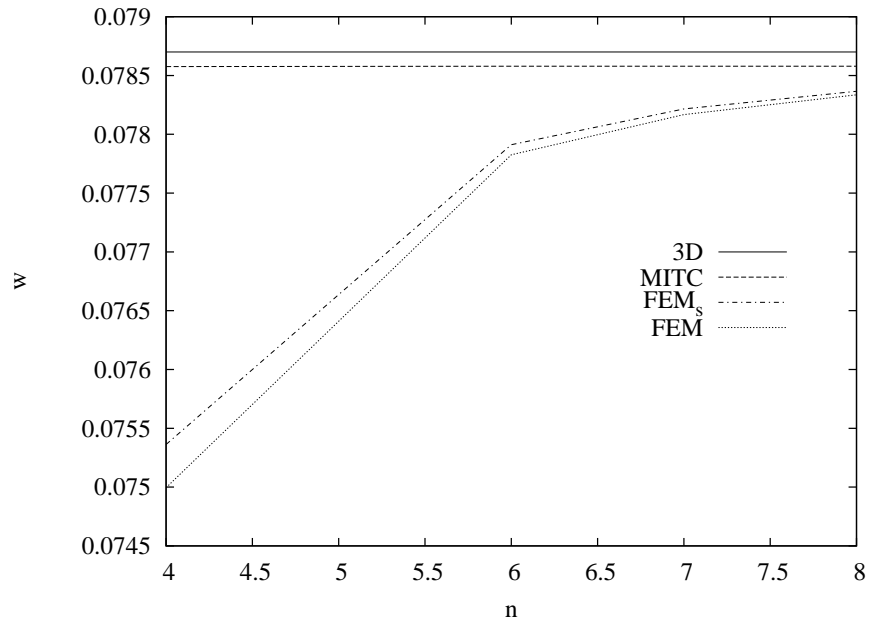


Figure 5.5: Ren shell. Convergence of the displacement \bar{w} by varying n . Thickness ratio $R/h = 100$. Theory: LD4.

n	2	4	6	8
ED4	0.07843	0.07849	0.07850	0.07850
err	0.34%	0.27%	0.25%	0.25%
LD4	0.07852	0.07857	0.07858	0.07858
err	0.23%	0.16%	0.15%	0.15%

Table 5.6: Ren cylindrical shell. Convergence of the transversal displacement $\bar{w}(\xi_3 = 0)$ by increasing the number of elements. Lamination $(90^\circ/0^\circ/90^\circ)$. Thickness ratio $R/h = 100$. Exact solution [30]: 0.0787.

respect to the exact solution is due only to the bi-dimensional approximation and not to the FEM approximation. This confirms also the efficiency of the MITC method in contrasting the locking, while the FEM_s and FEM solutions lock noticeably for very thin shells ($R/h = 100, 500$).

The Table 5.7 compares the results obtained using the different theories contained in

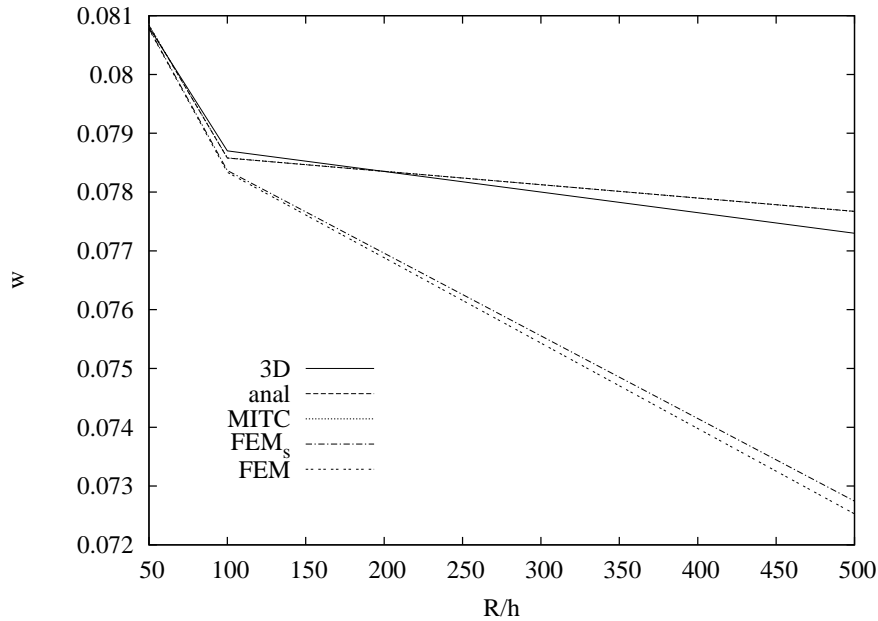


Figure 5.6: Ren shell. Convergence of the displacement \bar{w} by varying R/h . Theory: LD4. Mesh: 1×6 .

the CUF with the 3D elasticity solution and the CST (Classical Shell Theory) solution given by Ren in [30]. For some models (FSDT, ED4, ED2, LD4, LD1, EDZ2) also the analytical solution, indicated with the subscript a , is reported. In general, the results approach to the exact solution by increasing the order of expansion N , for the various thickness ratios. For both moderately thick and very thin shells, the solution coincides with the analytical one and this demonstrates that the element doesn't suffer the locking or other numerical phenomenons. For very low thickness ratio ($R/h = 2, 4$), there are some discrepancies between the two solutions because the two-dimensional approximation is erroneously applied to very thick shells and the aspect ratio of each element becomes very high. One can note that higher order ZZ models give a better solution in respect to ESL models, but only the LD4 model is able to exactly reproduce the 3D solution in the case of thick shell. This is due to the better approximation of transverse stresses obtained with the LW models, as it will be demonstrated in the following Section. Finally, one can conclude that the classical models (FSDT and CLT) give good results only when the shell is very thin ($R/h = 100, 500$). For thick shells, the CLT solution obtained with the CUF shell element is slightly higher than the CST one, because the CST model contains more assumptions along the thickness, such as the parameter H in the governing equations (5.7-5.9) is equal to 1.

R/h	2	4	10	50	100	500
3D[30]	1.436	0.457	0.144	0.0808	0.0787	0.773
CST[30]	0.0799	0.0781	0.0777	0.0776	0.0776	0.0776
CLT	0.09625	0.08712	0.08143	0.07834	0.07796	0.07766
FSDT	1.169	0.3329	0.1183	0.07976	0.07831	0.07766
FSDT _a	1.210	0.3354	0.1184	0.07977	0.07831	0.07766
ED4	1.368	0.4271	0.1364	0.08051	0.07850	0.07767
ED4 _a	1.383	0.4284	0.1365	0.08051	0.07850	0.07767
ED3	1.369	0.4272	0.1364	0.08051	0.07850	0.07767
ED2	1.104	0.3305	0.1191	0.07982	0.07832	0.07766
ED2 _a	1.111	0.3310	0.1191	0.07982	0.07832	0.07766
ED1	1.129	0.3324	0.1192	0.07982	0.07832	0.07766
LD4	1.460	0.4614	0.1442	0.08084	0.07858	0.07767
LD4 _a	1.435	0.4581	0.1440	0.08083	0.07858	0.07767
LD3	1.459	0.4614	0.1442	0.08084	0.07858	0.07767
LD2	1.411	0.4576	0.1441	0.08083	0.07858	0.07767
LD1	1.381	0.4435	0.1410	0.08068	0.07851	0.07764
LD1 _a	1.363	0.4407	0.1408	0.08067	0.07851	0.07764
EDZ3	1.412	0.4583	0.1441	0.08084	0.07858	0.07767
EDZ2	1.378	0.4430	0.1410	0.08071	0.07855	0.07767
EDZ2 _a	1.496	0.4420	0.1410	0.08071	0.07855	0.07767
EDZ1	1.400	0.4443	0.1408	0.08038	0.07821	0.07734

Table 5.7: Ren cylindrical shell. Lamination ($90^\circ/0^\circ/90^\circ$). Transversal displacement $\bar{w}(\xi_3 = 0)$.

The second problem considered is the structure analyzed by Varadan and Bhaskar [31] (see Fig.5.7). It is a composite cylinder, in which each layer is made of square symmetric unidirectional fibrous orthotropic material with the properties given in Table 5.8. L is the direction parallel to the fibres and T is the transverse direction.

The following problems are solved:

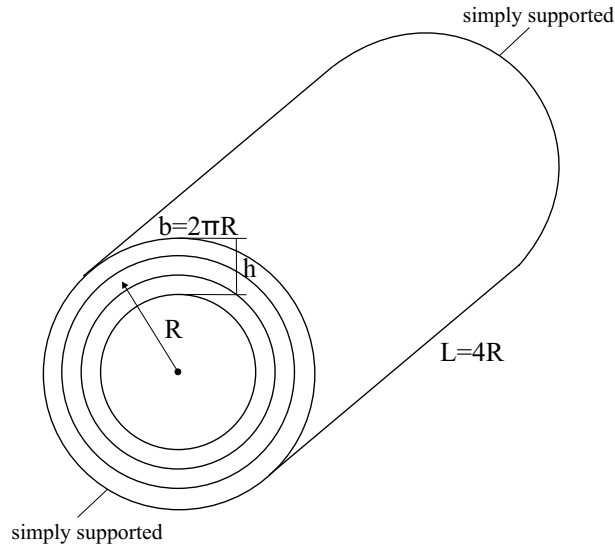


Figure 5.7: Varadan & Bhaskar cylinder.

Varadan & Bhaskar cylinder		
Young's modulus	E_L/E_T	25
Shear modulus	G_{LT}/E_T	0.5
Shear modulus	G_{TT}/E_T	0.2
Poisson's ratio	$\nu_{LT} = \nu_{TT}$	0.25
length	$L = 4R$	40
radius	R	10

Table 5.8: Physical data for Varadan & Bhaskar cylinder.

1. a two-layered ($90^\circ/0^\circ$) shell (90° for the outer layer and 0° for the inner layer, measured with respect to the ξ_1 axis);
2. a three-layered ($90^\circ/0^\circ/90^\circ$) shell.

In all these cases the layers are of equal thickness and the loading is internal sinusoidal pressure, applied normal to the bottom shell surface, and is given by:

$$p_3^+ = \hat{p}_3^+ \sin\left(\frac{m\pi\xi_1}{L}\right) \sin\left(\frac{n\pi\xi_2}{b}\right), \quad (5.19)$$

with amplitude $\hat{p}_3^+ = 1$ and wave numbers $m = 1$ and $n = 8$.

Due to the symmetry of both the geometry and the load, an octave of the cylinder is studied (1/2 in the axial direction and 1/4 in the hoop direction). The following symmetry conditions are applied:

$$\begin{aligned} v_s(\xi_1, 0) &= 0, \\ u_s(0, \xi_2) &= 0, \\ v_s(\xi_1, R\pi/2) &= 0, \end{aligned} \quad (5.20)$$

and the following boundary conditions are prescribed:

$$v_s(L/2, \xi_2) = w_s(L/2, \xi_2) = 0, \quad (5.21)$$

with $s = 0, 1, \dots, N$.

The results are presented for these cases for different thickness ratios R/h in terms of the following non-dimensional parameters:

$$\begin{aligned} \bar{w} &= \frac{w 10 E_L h^3}{\hat{p}_3^+ R^4}, \\ (\bar{\sigma}_{11}, \bar{\sigma}_{22}, \bar{\sigma}_{12}) &= \frac{(\sigma_{11}, \sigma_{22}, \sigma_{12}) 10 h^2}{\hat{p}_3^+ R^2}, \\ (\bar{\sigma}_{13}, \bar{\sigma}_{23}) &= \frac{(\sigma_{13}, \sigma_{23}) 10 h}{\hat{p}_3^+ R}, \\ \bar{\sigma}_{33} &= \frac{\sigma_{33}}{\hat{p}_3^+}, \end{aligned} \quad (5.22)$$

where the maximum values of the displacement and the stresses in the surface are considered.

Also in this case, a convergence analysis is performed for the lamination case ($90^\circ/0^\circ$). The Figures 5.8 and 5.9 show the convergence of the parameters \bar{w} and $\bar{\sigma}_{13}$ by varying the number of the elements n (a square mesh $n \times n$ is used) for the theory LD4 and the thickness ratio $R/h = 100$. The conclusions drawn for the Ren shell are here confirmed: the membrane locking is very important for both the displacements and the stresses and the MITC technique is very efficient in contrasting it. After this analysis, a mesh 8×8 is taken to perform the following analysis.

The Tables 5.9-5.12 and 5.13-5.14 show the results for the problems 1 and 2, respectively. The different theories contained in the CUF are used and the results are compared with the 3D solution given in [31]. Also the analytical solution is reported for the transversal displacement in the problem 2 (Table 5.13) in order to validate the numerical efficiency of the shell finite element. The results in terms of displacements (Tables 5.9 and 5.13) lead to the same conclusions made for the Ren shell: the results converge

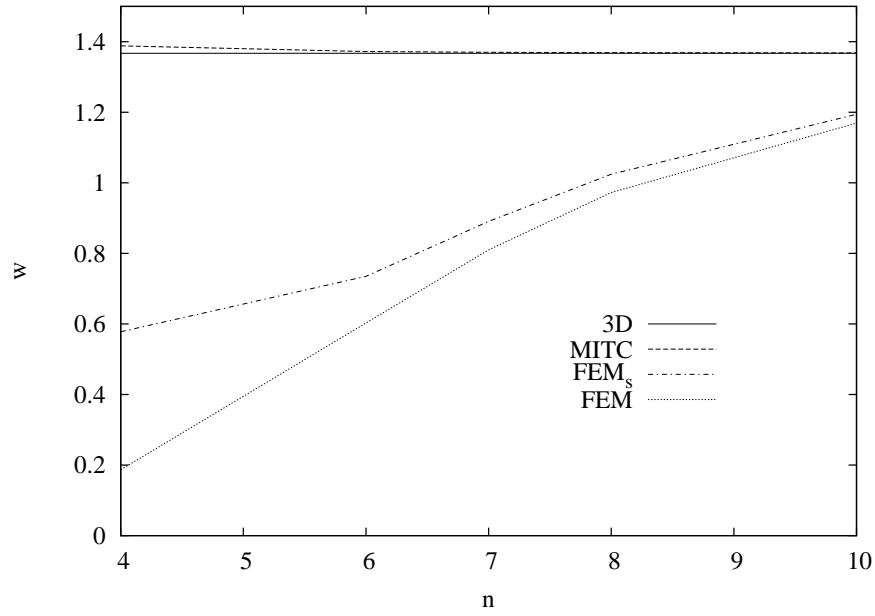


Figure 5.8: Varadan & Bhaskar cylinder. Convergence of the displacement \bar{w} by varying n . Lamination ($90^\circ/0^\circ$). Thickness ratio $R/h = 100$. Theory: LD4.

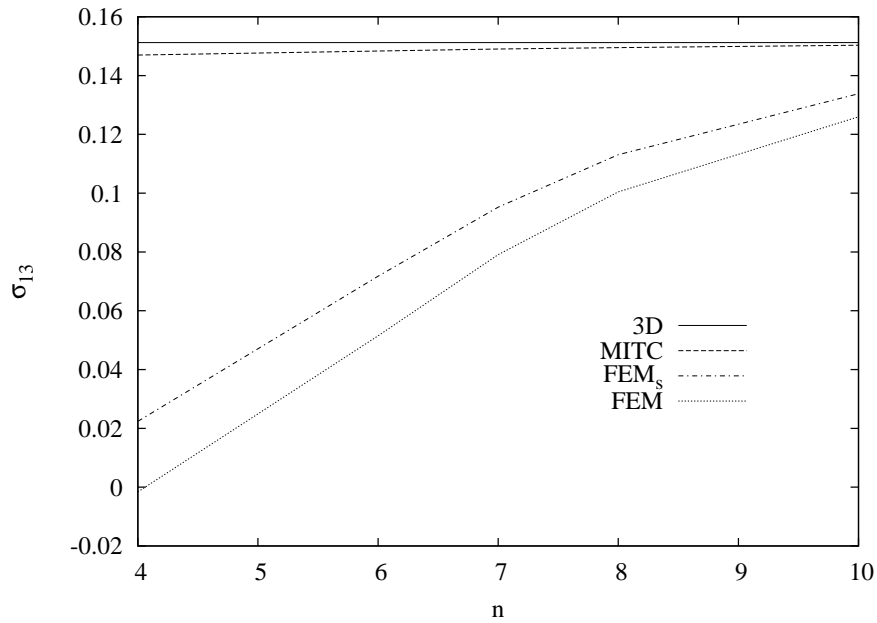


Figure 5.9: Varadan & Bhaskar cylinder. Convergence of the shear stress $\bar{\sigma}_{13}$ by varying n . Lamination ($90^\circ/0^\circ$). Thickness ratio $R/h = 100$. Theory: LD4.

to the exact solution by increasing the order of expansion N ; the LW models work better than the ESL and ZZ ones; and the CLT and FSDT model fail in the analysis of thick shells. If one considers the in-plane stresses (Tables 5.10, 5.11 and 5.13) the behavior is the same: higher-order layer wise models are necessary to match the reference solution in the thick shells, but the classical models are still able to give good results in the thin shell case. Looking at the transverse shear and normal stresses (Tables 5.12 and 5.14), one can note that neither the ED4 and EDZ3 models are able to reproduce the exact solution in both thick and thin shells (in particular in terms of σ_{33}). In this case, the use of the LD4 model becomes mandatory. This fact is simply explicable if one considers the distribution of shear and normal stresses along the thickness, given in the Figures 5.10-5.12. The LW model only is able to fulfill the continuity conditions of transverse stresses at the interfaces between layers, while the FSDT model gives a completely wrong result (Fig.5.11), even if the shell is very thin ($R/h = 100$). In particular, the Figures 5.10 ($R/h = 500$) and 5.12 ($R/h = 100$) show that the introduction of Murakami's zig-zag function improve the solution in respect to a simply ESL model, but it is not enough to correctly describe the distribution of the normal stress in the composite structures, because the interlaminar continuity conditions are not satisfied. For this reason, also the results in terms of displacements are better when a LW model is used.

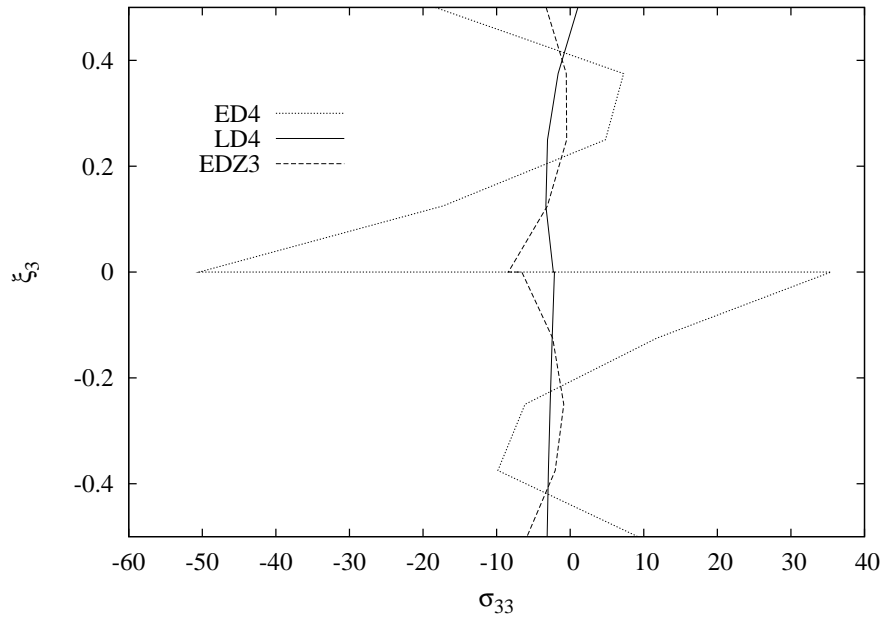
R/h	2	4	10	50	100	500
$\bar{w}(\xi_3 = 0)[31]$	14.034	6.100	3.330	2.242	1.367	0.1005
CLT	2.781	2.802	2.772	2.227	1.367	0.1007
FSDT	12.41	5.578	3.243	2.240	1.368	0.1007
ED4	14.08	6.075	3.319	2.242	1.369	0.1007
ED3	14.13	6.014	3.300	2.241	1.369	0.1007
ED2	13.07	5.717	3.255	2.240	1.369	0.1007
ED1	13.63	5.688	3.242	2.243	1.369	0.1009
LD4	14.33	6.164	3.337	2.242	1.369	0.1007
LD3	14.32	6.163	3.337	2.242	1.369	0.1007
LD2	13.80	5.921	3.284	2.241	1.369	0.1007
LD1	13.08	5.776	3.255	2.232	1.365	0.1007
EDZ3	14.20	6.009	3.299	2.241	1.369	0.1007
EDZ2	13.12	5.748	3.262	2.240	1.369	0.1007
EDZ1	13.67	5.759	3.247	2.232	1.365	0.1007

Table 5.9: Varadan & Bhaskar cylinder. Transversal displacement. Lamination ($90^\circ/0^\circ$).

R/h	2	4	10	50	100	500
$\bar{\sigma}_{11}(\xi_3 = \mp \frac{h}{2})[31]$	-2.660 0.2511	-0.9610 0.2120	-0.1689 0.1930	1.610 0.2189	2.300 0.1871	0.9436 0.0449
CLT	-0.5690 0.1464	-0.4752 0.1661	-0.1549 0.1864	1.594 0.2230	2.300 0.1903	0.9484 0.04535
FSDT	-1.216 0.2256	-0.6911 0.2018	-0.1523 0.1955	1.603 0.2236	2.302 0.1904	0.9484 0.04535
ED4	-2.649 0.2302	-0.9580 0.2181	-0.1785 0.1970	1.605 0.2216	2.303 0.1891	0.9486 0.04516
ED2	-2.172 0.1049	-0.8725 0.1156	-0.1649 0.1634	1.606 0.2226	2.303 0.1918	0.9483 0.04567
LD4	-2.678 0.2578	-0.9557 0.2210	-0.1702 0.2005	1.606 0.2241	2.303 0.1906	0.9484 0.04536
LD2	-2.610 0.1986	-0.9386 0.1732	-0.1703 0.1781	1.605 0.2204	2.302 0.1895	0.9484 0.04534
EDZ3	-2.703 0.2465	-0.9539 0.1970	-0.1685 0.1846	1.605 0.2206	2.302 0.1893	0.9484 0.04531
EDZ1	-1.950 0.01369	-0.8734 0.1234	-0.2031 0.1946	1.567 0.2483	2.278 0.2072	0.9468 0.04670
$\bar{\sigma}_{22}(\xi_3 = \mp \frac{h}{2})[31]$	-3.036 9.775	-1.789 10.31	-1.343 10.59	-0.9670 8.937	-0.5759 5.560	-0.0339 0.4345
CLT	-1.165 8.871	-1.243 10.33	-1.258 11.14	-1.003 9.405	-0.6023 5.845	-0.03596 0.4556
FSDT	-1.151 8.708	-1.236 10.25	-1.255 11.11	-1.001 9.392	-0.6017 5.840	-0.03596 0.4556
ED4	-2.785 10.36	-1.734 11.12	-1.358 11.26	-1.007 9.392	-0.6028 5.838	-0.03586 0.4553
ED2	-1.947 5.194	-1.534 8.827	-1.317 10.79	-1.004 9.380	-0.6023 5.840	-0.03608 0.4559
LD4	-2.843 11.24	-1.739 11.34	-1.354 11.30	-1.006 9.396	-0.6028 5.840	-0.03598 0.4555
LD2	-2.706 8.717	-1.668 10.23	-1.333 11.06	-1.006 9.385	-0.6028 5.838	-0.03598 0.4555
EDZ3	-2.860 10.20	-1.707 10.76	-1.336 11.17	-1.006 9.388	-0.6030 5.838	-0.03601 0.4555
EDZ1	-1.939 5.911	-1.585 9.151	-1.354 10.87	-1.027 9.383	-0.6168 5.847	-0.03711 0.4571

Table 5.10: Varadan & Bhaskar cylinder. In plane stresses. Lamination ($90^\circ/0^\circ$).

R/h	2	4	10	50	100	500
$\bar{\sigma}_{12}(\xi_3 = \mp \frac{h}{2})[31]$	-0.5016 0.2685	-0.2812 0.2007	-0.2325 0.1247	-0.3449 -0.0784	-0.3452 -0.1819	-0.1045 -0.0925
CLT	-0.1534 0.1504	-0.1761 0.1516	-0.2145 0.1227	-0.3588 -0.08235	-0.3617 -0.1915	-0.1099 -0.09736
FSDT	-0.2994 0.2532	-0.2431 0.1946	-0.2331 0.1273	-0.3604 -0.08313	-0.3620 -0.1917	-0.1099 -0.09736
ED4	-0.4812 0.3032	-0.2831 0.2199	-0.2391 0.1328	-0.3605 -0.08280	-0.3620 -0.1917	-0.1099 -0.09736
ED2	-0.3677 0.2541	-0.2521 0.2025	-0.2328 0.1299	-0.3602 -0.08275	-0.3620 -0.1916	-0.1099 -0.09736
LD4	-0.4910 0.3067	-0.2859 0.2216	-0.2400 0.1332	-0.3606 -0.08282	-0.3620 -0.1917	-0.1099 -0.09736
LD2	-0.4631 0.2861	-0.2732 0.2103	-0.2360 0.1309	-0.3603 -0.08276	-0.3620 -0.1916	-0.1099 -0.09736
EDZ3	-0.4852 0.2990	-0.2808 0.2147	-0.2374 0.1316	-0.3604 -0.08278	-0.3620 -0.1916	-0.1099 -0.09736
EDZ1	-0.3636 0.2715	-0.2553 0.2048	-0.2331 0.1297	-0.3589 -0.08242	-0.3611 -0.1912	-0.1099 -0.09735

Table 5.11: Varadan & Bhaskar cylinder. In plane shear stress. Lamination ($90^\circ/0^\circ$).Figure 5.10: Varadan & Bhaskar cylinder. Distribution of transverse normal stress $\bar{\sigma}_{33}$ along the thickness. Lamination ($90^\circ/0^\circ$). Thickness ratio $R/h = 500$.

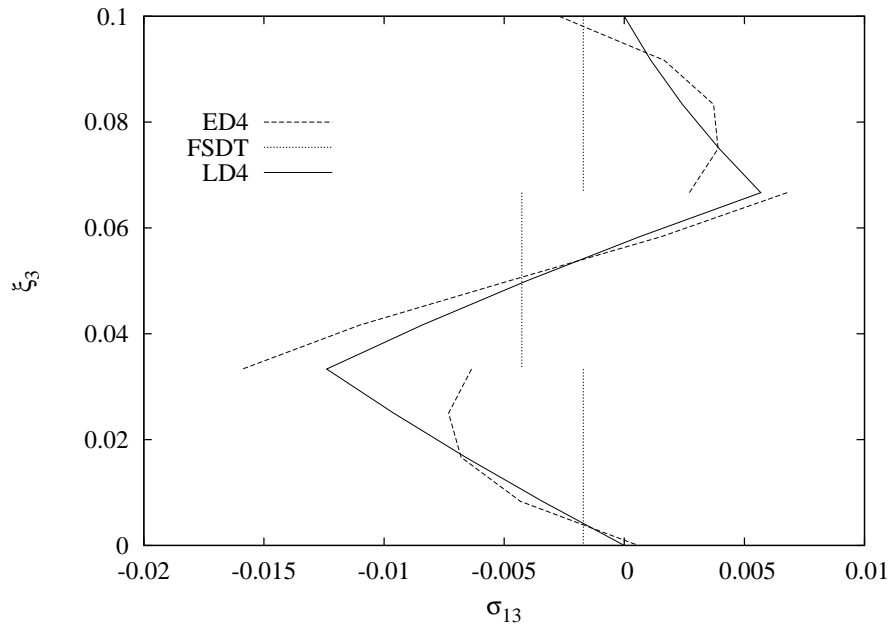
R/h	2	4	10	50	100	500
$\bar{\sigma}_{13}(\xi_3 = \frac{-h}{4})[31]$	0.4786	0.2758	0.1591	-0.0448	-0.1512	-0.0841
CLT	-	-	-	-	-	-
FSDT	0.3351	0.2401	0.1501	-0.1111	-0.2453	-0.1229
ED4	0.4142	0.2273	0.1257	-0.0560	-0.1503	-0.0797
ED2	0.3653	0.2187	0.1308	-0.0781	-0.1873	-0.0963
LD4	0.4783	0.2715	0.1578	-0.0418	-0.1495	-0.0843
LD2	0.3655	0.2090	0.1220	-0.0657	-0.1642	-0.0854
EDZ3	0.4144	0.2379	0.1350	-0.0969	-0.2165	-0.1090
EDZ1	0.3852	0.2081	0.1164	-0.0698	-0.1664	-0.0856
$\bar{\sigma}_{23}(\xi_3 = \frac{h}{4})[31]$	-2.931	-4.440	-5.457	-4.785	-2.972	-0.227
CLT	-	-	-	-	-	-
FSDT	-2.664	-3.216	-3.412	-2.065	-0.6314	0.3343
ED4	-2.928	-4.274	-4.931	-3.395	-1.446	0.2764
ED2	-2.477	-3.392	-3.762	-2.386	-0.8261	0.3219
LD4	-3.216	-4.791	-5.776	-5.024	-3.124	-0.2441
LD2	-2.675	-3.671	-4.197	-3.598	-2.238	-0.1769
EDZ3	-2.971	-3.896	-4.259	-2.784	-1.073	0.3019
EDZ1	-2.666	-3.494	-3.872	-2.486	-0.8902	0.3175
$\bar{\sigma}_{33}(\xi_3 = \frac{h}{4})[31]$	-0.31	-0.70	-1.68	-6.29	-7.71	-3.09
CLT	-	-	-	-	-	-
FSDT	-	-	-	-	-	-
ED4	-0.3358	-0.7126	-1.607	-5.072	-4.872	4.793
ED2	-0.3352	-0.6336	-1.330	-5.197	-7.752	-12.78
LD4	-0.3408	-0.7358	-1.754	-6.549	-8.000	-3.082
LD2	-0.3440	-0.6612	-1.397	-4.823	-5.847	-2.281
EDZ3	-0.3353	-0.6899	-1.454	-4.623	-5.071	-0.4819
EDZ1	-0.3489	-0.6867	-1.451	-4.927	-5.958	-2.315

Table 5.12: Varadan & Bhaskar cylinder. Transverse stresses. Lamination ($90^\circ/0^\circ$).

R/h	2	4	10	50	100	500
$\bar{w}(\xi_3 = 0)[31]$	10.1	4.009	1.223	0.5495	0.4715	0.1027
ED4	9.682	3.782	1.144	0.5456	0.4707	0.1029
ED4 _a	9.1582	3.7197	1.1409	0.5458	0.4708	0.1027
LD4	10.27	4.032	1.225	0.5493	0.4715	0.1029
LD4 _a	10.10	4.009	1.223	0.5495	0.4715	0.1027
$\bar{\sigma}_{11}(\xi_3 = \mp \frac{h}{2})[31]$	-0.8428 0.1761	-0.2701 0.1270	-0.0791 0.0739	-0.0225 0.0712	0.00018 0.0838	0.0379 0.0559
ED4	-0.9447 0.1433	-0.3011 0.1167	-0.0828 0.0734	-0.0240 0.0730	0.00062 0.0858	0.0381 0.0568
LD4	-0.8604 0.1841	-0.2733 0.1330	-0.0806 0.0773	-0.0241 0.0734	0.00029 0.0858	0.0377 0.0565
$\bar{\sigma}_{22}(\xi_3 = \mp \frac{h}{2})[31]$	-18.19 7.168	-9.323 6.545	-5.224 4.683	-3.987 3.930	-3.507 3.507	-0.7542 0.7895
ED4	-15.137 7.288	-9.146 6.845	-5.215 4.876	-4.146 4.129	-3.662 3.681	-0.7913 0.8289
LD4	-17.548 8.008	-9.418 7.103	-5.356 5.002	-4.152 4.135	-3.663 3.681	-0.7918 0.8285
$\bar{\sigma}_{12}(\xi_3 = \mp \frac{h}{2})[31]$	-0.2922 0.1797	-0.1609 0.1081	-0.0729 0.0374	-0.0760 -0.0118	-0.1038 -0.0478	-0.0889 -0.0766
ED4	-0.2770 0.1957	-0.1568 0.1127	-0.0713 0.0383	-0.0791 -0.0123	-0.1087 -0.0502	-0.0935 -0.0806
LD4	-0.2918 0.2015	-0.1642 0.1175	-0.0756 0.0398	-0.0795 -0.0124	-0.1088 -0.0503	-0.0935 -0.0806

Table 5.13: Varadan & Bhaskar cylinder. Transversal displacement and in-plane stresses. Lamination ($90^\circ/0^\circ/90^\circ$).

R/h	2	4	10	50	100	500
$\bar{\sigma}_{13}(\xi_3 = -\frac{1}{6}h)[31]$	0.3006	0.1736	0.0826	0.0894	0.1223	0.1051
ED4	0.4248	0.2321	0.1071	0.1175	0.1589	0.1339
LD4	0.3052	0.1745	0.0834	0.0909	0.1239	0.1059
$\bar{\sigma}_{23}(\xi_3 = 0)[31]$	-1.379	-2.349	-3.264	-3.491	-3.127	-0.691
ED4	-1.280	-2.025	-2.530	-2.613	-2.339	-0.5195
LD4	-1.442	-2.464	-3.421	-3.659	-3.279	-0.7287
$\bar{\sigma}_{33}(\xi_3 = 0)[31]$	-0.34	-0.62	-1.27	-4.85	-8.30	-9.12
ED4	-0.358	-0.684	-1.380	-5.184	-8.290	12.26
LD4	-0.343	-0.627	-1.296	-5.026	-8.621	-9.468

Table 5.14: Varadan & Bhaskar cylinder. Transverse stresses. Lamination ($90^\circ/0^\circ/90^\circ$).Figure 5.11: Varadan & Bhaskar cylinder. Distribution of transverse shear stress $\bar{\sigma}_{13}$ along the thickness. Lamination ($90^\circ/0^\circ/90^\circ$). Thickness ratio $R/h = 100$.

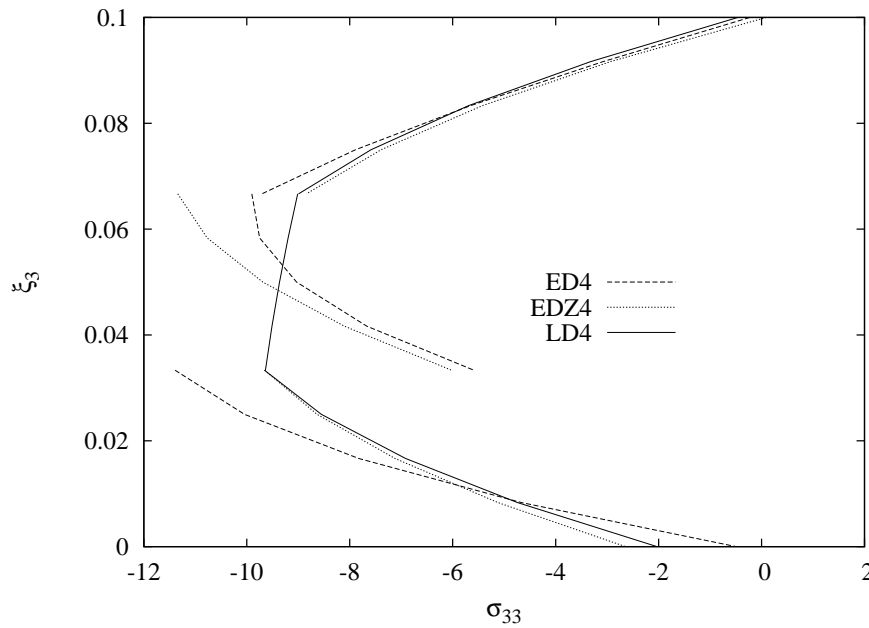


Figure 5.12: Varadan & Bhaskar cylinder. Distribution of transverse normal stress $\bar{\sigma}_{33}$ along the thickness. Lamination $(90^\circ/0^\circ/90^\circ)$. Thickness ratio $R/h = 100$.

5.3.1 Analysis of thick shells

The results presented in this chapter are obtained using the geometrical relations (2.21), in which the strain components are expressed in the 3D contravariant basis $(\mathbf{g}^1, \mathbf{g}^2, \mathbf{g}^3)$. From the tables provided above for composite shells, one can note that the solution calculated with LD4 theory (that is the best theory) gives the exact solution when the shell is thin, but there is an error in respect to the 3D solution when the shell is very thick $R/h = 2, 4$. Indeed, for thick shells, it isn't correct to assume that the basis $(\mathbf{g}^1, \mathbf{g}^2, \mathbf{g}^3)$ is coincident with the basis $(\mathbf{a}^1, \mathbf{a}^2, \mathbf{a}^3)$, and it is necessary to refer the strain components to the 2D basis. In this case, one needs to use the geometrical relations written by means of the differential matrixes in Eqs.(2.27-2.28).

The Tables 5.15 and 5.16 compare the results provided in the previous tables with the solution obtained using the correct geometrical relations, in the case of very thick shells $R/h = 2, 4$. Only the LD4 model is considered because it is the unique model that is able to reproduce the exact solution. In Table 5.15 (Ren shell), the transversal displacement \bar{w} obtained with the correct geometrical relations (LD4'), is compared with the result presented in Table 5.7 (LD4) and the analytical solution (LD4_a). One can note that the LD4' solution, differently from the LD4 solution, coincide exactly with the analytical solution and it approximates very well the 3D solution. In Table 5.16 (composite cylinder), the results are given in terms of both transversal displacement \bar{w} and transverse normal stress $\bar{\sigma}_{33}$. The table shows that, for both the laminations, the LD4' model reproduces the exact solution in terms of transversal displacement, while the LD4 solution presents a big error. Moreover, this fact influences the approximation of the trasverse normal stress that becomes better in the LD4' case. It might be demon-

strated also for the other stress components.

R/h	2	4
3D[30]	1.436	0.457
LD4 _a	1.435	0.4581
LD4	1.460	0.4614
LD4'	1.435	0.4581

Table 5.15: Ren cylindrical shell. Lamination ($90^\circ/0^\circ/90^\circ$). Transversal displacement $\bar{w}(\xi_3 = 0)$.

R/h	$(90^\circ/0^\circ)$		$(90^\circ/0^\circ/90^\circ)$	
	2	4	2	4
$\bar{w}[31]$	14.034	6.100	10.1	4.009
LD4	14.33	6.164	10.27	4.032
LD4'	14.001	6.097	10.095	4.007
$\bar{\sigma}_{33}[31]$	-0.31	-0.70	-0.34	-0.62
LD4	-0.341	-0.736	-0.343	-0.627
LD4'	-0.317	-0.7111	-0.335	-0.619

Table 5.16: Varadan & Bhaskar cylinder.

5.4 Analysis of FGM shells

The governing equations used for the analysis of FGM shells under pure-mechanical loads are the same presented in the Section 5.1, but in this case the material constants C_{ij} are dependent on the thickness coordinate ξ^3 . Differently from the analysis performed in Section 4.1, the material constants are not re-written using the Unified Formulation but they are directly integrated along ξ^3 with the thickness functions F_τ, F_s (the integrals are solved numerically).

The problem analyzed is the same of Section 4.1, but only the pure-mechanical case is considered. For the material properties, geometry and applied loads see Sec.4.1.2. The material index n_g is taken equal to 2 and different thickness ratios are considered: $R/h = 10, 100, 1000$. The reference solution is given in [133]. It is obtained using a

fourth-order CUF theory and taking a very high number of fictitious layers ($N_l = 100$) in the FGM shell, in which the mechanical properties are considered constant along the thickness and equal to the mean value between the top and bottom of the layer. In [133], it has been demonstrated that this procedure permits to calculate the quasi-3D solution of the static problem in FGM structures.

Table 5.17 shows the results in terms of displacements \bar{u} and \bar{w} and Table 5.18 in terms of the stresses $\bar{\sigma}_{22}$, $\bar{\sigma}_{13}$ and $\bar{\sigma}_{33}$. The comparison of FEM results, obtained with the different theories contained in the CUF, with the quasi-3D solution shows that the CUF element works very well for the analysis of FGM shells. It is demonstrated that a fourth-order of expansion of the displacements is necessary to ensure the convergence of the solution. The element provides very good results also for very thin shells ($R/h = 1000$) in spite of the membrane and shear locking phenomenon that usually affects the shell finite elements. One can note that the FSDT model is not able to accurately describe the distribution of displacements and stresses because it doesn't consider the variability of the mechanical behavior in FGMs along the thickness.

As discussed in [133], the influence of the material gradient on the variation of the transversal displacement is more evident in the thermal analysis and the use of higher-order models becomes mandatory in that case. For these reasons, a future work will be dedicated to the thermal analysis of functionally graded plates and shells by means of the CUF shell element.

For more details about the analysis of FGM structures by means of the CUF MITC9 shell element, one can refer to [227].

$R/h = 10$						
	Ref.[133]	FSDT	$N = 1$	$N = 2$	$N = 3$	$N = 4$
$\bar{u}_{(t)}$	0.0012	$1.048 \cdot 10^{-3}$	$7.937 \cdot 10^{-4}$	$6.659 \cdot 10^{-4}$	$1.089 \cdot 10^{-3}$	$1.152 \cdot 10^{-3}$
$\bar{u}_{(m)}$	-0.0006	$-2.562 \cdot 10^{-6}$	$-2.589 \cdot 10^{-4}$	$-6.100 \cdot 10^{-4}$	$-6.251 \cdot 10^{-4}$	$-5.739 \cdot 10^{-4}$
$\bar{u}_{(b)}$	-0.0010	$-1.053 \cdot 10^{-3}$	$-1.311 \cdot 10^{-3}$	$-5.911 \cdot 10^{-4}$	$-9.708 \cdot 10^{-3}$	$-1.004 \cdot 10^{-3}$
$\bar{w}_{(t)}$	0.0039	$2.338 \cdot 10^{-3}$	$3.503 \cdot 10^{-3}$	$3.499 \cdot 10^{-3}$	$3.835 \cdot 10^{-3}$	$3.876 \cdot 10^{-3}$
$\bar{w}_{(m)}$	0.0021	$2.338 \cdot 10^{-3}$	$2.327 \cdot 10^{-3}$	$1.950 \cdot 10^{-3}$	$2.158 \cdot 10^{-3}$	$2.126 \cdot 10^{-3}$
$\bar{w}_{(b)}$	0.0013	$2.338 \cdot 10^{-3}$	$1.152 \cdot 10^{-3}$	$9.847 \cdot 10^{-4}$	$1.306 \cdot 10^{-3}$	$1.331 \cdot 10^{-3}$
$R/h = 100$						
$\bar{u}_{(t)}$	0.0881	0.0887	0.0900	0.0876	0.0881	0.0881
$\bar{u}_{(m)}$	-0.0035	-0.0031	-0.0021	-0.0035	-0.0035	-0.0035
$\bar{u}_{(b)}$	-0.0952	-0.0949	-0.0943	-0.0946	-0.0951	-0.0951
$\bar{w}_{(t)}$	0.5984	0.5993	0.6006	0.5912	0.5944	0.5944
$\bar{w}_{(m)}$	0.5992	0.5993	0.6010	0.5956	0.5988	0.5989
$\bar{w}_{(b)}$	0.5964	0.5993	0.6015	0.5927	0.5960	0.5960
$R/h = 1000$						
$\bar{u}_{(t)}$	0.3157	0.3168	0.4970	0.3157	0.3163	0.3163
$\bar{u}_{(m)}$	-0.5553	-0.5547	-0.4285	-0.5551	-0.5549	-0.5549
$\bar{u}_{(b)}$	-1.426	-1.426	-1.354	-1.426	-1.426	-1.426
$\bar{w}_{(t)}$	55.45	55.50	58.92	55.44	55.47	55.47
$\bar{w}_{(m)}$	55.46	55.50	58.93	55.46	55.48	55.49
$\bar{w}_{(b)}$	55.47	55.50	58.94	55.46	55.49	55.49

Table 5.17: Non-dimensional in-plane displacement $\bar{u}(\frac{a}{2}, 0)$ and transversal displacement $\bar{w}(0, 0)$, calculated at the top (t), middle (m) and bottom (b) of the shell with material index $n_g = 2$.

$R/h = 10$						
	Ref.[133]	FSDT	$N = 1$	$N = 2$	$N = 3$	$N = 4$
$\bar{\sigma}_{22(t)}$	0.6770	0.2091	0.3929	0.5808	0.7466	0.6909
$\bar{\sigma}_{22(m)}$	0.1571	0.0439	0.3405	0.1365	0.1397	0.1602
$\bar{\sigma}_{22(b)}$	-0.2194	-0.2149	-0.1294	-0.0717	-0.3768	-0.2043
$\bar{\sigma}_{13(m)}$	-0.4440	-0.3347	-0.3322	-0.3107	-0.4521	-0.4574
$\bar{\sigma}_{33(m)}$	0.4486	–	0.5630	0.4346	0.4390	0.4570
$R/h = 100$						
$\bar{\sigma}_{22(t)}$	24.32	24.19	23.63	22.34	24.14	24.45
$\bar{\sigma}_{22(m)}$	11.03	10.88	9.794	12.22	11.07	11.05
$\bar{\sigma}_{22(b)}$	-11.22	-11.26	-12.68	-13.42	-10.82	-11.35
$\bar{\sigma}_{13(m)}$	-4.324	-2.910	-2.920	-3.147	-4.343	-4.339
$\bar{\sigma}_{33(m)}$	0.4689	–	5.419	2.757	0.5206	0.4802
$R/h = 1000$						
$\bar{\sigma}_{22(t)}$	955.9	958.8	916.0	932.8	955.5	959.0
$\bar{\sigma}_{22(m)}$	945.9	948.7	822.0	965.3	949.1	948.9
$\bar{\sigma}_{22(b)}$	780.1	781.9	600.4	748.6	788.2	782.2
$\bar{\sigma}_{13(m)}$	-3.862	-2.594	-2.775	-2.792	-3.878	-3.874
$\bar{\sigma}_{33(m)}$	0.4784	–	260.7	32.14	1.155	0.6914

Table 5.18: Non-dimensional stresses $\bar{\sigma}_{22}(0, 0)$, $\bar{\sigma}_{13}(\frac{a}{2}, 0)$ and $\bar{\sigma}_{33}(0, 0)$, calculated at the top (t), middle (m) and bottom (b) of the shell with material index $n_g = 2$.

Chapter 6

RBF solutions

In this chapter, some results obtained from the analysis of composite and FGM shells by means of the Radial Basis Functions method are presented. The governing equations are derived in strong form from the PVD for the static analysis and the free vibration analysis of shells. Note that every calculation is made referring to the double-curvature geometry and relative notation (see Section 2.2.1), even when the shell is cylindrical. Only the pure-mechanical problem is considered. New theories, different from those presented in Chapter 2, are used for the analysis. These are the Sinusoidal Shear Deformation Theory (SSDT) and the High-order Shear Deformation Theory (HSDT) and they are implemented by means of the Unified Formulation. The results are compared with analytical solutions given in literature and they show that the RBF method is very efficient for the study of both composite and FGM structures. Also a comparison with FEM results is provided in order to prove the advantages of radial basis functions that are the absence of mesh, the ease of discretization of boundary conditions and equations of equilibrium.

6.1 Governing equations

The differential equations for the analysis of doubly-curved shells by means of the RBF method are obtained following the procedure exposed in Section 3.1. The geometrical relations (Eqs.(2.29)), the constitutive equations (Eqs.(2.36)) and the Unified Formulation (Eqs.(2.1)) are substituted in the PVD (Eq.3.2) and the integration by parts (see Eq.(3.9) is applied in order to calculate the strong solution. The final compact form of governing equations and relative boundary conditions is given in the equations (5.3) and (3.15), respectively. The explicit expression of the fundamental nuclei $\mathbf{K}_{uu}^{k\tau s}$, $\mathbf{\Pi}_{uu}^{k\tau s}$

and $M_{uu}^{k\tau s}$ is the following:

$$\begin{aligned}
(\mathbf{K}_{uu}^{\tau sk})_{11} &= -C_{11}^k J_{\beta/\alpha}^{k\tau s} \partial_\alpha^s \partial_\alpha^\tau - C_{16}^k J^{k\tau s} \partial_\alpha^\tau \partial_\beta^s - C_{16}^k J^{k\tau s} \partial_\alpha^s \partial_\beta^\tau - C_{66}^k J_{\alpha/\beta}^{k\tau s} \partial_\beta^s \partial_\beta^\tau \\
&\quad + C_{55}^k \left(J_{\alpha\beta}^{k\tau s z} - \frac{1}{R_{\alpha_k}} J_\beta^{k\tau s z} - \frac{1}{R_{\alpha_k}} J_\beta^{k\tau s z} + \frac{1}{R_{\alpha_k}^2} J_{\beta/\alpha}^{k\tau s} \right), \\
(\mathbf{K}_{uu}^{\tau sk})_{12} &= -C_{12}^k J^{k\tau s} \partial_\alpha^\tau \partial_\beta^s - C_{16}^k J_{\beta/\alpha}^{k\tau s} \partial_\alpha^\tau \partial_\alpha^s - C_{26}^k J_{\alpha/\beta}^{k\tau s} \partial_\beta^\tau \partial_\beta^s - C_{66}^k J^{k\tau s} \partial_\alpha^s \partial_\beta^\tau \\
&\quad + C_{45}^k \left(J_{\alpha\beta}^{k\tau s z} - \frac{1}{R_{\beta_k}} J_\alpha^{k\tau s z} - \frac{1}{R_{\alpha_k}} J_\beta^{k\tau s z} + \frac{1}{R_{\alpha_k}} \frac{1}{R_{\beta_k}} J^{k\tau s} \right), \\
(\mathbf{K}_{uu}^{\tau sk})_{13} &= -C_{11}^k \frac{1}{R_{\alpha_k}} J_{\beta/\alpha}^{k\tau s} \partial_\alpha^\tau - C_{12}^k \frac{1}{R_{\beta_k}} J^{k\tau s} \partial_\alpha^\tau - C_{13}^k J_\beta^{k\tau s z} \partial_\alpha^\tau \\
&\quad - C_{16}^k \frac{1}{R_{\alpha_k}} J^{k\tau s} \partial_\beta^\tau - C_{26}^k \frac{1}{R_{\beta_k}} J_{\alpha/\beta}^{k\tau s} \partial_\beta^\tau - C_{36}^k J_\alpha^{k\tau s z} \partial_\beta^\tau \\
&\quad + C_{45}^k \left(J_\alpha^{k\tau s z} \partial_\beta^s - \frac{1}{R_{\alpha_k}} J^{k\tau s} \partial_\beta^s \right) + C_{55}^k \left(J_\beta^{k\tau s z} \partial_\alpha^s - \frac{1}{R_{\alpha_k}} J_{\beta/\alpha}^{k\tau s} \partial_\alpha^s \right), \\
(\mathbf{K}_{uu}^{\tau sk})_{21} &= -C_{12}^k J^{k\tau s} \partial_\alpha^s \partial_\beta^\tau - C_{16}^k J_{\beta/\alpha}^{k\tau s} \partial_\alpha^s \partial_\alpha^\tau - C_{26}^k J_{\alpha/\beta}^{k\tau s} \partial_\beta^s \partial_\beta^\tau - C_{66}^k J^{k\tau s} \partial_\alpha^\tau \partial_\beta^s \\
&\quad + C_{45}^k \left(J_{\alpha\beta}^{k\tau s z} - \frac{1}{R_{\beta_k}} J_\alpha^{k\tau s z} - \frac{1}{R_{\alpha_k}} J_\beta^{k\tau s z} + \frac{1}{R_{\alpha_k}} \frac{1}{R_{\beta_k}} J^{k\tau s} \right), \\
(\mathbf{K}_{uu}^{\tau sk})_{22} &= -C_{22}^k J_{\alpha/\beta}^{k\tau s} \partial_\beta^s \partial_\beta^\tau - C_{26}^k J^{k\tau s} \partial_\alpha^s \partial_\beta^\tau - C_{26}^k J^{k\tau s} \partial_\alpha^\tau \partial_\beta^s - C_{66}^k J_{\beta/\alpha}^{k\tau s} \partial_\alpha^s \partial_\alpha^\tau \\
&\quad + C_{44}^k \left(J_{\alpha\beta}^{k\tau s z} - \frac{1}{R_{\beta_k}} J_\alpha^{k\tau s z} - \frac{1}{R_{\beta_k}} J_\alpha^{k\tau s z} + \frac{1}{R_{\beta_k}^2} J_{\alpha/\beta}^{k\tau s} \right), \\
(\mathbf{K}_{uu}^{\tau sk})_{23} &= -C_{12}^k \frac{1}{R_{\alpha_k}} J^{k\tau s} \partial_\beta^\tau - C_{22}^k \frac{1}{R_{\beta_k}} J_{\alpha/\beta}^{k\tau s} \partial_\beta^\tau - C_{23}^k J_\alpha^{k\tau s z} \partial_\beta^\tau \\
&\quad - C_{16}^k \frac{1}{R_{\alpha_k}} J_{\beta/\alpha}^{k\tau s} \partial_\alpha^\tau - C_{26}^k \frac{1}{R_{\beta_k}} J^{k\tau s} \partial_\alpha^\tau - C_{36}^k J_\beta^{k\tau s z} \partial_\alpha^\tau \\
&\quad + C_{45}^k \left(J_\beta^{k\tau s z} \partial_\alpha^s - \frac{1}{R_{\beta_k}} J^{k\tau s} \partial_\alpha^s \right) + C_{44}^k \left(J_\alpha^{k\tau s z} \partial_\beta^s - \frac{1}{R_{\beta_k}} J_{\alpha/\beta}^{k\tau s} \partial_\beta^s \right), \\
(\mathbf{K}_{uu}^{\tau sk})_{31} &= C_{11}^k \frac{1}{R_{\alpha_k}} J_{\beta/\alpha}^{k\tau s} \partial_\alpha^s + C_{12}^k \frac{1}{R_{\beta_k}} J^{k\tau s} \partial_\alpha^s + C_{13}^k J_\beta^{k\tau s z} \partial_\alpha^s \\
&\quad + C_{16}^k \frac{1}{R_{\alpha_k}} J^{k\tau s} \partial_\beta^s + C_{26}^k \frac{1}{R_{\beta_k}} J_{\alpha/\beta}^{k\tau s} \partial_\beta^s + C_{36}^k J_\alpha^{k\tau s z} \partial_\beta^s \\
&\quad - C_{45}^k \left(J_\alpha^{k\tau s z} \partial_\beta^\tau - \frac{1}{R_{\alpha_k}} J^{k\tau s} \partial_\beta^\tau \right) - C_{55}^k \left(J_\beta^{k\tau s z} \partial_\alpha^\tau - \frac{1}{R_{\alpha_k}} J_{\beta/\alpha}^{k\tau s} \partial_\alpha^\tau \right),
\end{aligned}$$

$$\begin{aligned}
(\mathbf{K}_{uu}^{\tau sk})_{32} &= C_{12}^k \frac{1}{R_{\alpha_k}} J^{k\tau s} \partial_\beta^s + C_{22}^k \frac{1}{R_{\beta_k}} J_{\alpha/\beta}^{k\tau s} \partial_\beta^s + C_{23}^k J_\alpha^{k\tau z s} \partial_\beta^s \\
&\quad + C_{16}^k \frac{1}{R_{\alpha_k}} J_{\beta/\alpha}^{k\tau s} \partial_\alpha^s + C_{26}^k \frac{1}{R_{\beta_k}} J^{k\tau s} \partial_\alpha^s + C_{36}^k J_\beta^{k\tau z s} \partial_\alpha^s \\
&\quad - C_{45}^k \left(J_\beta^{k\tau s z} \partial_\alpha^\tau - \frac{1}{R_{\beta_k}} J^{k\tau s} \partial_\alpha^\tau \right) - C_{44}^k \left(J_\alpha^{k\tau s z} \partial_\beta^\tau - \frac{1}{R_{\beta_k}} J_{\alpha/\beta}^{k\tau s} \partial_\beta^\tau \right), \\
(\mathbf{K}_{uu}^{\tau sk})_{33} &= C_{11}^k \frac{1}{R_{\alpha_k}^2} J_{\beta/\alpha}^{k\tau s} + C_{22}^k \frac{1}{R_{\beta_k}^2} J_{\alpha/\beta}^{k\tau s} + C_{33}^k J_{\alpha\beta}^{k\tau z s z} \\
&\quad + 2C_{12}^k \frac{1}{R_{\alpha_k}} \frac{1}{R_{\beta_k}} J^{k\tau s} + C_{13}^k \frac{1}{R_{\alpha_k}} (J_\beta^{k\tau z s} + J_\beta^{k\tau s z}) + C_{23}^k \frac{1}{R_{\beta_k}} (J_\alpha^{k\tau z s} + J_\alpha^{k\tau s z}) \\
&\quad - C_{44}^k J_{\alpha/\beta}^{k\tau s} \partial_\beta^s \partial_\beta^\tau - C_{55}^k J_{\beta/\alpha}^{k\tau s} \partial_\alpha^s \partial_\alpha^\tau - C_{45}^k J^{k\tau s} \partial_\alpha^s \partial_\beta^\tau - C_{45}^k J^{k\tau s} \partial_\alpha^\tau \partial_\beta^s, \tag{6.1}
\end{aligned}$$

$$\begin{aligned}
(\mathbf{\Pi}_{uu}^{\tau sk})_{11} &= n_\alpha C_{11}^k J_{\beta/\alpha}^{k\tau s} \partial_\alpha^s + n_\beta C_{66}^k J_{\alpha/\beta}^{k\tau s} \partial_\beta^s + n_\beta C_{16}^k J^{k\tau s} \partial_\alpha^s + n_\alpha C_{16}^k J^{k\tau s} \partial_\beta^s, \\
(\mathbf{\Pi}_{uu}^{\tau sk})_{12} &= n_\alpha C_{16}^k J_{\beta/\alpha}^{k\tau s} \partial_\alpha^s + n_\beta C_{26}^k J_{\alpha/\beta}^{k\tau s} \partial_\beta^s + n_\alpha C_{12}^k J^{k\tau s} \partial_\beta^s + n_\beta C_{66}^k J^{k\tau s} \partial_\alpha^s, \\
(\mathbf{\Pi}_{uu}^{\tau sk})_{13} &= n_\alpha \frac{1}{R_{\alpha_k}} C_{11}^k J_{\beta/\alpha}^{k\tau s} + n_\alpha \frac{1}{R_{\beta_k}} C_{12}^k J^{k\tau s} + n_\alpha C_{13}^k J_\beta^{k\tau s z} + n_\beta \frac{1}{R_{\alpha_k}} C_{16}^k J^{k\tau s} + \\
&\quad n_\beta \frac{1}{R_{\beta_k}} C_{26}^k J_{\alpha/\beta}^{k\tau s} + n_\beta C_{36}^k J_\alpha^{k\tau s z}, \\
(\mathbf{\Pi}_{uu}^{\tau sk})_{21} &= n_\alpha C_{16}^k J_{\beta/\alpha}^{k\tau s} \partial_\alpha^s + n_\beta C_{26}^k J_{\alpha/\beta}^{k\tau s} \partial_\beta^s + n_\beta C_{12}^k J^{k\tau s} \partial_\alpha^s + n_\alpha C_{66}^k J^{k\tau s} \partial_\beta^s, \\
(\mathbf{\Pi}_{uu}^{\tau sk})_{22} &= n_\alpha C_{66}^k J_{\beta/\alpha}^{k\tau s} \partial_\alpha^s + n_\beta C_{22}^k J_{\alpha/\beta}^{k\tau s} \partial_\beta^s + n_\beta C_{26}^k J^{k\tau s} \partial_\alpha^s + n_\alpha C_{26}^k J^{k\tau s} \partial_\beta^s, \\
(\mathbf{\Pi}_{uu}^{\tau sk})_{23} &= n_\alpha \frac{1}{R_{\alpha_k}} C_{16}^k J_{\beta/\alpha}^{k\tau s} + n_\alpha \frac{1}{R_{\beta_k}} C_{26}^k J^{k\tau s} + n_\alpha C_{36}^k J_\beta^{k\tau s z} + n_\beta \frac{1}{R_{\alpha_k}} C_{12}^k J^{k\tau s} + \\
&\quad n_\beta \frac{1}{R_{\beta_k}} C_{22}^k J_{\alpha/\beta}^{k\tau s} + n_\beta C_{23}^k J_\alpha^{k\tau s z}, \\
(\mathbf{\Pi}_{uu}^{\tau sk})_{31} &= -n_\alpha \frac{1}{R_{\alpha_k}} C_{55}^k J_{\beta/\alpha}^{k\tau s} + n_\alpha C_{55}^k J_\beta^{k\tau s z} - n_\beta \frac{1}{R_{\alpha_k}} C_{45}^k J^{k\tau s} + n_\beta C_{45}^k J_\alpha^{k\tau s z}, \\
(\mathbf{\Pi}_{uu}^{\tau sk})_{32} &= -n_\alpha \frac{1}{R_{\beta_k}} C_{45}^k J^{k\tau s} + n_\alpha C_{45}^k J_\beta^{k\tau s z} - n_\beta \frac{1}{R_{\beta_k}} C_{44}^k J_{\alpha/\beta}^{k\tau s} + n_\beta C_{44}^k J_\alpha^{k\tau s z}, \\
(\mathbf{\Pi}_{uu}^{\tau sk})_{33} &= n_\alpha C_{55}^k J_{\beta/\alpha}^{k\tau s} \partial_\alpha^s + n_\beta C_{44}^k J_{\alpha/\beta}^{k\tau s} \partial_\beta^s + n_\beta C_{45}^k J^{k\tau s} \partial_\alpha^s + n_\alpha C_{45}^k J^{k\tau s} \partial_\beta^s, \tag{6.2}
\end{aligned}$$

$$\begin{aligned}
\mathbf{M}_{11}^{k\tau s} &= \rho^k J_{\alpha\beta}^{k\tau s}, \\
\mathbf{M}_{12}^{k\tau s} &= 0, \\
\mathbf{M}_{13}^{k\tau s} &= 0, \\
\mathbf{M}_{21}^{k\tau s} &= 0, \\
\mathbf{M}_{22}^{k\tau s} &= \rho^k J_{\alpha\beta}^{k\tau s}, \\
\mathbf{M}_{23}^{k\tau s} &= 0, \\
\mathbf{M}_{31}^{k\tau s} &= 0, \\
\mathbf{M}_{32}^{k\tau s} &= 0, \\
\mathbf{M}_{33}^{k\tau s} &= \rho^k J_{\alpha\beta}^{k\tau s},
\end{aligned} \tag{6.3}$$

where the integrals J are the same introduced for the Navier method in Section 4.1.1.

6.2 Analysis of laminated shells

Three different theories are used for the analysis of laminated shells by means of the RBF and they are implemented by means of the CUF.

The first is a sinus shear deformation theory (SSDT) that involves the following expansion of displacements:

$$u = u_0 + zu_1 + \sin\left(\frac{\pi z}{h}\right)u_3, \quad v = v_0 + zv_1 + \sin\left(\frac{\pi z}{h}\right)v_3, \quad w = w_0 + zw_1 + \sin\left(\frac{\pi z}{h}\right)w_3, \tag{6.4}$$

where u_0, v_0 and w_0 are translations of a point at the middle-surface of the plate, and u_1, v_1, u_3, v_3 denote rotations. This theory is an expansion of early developments by Touratier [228]-[230], and Vidal and Polit [231]. It considers a sinusoidal variation of all displacements u, v, w , allowing for through-the-thickness deformations. In the framework of the Unified Formulation, one can define the following vector of the thickness functions:

$$F_s = \left[1, z, \sin\left(\frac{\pi z}{h}\right)\right]. \tag{6.5}$$

The second theory considered is an EDZ1 model that takes into account the ZZ effects and transverse normal strains. The relative expression of the displacement field is the following:

$$u = u_0 + zu_1 + (-1)^k \frac{2}{h_k} \left(z - \frac{1}{2}(z_k + z_{k+1})\right) u_Z, \tag{6.6}$$

$$v = v_0 + zv_1 + (-1)^k \frac{2}{h_k} \left(z - \frac{1}{2}(z_k + z_{k+1})\right) v_Z, \tag{6.7}$$

$$w = w_0 + zw_1 + (-1)^k \frac{2}{h_k} \left(z - \frac{1}{2}(z_k + z_{k+1})\right) w_Z, \tag{6.8}$$

where z_k, z_{k+1} are the bottom and top z -coordinates at each layer and h_k is the thickness of the layer. The additional degrees of freedom u_Z, v_Z have a meaning of displacement,

and its amplitude is layer independent. In this case, the vector of thickness functions is:

$$F_s = \left[1, z, (-1)^k \frac{2}{h_k} \left(z - \frac{1}{2}(z_k + z_{k+1}) \right) \right]. \quad (6.9)$$

Finally, a LD1 model is used, in which each layer k of the given multi-layered structure is separately considered. According to the CUF, the three displacement components u_α , u_β and u_z and their relative variations can be modelled as:

$$(u_\alpha^k, u_\beta^k, u_z^k) = F_s^k (u_{\alpha s}^k, u_{\beta s}^k, u_{zs}^k), \quad (\delta u_\alpha^k, \delta u_\beta^k, \delta u_z^k) = F_\tau^k (\delta u_{\alpha \tau}^k, \delta u_{\beta \tau}^k, \delta u_{z \tau}^k). \quad (6.10)$$

Therefore, the vector of thickness functions is defined as follows:

$$F_s = \left[\frac{1 - 2/h_k (z - \frac{1}{2}(z_k + z_{k+1}))}{2}, \quad \frac{1 + 2/h_k (z - \frac{1}{2}(z_k + z_{k+1}))}{2} \right].$$

6.2.1 Results and discussion

All numerical examples consider a Chebyshev grid and a Wendland function, defined as

$$\phi(r) = (1 - cr)_+^8 (32(cr)^3 + 25(cr)^2 + 8cr + 1), \quad (6.11)$$

where the shape parameter (c) was obtained by an optimization procedure, as detailed in Ferreira and Fasshauer [232].

A laminated composite spherical shell is here considered, of side a and thickness h , composed of layers oriented at $[0^\circ/90^\circ/0^\circ]$ and $[0^\circ/90^\circ/90^\circ/0^\circ]$. The shell is subjected to a sinusoidal vertical pressure of the form

$$p_z = P \sin\left(\frac{\pi x}{a}\right) \sin\left(\frac{\pi y}{a}\right),$$

with the origin of the coordinate system located at the lower left corner on the mid-plane and P the maximum load (at center of shell).

The orthotropic material properties for each layer are given by:

$$E_1 = 25.0E_2, \quad G_{12} = G_{13} = 0.5E_2, \quad G_{23} = 0.2E_2, \quad \nu_{12} = 0.25.$$

The in-plane displacements, the transverse displacements, the normal stresses and the in-plane and transverse shear stresses are presented in normalized form as:

$$\begin{aligned} \bar{w} &= \frac{10^3 w_{(a/2, a/2, 0)} h^3 E_2}{Pa^4}, \quad \bar{\sigma}_{xx} = \frac{\sigma_{xx(a/2, a/2, h/2)} h^2}{Pa^2}, \quad \bar{\sigma}_{yy} = \frac{\sigma_{yy(a/2, a/2, h/4)} h^2}{Pa^2}, \\ \bar{\tau}_{xz} &= \frac{\tau_{xz(0, a/2, 0)} h}{Pa}, \quad \bar{\tau}_{xy} = \frac{\tau_{xy(0, 0, h/2)} h^2}{Pa^2}. \end{aligned}$$

The shell is simply-supported on all edges.

In table 6.1, an assessment of the RBF method is presented for the plate case ($R \rightarrow \infty$). We compare the deflections obtained with the RBF method and an the LD1 model with the LW analytical solution given in [73] and the results obtained with two different shell finite elements: MITC4 and MITC9. These elements are based on CUF and they are described in details in [233] and [127], respectively. Various thickness ratios and laminations are considered. In all the cases, the table shows that the present method is in good agreement with the FEM solution.

In table 1, the static deflections for the present shell models are compared with results

	Method	$a/h = 10$	$a/h = 100$
[0°/90°/0°]	LW [73]	7.4095	4.3400
	LD1 (13 × 13)	7.2739	4.2924
	LD1 (17 × 17)	7.2743	4.2941
	LD1 (21 × 21)	7.2743	4.2943
	MITC4 (13 × 13)	7.2955	4.2573
	MITC4 (17 × 17)	7.3427	4.2915
	MITC4 (21 × 21)	7.3657	4.3082
	MITC9 (5 × 5)	7.4067	4.3375
	MITC9 (9 × 9)	7.4092	4.3397
	MITC9 (13 × 13)	7.4095	4.3399
[0°/90°/90°/0°]	LW [73]	7.3148	4.3420
	LD1 (13 × 13)	7.1722	4.2871
	LD1 (17 × 17)	7.1726	4.2887
	LD1 (21 × 21)	7.1726	4.2889
	MITC4 (13 × 13)	7.2011	4.2593
	MITC4 (17 × 17)	7.2482	4.2935
	MITC4 (21 × 21)	7.2711	4.3102
	MITC9 (5 × 5)	7.3120	4.3396
	MITC9 (9 × 9)	7.3145	4.3418
	MITC9 (13 × 13)	7.3147	4.3420

Table 6.1: Non-dimensional central deflection, $\bar{w} = w \frac{10^2 E_2 h^3}{P_0 a^4}$ for different cross-ply laminated plates.

of Reddy shell formulation using first-order and third-order shear-deformation theories [234]. Nodal grids with 13×13 , 17×17 , and 21×21 points are considered. Various values of R/a and two values of a/h (10 and 100) are taken for the analysis. Results are in good agreement for various a/h ratios with the higher-order results of Reddy [234].

In tables 6.4 and 6.5 the nondimensionalized natural frequencies from the present theories for various cross-ply spherical shells are compared with analytical solutions by Reddy and Liu [234], who considered both the First-order Shear Deformation Theory (FSDT) and the High-order Shear Deformation Theory (HSDT). The first-order the-

a/h	Method	R/a					
		5	10	20	50	100	10^9
10	SSDT (13×13)	6.6874	6.9044	6.9615	6.9781	6.9806	6.9816
	SSDT (17×17)	6.6879	6.9047	6.9618	6.9784	6.9809	6.9819
	SSDT (21×21)	6.6880	6.9048	6.9618	6.9784	6.9809	6.9820
	EDZ1 (13×13)	6.8510	7.0818	7.1429	7.1609	7.1637	7.1649
	EDZ1 (17×17)	6.8516	7.0822	7.1433	7.1612	7.1640	7.1653
	EDZ1 (21×21)	6.8516	7.0822	7.1433	7.1612	7.1640	7.1653
	LD1 (13×13)	6.9514	7.1891	7.2518	7.2700	7.2728	7.2739
	LD1 (17×17)	6.9520	7.1895	7.2521	7.2703	7.2731	7.2743
	LD1 (21×21)	6.9521	7.1895	7.2522	7.2704	7.2732	7.2743
	HSDT [234]	6.7688	7.0325	7.1016	7.1212	7.1240	7.125
	FSDT [234]	6.4253	6.6247	6.6756	6.6902	6.6923	6.6939
100	SSDT (13×13)	1.0244	2.3651	3.5151	4.0692	4.1629	4.1951
	SSDT (17×17)	1.0249	2.3661	3.5165	4.0707	4.1644	4.1966
	SSDT (21×21)	1.0250	2.3662	3.5167	4.0709	4.1646	4.1966
	EDZ1 (13×13)	1.0245	2.3658	3.5167	4.0714	4.1652	4.1975
	EDZ1 (17×17)	1.0250	2.3667	3.5181	4.0728	4.1667	4.1990
	EDZ1 (21×21)	1.0250	2.3669	3.5183	4.0731	4.1669	4.1992
	LD1 (13×13)	1.0300	2.3956	3.5832	4.1606	4.2587	4.2924
	LD1 (17×17)	1.0305	2.3966	3.5846	4.1622	4.2603	4.2941
	LD1 (21×21)	1.0306	2.3968	3.5848	4.1625	4.2606	4.2943
	HSDT [234]	1.0321	2.4099	3.617	4.2071	4.3074	4.3420
	FSDT [234]	1.0337	2.4109	3.6150	4.2027	4.3026	4.3370

Table 6.2: Non-dimensional central deflection, $\bar{w} = w \frac{10^2 E_2 h^3}{P_0 a^4}$ variation with various number of grid points per unit length, N for different R/a ratios, for $R_1 = R_2$. Laminate $[0^\circ/90^\circ/0^\circ]$.

ory overpredicts the fundamental natural frequencies of symmetric thick shells and symmetric shallow thin shells. The present radial basis function method is compared with analytical results by Reddy [234] and shows excellent agreement.

This meshless approach demonstrated that is very successful in the static deformations and free vibration analysis of laminated composite shells. Advantages of radial basis functions are absence of mesh, ease of discretization of boundary conditions and equations of equilibrium or motion and very easy coding. For further details about the analysis of laminated shells by means of the RBF method, one can refer to the works [235]-[237].

a/h	Method	R/a					
		5	10	20	50	100	10^9
10	SSDT (13×13)	6.7199	6.9418	7.0004	7.0174	7.0201	7.0211
	SSDT (17×17)	6.7204	6.9423	7.0007	7.0178	7.0204	7.0214
	SSDT (21×21)	6.7205	6.9423	7.0008	7.0178	7.0204	7.0215
	EDZ1 (13×13)	6.7737	7.0012	7.0614	7.0791	7.0819	7.0831
	EDZ1 (17×17)	6.7742	7.0015	7.0618	7.0795	7.0822	7.0834
	EDZ1 (21×21)	6.7742	7.0015	7.0618	7.0795	7.0822	7.0834
	LD1 (13×13)	6.8580	7.0902	7.1511	7.1686	7.1712	7.1722
	LD1 (17×17)	6.8585	7.0905	7.1514	7.1690	7.1716	7.1726
	LD1 (21×21)	6.8586	7.0906	7.1515	7.1690	7.1716	7.1726
	HSDT [234]	6.7865	7.0536	7.1237	7.1436	7.1464	7.1474
	FSDT [234]	6.3623	6.5595	6.6099	6.6244	6.6264	6.6280
100	SSDT (13×13)	1.0190	2.3581	3.5119	4.0694	4.1638	4.1962
	SSDT (17×17)	1.0195	2.3591	3.5132	4.0708	4.1653	4.1978
	SSDT (21×21)	1.0195	2.3592	3.5134	4.0711	4.1655	4.1980
	EDZ1 (13×13)	1.0190	2.3583	3.5125	4.0702	4.1647	4.1972
	EDZ1 (17×17)	1.0194	2.3593	3.5138	4.0717	4.1662	4.1987
	EDZ1 (21×21)	1.0195	2.3594	3.5140	4.0719	4.1664	4.1989
	LD1 (13×13)	1.0242	2.3865	3.5753	4.1548	4.2533	4.2871
	LD1 (17×17)	1.0247	2.3874	3.5766	4.1563	4.2548	4.2887
	LD1 (21×21)	1.0247	2.3876	3.5768	4.1565	4.2551	4.2889
	HSDT [234]	1.0264	2.4024	3.6133	4.2071	4.3082	4.3430
	FSDT [234]	1.0279	2.4030	3.6104	4.2015	4.3021	4.3368

Table 6.3: Non-dimensional central deflection, $\bar{w} = w \frac{10^2 E_2 h^3}{P_0 a^4}$ variation with various number of grid points per unit length, N for different R/a ratios, for $R_1 = R_2$. Laminate $[0^\circ/90^\circ/90^\circ/0^\circ]$.

6.3 Free vibration analysis of FGM shells

For the analysis of FGM shells, an higher-order shear deformation theory (HSDT) is used, that involves the following expansion of displacements:

$$u(\alpha, \beta, z, t) = u_0(\alpha, \beta, t) + zu_1(\alpha, \beta, t) + z^3 u_3(\alpha, \beta, t), \quad (6.12)$$

$$v(\alpha, \beta, z, t) = v_0(\alpha, \beta, t) + zv_1(\alpha, \beta, t) + z^3 v_3(\alpha, \beta, t), \quad (6.13)$$

$$w(\alpha, \beta, z, t) = w_0(\alpha, \beta, t) + zw_1(\alpha, \beta, t) + z^2 w_2(\alpha, \beta, t), \quad (6.14)$$

where u , v , and w are the displacements in the α -, β -, and z - directions, respectively. u_0 , u_1 , u_3 , v_0 , v_1 , v_3 , w_0 , w_1 , and w_2 are functions to be determined. u_0 , v_0 and

a/h	Method	R/a					
		5	10	20	50	100	10^9
10	SSDT (13×13)	12.0999	11.9378	11.8967	11.8851	11.8835	11.8829
	SSDT (17×17)	12.0995	11.9375	11.8964	11.8849	11.8832	11.8827
	SSDT (21×21)	12.0994	11.9375	11.8964	11.8849	11.8832	11.8827
	EDZ1 (13×13)	12.0527	11.8889	11.8474	11.8357	11.8340	11.8335
	EDZ1 (17×17)	12.0523	11.8886	11.8471	11.8355	11.8338	11.8332
	EDZ1 (21×21)	12.0522	11.8885	11.8470	11.8355	11.8338	11.8332
	LD1 (11×11)	11.9560	11.7900	11.7478	11.7360	11.7343	11.7337
	LD1 (13×13)	11.9549	11.7892	11.7472	11.7353	11.7337	11.7331
	LD1 (17×17)	11.9544	11.7889	11.7469	11.7351	11.7334	11.7329
	LD1 (19×19)	11.9544	11.7889	11.7469	11.7351	11.7334	11.7328
	HSDT [234]	12.040	11.840	11.790	11.780	11.780	11.780
100	SSDT (13×13)	31.2175	20.5753	16.8713	15.6760	15.4977	15.4378
	SSDT (17×17)	31.2076	20.5690	16.8663	15.6714	15.4931	15.4333
	SSDT (21×21)	31.2063	20.5683	16.8658	15.6711	15.4929	15.4331
	EDZ1 (13×13)	31.2170	20.5742	16.8698	15.6744	15.4960	15.4361
	EDZ1 (17×17)	31.2072	20.5679	16.8648	15.6698	15.4915	15.4316
	EDZ1 (21×21)	31.2059	20.5672	16.8642	15.6693	15.4910	15.4311
	LD1 (11×11)	31.1653	20.4712	16.7365	15.5286	15.3482	15.2876
	LD1 (13×13)	31.1374	20.4524	16.7208	15.5138	15.3336	15.2730
	LD1 (17×17)	31.1275	20.4460	16.7157	15.5092	15.3290	15.2684
	LD1 (19×19)	31.1265	20.4455	16.7153	15.5088	15.3287	15.2681
	HSDT [234]	31.100	20.380	16.630	15.420	15.230	15.170

Table 6.4: Nondimensionalized fundamental frequencies of cross-ply laminated spherical shells, $\bar{\omega} = \omega \frac{a^2}{h} \sqrt{\rho/E_2}$, laminate ($[0^\circ/90^\circ/90^\circ/0^\circ]$)

w_0 are translations of a point at the middle-surface of the shell, and u_1, v_1, u_3, v_3 denote rotations. The consideration of higher-order terms in w allows the study of the thickness-stretching effects. The vector of the thickness functions is defined as follows:

$$F_{su} = F_{sv} = \begin{bmatrix} 1 & z & z^3 \end{bmatrix}, \quad (6.15)$$

for in-plane displacements u, v and:

$$F_{sw} = \begin{bmatrix} 1 & z & z^2 \end{bmatrix}, \quad (6.16)$$

for transverse displacement w .

The computation of elastic constants C_{ij} considers the following steps:

1. computation of volume fraction of the ceramic and metal phases;

a/h	Method	R/a					
		5	10	20	50	100	10^9
10	SSDT (13×13)	12.1258	11.9661	11.9256	11.9142	11.9126	11.9120
	SSDT (17×17)	12.1254	11.9658	11.9253	11.9140	11.9123	11.9112
	SSDT (21×21)	12.1253	11.9658	11.9253	11.9140	11.9123	11.9112
	EDZ1 (13×13)	11.9831	11.8192	11.7777	11.7660	11.7643	11.7638
	EDZ1 (17×17)	11.9827	11.8190	11.7774	11.7658	11.7641	11.7635
	EDZ1 (21×21)	11.9827	11.8190	11.7774	11.7658	11.7641	11.7635
	LD1 (11×11)	11.8748	11.7803	11.6660	11.6542	11.6524	11.6519
	LD1 (13×13)	11.8736	11.7075	11.6654	11.6535	11.6518	11.6513
	LD1 (17×17)	11.8732	11.7073	11.6652	11.6533	11.6516	11.6511
	LD1 (19×19)	11.8732	11.7072	11.6651	11.6533	11.6516	11.6510
	HSDT[234]	12.060	11.860	11.810	11.790	11.790	11.790
100	SSDT (13×13)	31.1360	20.5441	16.8634	15.6764	15.4993	15.4398
	SSDT (17×17)	31.1262	20.5388	16.8584	15.6718	15.4948	15.4353
	SSDT (21×21)	31.1249	20.5381	16.8579	15.6714	15.4944	15.4349
	EDZ1 (13×13)	31.1343	20.5420	16.8595	15.6721	15.4950	15.4355
	EDZ1 (17×17)	31.1244	20.5357	16.8545	15.6675	15.4905	15.4310
	EDZ1 (21×21)	31.1231	20.5350	16.8540	15.6671	15.4901	15.4306
	LD1 (11×11)	31.0775	20.4310	16.7165	15.5158	15.4993	15.4398
	LD1 (13×13)	31.0501	20.4133	16.7023	15.5028	15.4948	15.4353
	LD1 (17×17)	31.0402	20.4070	16.6973	15.4982	15.4944	15.4349
	LD1 (19×19)	31.0402	20.4065	16.6969	15.6714	15.4944	15.4349
	HSDT[234]	31.020	20.350	16.620	15.420	15.240	15.170

Table 6.5: Nondimensionalized fundamental frequencies of cross-ply laminated spherical shells, $\bar{\omega} = \omega \frac{a^2}{h} \sqrt{\rho/E_2}$, laminate ($[0^\circ/90^\circ/0^\circ]$)

2. computation of elastic properties E and ν ;

3. computation of elastic constants C_{ij} ;

In the present work, the volume fraction of the ceramic phase is defined according to the power-law:

$$V_c = \left(0.5 + \frac{z}{h}\right)^p, \quad (6.17)$$

being $z \in [-h/2, h/2]$, h the thickness of the shell, and the exponent p a scalar parameter that defines gradation of material properties across the thickness direction. The volume fraction of the metal phase is given as $V_m = 1 - V_c$.

The Young's modulus, E , and Poisson's ratio, ν , are computed by the law-of-mixtures:

$$E(z) = E_m V_m + E_c V_c, \quad \nu(z) = \nu_m V_m + \nu_c V_c. \quad (6.18)$$

Then, the computation of the elastic constants C_{ij} is performed, depending on the as-

sumption of ϵ_{zz} . If $\epsilon_{zz} = 0$, then C_{ij} are the plane-stress reduced elastic constants:

$$C_{11} = \frac{E}{1 - (\nu)^2}, \quad C_{12} = \nu \frac{E}{1 - (\nu)^2}, \quad C_{44} = \frac{E}{2(1 + \nu)}, \quad C_{33} = 0, \quad (6.19)$$

where E is the modulus of elasticity, ν is the Poisson's ratio found in previous step. If $\epsilon_{zz} \neq 0$ (thickness-stretching), then C_{ij} are the three-dimensional elastic constants, given by:

$$C_{11} = \frac{E(1 - (\nu)^2)}{1 - 3(\nu)^2 - 2(\nu)^3}, \quad C_{12} = \frac{E(\nu + (\nu)^2)}{1 - 3(\nu)^2 - 2(\nu)^3}, \quad (6.20)$$

$$C_{44} = \frac{E}{2(1 + \nu)}, \quad C_{33} = \frac{E(1 - (\nu)^2)}{1 - 3(\nu)^2 - 2(\nu)^3}. \quad (6.21)$$

As in Section 5.4, the material constants are directly integrated with the thickness functions using the Gauss integration method.

6.3.1 Results and discussion

In this section, the higher-order shear deformation theory is combined with radial basis functions collocation for the free vibration analysis of functionally graded shell panels. Examples include spherical ($R_x = R_y = R$) as well as cylindrical ($R_x = R$ and $R_y = \infty$) shell panels with all edges clamped (CCCC) or simply supported (SSSS). Particular cases of these are also considered: isotropic materials (fully ceramic, $p = 0$, and fully metal, $p = \infty$) and plates ($R_x = R_y = \infty$).

To study the effect of $\epsilon_{zz} \neq 0$ in these problems, the case $\epsilon_{zz} = 0$ is implemented by considering $w = w_0$ instead (6.14).

Results are compared with those from Pradyumna and Bandyopadhyay [238], who used finite elements formulation and a HSDT disregarding through-the-thickness deformations.

The following material properties are used:

silicon nitride (Si_3N_4):

$$E_c = 322.2715 GPa, \quad \nu_c = 0.24, \quad \rho_c = 2370 Kg/m^3, \quad (6.22)$$

stainless steel ($SUS304$):

$$E_m = 207.7877 GPa, \quad \nu_m = 0.31776, \quad \rho_m = 8166 Kg/m^3 \quad (6.23)$$

aluminum:

$$E_m = 70 GPa, \quad \nu_m = 0.3, \quad \rho_m = 2707 Kg/m^3, \quad (6.24)$$

alumina:

$$E_c = 380 GPa, \quad \nu_c = 0.3, \quad \rho_c = 3000 Kg/m^3. \quad (6.25)$$

The non-dimensional frequency is given as:

$$\bar{w} = wa^2 \sqrt{\frac{\rho_m h}{D}}, \quad \text{where} \quad D = \frac{E_m h^3}{12(1 - \nu_m^2)}. \quad (6.26)$$

In all numerical examples a Chebyshev grid is employed (see figure 6.1) and the Wendland function defined as:

$$\phi(r) = (1 - cr)_+^8 (32(cr)^3 + 25(cr)^2 + 8cr + 1) . \quad (6.27)$$

Here, the shape parameter (c) is obtained by an optimization procedure, as detailed in Ferreira and Fasshauer [232].

An initial study was performed to show the convergence of the present approach and

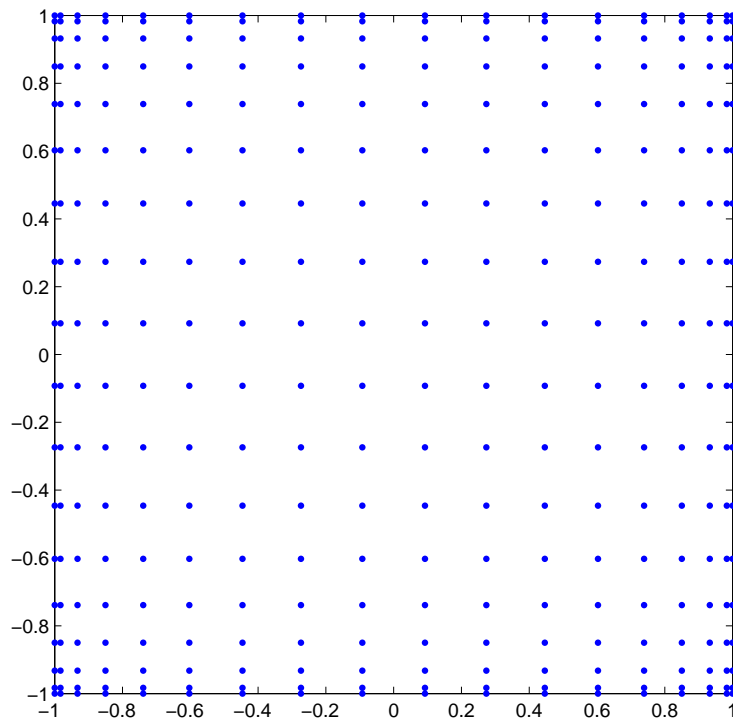


Figure 6.1: A sketch of a Chebyshev grid for 17^2 points

select the number of points to use in the computation of the vibration problems. Results are presented in table 6.6 and refer to the first four vibration modes of a clamped functionally graded cylindrical shell panel composed of silicon nitride (6.22) and stainless steel (6.23), with side-to-thickness ratio $a/h = 10$, side-to-radius ratio $a/R = 0.1$, power law exponent $p = 0.2$, and $a = b = 2$. A 17^2 grid was chosen for the following vibration problems.

Clamped functionally graded cylindrical shell panel

The free vibration of clamped FG cylindrical shell panels is analysed.

In table 6.7 the first 4 vibration modes of a square clamped FG cylindrical shell panel

grid	13^2	17^2	19^2	21^2
1^{st}	60.3483	60.3431	60.3499	60.3479
2^{nd}	115.2450	115.2134	115.2315	115.2044
3^{rd}	115.3917	115.3665	115.3755	115.3347
4^{th}	162.1741	162.0337	162.0727	162.0860

Table 6.6: Initial study. Square CCCC FG cylindrical panel, Si_3N_4 and $SUS304$, $a/h = 10$, $a/R = 0.1$, $p = 0.2$.

mode	source	$p = 0$ (Si_3N_4)	$p = 0.2$	$p = 2$	$p = 10$	$p = \infty$ ($SUS304$)
1	ref. [238]	72.9613	60.0269	39.1457	33.3666	32.0274
	ref. [239]	74.518	57.479	40.750	35.852	32.761
	present $\epsilon_{zz} = 0$	74.2634	60.0061	40.5259	35.1663	32.6108
	present $\epsilon_{zz} \neq 0$	74.5821	60.3431	40.8262	35.4229	32.8593
2	ref. [238]	138.5552	113.8806	74.2915	63.2869	60.5546
	ref. [239]	144.663	111.717	78.817	69.075	63.314
	present $\epsilon_{zz} = 0$	141.6779	114.3788	76.9725	66.6482	61.9329
	present $\epsilon_{zz} \neq 0$	142.4281	115.2134	77.6639	67.1883	62.4886
3	ref. [238]	138.5552	114.0266	74.3868	63.3668	60.6302
	ref. [239]	145.740	112.531	79.407	69.609	63.806
	present $\epsilon_{zz} = 0$	141.8485	114.5495	77.0818	66.7332	62.0082
	present $\epsilon_{zz} \neq 0$	142.6024	115.3665	77.7541	67.2689	62.5668
4	ref. [238]	195.5366	160.6235	104.7687	89.1970	85.1788
	ref. [239]	206.992	159.855	112.457	98.386	90.370
	present $\epsilon_{zz} = 0$	199.1566	160.7355	107.9484	93.3350	86.8160
	present $\epsilon_{zz} \neq 0$	200.3158	162.0337	108.9677	94.0923	87.6341

Table 6.7: First 4 modes of a CCCC square FG cylindrical shell panel, Si_3N_4 and $SUS304$, $a/h = 10$, $a/R = 0.1$, for several p .

with constituents silicon nitride (6.22) and stainless steel (6.23), side-to-thickness ratio $a/h = 10$, side-to-radius ratio $a/R = 0.1$, and several power law exponents p are presented. Results are compared with [238] and those from Yang and Shen [239], with the differential quadrature approximation and Galerkin technique, both neglecting through-the-thickness deformations.

The fundamental frequency of square clamped FG cylindrical shell panels composed of aluminum (6.24) and alumina (6.25), with side-to-radius ratio $a/R = 0.1$, various side-to-thickness ratios a/h and power law exponents p are presented in table 6.8.

The results of the present approach in tables 6.7 and 6.8 compare well with references. The combination of present HSDT and the meshless technique based on collocation with radial basis function shows very good accuracy in the free vibration analysis of FG shells.

In table 6.9 the fundamental frequency of square clamped FG cylindrical shell panels composed of aluminum (6.24) and alumina (6.25), with side-to-thickness ratios

p	source	$a/h = 5$	$a/h = 10$	$a/h = 15$	$a/h = 20$	$a/h = 50$	$a/h = 100$
0	FSDT	56.5548	70.8035	75.7838	77.5654	85.4346	103.4855
	ref. [238]	58.2858	71.7395	75.0439	77.0246	84.8800	102.9227
	present $\epsilon_{zz} = 0$	59.0433	72.3272	76.4904	78.4918	85.6073	102.3351
	present $\epsilon_{zz} \neq 0$	59.7741	72.8141	76.8148	78.7342	85.7713	102.7871
0.5	FSDT	47.2468	57.7597	62.2838	63.8393	70.3199	87.1049
	ref. [238]	48.7185	58.5305	61.5835	63.1381	69.8604	86.5452
	present $\epsilon_{zz} = 0$	49.3050	59.5188	62.6780	64.2371	70.4237	85.4780
	present $\epsilon_{zz} \neq 0$	49.9508	59.9353	62.9544	64.4438	70.5664	85.9029
1	FSDT	42.0305	51.0884	55.4209	56.7991	62.8458	77.7762
	ref. [238]	43.4243	52.0173	54.7015	56.0880	62.2152	77.0774
	present $\epsilon_{zz} = 0$	43.9548	52.8776	55.6437	57.0255	62.7088	76.6386
	present $\epsilon_{zz} \neq 0$	44.5754	53.2759	55.9081	57.2226	62.8414	77.0381

Table 6.8: Fundamental frequencies of CCCC square FG cylindrical shell panels composed of aluminum and alumina, $R/a = 0.1$, for various a/h and p .

$a/h = 10$, are presented considering various side-to-radius ratio a/R , and power law exponents p .

Simply supported functionally graded cylindrical shell panel

The free vibration of simply supported FG cylindrical shell panels is now analysed. Table 6.10 presents the fundamental frequency of a square simply supported FG cylindrical shell panel with constituents aluminum (6.24) and alumina (6.25), length-to-thickness ratio $a/h = 10$, and several length-to-radius ratio a/R and several power law exponents p as well.

Clamped functionally graded spherical shell panel

We now study the free vibration of clamped FG spherical shell panels. The fundamental frequency of a square clamped FG spherical shell panel with constituents aluminum (6.24) and alumina (6.25), and side-to-thickness ratio $a/h = 10$, considering various side-to-radius ratios a/R , and several power law exponents p are presented in table 6.11.

Simply supported functionally graded spherical shell panel

This example considers the free vibration of simply supported FG spherical shell panels.

The fundamental frequency of a square simply supported FG spherical shell panel composed of aluminum (6.24) and alumina (6.25), with side-to-thickness ratio $a/h = 10$, are presented in table 6.12 considering various side-to-radius ratios a/R as well

p	source	$R/a = 0.5$	$R/a = 1$	$R/a = 5$	$R/a = 10$	$R/a = 50$	Plate
0	ref. [238]	129.9808	94.4973	71.8861	71.0394	70.7660	70.7546
	present $\epsilon_{zz} = 0$	133.6037	95.5849	73.1640	72.3304	72.0614	72.0502
	present $\epsilon_{zz} \neq 0$	134.5056	96.0131	73.6436	72.8141	72.5465	72.5353
0.2	ref. [238]	119.6109	87.3930	68.1152	67.3320	67.0801	67.0698
	present $\epsilon_{zz} = 0$	121.8612	87.8148	66.6620	65.8808	65.6371	65.6299
	present $\epsilon_{zz} \neq 0$	122.7375	88.1659	67.1004	66.3235	66.0814	66.0743
0.5	ref. [238]	108.1546	79.5689	63.1896	62.4687	62.2380	62.2291
	present $\epsilon_{zz} = 0$	110.2017	80.0146	60.2477	59.5215	59.3022	59.2985
	present $\epsilon_{zz} \neq 0$	111.0739	80.3049	60.6568	59.9353	59.7178	59.7142
1	ref. [238]	96.0666	71.2453	56.5546	55.8911	55.6799	55.6722
	present $\epsilon_{zz} = 0$	97.9069	71.6716	53.5430	52.8800	52.6864	52.6856
	present $\epsilon_{zz} \neq 0$	98.7955	71.9167	53.9340	53.2759	53.0841	53.0835
2	ref. [238]	84.4431	62.9748	36.2487	35.6633	35.4745	35.4669
	present $\epsilon_{zz} = 0$	86.3088	63.4398	47.5205	46.9447	46.7820	46.7835
	present $\epsilon_{zz} \neq 0$	87.2271	63.6675	47.9060	47.3343	47.1726	47.1741
10	ref. [238]	69.8224	51.3803	33.6611	33.1474	32.9812	32.9743
	present $\epsilon_{zz} = 0$	71.7634	52.0900	40.8099	40.4145	40.3028	40.3037
	present $\epsilon_{zz} \neq 0$	72.3922	52.2780	41.0985	40.7046	40.5923	40.5929
∞	ref. [238]	61.0568	44.2962	32.4802	32.0976	31.9741	31.9689
	present $\epsilon_{zz} = 0$	60.3660	43.1880	33.0576	32.6810	32.5594	32.5543
	present $\epsilon_{zz} \neq 0$	60.7735	43.3815	33.2743	32.8995	32.7786	32.7735

Table 6.9: Fundamental frequencies of CCCC square FG cylindrical shell panels composed of aluminum and alumina, $a/h = 10$, for various R/a and p .

p	source	$R/a = 0.5$	$R/a = 1$	$R/a = 5$	$R/a = 10$	$R/a = 50$	Plate
0	ref. [238]	68.8645	51.5216	42.2543	41.9080	41.7963	41.7917
	present $\epsilon_{zz} = 0$	70.1594	52.1938	42.6701	42.3153	42.2008	42.1961
	present $\epsilon_{zz} \neq 0$	69.9872	52.1101	42.7172	42.3684	42.2560	42.2513
0.2	ref. [238]	64.4001	47.5968	40.1621	39.8472	39.7465	39.7426
	present $\epsilon_{zz} = 0$	65.3889	47.9338	38.7168	38.3840	38.2842	38.2827
	present $\epsilon_{zz} \neq 0$	65.2100	47.8590	38.7646	38.4368	38.3384	38.3368
0.5	ref. [238]	59.4396	43.3019	37.2870	36.9995	36.9088	36.9057
	present $\epsilon_{zz} = 0$	60.4255	43.6883	34.8768	34.5672	34.4809	34.4820
	present $\epsilon_{zz} \neq 0$	60.2422	43.6239	34.9273	34.6219	34.5365	34.5376
1	ref. [238]	53.9296	38.7715	33.2268	32.9585	32.8750	32.8726
	present $\epsilon_{zz} = 0$	54.8909	39.1753	30.9306	30.6485	30.5759	30.5792
	present $\epsilon_{zz} \neq 0$	54.7074	39.1246	30.9865	30.7077	30.6355	30.6386
2	ref. [238]	47.8259	34.3338	27.4449	27.1789	27.0961	27.0937
	present $\epsilon_{zz} = 0$	48.7807	34.7654	27.5362	27.2979	27.2423	27.2472
	present $\epsilon_{zz} \neq 0$	48.6005	34.7289	27.5977	27.3616	27.3055	27.3102
10	ref. [238]	37.2593	28.2757	19.3892	19.1562	19.0809	19.0778
	present $\epsilon_{zz} = 0$	38.2792	28.8072	24.2472	24.1063	24.0762	24.0802
	present $\epsilon_{zz} \neq 0$	38.1172	28.7611	24.2839	24.1444	24.1125	24.1171
∞	ref. [238]	31.9866	24.1988	19.0917	18.9352	18.8848	18.8827
	present $\epsilon_{zz} = 0$	31.7000	23.5827	19.2796	19.1193	19.0675	19.0654
	present $\epsilon_{zz} \neq 0$	31.6222	23.5448	19.3008	19.1433	19.0924	19.0903

Table 6.10: Fundamental frequencies of SSSS square FG cylindrical shell panels composed of aluminum and alumina, $a/h = 10$, for various R/a and p .

p	source	$R/a = 0.5$	$R/a = 1$	$R/a = 5$	$R/a = 10$	$R/a = 50$	Plate
0	ref. [238]	173.9595	120.9210	73.5550	71.4659	70.7832	70.7546
	present $\epsilon_{zz} = 0$	176.8125	122.0934	74.8207	72.7536	72.0784	72.0502
	present $\epsilon_{zz} \neq 0$	176.8356	122.3533	75.2810	73.2322	72.5633	72.5353
0.2	ref. [238]	161.3704	112.2017	69.6597	67.7257	67.0956	67.0698
	present $\epsilon_{zz} = 0$	163.0852	112.7143	68.2142	66.2686	65.6498	65.6299
	present $\epsilon_{zz} \neq 0$	163.0460	112.8132	68.6329	66.7063	66.0938	66.0743
0.5	ref. [238]	147.4598	102.5983	64.6114	62.8299	62.2519	62.2291
	present $\epsilon_{zz} = 0$	149.0931	103.1804	61.6902	59.8745	59.3112	59.2985
	present $\epsilon_{zz} \neq 0$	149.0095	103.1490	62.0789	60.2831	59.7265	59.7142
1	ref. [238]	132.3396	92.2147	57.8619	56.2222	55.6923	55.6722
	present $\epsilon_{zz} = 0$	133.8751	92.8282	54.8597	53.1956	52.6921	52.6856
	present $\epsilon_{zz} \neq 0$	133.7710	92.6962	55.2302	53.5864	53.0895	53.0835
2	ref. [238]	116.4386	81.3963	37.3914	35.9568	35.4861	35.4669
	present $\epsilon_{zz} = 0$	118.0167	82.0948	48.6656	47.2135	46.7849	46.7835
	present $\epsilon_{zz} \neq 0$	117.9317	81.9179	49.0328	47.5990	47.1754	47.1741
10	ref. [238]	92.1387	64.8773	34.6658	33.4057	32.9916	32.9743
	present $\epsilon_{zz} = 0$	93.9111	65.8103	41.6016	40.5998	40.3049	40.3037
	present $\epsilon_{zz} \neq 0$	93.8398	65.7018	41.8796	40.8883	40.5946	40.5929
∞	ref. [238]	80.7722	56.2999	33.2343	32.2904	31.9819	31.9689
	present $\epsilon_{zz} = 0$	79.8889	55.1653	33.8061	32.8722	32.5671	32.5543
	present $\epsilon_{zz} \neq 0$	79.8994	55.2827	34.0141	33.0884	32.7862	32.7735

Table 6.11: Fundamental frequencies of CCCC square FG spherical shell panels composed of aluminum and alumina, $a/h = 10$, for various R/a and p .

p	source	$R/a = 0.5$	$R/a = 1$	$R/a = 5$	$R/a = 10$	$R/a = 50$	Plate
0	ref. [238]	124.1581	78.2306	44.0073	42.3579	41.8145	41.7917
	present $\epsilon_{zz} = 0$	126.2994	79.2626	44.4455	42.7709	42.2192	42.1961
	present $\epsilon_{zz} \neq 0$	126.0882	79.0008	44.4697	42.8180	42.2741	42.2513
0.2	ref. [238]	115.7499	72.6343	41.7782	40.2608	39.7629	39.7426
	present $\epsilon_{zz} = 0$	117.3053	73.2663	40.3936	38.8074	38.2988	38.2827
	present $\epsilon_{zz} \neq 0$	117.0197	73.0034	40.4211	38.8551	38.3528	38.3368
0.5	ref. [238]	106.5014	66.5025	38.7731	37.3785	36.9234	36.9057
	present $\epsilon_{zz} = 0$	108.0044	67.1623	36.4453	34.9574	34.4922	34.4820
	present $\epsilon_{zz} \neq 0$	107.6572	66.9033	36.4782	35.0080	34.5478	34.5376
1	ref. [238]	96.2587	59.8521	34.6004	33.3080	32.8881	32.8726
	present $\epsilon_{zz} = 0$	97.6938	60.5121	32.3691	31.0012	30.5840	30.5792
	present $\epsilon_{zz} \neq 0$	97.2968	60.2636	32.4101	31.0572	30.6437	30.6386
2	ref. [238]	84.8206	52.7875	28.7459	27.5110	27.1085	27.0937
	present $\epsilon_{zz} = 0$	86.2288	53.4659	28.7833	27.5984	27.2474	27.2472
	present $\epsilon_{zz} \neq 0$	85.8028	53.2311	28.8329	27.6602	27.3109	27.3102
10	ref. [238]	65.2296	41.6702	20.4691	19.4357	19.0922	19.0778
	present $\epsilon_{zz} = 0$	66.7088	42.4365	25.0772	24.3034	24.0791	24.0802
	present $\epsilon_{zz} \neq 0$	66.3594	42.2155	25.1038	24.3401	24.1168	24.1171
∞	ref. [238]	57.2005	36.2904	19.8838	19.1385	18.8930	18.8827
	present $\epsilon_{zz} = 0$	57.0657	35.8131	20.0818	19.3251	19.0759	19.0654
	present $\epsilon_{zz} \neq 0$	56.9702	35.6948	20.0927	19.3464	19.1006	19.0903

Table 6.12: Fundamental frequencies of SSSS square FG spherical shell panels composed of aluminum and alumina, $a/h = 10$, for various R/a and p .

power law exponents p .

Discussion

All results presented in tables 6.7 to 6.12 are in excellent agreement with references considered. Exceptions are $p = 10$ and $R/a = 5, 10, 50$ for the SSSS panels, and $p = 2, 10$ and $R/a = 5, 10, 50$ for the CCCC panels. The authors did not find any explanation for these exceptions.

A detailed analysis of previous tables lead us to the following conclusions:

- **Boundary conditions:** Clamped FG shell panels present higher frequency values than simply supported ones.
- **Geometry:** Lower radii of curvature values present higher frequency values, i. e., the fundamental frequency decreases as the ratio R/a increases.
- **Material properties:** The fundamental frequency of FG shell panels decreases as the exponent p in power-law increases.

Another conclusion from all tables is that the fundamental frequency decreases as the radius of curvature increases. The fall-off is faster for smaller values of R (R/a) and then shows fast convergence.

The effect of $\epsilon_{zz} \neq 0$ shows significance in thicker shells (see table 6.7) and seems independent of the radius of curvature (see tables 6.9 to 6.12).

Chapter 7

Conclusions

The analysis of advanced structures involved in multi-field problems has been considered in this thesis. In particular, the analysis of composite shells, the thermal and mechanical analysis of FGM shells, the electromechanical analysis of shell structures embedding piezoelectric layers and the analysis of carbon nanotubes have been performed.

The shell models contained in the CUF have been used to model the field variables: displacements, temperature, electrical potential, transverse stress components and normal electrical displacement (in the case of FGM structures, the CUF can be used also to model the material properties). These models differ in the variable description (Equivalent Single Layer (ESL) or Layer Wise (LW)) and in the order of expansion in the thickness direction used for the primary variables of the problem. Moreover, refined or advanced models can be considered in the CUF, depending on the variational statement employed for the derivation of governing equations. The refined models are developed in the framework of the Principle of Virtual Displacements (PVD) with the possibility of a priori modelling the displacements, the electric potential and the temperature. The advanced models, also called mixed models, are developed in the framework of Reissner's Mixed Variational Theorem (RMVT), which permits the displacements, the electric potential, the temperature, the transverse shear/normal stresses and the transverse normal electric displacement, to be considered as independent variables. The obtained governing equations have been solved in analytical way using the Navier method or in numerical way, using the Finite Element Method and the Radial Basis Functions method. In particular, this last is a meshless method recently proposed to overcome the numerical problems of the finite element method relative to the mesh. Note that, the cases of FEM and RBF methods combined with the Unified Formulation and shell geometries is a new approach that has been firstly introduced in this thesis.

The main results have been organized in three parts: the analytical solutions obtained using the Navier method, the solutions obtained by means of the FEM and the solutions calculated with the RBF method.

In the first part, an extension of the Carrera's Unified Formulation which accounts

for functionally graded shells subjected to thermal loads has been presented. It has been shown that the unified treatment of all the considered variables (displacements, temperature, material) can include any kind of material gradient. The CUF provides very accurate results, compared to reference solutions, although the use of higher order expansions in the thickness direction are mandatory. It has been found that the temperature profile cannot be assumed linear in an FGM layer, even when a very thin shell is considered. The assumption of a constant transverse deflection through the thickness direction is not valid in the thermal case; lower errors are produced in the case of the mechanical loading. The influence of material gradient is more significant for a thermal loading than for mechanical loadings.

Then, the electromechanical problem has been analyzed using both the Principle of Virtual Displacements and Reissner's Mixed Variational Theorem. In particular, various forms of RMVT have been discussed in which the transverse shear/normal stresses and/or the transverse normal electric displacement are a priori modelled. The governing differential equations are derived according to Carrera's Unified Formulation for multilayered shells and the closed-form solutions of the free vibration problem of simply supported, orthotropic piezoelectric laminates in closed circuit configurations (electric potential imposed to zero at the top and bottom) have been calculated. The frequencies obtained from the free vibrations analysis of a multilayered ring shell have been compared with the three-dimensional solution and the following conclusions have been drawn:

1. The use of Layer Wise models is mandatory to achieve a 3D solution, whereas Equivalent Single Layer models give erroneous results even when higher orders of expansion are used; classical theories such as CLT and FSDT could lead to large errors.
2. Mixed theories do not significantly improve the results in terms of circular frequency parameters; however, their use becomes mandatory to predict the correct 'through the thickness' modes for both transverse mechanical and electrical variables.
3. The effect produced by the electromechanical interaction on the frequency response approximately increases with the thickness ratio of the shell but decreases with the wave numbers m and n . However this effect depends no more on wave number when the shell is very thin.

Finally, the refined shell models contained in the Unified Formulation have been applied to the study of the dynamic response in double-walled carbon nanotubes. The DWNT was assumed to be an equivalent continuum cylindrical shell made up of two layers and both ESL and LW models have been employed in the analysis. In particular, the LW models have been modified in order to consider two DWNT tubes as separately vibrating and to account for the van der Waals interaction between them. The following conclusions have been made:

- refined shell models can successfully be extended to the free vibration analysis of

DWNTs and they give a satisfactory analysis for both long and short CNTs, for both lower and higher frequencies;

- the introduction of the van der Waals forces makes it possible to consider two adjacent tubes and leads to lower frequency values;
- the introduction of the vdW forces is mandatory for short CNTs and/or higher frequencies.

The second part of this thesis is dedicated to the FEM analysis of composite and FGM shells. The governing equations are derived from the PVD for the pure-mechanical problem. Firstly, an assessment of the shell finite element based on the CUF has been presented. In this element, the Mixed Interpolation of Tensorial Components method has been employed to contrast the membrane and shear locking phenomenon. The results obtained by analyzing two classical test problems, such as pinched shell and Scordelis-Lo problem, have shown that:

- The MITC9 shell element presents good properties of convergence and robustness;
- The MITC method remains effective in the case of shell FEs formulated on the basis of higher-order theories contained in the Unified Formulation;
- The MITC9 element is completely locking free.

Then, the static analysis of cylindrical composite structures has been performed. The results have been provided in terms of both displacement, in plane stresses and transverse stresses, for various thickness ratios from very thick to very thin shells. The performances of the shell element have been tested and the different theories (classical and refined) contained in the CUF have been compared. The conclusions that can be drawn are the following:

1. the shell element is completely locking free, even when the shell is very thin;
2. the results converge to the exact solution by increasing the number of the elements and the order of expansion of the displacements in the thickness direction;
3. when the shell is very thick, the LW models work better than ZZ ones, and these last work better than ESL models;
4. the classical models, such as CLT and FSDT completely fail in the analysis of thick shells;
5. the use of LW models is mandatory for both thick and thin shells, if one needs to accurately describe the distribution of trasverse stresses in the thickness and to satisfy the interlaminar continuity conditions.

Finally, the CUF shell finite element has been used for the mechanical analysis of FGM shells and the grading material variation in the thickness direction has been taken into account. The shell considered is simply supported and subjected to a bi-sinusoidal pressure load. These conditions permit to calculate the quasi-3D analytical solution of the problem by means of the Navier method and higher-order models. The comparison of the FEM results with the quasi-3D solution has shown that the shell element provides very accurate results. The locking phenomenon doesn't appear, even if the considered structure is very thin. The use of higher-order expansions is necessary to correctly describe the distribution of displacements and stresses along the thickness in functionally graded shells. Moreover, it has been confirmed that the assumption of constant transversal displacement, on which the FSDT is based, is not valid in FGMs.

The Radial Basis Functions method has been used in the last part of this thesis. A sinusoidal shear deformation theory (SSDT), EDZ1 and LD1 models have been implemented for the analysis of laminated orthotropic elastic shells through a multiquadrics discretization of equations of motion and boundary conditions. Firstly, an assessment of the RBF method has been presented for the plate case. The results have been compared with the analytical solution and the FEM results obtained with two different shell finite elements: MITC4 and MITC9 based on the CUF. In both cases, the RBF method was in good agreement with the reference solution. Then, the solutions of both shell bending and free vibration problem have been presented. The results have been provided in terms of static deformations and natural frequencies and they have been compared with other sources. The present meshless approach demonstrated that is very successful in the analysis of laminated composite shells. Advantages of radial basis functions are absence of mesh, ease of discretization of boundary conditions and equations of equilibrium or motion and very easy coding. The static displacements and the natural frequencies obtained have been shown to be in excellent agreement with analytical solutions.

Finally, the Carrera's Unified Formulation have been combined with the Radial Basis Functions collocation technique for the free vibration analysis of functionally graded shells. A higher-order shear deformation theory that allows extensibility in the thickness direction have been implemented and the effect of $\epsilon_{zz} \neq 0$ have been studied. Numerical results have been compared with other sources and also in this case the present approach demonstrated to be successful in the free vibration analysis of functionally graded shells and easy to implement.

7.1 Outlooks

The first objective of the future work is the implementation of an *isoparametric* shell element based on the CUF, that permits to analyze structures with arbitrary geometry. Similarly to the geometrically exact shell element presented in this thesis, the geometrical relations are derived from the Green-Lagrange strain tensor (Eq.(2.8)), considering the following approximations by means of Lagrangian shape functions for both the

displacement and the position vector:

$$\mathbf{u} = N_i \mathbf{u}_i, \quad \mathbf{R} = N_i \mathbf{R}_i, \quad (7.1)$$

with $i = 1, \dots, 9$. The vectors \mathbf{u} and \mathbf{R} contains the displacement components and the coordinates of a generic point in the volume of the shell, respectively, expressed in the cartesian reference system (x, y, z) . Therefore, the geometry of the shell is approximated by knowing the position vector of the nodes of the element.

In order to derive the geometrical relations, it is necessary also to define a unique normal vector to the surface, called director field \mathbf{D} , in each node of the element. As the position vector, the director field is interpolated on the nodes by means of the shape functions:

$$\mathbf{D} = N_i \mathbf{D}_i. \quad (7.2)$$

The MITC method will be applied to contrast the membrane and shear locking phenomenon as shown in Section 3.3.1.

Another objective is to extend the present shell finite element to the mixed models contained in the CUF. In this case, the use of the RMTV permits not only to fulfil the C_z^0 requirements for the transverse stresses, but also to contrast the locking. Indeed, following the same strategy of the MITC method, the stresses, that are modelled a priori, can be opportunely interpolated in the domain of the element using points that are different from the interpolation points of the displacements.

The analysis of the results presented in Chapter 4 has demonstrated the superiority of the refined and advanced shell models contained in the CUF in the study of multi-field problems. For these reasons, it is reasonable to extend the present shell element to the thermo-mechanical analysis of FGM structures and the electromechanical analysis of piezoelectric shells in order to overcome the limits of classical shell elements proposed in literature.

At the same time, also the RBF method, that is a good alternative to the FEM, will be extended to mixed formulations and multi-field problems.

Conclusioni

In questa tesi è stata considerata l'analisi di strutture avanzate coinvolte in problemi multi campo. I modelli guscio contenuti nella CUF sono stati utilizzati per modellare le diverse variabili di campo (spostamenti, temperatura, potenziale elettrico, tensioni trasversali e spostamento elettrico normale). Le equazioni di governo sono state risolte sia analiticamente, tramite il metodo di Navier, che numericamente, usando il metodo degli elementi finiti (FEM) e il metodo delle collocazioni tramite radial basis functions (RBF). I risultati ottenuti sono stati organizzati in tre parti: soluzioni analitiche, soluzioni FEM e soluzioni RBF.

Nella prima parte, è stata presentata l'analisi di gusci FGM soggetti a carichi termici e meccanici. E' stato dimostrato che il profilo di temperatura lungo lo spessore non può essere considerato lineare in uno strato FGM, anche quando il guscio è molto sottile. Di conseguenza, lo spostamento trasversale non può essere assunto costante lungo lo spessore, come si ritrova nelle teorie classiche. Questo è vero anche nei gusci FGM soggetti a carico meccanico puro, anche se in maniera meno evidente. Successivamente, è stato analizzato il problema elettromeccanico in strutture contenenti strati in materiale piezoelettrico. I modelli misti basati sul principio variazionale RMVT sono stati utilizzati per l'analisi. Principalmente, si è visto che l'uso dei modelli misti è necessario per descrivere correttamente l'andamento lungo lo spessore delle variabili trasversali sia meccaniche (tensioni trasversali) che elettriche (spostamento elettrico normale). Infine, è stata effettuata l'analisi dinamica di un double-walled carbon nanotube tramite i modelli LW contenuti nella CUF, che permettono di tener conto delle forze di Van der Waals che agiscono tra le due pareti. I risultati hanno mostrato una buona concordanza con la soluzione di riferimento data in letteratura.

La seconda parte della tesi è dedicata all'analisi meccanica di strutture guscio tramite l'elemento finito basato sulla CUF. Innanzitutto, è stato verificato che l'elemento finito fosse libero dal fenomeno del locking. E' stata effettuata l'analisi di alcuni problemi discriminanti presi dalla letteratura che riguardano gusci isotropi molto sottili ed è stato dimostrato che l'elemento presenta buone proprietà di convergenza numerica. Successivamente, sono stati presentati i risultati ottenuti dall'analisi di gusci in materiale composito ed è stata evidenziata l'importanza di utilizzare i modelli LW per descrivere correttamente l'andamento delle tensioni trasversali lungo lo spessore del guscio. Infine, sono stati analizzati gusci FGM e sono state confermate le conclusioni viste con il metodo analitico.

Nell'ultima parte della tesi il metodo RBF è stato utilizzato per l'analisi di gusci in materiale composito e FGM. I risultati ottenuti sono stati comparati con i risultati analitici e i risultati FEM ed è stato provato che il metodo funziona molto bene. In pratica, e' stato dimostrato che l'utilizzo del metodo RBF è vantaggioso rispetto al FEM perché non presenta problemi numerici legati alla mesh, quali il locking, e la discretizzazione e l'implementazione delle equazioni di

governo risultano molto semplici.

Conclusions

Dans cette thèse, on a considéré l'analyse de structures avancées dans un cadre multi-physique. Les modèles coques dérivés de la CUF ont été utilisés pour modéliser les différentes variables du champ (déplacement, température, potentiel électrique, contraintes transversales et déplacement électrique normal). Les équations fondamentales ont été résolues analytiquement au moyen de la méthode de Navier, et numériquement, en utilisant la méthode des éléments finis (FEM) et la méthode sans maillage utilisant des fonctions de base radiale (RBF).

Les résultats obtenus ont été organisés en trois parties: solutions analytiques, solutions FEM et solutions RBF. Dans la première partie on a présenté l'analyse des coques FGM soumises à des chargements thermiques et mécaniques. On a démontré que le profil de température le long de l'épaisseur ne peut pas être considéré comme linéaire pour une coque FGM, même quand la coque est très mince. En conséquence le déplacement transversale ne peut être supposé constant le long de l'épaisseur, comme dans les théories classiques. C'est aussi vrai pour les coques FGM soumises à des chargements mécaniques pures. Ensuite, des problèmes électromécaniques ont été traités pour des coques piézo-électrique. Les modèles mixtes, basés sur le principe variationnel RMVT, ont été utilisés. On a observé que l'utilisation des modèles mixtes est nécessaires pour décrire correctement la distribution le long de l'épaisseur des contraintes transversales et du déplacement électrique. Enfin, l'analyse dynamique d'un carbon nanotube à double paroi en utilisant les modèles LW de la CUF a été présenté. Cela permet de tenir compte des forces de Van der Waals qui agissent entre les deux parois. Les résultats ont démontré une bonne adéquation avec les solutions de référence de la littérature.

La deuxième partie a été consacrée à l'analyse mécanique des structures coques au moyen d'un nouvel élément fini utilisant la CUF. Cet EF n'est pas sensible au phénomène de verrouillage. On a réalisé l'analyse de certains problèmes discriminants trouvés dans la littérature et qui concernent les coques isotropes très minces. Cette analyse a permis de démontrer que cet EF présente de bonnes propriétés de convergence numérique. Des tests concernant des coques en matériaux composites ont ensuite été présentés. Cela a permis de mettre en évidence l'importance de l'utilisation des modèles LW pour décrire correctement la distribution des contraintes transversales à travers la coque. Les coques FGM ont enfin été analysées permettant de confirmer les conclusions observées en utilisant la méthode analytique.

Dans la dernière partie, la méthode RBF a été utilisée pour l'analyse des coques composite et FGM. Les résultats obtenus ont été comparés avec les résultats analytiques et FEM. On a pu constater que la méthode fonctionnait parfaitement. L'utilisation de la méthode RBF présente les avantages des méthodes sans maillage par rapport à la FEM. De plus, l'obtention des équations fondamentales est assez simple.

Bibliography

- [1] PANTELAKIS, SP.G., ALEXOPOULOS, N.D., *Assessment of the ability of conventional and advanced wrought aluminum alloys for mechanical performance in light-weight applications*, Materials & Design, 29(1), 80-91, 2008.
- [2] REDDY, J.N., *Mechanics of Laminated Composite Plates and Shells. Theory and Analysis*, CRC Press, 2004, New York (USA).
- [3] JONES, R.M., *Mechanics of Composite Materials*, Second Edition, Taylor & Francis, 1999, PA (USA).
- [4] GIBSON, R.F., *Principle of Composite Material Mechanics*, McGraw-Hill, 1994, New York (USA).
- [5] CHEN, A., DAVALOS, J.F., *A solution including skin effect for stiffness and stress field of sandwich honeycombe core*, International Journal of Solids and Structures, 42(9-10), 2711-2739, 2005.
- [6] ZHOU, D., STRONGE, W.J., *Mechanical properties of fibrous core sandwich panels*, International Journal of Mechanical Sciences, 47(4-5), 775-798, 2005.
- [7] CHOPRA, I., *Review of state of art of smart structures and integrated systems*, AIAA Journal, 40(11), 2145-2187, 2002.
- [8] TANI, J., TAKAGI, T., QIU, J., *Intelligent materials systems: application of functional materials*, Applied Mechanics Reviews, 51(8), 505-521, 1998.
- [9] RAO, S.S., SUNAR, M., *Piezoelectricity and its use in disturbance sensing and controll of flexible structures: a survey*, Applied Mechanics Reviews, 47(4), 113-123, 1994.
- [10] SURESH, S., MORTENSEN, A., *Fundamentals of Functionally Graded Materials, Processing and Thermomechanical Behavior of Graded Metals and Metal- Ceramic Composites*, IOM Communications Ltd, 1998, London (UK).
- [11] PINDER, M.-J., ARNOLD, S.M., ABOUDI, J., HUI, D., *Use of composites in functionally graded materials*, Composites Engineering, 4(1), 1-145, 1994.
- [12] BIRMAN, V., BYRD, L.W., *Modeling and analysis of functionally graded materials and structures*, Applied Mechanics Reviews, 60(5), 195-216, 2007.

- [13] REITER, T., DVORAK, G.J., TVERGAARD, V., *Micromechanical models for graded composite materials*, Journal of the Mechanics and Physics and Solids, 45(8), 1281-1302, 1997.
- [14] GASIK, M.M., *Micromechanical modelling of functionally graded materials*, Computational Materials Science, 13(1-3), 42-55, 1998.
- [15] GRUJICIC, M., ZHANG, Y., *Determination of effective elastic properties of functionally graded materials using Voronoi cell finite element method*, Materials Science and Engineering A, 251(1-2), 64-76, 1998.
- [16] LIU, G.R., HAN, X., LAM, K.Y., *Stress waves in functionally gradient materials and its use for material characterization*, Composites. Part B: Engineering, 30(4), 383-394, 1999.
- [17] RAHMAN, S., CHAKRABORTY, A., *A stochastic micromechanical model for elastic properties of functionally graded materials*, Mechanics of Materials, 39(6), 548-563, 2007.
- [18] MORI, T., TANAKA, K., *Average stress in matrix and average elastic energy of materials with misfitting inclusions*, Acta Metallurgica, 21(5), 571-574, 1973.
- [19] IJAM, S., *Helical microtubules of graphitic carbon*, Nature, 354, 56-58, 1991.
- [20] SANDLER, J., WERNER, P., SHAFFER, M.S.P., DEMCHUK, V., ALTSTADT, V., WINDLE, A.H., *Carbon-nanofibre-reinforced poly(ether ether ketone) composites*, Composites Part A, 33(8), 1033-1039, 2002.
- [21] GONG, X., LIU, J., BASKARAN, S., VOISE, R.D., YOUNG, J.S., *Surfactant assisted processing of carbon nanotube/polymer composite*, Chemistry of Materials, 12, 1049-1052, 2000.
- [22] WONG, E.W., SHEEHAN, P.E., LIEBER, C.M., *Nanobeam mechanics: elasticity, strength, and toughness of nanorods and nanotubes*, Science, 277, 1971-1975, 1997.
- [23] WANG, Q., WUEK, S., VARADAN, V., *Torsional buckling of carbon nanotubes*, Physics Letters A, 367, 135-139, 2007.
- [24] WANG, X., CAI, H., *Effects of initial stress on non-coaxial resonance of multi-wall carbon nanotubes*, Acta Materialia, 54, 2067-2074, 2006.
- [25] KOITER, W.T., *A consistent first approximations in the general theory of thin elastic shells*, Proceedings of the Symposium on the Theory of Thin Elastic Shells, North-Holland, Amsterdam, 1959, 12-23.
- [26] CARRERA, E., *A class of two dimensional theories for multilayered plates analysis*, Atti Accademia delle Scienze di Torino, Mem. Sci. Fis., 19-20, 49-87, 1995.

- [27] NOOR, A.K., RARIG, P.L., *Three-dimensional solutions of laminated cylinders*, Computer Methods in Applied Mechanics and Engineering, 3, 319-334, 1974.
- [28] NOOR, A.K., PETERS, W.S., *Stress, vibration and buckling of multilayered cylinders*, Journals of Structural Engineering, 115, 68-89, 1989.
- [29] NOOR, A.K., PETERS, W.S., *A posteriori estimates for shear correction factors in multilayered composite cylinders*, Journals of Engineering Mechanics, 115, 1225-1245, 1989.
- [30] REN, J.G., *Exact solutions for laminated cylindrical shells in cylindrical bending*, Composite Science and Technology, 29, 169-187, 1987.
- [31] VARADAN, T.K., BHASKAR, K., *Bending of laminated orthotropic cylindrical shells - an elasticity approach*, Composite Structures, 17, 141-156, 1991.
- [32] SHAYERMAN, I.YA., *Theory of symmetrical deformation of anisotropic elastic shells*, Izvestia Kievsk Politekh i Del-Khoz Inst, 1, 54-72, 1924.
- [33] AMBARTSUMIAN, S.A., *On general theory of anisotropic shells*, Prikladnaya Matematika Mekhanika, 22(2), 226-237, 1958.
- [34] GOLDENVAIZER, A.N., *Theory of Thin Elastic Shells*, International Series of Monograph in Aeronautics and Astronautics, Pergamon, 1961, New York (USA).
- [35] GOLDENVAIZER, L., *Derivation of an approximated theory of shells by means of asymptotic integration of the equations of the theory of elasticity*, Prikladnaya Matematika Mekhanika, 27(4), 593-608, 1963.
- [36] CICALA, P., *Systematic Approach to Linear Shell Theory*, Levrotto and Bella, 1965, Turin, Italy.
- [37] BERDICHEVSKY, V.L., *Variational-asymptotic method of shell theory construction*, Prikladnaya Matematika Mekhanika, 43(4), 664-687, 1979.
- [38] BERDICHEVSKY, V.L., *Variational-asymptotic method of constructing the nonlinear shell theory*, Theory of Thin Shells, North-Holland, Amsterdam, 137-161, 1980.
- [39] BERDICHEVSKY, V.L., *Variational Principles of Continuum Mechanics*, Nauka, 1983, Moscow.
- [40] BERDICHEVSKY, V.L., MISYURA, V., *Effect of accuracy loss in classical shell theory*, Journals of Applied Mechanics, 59(2), 217-223, 1992.
- [41] BERT, C.W., *Analysis of Shells*, Analysis and Performance of Composites, edited by L. J. Broutman, Wiley, New York, 207-258, 1980.
- [42] LIBRESCU, L., *Elasto-statics and kinetics of anisotropic and heterogeneous shell-type structures*, Noordhoff International, 1975, Leyden, The Netherlands.

- [43] GRIGOLYUK, E.I., KULIKOV, G.M., *General direction of the development of the theory of shells*, *MekhanikaKompozitnykhMaterialov*, 24(2), 287-298, 1988.
- [44] DENNIS, S.T., PALAZOTTO, A.N., *Transverse shear deformation in orthotropic cylindrical pressure vessels using a higher-order shear theory*, *AIAA Journal*, 27(10), 1441-1447, 1989.
- [45] MERK, J., *Hierarchische, kontinuumbasiert shalenelemente höhere ordnung*, Ph.D Dissertation, Inst. for Statics and Dynamics, Universität Stuttgart, 1995, Stuttgart, Germany.
- [46] DI, S., RAMM, E., *Hybrid stress formulation for higher-order theory of laminated shell analysis*, *Computer Method in Applied Mechanics and Engineering*, 109, 359-365, 1993.
- [47] FETTAHLIOGLU, O.A., STEELE, C.R., *Asymptotic solutions for orthotropic non-homogeneous shells of revolution*, *Journal of Applied Mechanics*, 41, 753-758, 1974.
- [48] WIDERA, G.E.O., LOGAN, D.L., *Refined theories for non-homogeneous anisotropic, cylindrical shells: Part I-Derivation*, *Journal of Engineering Mechanics Division, ACSE*, 106, 1053-1073, 1980.
- [49] WIDERA, G.E.O., FAN, H., *On the derivation of a refined theory for non-homogeneous anisotropic shells of revolution*, *Journal of Applied Mechanics*, 110, 102-105, 1988.
- [50] SPENCER, A.J.M., WATSON, P., ROGERS, T.G., *Stress analysis of laminated circular cylindrical shells*, *Recent Developments in Composite Materials Structures*, American Society of Mechanical Engineering, 1990, New York.
- [51] KAPANIA, R.K., *A review on the analysis of laminated shells*, *Journal of Pressure Vessel Technology*, 111, 88-96, 1989.
- [52] NOOR, A.K., BURTON, W.S., *Assessment of computational models for multilayered composite shells*, *Applied Mechanics Review*, 43, 67-97, 1990.
- [53] HSU, T., WANG, J.T., *A theory of laminated cylindrical shells consisting of layers of orthotropic laminae*, *AIAA Journal*, 8(12), 2141-2146, 1970.
- [54] CHEUNG, Y.K., WU, C.I., *Free vibrations of thick, layered cylinders having finite length with various boundary conditions*, *Journal of Sound and Vibration*, 24, 189-200, 1972.
- [55] BARBERO, E.J., REDDY, J.N., TEPLY, J.L., *General two-dimensional theory of laminated cylindrical shells*, *AIAA Journal*, 28(3), 544-553, 1990.
- [56] HILDEBRAND, F.B., REISSNER, E., THOMAS, G.B., *Note on the foundations of the theory of small displacements of orthotropic shells*, *NACA TN-1833*, 1949.
- [57] WHITNEY, J.M., SUN, C.T., *A Refined theory for laminated anisotropic, cylindrical shells*, *Journal of Applied Mechanics*, 41, 471-476, 1974.

- [58] REDDY, J.N., LIU, C.F., *A higher-order shear deformation theory of laminated elastic shells*, International Journal of Engineering Sciences, 23, 319-330, 1985.
- [59] LIBRESCU, L., KHDEIR, A.A., FREDERICK, D., *A shear deformable theory of laminated composite shallow shell-type panels and their response analysis. Part II: static response*, Acta Mechanica, 77, 1-12, 1989.
- [60] DENNIS, S.T., PALAZOTTO, A.N., *Laminated shell in cylindrical bending, two-Dimensional approach vs exact*, AIAA Journal, 29(4), 647-650, 1991.
- [61] RATH, B.K., DAS, Y.C., *Vibration of layered shells*, Journal of Sound Vibration, 28, 737-757, 1973.
- [62] DISCIUVA, M., CARRERA, E., *Elasto-dynamic behavior of relatively thick, symmetrically laminated, anisotropic circular cylindrical shells*, Journal of Applied Mechanics, 59, 222-223, 1992.
- [63] REISSNER, E., *On a certain mixed variational theory and a proposed applications*, International Journal of Numerical Methods in Engineering, 20, 1366-1368, 1984.
- [64] REISSNER, E., *On a mixed variational theorem and on a shear deformable plate theory*, International Journal of Numerical Methods in Engineering, 23, 193-198, 1986.
- [65] BHASKAR, K., VARADAN, T.K., *Reissner's new mixed variational principle applied to laminated cylindrical shells*, Journal of Pressure Vessel Technology, 114, 115-119, 1992.
- [66] JING, H., TZENG, K., *Refined shear deformation theory of laminated shells*, AIAA Journal, 31(4), 765-773, 1993.
- [67] CARRERA, E., *C_z^0 -requirements: models for the two-dimensional analysis of multilayered structures*, Composite Structures, 37, 373-384, 1997.
- [68] CARRERA, E., *Sviluppi recenti di una equazione mista di Reissner nello studio delle strutture multistrato*, Associazione Italiana di Aeronautica e Astronautica XIII Conference, 3, 967-976, 1997, Naples, Italy.
- [69] CARRERA, E., *Mixed layer-wise models for multilayered plates analyses*, Composite Structure, 43(44), 57-70, 1998.
- [70] CARRERA, E., *Evaluation of layer-wise mixed theories for laminated plates analysis*, AIAA Journal, 36(5), 830-839, 1998.
- [71] CARRERA, E., *Layer-wise mixed models for accurate vibration analysis of multilayered plates*, Journal of Applied Mechanics, 65(44), 820-829, 1998.
- [72] CARRERA, E., *Multilayered shell theories accounting for layerwise mixed description, part 1: governing equations*, AIAA Journal, 37(9), 1107-1116, 1999.

- [73] CARRERA, E., *Multilayered shell theories accounting for layerwise mixed description, 2: numerical evaluations*, AIAA Journal, 37(9), 1117-1124, 1999.
- [74] KRAUSE, H., *Thin elastic shells*, Wiley, 1967, New York.
- [75] FLUGGE, W., *Stresses in shells*, Springer-Verlag, 1960, Berlin.
- [76] NOVOZHILOV, V.V., *The theory of thin shells*, Noordhoff, Groningen, 1959, The Netherlands.
- [77] VOYIADIS, G.Z., SHI, G., *A refined two-dimensional theory for thick cylindrical shells*, International Journal of Solids and Structures, 27, 261-282, 1991.
- [78] SOLDATOS, K.P., *A comparison of some shell theories used for the dynamic analysis of cross-ply laminated circular cylindrical shells*, Journal of Sound and Vibration, 97, 305-319, 1994.
- [79] CARRERA, E., *The effects of shear deformation and curvature on buckling and vibrations of cross-ply laminated composite shells*, Journal of Sound and Vibration, 151, 405-433, 1991.
- [80] ROBBINS, D.H., CHOPRA, I., *The effect of laminated kinematic assumptions on the global response of actuated plates*, Journal of Intelligent Material Systems and Structures, 17(4), 273-299, 2006.
- [81] CARRERA, E., *Developments, ideas and evaluations based upon the Reissner's Mixed Theorem in the modelling of multilayered plates and shells*, Applied Mechanics Reviews, 54(4), 301-329, 2001.
- [82] CARRERA, E., *Theories and finite elements for multilayered plates and shells: a unified compact formulation with numerical assessment and benchmarking*, Archives of Computational Methods in Engineering, 10(3), 215-296, 2003.
- [83] BALLHAUSE, D., D'OTTAVIO, M., KRÖPLIN, B., CARRERA, E., *A unified formulation to assess multilayered theories for piezoelectric plates*, Computers and Structures, 83(15-16), 1217-1235, 2004.
- [84] ROBALDO, A., CARRERA, E., BENJEDDOU, A., *A unified formulation for finite element analysis of piezoelectric adaptive plates*, Computers and Structures, 84(22-23), 1415-1505, 2006.
- [85] D'OTTAVIO, M., KRÖPLIN, B., *An extension of Reissner mixed variational theorem to piezoelectric laminates*, Mechanics of Advanced Materials and Structures, 13(2), 139-150, 2006.
- [86] CARRERA, E., BOSCOLO, M., *Classical and mixed finite elements for static and dynamics analysis of piezoelectric plates*, International Journal of Numerical Methods in Engineering, available on line, 2006.

- [87] CARRERA, E., FAGIANO, C., *Mixed piezoelectric plate elements with continuous transverse electric displacements*, Journal of Mechanics of Materials and Structures, 2(3), 421-438, 2007.
- [88] HEYLIGER, P., PEI, K.C., SARAVANOS, D., *Layerwise mechanics and finite element model for laminated piezoelectric shells*, AIAA Journal, 34(11), 2353-2360, 1996.
- [89] LAMMERING, R., MESECKE-RISCHMANN, S., *Multifield variational formulations and related finite elements for piezoelectric shells*, Smart Materials and Structures, 12(6), 904-913, 2003.
- [90] CHO, M., ROH, H.Y., *Development of geometrically exact new shell elements based on general curvilinear co-ordinates*, International Journal of Numerical Methods in Engineering, 56(1), 81-115, 2003.
- [91] KÖGL, M., BUCALEM, M.L., *Analysis of smart laminates using piezoelectric MITC plate and shell elements*, Computers and Structures, 83(15-16), 1153-1163, 2005.
- [92] SARAVANOS, D.A., HEYLIGER, P.R., *Mechanics and computational models for laminated piezoelectric beams, plates, and shells*, Applied Mechanics Reviews, 52(10), 305-320, 1999.
- [93] WANG, H.M., DING, H.J., CHEN, Y.M., *Dynamic solution of a multilayered orthotropic piezoelectric hollow cylinder for axisymmetric plane strain problems*, International Journal of Solids and Structures, 42(1), 85-102, 2005.
- [94] SHAKERI, M., ESLAMI, M., DANESHMEHR, A., *Dynamic analysis of thick laminated shell panel with piezoelectric layer based on three dimensional elasticity solution*, Computers and Structures, 84(22-23), 1519-1526, 2006.
- [95] CHEN, C.-Q., SHEN, Y.-P., WANG, X.-M., *Exact solution of orthotropic cylindrical shell with piezoelectric layers under cylindrical bending*, International Journal of Solids and Structures, 33(30), 4481-4494, 1996.
- [96] DUMIR, P., DUBE, G., KAPURIA, S., *Exact piezoelastic solution of simply-supported orthotropic circular cylindrical panel in cylindrical bending*, International Journal of Solids and Structures, 34(6), 685-702, 1997.
- [97] CARRERA, E., BRISCHETTO, S., *Piezoelectric shell theories with a priori continuous transverse electromechanical variables*, Journal of Mechanics of Materials and Structures, 2(2), 377-399, 2007.
- [98] CARRERA, E., BRISCHETTO, S., CINEFRA, M., *Variable kinematics and advanced variational statements for free vibrations analysis of piezoelectric plates and shells*, Computer Modeling in Engineering and Sciences, 65, 259-342, 2010.
- [99] D'OTTAVIO, M., BALLHAUSE, D., KRÖPLIN, B., CARRERA, E., *Closed-form solutions for the free vibration problem of multilayered piezoelectric shells*, Computers and Structures, 84(22-23), 1506-1518, 2006.

- [100] CARRERA, E., BRISCHETTO, S., *Reissner mixed theorem applied to static analysis of piezoelectric shells*, Journal of Intelligent Material Systems and Structures, 18, 1083-1107, 2007.
- [101] PELLETIER, J.L., VEL, S.S., *An exact solution for the steady-state thermoelastic response of functionally graded orthotropic cylindrical shells*, International Journal of Solids and Structures, 43, 1131-1158, 2006.
- [102] SHAO, Z.S., *Mechanical and thermal stresses of a functionally graded circular hollow cylinder with finite length*, International Journal of Pressure Vessels and Piping, 82, 155-163, 2005.
- [103] LIEW, K.M., KITIPORNCHAI, S., ZHANG, X.Z., LIM, C.W., *Analysis of the thermal stress behaviour of functionally graded hollow circular cylinders*, International Journal of Solids and Structures, 40, 2355-2380, 2003.
- [104] VEL, S.S., BASKIYAR, R., *Thermally induced stresses in functionally graded thick tubes*, AIP Conference Proceedings, 973, 688-693, 2008.
- [105] ABRINIA, K., NAEI, H., SADEGHI, F., DJAVANROODI, F., *New analysis for the FGM thick cylinders under combined pressure and temperature loading*, American Journal of Applied Sciences, 5(7), 852-859, 2008.
- [106] SHAO, Z.S., WANG, T.J., *Three-dimensional solutions for the stress fields in functionally graded cylindrical panel with finite length and subjected to thermal/mechanical loads*, International Journal of Solids and Structures, 43, 3856-3874, 2006.
- [107] SHAO, Z.S., WANG, T.J., *Vibrational analysis of single-walled carbon nanotubes using beam element*, Thin-Walled Structures, 47, 646-652, 2009.
- [108] MIR, M., HOSSEINI, A., MAJZOBI, G.H., *A numerical study of vibrational properties of single-walled carbon nanotubes*, Computational Materials Science, 43, 540-548, 2008.
- [109] WANG, C.M., TAN, V.B.C., ZHANG, Y.Y., *Timoshenko beam model for vibration analysis of multiwalled carbon nanotubes*, Journal of Sound and Vibration, 294, 1060-1072, 2006.
- [110] AYDOGDU, M., *Vibration of multi-walled carbon nanotubes by generalized shear deformation theory*, International Journal of Mechanical Sciences, 50, 837-844, 2008.
- [111] AYDOGDU, M., *Effects of shear deformation on vibration of doublewalled carbon nanotubes embedded in an elastic medium*, Archive of Applied Mechanics, 78, 711-723, 2008.
- [112] AMIN, S.S., DALIR, H., FARSHIDIANFAR, A., *Carbon nanotube-reinforced composites: frequency analysis theories based on the matrix stiffness*, Computational Mechanics, 43, 515-524, 2009.

- [113] CHANG, W.J., LEE, H.L., *Free vibration of a single-walled carbon nanotube containing a fluid flow using the Timoshenko beam model*, Physics Letters A, 373, 982-985, 2009.
- [114] ZHANG, Y.Y., WANG, C.M., TAN, V.B.C., *Assessment of Timoshenko beam models for vibrational behavior of single-walled carbon nanotubes using Molecular Dynamics*, Advanced in Applied Mathematics and Mechanics, 1(1), 89-106, 2009.
- [115] DONG, K., ZHU, S.Q., WANG, X., *Wave propagation in multiwall carbon nanotubes embedded in a matrix material*, Composite Structures, 82, 1-9, 2008.
- [116] FOO, C.N., *Vibration of single-walled carbon nanotubes based on cylindrical shell model*, <http://www.nus.edu.sg/nurop/2009/FoE/U076369B.PDF>.
- [117] WANG, C.Y., ZHANG, L.C., *An elastic shell model for characterizing single-walled carbon nanotubes*, Nanotechnology, 19, 195704, 2008.
- [118] HE, X.Q., EISENBERGER, M., LIEW, K.M., *The effect of van der Waals interaction modeling on the vibration characteristics of multiwalled carbon nanotubes*, Journal of Applied Physics, 100, 1-12, 2006.
- [119] HE, X.Q., KITIPORNCHAI, S., LIEW, K.M., *Buckling analysis of multi-walled carbon nanotubes: a continuum model accounting for van der Waals interaction*, Journal of Mechanics and Physics of Solids, 53, 303-326, 2005.
- [120] YAO, X., HAN, Q., *Torsional buckling and postbuckling equilibrium path of double-walled carbon nanotubes*, Composites Science and Technology, 68, 113-120, 2008.
- [121] CARRERA, E., BRISCHETTO, S., *Analysis of thickness locking in classical, refined and mixed multilayered plate theories*, Composites Structures, 82(4), 549-562, 2008.
- [122] CARRERA, E., BRISCHETTO, S., *Analysis of thickness locking in classical, refined and mixed theories for layered shells*, Composites Structures, 85(1), 83-90, 2008.
- [123] MURAKAMI, H., *Laminated composite plate theory with improved in-plane responses*, Journal of Applied Mechanics, 53, 661-666, 1986.
- [124] LEISSA, A.W., *Vibration of shells*, NASA SP-288, 1973, Washington, D.C. (USA).
- [125] LEISSA, A.W., *Vibration of plates*, NASA SP-160, 1969, Washington, D.C. (USA).
- [126] CHAPELLE, D., BATHE, K.J., *The finite element analysis of shells.-Fundamentals*, Springer, 2003, Berlin.
- [127] CINEFRA, M., CHINOSI, C., DELLA CROCE, L., *MITC9 shell elements based on refined theories for the analysis of isotropic cylindrical structures*, Mechanics of Advanced Materials and Structures, in press.

- [128] BRISCHETTO, S., *MITC9 shell elements based on refined theories for the analysis of isotropic cylindrical structures, Classical and mixed multilayered plate/shell models for multifield problems analysis*, Ph.D. Thesis, 2009, Politecnico di Torino, Turin.
- [129] CARRERA, E., BRISCHETTO, S., NALI, P., *Variational statements and computational models for multifield problems and multilayered structures*, Mechanics of Advanced Materials and Structures, 15(3), 182-198, 2008.
- [130] CARRERA, E., BOSCOLO, M., ROBALDO, A., *Hierarchic multilayered plate elements for coupled multifield problems of piezoelectric adaptive structures: formulation and numerical assessment*, Archives of Computational Methods in Engineering, 14(4), 383-430, 2007.
- [131] ALTAY, G.A., DÖKMECI, M.C., *Fundamental variational equations of discontinuous thermopiezoelectric fields*, International Journal of Engineering Sciences, 34(7), 769-782, 1996.
- [132] NOWINSKI, J.L., *Theory of Thermoelasticity with Applications*, Sijthoff & Noordhoff, 1978, The Netherlands.
- [133] CINEFRA, M., CARRERA, E., BRISCHETTO, S., BELOUETTAR, S., *Thermo-mechanical analysis of functionally graded shells*, Journal of Thermal Stresses, 33(10), 942-963, 2010.
- [134] CINEFRA, M., BELOUETTAR, S., SOAVE, M., CARRERA, E., *Variable kinematic models applied to free vibration analysis of functionally graded materials shells*, European Journal of Mechanics-A/Solids, 29, 1078-1087, 2010.
- [135] MACNEAL, R.H., *Perspective on finite elements for shell analysis*, Finite Elements in Analysis and Design, 30, 175-186, 1998.
- [136] ARGYRIS, J.H., *Matrix displacement analysis of plates and shells, Prolegomena to a General Theory, Part I*, Ingenieur-Archiv, 35, 102-142, 1966.
- [137] SABIR, A.B., LOCK, A.C., *The application of finite elements to the large deflection geometrically non-linear behaviour of cylindrical shells*, Variational Methods in Engineering 2, (Eds. C.A. Brebbia, H. Tottenham). Southampton University Press, 7/66-7/75, 1972.
- [138] WEMPNER, G.A., ODEN, J.T., KROSS, D.A., *Finite element analysis of thin shells*, Journal of Engineering Mechanics ASCE 94, 94, 1273-1294, 1968.
- [139] ABEL, J.F., POPOV, E.P., *Static and dynamic finite element analysis of sandwich structures*, Proceedings of the Second Conference of Matrix Methods in Structural Mechanics, AFFSL-TR-68-150, 213-245, 1968.
- [140] MONFORTON, G.R., SCHMIDT, L.A., *Finite element analyses of sandwich plates and cylindrical shells with laminated faces*, Proceedings of the Second Conference of Matrix Methods in Structural Mechanics, AFFSL-TR-68-150, 573-308, 1968.

- [141] PRYOR, C.W., BARKER, R.M., *A finite element analysis including transverse shear effect for applications to laminated plates*, American Institute of Aeronautics and Astronautics Journal, 9, 912-917, 1971.
- [142] NOOR, A.K., *Finite Element Analysis of Anisotropic Plates*, American Institute of Aeronautics and Astronautics Journal, 11, 289-307, 1972.
- [143] HUGHES, T.J.R., TEZDUYAR, T., *Finite elements based upon Mindlin plate theory with particular reference to the four-node isoparametric element*, Journal of Applied Mechanics, 48, 587-596, 1981.
- [144] PANDA, S.C., NATARAJAN, R., *Finite Element Analysis of Laminated Composites Plates*, International Journal for Numerical Methods in Engineering, 14, 69-79, 1979.
- [145] PARISCH, H., *A critical survey of the 9-node degenerated shell element with special emphasis on thin shell application and reduced integration*, Computer Methods in Applied Mechanics and Engineering, 20, 323-350, 1979.
- [146] FERREIRA, A.J.M., BARBOSA, J.T., MARQUES, A.T., DE SÀ, J.C., *Non-linear analysis of sandwich shells: the effect of core plasticity*, Computers & Structures, 76, 337-346, 2000.
- [147] ZIENKIEWICZ, O.C., TAYLOR, R.L., TOO, J.M., *Reduced intergration technique in general analysis of plates and shells*, International Journal for Numerical Methods in Engineering, 3, 275-290, 1973.
- [148] CHINOSI, C., LOVADINA, C., *Remarks on partial selective reduced integration method for Reissner-Mindlin plate problem*, Computers & Structures, 73, 73-78, 1999.
- [149] PUGH, E.D.L., HINTONAND, E., ZIENKIEWICZ, O.C., *A study of quadrilater plate bending elements with reduced integration*, International Journal for Numerical Methods in Engineering, 12, 1059-1079, 1978.
- [150] HUGHES, T.J.R., COHEN, M., HORAUN, M., *Reduced and selective integration techniques in the finite element methods*, Nuclear Engineering and Design, 46, 203-222, 1978.
- [151] MALKUS, D.S., HUGHES, T.J.R., *Mixed finite element methods - reduced and selective integration techniques: a unified concepts*, Computer Methods in Applied Mechanics and Engineering, 15, 63-81, 1978.
- [152] CHINOSI, C., DELLA CROCE, L., SCAPOLLA, T., *Solving thin Naghdi shells with special finite elements*, Mathematical Modeling & Scientific Computing, 8, 231-240, 1997.
- [153] CHINOSI, C., DELLA CROCE, L., SCAPOLLA, T., *Hierarchic finite elements for thin Naghdi shell model*, International Journal of Solids and Structures, 35(16), 1863-1880, 1998.

- [154] NAGHDI, P.M., *The theory of shells and plates*, Handbuch der Physik, 4, 425-640, 1972, Springer, Berlin.
- [155] BATHE, K.J., DVORKIN, E.N., *A four node plate bending element based on Mindlin/Reissner plate theory and mixed interpolation*, International Journal for Numerical Methods in Engineering, 21, 367-383, 1985.
- [156] BATHE, K.J., BREZZI, F., CHO, S.W., *The MITC7 and MITC9 plate elements*, Computers and Structures, 32, 797-814, 1989.
- [157] BATHE, K.J., BREZZI, F., FORTIN, M., *Mixed interpolated elements for Reissner-Mindlin plates*, International Journal for Numerical Methods in Engineering, 28, 1787-1801, 1989.
- [158] HUANG, N.C., HINTON, E., *A nine node Lagrangian Mindlin plate element with enhanced shear interpolation*, Engineering Computations, 1, 369-379, 1984.
- [159] AURICCHIO, F., SACCO, L., *A mixed-enhanced finite elements for the analysis of laminated composites*, International Journal for Numerical Methods in Engineering, 44, 1481-1504, 1999.
- [160] BRANK, B., CARRERA, E., *A Family of Shear-Deformable Shell Finite Elements for Composite Structures*, Computer & Structures, 76, 297-297, 2000.
- [161] ARNOLD, D.N., BREZZI, F., *Locking-free finite element methods for shells*, Mathematics of Computation, 66(217), 1-14, 1997.
- [162] BÜCHTER, N., RAMM, E., *3d-extension of non-linear shell equations based on the enhanced assumed strain concept*, Computational Methods in Applied Sciences, 55-62, 1992, Hirsch C.(ed). Elsevier.
- [163] BISCHOFF, M., RAMM, E., *Shear-deformable shell elements for large strains and rotations*, International Journal for Numerical Methods in Engineering, 40, 4427-4449, 1997.
- [164] BISCHOFF, M., RAMM, E., *On the physical significance of higher-order kinematic and static variables in a three-dimensional shell formulation*, International Journal of Solids and Structures, 37, 6933-6960, 2000.
- [165] BLETZINGER, K.U., BISCHOFF, M., RAMM, E., *A unified approach for shear-locking-free triangular and rectangular shell finite elements*, Computers & Structures, 75, 321-334, 2000.
- [166] BRAUN, M., BISCHOFF, M., RAMM, E., *Non linear shell formulations for complete three-dimensional constitutive laws including composites and laminates*, Computational Mechanics, 15, 1-18, 1994.

- [167] SIMO, J.C., RAFAI, S., *A class of mixed assumed strain methods and the method of incompatible modes*, International Journal for Numerical Methods in Engineering, 29, 1595-1638, 1990.
- [168] KANT, T., OWEN, D.R.J., ZIENKIEWICZ, O.C., *Refined higher order C^0 plate bending element*, Computer & Structures, 15, 177-183, 1982.
- [169] KANT, T., KOMMINENI, J.R., *Large Amplitude Free Vibration Analysis of Cross-Ply Composite and Sandwich Laminates with a Refined Theory and C^0 Finite Elements*, Computer & Structures, 50, 123-134, 1989.
- [170] DAU, F., POLIT, O., TOURATIER, M., *An efficient C^1 finite element with continuity requirements for multilayered/sandwich shell structures*, Computer & Structures, 82, 1889-1899, 2004.
- [171] DAU, F., POLIT, O., TOURATIER, M., *C^1 plate and shell finite elements for geometrically nonlinear analysis of multilayered structures*, Computer & Structures, 84, 1264-1274, 2006.
- [172] POLIT, O., TOURATIER, M., *A new laminated triangular finite element assuring interface continuity for displacements and stresses*, Composite Structures, 38(1-4), 37-44, 1997.
- [173] POLIT, O., TOURATIER, M., *High-order triangular sandwich plate finite element for linear and non-linear analyses*, Computational Methods in Applied Mechanics and Engineering, 185, 305-324, 2000.
- [174] POLIT, O., TOURATIER, M., *A multilayered/sandwich triangular finite element applied to linear and non-linear analyses*, Composite Structures, 58, 121-128, 2002.
- [175] TESSLER, A., *A Higher-order plate theory with ideal finite element suitability*, Computer Methods in Applied Mechanics and Engineering, 85, 183-205, 1991.
- [176] REDDY, J.N., *Mechanics of Laminated Composite Plates. Theory and Analysis*, CRC Press, 1997, New York (USA).
- [177] PALAZOTTO, A.N., DENNIS, S.T., *Nonlinear analysis of shell structures*. AIAA Series, 1992.
- [178] DISCIUVA, M., CICORELLO, A., DALLE MURA, E., *A class of multilayered anisotropic plate elements including the effects of transverse shear deformability*, Proceedings of AIDAA Conference, 877-892, 1985, Torino.
- [179] BEKOU, A., TOURATIER, M., *A Rectangular Finite Element for analysis composite multilayered shallow shells in static, vibration and buckling*, International Journal for Numerical Methods in Engineering, 36, 627-653, 1993.
- [180] REISSNER, E., *On a certain mixed variational theorem and on laminated elastic shell theory*, Proceedings of the Euromech-Colloquium, 219, 17-27, 1986.

- [181] RAO, K.M., MEYER-PIENING, H.R., *Analysis of thick laminated anisotropic composites plates by the finite element method*, Composite Structures, 15, 185-213, 1990.
- [182] BRANK, B., CARRERA, E., *Multilayered Shell Finite Element with Interlaminar Continuous Shear Stresses: A Refinement of the Reissner-Mindlin Formulation*, International Journal for Numerical Methods in Engineering, 48, 843-874, 2000.
- [183] NOOR, A.K., BURTON, W.S., *Assessment of computational models for multi-layered composite shells*, Applied Mechanics Review, 43, 67-97, 1990.
- [184] REDDY, J.N., *An evaluation of equivalent single layer and layer-wise theories of composite laminates*, Composite Structures, 25, 21-35, 1993.
- [185] MAWENYA, A.S., DAVIES, J.D., *Finite element bending analysis of multilayer plates*, International Journal for Numerical Methods in Engineering, 8, 215-225, 1974.
- [186] PINSKY, P.M., KIM, K.O., *A multi-director formulation for nonlinear elastic-viscoelastic layered shells*, Computers & Structures, 24, 901-913, 1986.
- [187] CHAUDHURI, R.A., SEIDE, P., *An approximate method for prediction of transverse shear stresses in a laminated shell*, International Journal of Solids and Structures, 23, 1145-1161, 1987.
- [188] RAMMERSTORFER, F.G., DORNINGER, K., STARLINGER, A., *Composite and sandwich shells*, in Non-linear Analysis of Shells by Finite Elements, 131-194, 1992.
- [189] CHAUDHURI, R.A., SEIDE, P., *An approximate method for prediction of transverse shear stresses in a laminated shell*, International Journal of Solids and Structures, 23, 1145-1161, 1987.
- [190] KANSA, E.J., *Multiquadrics- a scattered data approximation scheme with applications to computational fluid dynamics. i: Surface approximations and partial derivative estimates*, Computers and Mathematics with Applications, 19(8/9), 127-145, 1990.
- [191] HON, Y.C., LU, M.W., XUE, W.M., ZHU, Y.M., *Multiquadric method for the numerical solution of byphasic mixture model*, Applied Mathematics and Computation, 88, 153-175, 1997.
- [192] HON, Y.C., CHEUNG, K.F., MAO, X.Z., KANSA, E.J., *A multiquadric solution for the shallow water equation*, ASCE Journal of Hydraulic Engineering, 125(5), 524-533, 1999.
- [193] WANG, J.G., LIU, G.R., LIN, P., *Numerical analysis of biot's consolidation process by radial point interpolation method*, International Journal of Solids and Structures, 39(6), 1557-1573, 2002.
- [194] LIU, G.R., GU, Y.T., *A local radial point interpolation method (lrpim) for free vibration analyses of 2-d solids*, Journal of Sound and Vibration, 246(1), 29-46, 2001.

- [195] LIU, G.R., WANG, J.G., *A point interpolation meshless method based on radial basis functions*, International Journal for Numerical Methods in Engineering, 54, 1623-1648, 2002.
- [196] WANG, J.G., LIU, G.R., *On the optimal shape parameters of radial basis functions used for 2-d meshless methods*, Computer Methods in Applied Mechanics and Engineering, 191, 2611-2630, 2002.
- [197] CHEN, X.L., LIU, G.R., LIM, S.P., *An element free galerkin method for the free vibration analysis of composite laminates of complicated shape*, Composite Structures, 59, 279-289, 2003.
- [198] DAI, K.Y., LIU, G.R., LIM, S.P., CHEN, X.L., *An element free galerkin method for static and free vibration analysis of shear-deformable laminated composite plates*, Journal of Sound and Vibration, 269, 633-652, 2004.
- [199] LIU, G.R., CHEN, X.L., *Buckling of symmetrically laminated composite plates using the element-free galerkin method*, International Journal of Structural Stability and Dynamics, 2, 281-294, 2002.
- [200] LIEW, K.M., CHEN, X.L., REDDY, J.N., *Mesh-free radial basis function method for buckling analysis of non-uniformity loaded arbitrarily shaped shear deformable plates*, Computer Methods in Applied Mechanics and Engineering, 193, 205-225, 2004.
- [201] HUANG, Y.Q., LI, Q.S., *Bending and buckling analysis of antisymmetric laminates using the moving least square differential quadrature method*, Computer Methods in Applied Mechanics and Engineering, 193, 3471-3492, 2004.
- [202] LIU, L., LIU, G.R., TAN, V.C.B., *Element free method for static and free vibration analysis of spatial thin shell structures*, Computer Methods in Applied Mechanics and Engineering, 191, 5923-5942, 2002.
- [203] XIANG, S., WANG, K.M., AI, Y.T., SHA, Y.D., SHI, H., *Analysis of isotropic, sandwich and laminated plates by a meshless method and various shear deformation theories*, Composite Structures, 91(1), 31-37, 2009.
- [204] XIANG, S., SHI, H., WANG, K.M., AI, Y.T., SHA, Y.D., *Thin plate spline radial basis functions for vibration analysis of clamped laminated composite plates*, European Journal of Mechanics A/Solids, 29, 844-850, 2010.
- [205] HARDY, R.L., *Multiquadric equations of topography and other irregular surfaces*, Geophysical Research, 176, 1905-1915, 1971.
- [206] FORNBERG, B., WRIGHT, G., LARSSON, E., *Some observations regarding interpolants in the limit of flat radial basis functions*, Computers & Mathematics with Applications, 47, 37-55, 2004.

- [207] SHU, C., DING, H., YEO, K.S., *Local radial basis function-based differential quadrature method and its application to solve twodimensional incompressible Navier-Stokes equations*, Computer Methods in Applied Mechanics and Engineering, 192, 941-954, 2003.
- [208] WU, W.X., SHU, C., WANG, C.M., *Vibration analysis of arbitrarily shaped membranes using local radial basis function-based differential quadrature method*, Journal of Sound and Vibration, 306, 252-270, 2007.
- [209] BELLMAN, R.E., KASHEF, B.G., CASTI, J., *Differential quadrature: a technique for the rapid solution of nonlinear partial differential equations*, Journal of Computational Physics, 10, 40-52, 1972.
- [210] CARRERA, E., CIUFFREDA, A., *Closed form solution to assess multilayered plates theories for various thermal stress problem*, Journal of Thermal Stresses, 27, 1001-1031, 2004.
- [211] BRISCHETTO, S., LEETSCH, R., CARRERA, E., WALLMERSRERGER, T., KRÖPLIN, B., *Thermo-machanical bending of functionally graded plates*, Journal of Thermal Stresses, 31(3), 286-308, 2008.
- [212] REDDY, J.N., CHEN, Z.N., *Three-dimensional thermomechanical deformations of functionally graded rectangular plates*, European Journal of Mechanics A/Solids, 20(5), 841-855, 2001.
- [213] MORI, T., TANAKA, K., *Average stress in matrix and average elastic energy of materials with misfitting inclusions*, Acta Metallurgica, 21, 571-574, 1973.
- [214] BENVENISTE, Y., *A new approach to the application of Mori-Tanaka's theory in composite materials*, Mechanics of Materials, 6, 147-157, 1987.
- [215] HATTA, H., TAYA, M., *Effective thermal conductivity of a misoriented short fiber composite*, Journal of Applied Physics, 58, 2478-2486, 1985.
- [216] LEVIN, V.M., *Thermal expansion coefficients of heterogeneous materials*, Mekh. Tverd. Tela, 2, 88-94, 1967.
- [217] SHAPERY, R.A., *Thermal expansion coefficients of composite materials based on energy principles*, Journal of Composite Materials, 2, 380-404, 1968.
- [218] CARRERA, E., BRISCHETTO, S., D'OTTAVIO, M., *Vibration of Piezo-Electric Shells by Unified Formulation and Reissner's Mixed Theorem*, II ECCOMAS Thematic Conference on Smart Structures and Materials, July 18-21, 2005, Lisbon (Portugal).
- [219] D'OTTAVIO, M., BALLHAUSE, D., KRÖPLIN, B., CARRERA, E., *Closed-form solutions for the free-vibration problem of multilayered piezoelectric shells*, Computers and Structures, 84(22-23), 1506-1518, 2006.

- [220] HEYLIGER, P., PEI, K.C., SARAVANOS, D., *Layerwise mechanics and finite element model for laminated piezoelectric shells*, AIAA Journal, 34:1111, 2353-2360, 1996.
- [221] AYDOGDU, M., *Effects of shear deformation on vibration of doublewalled carbon nanotubes embedded in an elastic medium*, Archive of Applied Mechanics, 78, 711-723, 2008.
- [222] CINEFRA, M., CARRERA, E., BRISCHETTO, S., *Refined shell models for the vibration analysis of multi-walled carbon nanotubes*, Mechanics of Advanced Materials and Structures, in press.
- [223] CINEFRA, M., CHINOSI, C., DELLA CROCE, L., *MITC9 shell elements based on refined theories for the analysis of isotropic cylindrical structures*, Mechanics of Advanced Materials and Structures, in press.
- [224] FLÜGGE, W., *Stresses in shells*, 2nd edn. Springer, 1960, Berlin.
- [225] SCORDELIS, A., LO, K.S., *Computer analysis in cylindrical shells*, Journal of American Concrete Institute, 61, 561-593, 1964.
- [226] MCNEAL, R.H., HARDER, R.L., *A proposed standard set of problems to test finite element accuracy*, Finite Elements in Analysis and Design, 1, 3-20, 1985.
- [227] CINEFRA, M., CARRERA, E., DELLA CROCE, L., CHINOSI, C., *Refined shell elements for the analysis of functionally graded structures*, Composite Structures, 94, 415-422, 2012.
- [228] TOURATIER, M., *A generalization of shear deformation theories for axisymmetric multilayered shells*, International Journal of Solids and Structures, 29, 1379-1399, 1992.
- [229] TOURATIER, M., *An efficient standard plate theory*, International Journal of Engineering Science, 29, 901-916, 1991.
- [230] TOURATIER, M., *A refined theory of laminated shallow shells*, International Journal of Solids and Structures, 29, 1401-1415, 1992.
- [231] VIDAL, P., POLIT, O., *A family of sinus finite elements for the analysis of rectangular laminated beams*, Composite Structures, 84, 56-72, 2008.
- [232] FERREIRA, A.J.M., FASSHAUER, G.E., *Computation of natural frequencies of shear deformable beams and plates by a rbf-pseudospectral method*, Computer Methods in Applied Mechanics and Engineering, 196, 134-146, 2006.
- [233] CINEFRA, M., CARRERA, E., NALI, P., *MITC technique extended to variable kinematic multilayered plate elements*, Composite Structures, 92, 1888-1895, 2010.
- [234] REDDY, J.N., LIU, C.F., *A higher-order shear deformation theory of laminated elastic shells*, International Journal of Engineering Science, 23, 319-330, 1985.

- [235] FERREIRA, A.J.M., ROQUE, C.C., CARRERA, E., CINEFRA, M., POLIT, O., *Analysis of laminated shells by a sinusoidal shear deformation theory and Radial Basis Functions collocation, accounting for through-the-thickness deformations*, Composites Part B, 42, 1276-1284, 2011.
- [236] FERREIRA, A.J.M., ROQUE, C.C., CARRERA, E., CINEFRA, M., *Analysis of laminated shells by Murakami's Zig-Zag theory and Radial Basis Functions collocation*, Journal of Engineering Mechanics, submitted.
- [237] FERREIRA, A.J.M., ROQUE, C.C., CARRERA, E., CINEFRA, M., *Analysis of laminated doubly-curved shells by a layer-wise theory and radial basis functions collocation, accounting for through-the-thickness deformations*, Computational Mechanics, 48(1), 13-25, 2011.
- [238] YANG, J., SHEN, H.S., *Free vibration analysis of functionally graded curved panels using a higher-order finite element formulation*, Journal of Sound and Vibration,, 318(1-2), 176-192, 2008.
- [239] YANG, J., SHEN, H.S., *Free vibration and parametric resonance of shear deformable functionally graded cylindrical panels*, Journal of Sound and Vibration, 261(5), 871-893, 2003.

Curriculum Vitae

Name	Maria Cinefra
Date of birth	26 September 1984
Place of birth	Francavilla Fontana (BR), Italy
e-mail	maria.cinefra@polito.it

Education

January 2009 - December 2011	Ph.D. student at Politecnico di Torino and Université Paris X
March 2007 - December 2008	Magistral degree in Aerospace engineering at Politecnico di Torino
September 2003 - March 2007	Bachelor degree in Aerospace engineering at Politecnico di Torino
September 1998 - July 2003	Higher education at secondary sciences school "Francesco Ribezzo", Francavilla Fontana (BR), Italy

Professional experience

January 2009 - March 2011	Research fellowship with CRP H. Tudor of Luxembourg
Since June 2011	Research assistantships at Politecnico di Torino

Teaching activities

Since March 2010	Teaching assistant of the courses "Non-linear analysis" and "Structures for aerospace vehicles" at Politecnico di Torino
------------------	--